UNIVERSITY OF SOUTHAMPTON

FACULTY OF NATURAL AND ENVIRONMENTAL SCIENCES

Chemistry

Volume 1 of 1

Application of Separation Science and Mass Spectrometry to the Analysis of Fuels

by

Waraporn Ratsameepakai

Thesis for the degree of Doctor of Philosophy

February 2016

UNIVERSITY OF SOUTHAMPTON

<u>ABSTRACT</u>

FACULTY OF NATURAL AND ENVIRONMENTAL SCIENCES

<u>Chemistry</u>

Thesis for the degree of Doctor of Philosophy

APPLICATION OF SEPARATION SCIENCE AND MASS SPECTROMETRY TO THE ANALYSIS OF FUELS

Waraporn Ratsameepakai

Abstract: Biodiesel has been used as alternative energy because of the shortage of petroleum fuel resources. Biodiesel is a mixture of fatty acid methyl esters (FAMEs) having different molecular structures with varying chain lengths, and levels of unsaturation. Electrochemistry-mass spectrometry (EC-MS) was used for investigation and monitoring oxidation products of FAMEs. Through direct coupling of this device to the electrospray ion source of the mass spectrometer typical oxidation products were observed in minutes compared to months/years for the auto-oxidation process. The efficiency of glassy carbon (GC) and magic diamond (MD) working electrodes was compared. Oxygenated species for methyl oleate (C18:1), methyl linoleate (C18:2) and methyl linolenate (C18:3) with up to +2(O), + 6(O), and + 9(O), (2.5 V, GC electrode) and +6(O), +8(O), and + 12(O) (3.0 V, MD electrode) respectively were observed. The potentials of oxidation increased in the order methyl esters of C18:3 <

C18:2 < C18:1 for both MD and GC electrodes. The primary oxidation products, hydroperoxides-FAME, in the auto-oxidation of unsaturated FAMEs (C18:1, C18:2, C18:3) can undergo further oxidation to produces a numerous of volatile and non-volatile secondary oxidation products. The volatile oxidation products, *e.g.* 2,4-decadienal and methyl 9-oxo-nonanoate were observed in the gas chromatography-electron ionisation mass spectrometry (GC-EI MS) analyses whereas the less volatile species require electrospray ionisation (ESI) and chromatographic introduction of the samples.

High performance liquid chromatography-electrospray ionisation mass spectrometry (HPLC-ESI MS), ultra-high performance liquid chromatography-electrospray ionisation mass spectrometry (UHPLC-ESI MS) and ultra-high performance supercritical fluid chromatography-electrospray ionisation mass spectrometry (UHPSFC-ESI MS) can be used for the separation of non-volatile species of the oxidation products. The elemental formula for these oxidised FAMEs were determined by ultra-high performance liquid chromatography-quadrupole-time of flight mass spectrometry (UHPLC-Q-TOF MS) and infusion Fourier transform-ion cyclotron resonance mass spectrometry (FT-ICR MS). The presence of oxygenated species up to 6 oxygen atoms of the ion at *m/z* 411.1999 $[C_{19}H_{32}O_8 + Na]^+$ with a 2.6 ppm error observed in positive ion ESI-FT-ICR MS. It expected as the hydroperoxy bis-cyclic peroxides from auto-oxidised methyl linolenate.

Revision of the Energy Institute IP/585 reference method for quantitation of rapeseed methyl esters (RME) by GC-MS was required to afford quantitation of the short chain FAMEs in aviation turbine fuel (AVTUR) now appearing in certain geographic regions of the world. The revised method has delivered showed partial success and an improvement in qualitatively detecting and a positive move towards quantitation of the major components of coconut methyl ester (CME). HPLC and UHPLC coupled to MS offer alternative orthogonal approaches for analysis of these materials. The selective ionisation afforded by ESI affords ready detection of the FAMEs though the reversed-phase chromatography does not fully separate the FAME from the AVTUR fuel matrix, this would lead to matrix effects and ion suppression issues which could compromise any quantitative analysis. UHPSFC-MS provides a solution where the coconut methyl ester (CME) and rapeseed methyl ester (RME) are completely separated from the AVTUR whilst still delivering the benefits of the selective ionisation provided by the electrospray interface. Further supercritical fluid carbon dioxide (scCO$_2$) is readily compatible with direct injection of the AVTUR fuel with the analytical benefits of supercritical fluid chromatography delivering base-line resolved peaks for all the FAMEs of interest in under 3 min.

Table of Contents

List of Tables

List of Figures

xiv

DECLARATION OF AUTHORSHIP

I, WARAPORN RATSAMEEPAKAI

declare that this thesis and the work presented in it are my own and has been generated by me as the result of my own original research.

Application of Separation Science and Mass Spectrometry to

the Analysis of Fuels

I confirm that:

1. This work was done wholly or mainly while in candidature for a research degree at this University;

2. Where any part of this thesis has previously been submitted for a degree or any other qualification at this University or any other institution, this has been clearly stated;

3. Where I have consulted the published work of others, this is always clearly attributed;

4. Where I have quoted from the work of others, the source is always given. With the exception of such quotations, this thesis is entirely my own work;

5. I have acknowledged all main sources of help;

6. Where the thesis is based on work done by myself jointly with others, I have made clear exactly what was done by others and what I have contributed myself;

7. Parts of this work have been published as:

   "W. Ratsameepakai, J. M. Herniman, T. J. Jenkins, G. J. Langley. Evaluation of ultrahigh-performance supercritical fluid chromatography–mass spectrometry as an alternative approach for the analysis of fatty acid methyl esters in aviation turbine fuel. Energy & Fuels **2015**, *29*, 2485." http://dx.doi.org/10.1021/acs.energyfuels.5b00103

Signed:..

Date:..

Acknowledgements

xxx

Definitions and Abbreviations

abr. unit   Arbitrary unit

APCI   Atmospheric pressure chemical ionisation

ASTM   American Society for Testing and Materials

AVTUR   Aviation turbine fuel

°C   degree Celsius

CFPP   Cold filter plugging point

CID   Collision induced dissociation

CME   Coconut methyl ester

CN   Cetane number

CP   Cloud point

cSt   Centistokes

EC   Electrochemistry

EI   Electron ionisation

ELSD   Evaporative light-scattering detector

ESI   Electrospray ionisation

EN   European standard

eV   electron volt

FAMEs   Fatty acid methyl esters

FT-ICR	Fourier transform-ion cyclotron resonance
GC	Gas chromatography
GC × GC	Comprehensive two-dimensional gas chromatography
GC electrode	Glassy carbon electrode
HPLC	High performance liquid chromatography
HRMS	High resolution mass spectrometry
LC	Liquid chromatography
LOD	Limit of detection
MD electrode	Magic diamond electrode
min	Minute
mg/kg	Milligram per kilogram
MS	Mass spectrometry
MS/MS	Tandem mass spectrometry
m/z	Mass-to-charge ratio
NP-HPLC	Normal phase-high performance liquid chromatography
PP	Pour point
ppm	Part per million
PV	Peroxide value

QTOF	Quadrupole time of flight
RP-HPLC	Reversed phase-high performance liquid chromatography
RICC	Reconstructed ion current chromatogram
RME	Rapeseed methyl esters
SFC	Supercritical fluid chromatography
SME	Soybean methyl ester
T	Tesla
TICC	Total ion current chromatogram
TOF	Time of flight
t_R	Retention time
UHPLC	Ultra high performance liquid chromatography
UHPSFC	Ultra high performance supercritical fluid chromatography
UPC^2	Ultra performance convergence chromatography
v/v	Volume by volume
w/w	Weight by weight

Chapter 1:   Introduction

The world has been facing an energy crisis since the 1970s, and oil prices increased to a record high in recent years. However, global energy consumption remains reliant on energy from fossil fuels, and they are used as the primary source of electricity and transportation fuels. Since the 1970s energy crisis, with increasing awareness of the limitations of fossil fuel resources and environmental issues, renewable energy resources (solar, wind, geothermal and biofuels) have become more attractive for the production of alternatives fuels. Biodiesel is now an area of great interest since it has a similar chemical structure and energy content to conventional diesel fuel.[1]

1.1   Background of biodiesel

The first concept of the direct use of vegetable oils as diesel fuel occurred before the energy crisis. Rudolf Diesel used neat vegetable oil (peanut oil) as diesel fuel for his diesel engines at the Paris Exposition in 1900.[2][3] Crude vegetable oils continued in use until the 1920s before fossil-based diesel completely replaced vegetable oils in the market because of their cheaper price and higher availability. Diesel engines had been also developed to operate on petrodiesel fuel, thus modern diesel engines are not compatible with the direct introduction of high viscosity and low volatility neat vegetable oils. With the high viscosity and introduction of crude vegetable oils issues such as deposit formation in the injection system began to occur.[4] At that time, the availability of fossil

fuel resources was not seen as a problem, hence research and development of vegetable oils as a source of diesel fuel was not taken seriously.[1]

1.2 What is biodiesel?

According to the American Society for Testing and Materials (ASTM) D675, "biodiesel" is defined as mono-alkyl esters of long chain fatty acids derived from vegetable oils and animal fats, designated as "B100".[2] Biodiesel is produced from triglycerides from vegetable oils or animal fats *via* transesterification with alcohols, in the presence of a base catalyst, to produce fatty acid alkyl esters as the main product and glycerol as a by-product.

1.3 Feedstocks for biodiesel production

Various feedstocks for biodiesel production include edible oils, non-edible oils, animal fats, waste cooking oils and microalgae. Feedstocks for biodiesel production can be divided into three types[5][6]: first generation feedstocks which include edible vegetable oils such as rapeseed, soybean, peanut, sunflower, palm and coconut oils; second generation feedstocks which include non-edible vegetable oil[7][8][9][10][11] (Jatropha, castor oil, rubber seed), animal fats[12] and waste cooking oils,[13][14] and alternatively, microalgae (unicellular micro-organisms) are considered as third generation feedstocks for biodiesel.[7][15][[16] Table 1-1 shows some feedstocks used for biodiesel production.

Table 1-1   Biodiesel feedstocks[4][5][7][17][18]

First generation	Second generation	Third generation
Edible oils	Non-edible oils	Algae (cyanobacteria)
Soybean	Jatropha	Fungi
Rapeseed	Cotton seed	Bacteria
Canola	Neem	Fungi
Peanut	Rubber seed tree	Microalgae
Coconut	Animal fats	
Palm	Pork lard	
	Beef tallow	
	Poultry Fat	
	Fish oil	
	Chicken fat	

However, the selection criteria of feedstocks to produce biodiesel are highly dependent upon the region, climate, soil condition and geography, availability, cost and oil composition. Therefore, different regions are focusing on different types of feedstock for biodiesel production, for example, rapeseed oil is the dominant feedstock for biodiesel production in Europe, soybean oil in the United States of America and palm oil in tropical countries such as Malaysia.[19][20] Coconut oil is another feedstock used for biodiesel production in the Pacific Rim region such as Malaysia and Indonesia.[21][22][23][24] Table 1-2 shows some potential feedstocks used for biodiesel production worldwide.

Table 1-2   Examples of some feedstocks used for biodiesel production worldwide[4][18][24]

Feedstock	Countries
Edible oils	
Coconut	Indonesia; Philippines, Thailand
Palm	Brazil, Indonesia, Malaysia
Rapeseed	China, France, Germany, Sweden, UK
Soybean	Argentina, Brazil, Canada, Russia, USA
Non-edible oils	
Jatropha	India, Indonesia, Philippines
Animal fats/waste cooking oils	Australia, Finland, Mexico, New Zealand, USA

The physical and chemical properties of biodiesel depend on the fatty acid compositions of the feedstocks used in the production. The composition of fatty acid from coconut, soybean and rapeseed oils used in biodiesel production are shown in Table 1-3. The structures, molecular formula and respective relative molecular weights of fatty acids are shown in Table 1-4.

Table 1-3   Fatty acid composition of some feedstocks used as biodiesel[25]

Fatty acid composition (wt %)	Oil		
	Coconut	**Rapeseed**	**Soybean**
Octanoic acid (C8:0)	4.6-9.5	-	-
Decanoic acid (C10:0)	4.5-9.7	-	-
Dodecanoic acid (C12:0)	44-51	-	-
Tetradecanoic acid (C14:0)	13-20.6	0-1.5	-
Hexadecanoic acid (C16:0)	7.5-10.5	1-6	2.3-13.3
Octadecanoic acid (C18:0)	1-3.5	0.5-3.5	2.4-6
(9Z)-9-Octadecenoic acid (C18:1)	5-8.2	60	17.7-30.8
(9Z, 12Z)-9,12 Octadecadienoic acid (C18:2)	1.0-2.6	9.5-23	49-57.1
(9Z, 12Z, 15Z)-9,12,15 Octadecatrienoic acid (C18:3)	0-0.2	1-13	2-10.5

Note: CX: Y where the X is the number of carbon atoms in the fatty acid chain and Y is the number of double bonds.

Table 1-4   Structures, formulae and relative molecular masses of fatty acids
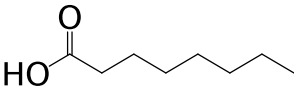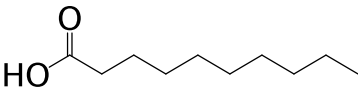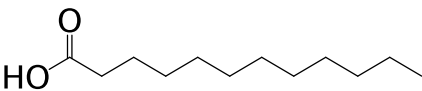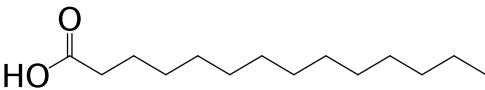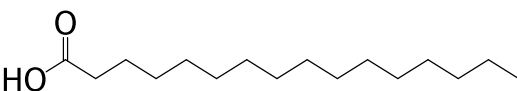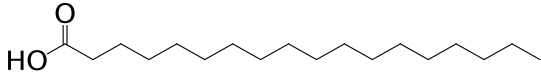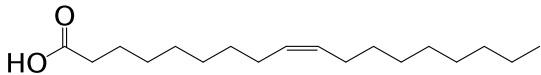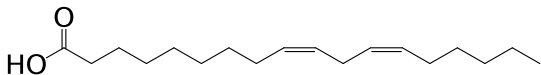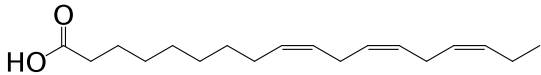
Structure	Details
(C8:0)	Systematic name: Octanoic acid Common name: Caprylic acid Molecular formula: $C_8H_{16}O_2$ Monoisotopic mass: 144.1150 Da
(C10:0)	Systematic name: Decanoic acid Common name: Capric acid Molecular formula: $C_{10}H_{20}O_2$ Monoisotopic mass: 172.1463 Da
(C12:0)	Systematic name: Dodecanoic acid Common name: Lauric acid Molecular formula: $C_{12}H_{24}O_2$ Monoisotopic mass: 200.1776 Da
(C14:0)	Systematic name: Tetradecanoic acid Common name: Myristic acid Molecular formula: $C_{14}H_{28}O_2$ Monoisotopic mass: 228.2089 Da
(C16:0)	Systematic name: Hexadecanoic acid Common name: Palmitic acid Molecular formula: $C_{16}H_{32}O_2$ Monoisotopic mass: 256.2402 Da

Table 1-4   (continued) Structures, formulae and relative molecular masses of fatty acids

Structure	Details
(C18:0)	Systematic name: Octadecanoic acid Common name: Stearic acid Molecular formula: $C_{18}H_{36}O_2$ Monoisotopic mass: 284.2715 Da
(C18:1)	Systematic name: (9Z)-Octadec-9-enoic acid Common name: Oleic acid Molecular formula: $C_{18}H_{34}O_2$ Monoisotopic mass: 282.2559 Da
(C18:2)	Systematic name: (9Z, 12Z)-9,12-Octadecadienoic acid Common name: Linoleic acid Molecular formula: $C_{18}H_{32}O_2$ Monoisotopic mass: 280.2402 Da
(C18:3)	Systematic name: (9Z, 12Z, 15Z)-9,12,15 Octadecatrienoic acid Common name: Linoleic acid Molecular formula: $C_{18}H_{30}O_2$ Monoisotopic mass: 278.22462 Da

1.4   Biodiesel production

The viscosity of vegetable oils (30–200 centistokes (cSt)) is higher than that of diesel fuel (4 cSt) at 40 °C.[26] The direct use of vegetable oils in diesel engines leads to various problems, such as poor atomisation of fuel, incomplete combustion with heavy smoke emission, carbon deposition, sticking of oil rings, injector coking[24], and gelling of the engine lubricant oil.[27] Four primary methods have been used to reduce the viscosity of neat vegetable oils including blending with diesel[28], thermal cracking or pyrolysis[29], micro-emulsification[30] and transesterification.[31][32][33] Transesterification is the most commonly used method to reduce the final viscosity of vegetable oils to produce biodiesel.

1.4.1   Transesterification for biodiesel production

Transesterification is a process of reacting a triglyceride with an alcohol, usually methanol in the presence of a base catalyst sodium hydroxide (NaOH) or potassium hydroxide (KOH) to produce the fatty acid methyl esters (FAMEs) as the main product and glycerol as a by-product. This reaction involves three sequential and reversible reactions. A mole of triglyceride initially reacts with three moles of methanol to produce a mole of glycerol and three moles of fatty acid alkyl esters. A triglyceride is transformed to diglyceride, monoglyceride, and finally monoalkyl ester, glycerol, as shown in Figure 1-1. Transesterification is the equilibrium reaction. It is necessary to use a more excess of the alcohol in order to the shift the equilibrium to the right.[34]
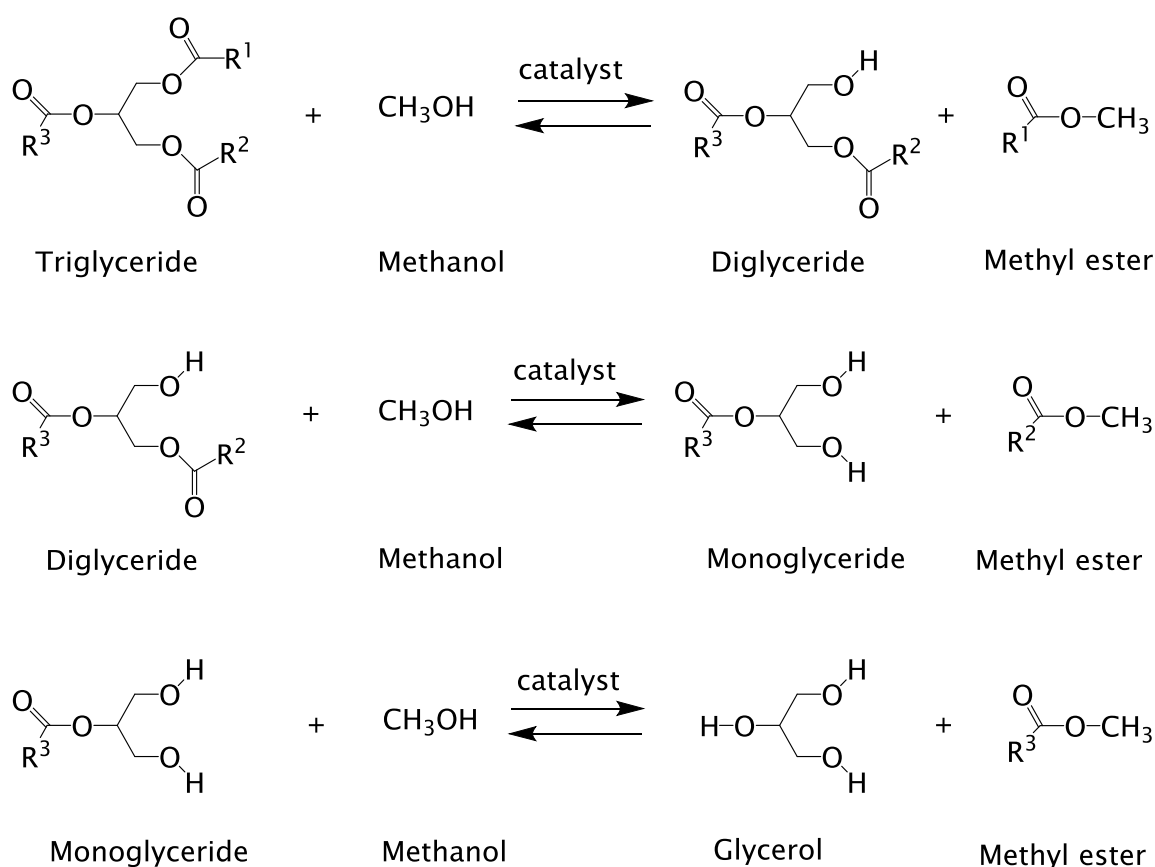
Figure 1-1   Transesterification of triglycerides with methanol for biodiesel production. R¹, R², R³ are represented as a mixture of various fatty acid chains.

Various alcohols such as methanol, ethanol, propanol, butanol, hexanol, octanol and decanol have been used in the transesterification process for biodiesel production.[35] Methanol and ethanol are most commonly used, especially methanol in commercial biodiesel production in Europe due to its low cost[1][36], it being polar and shortest chain alcohol.[37] Some researchers state that ethanol is the preferred alcohol[38] because ethanol is produced from agricultural products, is renewable[39] and is biologically friendly.[40][41]

1.5   Properties of biodiesel

Biodiesel derived from different feedstocks has different physiochemical characteristics and chemical compositions. The physical and chemical fuel properties of biodiesel basically depend on feedstock and their fatty acids composition. Then, the several parameters affecting the fuel properties of the biodiesel must be considered. Each country established and developed standard specifications for biodiesel such as Germany (DIN 51606), Austria (ON) and the Czech Republic (CSN).[18] Due to the climate-related requirements for biodiesel in different countries, standards for different regions are slightly modified. However, the most popular established standards for biodiesel are the European standard EN 14214 in Europe and the American Society for Testing and Materials (ASTM) D6751 in the USA.[42] The following sections discuss some properties of biodiesel.

1.5.1   Density

In general, densities of biodiesel fuels are slightly higher than those of diesel. The density of biodiesel is strongly affected by the degree of unsaturation, with higher unsaturation leading to increased density. Table 1-5 shows soy methyl ester (SME) has the highest density (880.0-885.0 kg/m³) because polyunsaturated FAMEs likely C18:2 is rich in SME. Coconut methyl ester (CME) has the lowest density ranging from 849.2–870.0 kg/m³. Diesel has a density range of 816.0-843.5 kg/m³. High density biodiesel will lead to poor vaporisation, possible blockage of the injector nozzle and incomplete combustion of the injected fuel.[1]

1.5.2 Kinematic viscosity

Viscosity is the most important property of any fuel as it indicates the ability of a fuel to flow. The kinematic viscosity of biodiesel is higher than that of diesel. The viscosity of biodiesel increases with an increase in the carbon chain length, the degree of saturation of the fatty acid and its ester[43] and the presence of free fatty acids and oxidation products.

Viscosity of CME has lower when compared with RME and SME due to the shorter chain length (C8–C14) of the fatty acid components. High viscosity causes poor flow of fuel in the engine combustion chamber during the intake stroke and takes longer to mix with the air, resulting in delayed combustion. Moreover, *cis/trans* configuration of FAMEs can affect oxidative stability at high temperature. A *trans*-monoene is more stable than a *cis*-monoene, whereas a *trans*-conjugated diene is more susceptible to oxidation than neighbouring *cis*-conjugated diene.[44] Figure 1-2 shows the order stability of alkene isomers. Then, the isomerisation of the double bonds, usually *cis* to *trans*, along with the formation of high molecular weight products leads to high viscosity.
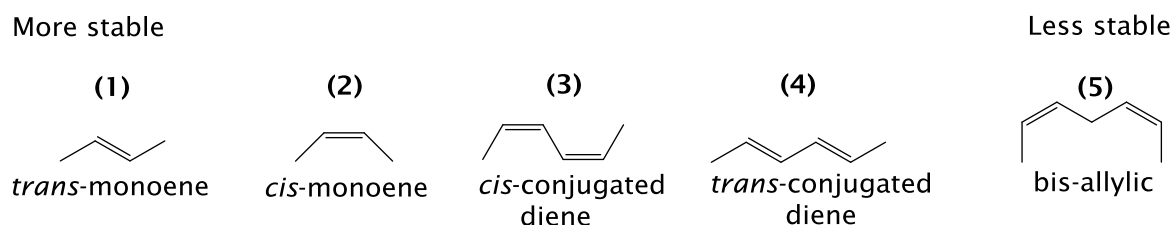
Figure 1-2   Stability order of alkene isomers.

Viscosity is therefore a useful measurement for the oxidation progression of biodiesel. The polymeric secondary oxidation products of biodiesel can cause the formation of soluble gums and insoluble materials and will result in a further increase in viscosity.[42] The formation of insoluble compounds occurring in oxidised biodiesel has been investigated by several researches. Fang and McCormick[45] proposed the pathway leading to the formation of insoluble materials, oligomers, from biodiesel oxidation products. Peroxides formed in the initial step of oxidation can decompose to form aldehydes, ketones, and acids. These compounds undergo aldol condensation to form oligomeric and polymeric compounds, see Figure 1-3. The physical property of the oligomer and polymer can be devastating fuel system.[46]

Aldol-condensation

$$R^1-\underset{\underset{O}{\|}}{C}-H \quad + \quad H_3C-\underset{\underset{O}{\|}}{C}-R^2 \quad \longrightarrow \quad R^1-HC{=}HC-\underset{\underset{O}{\|}}{C}-R^2 \quad + \quad H_2O$$

Aldehyde   Ketone
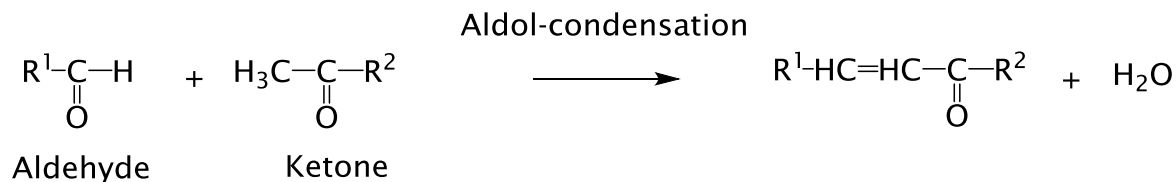
Figure 1-3   Aldol-condensation to form oligomeric compounds.[47]

Additionally, dimers and polymers are formed during the autoxidation of methyl linoleate and linoleate hydroperoxides under room temperature (25-40 °C) by cross linkage either peroxide or ether linkages and contained hydroperoxy, hydroxy and oxo groups.[48][49] Example of dimeric compounds from auto-oxidised FAMEs is shown in Figure 1-4.
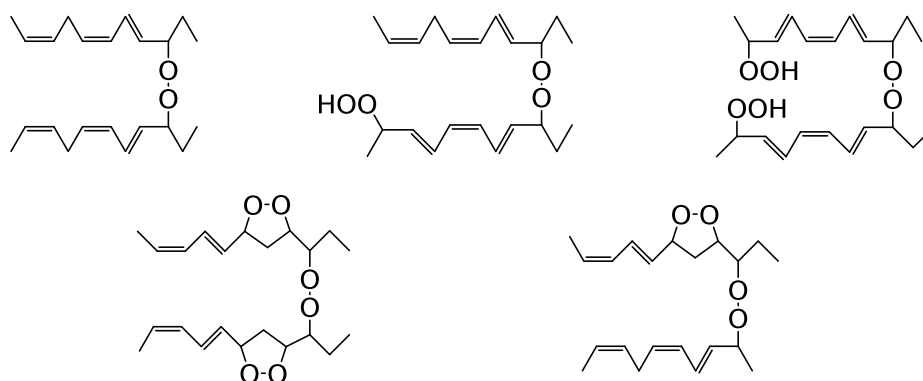
Figure 1-4   Dimeric compounds from autoxidised methyl linolenate at 40 °C.[48]

Waynick[50] proposed the vinyl polymerisation for the pathway of the formation of insoluble material in biodiesel. In the vinyl polymerisation, an allyl radical (R•) is added directly to a double bond to form a C-C and another free radical. This free radical reacts another molecule to create of the oligomer, see Figure 1-5.
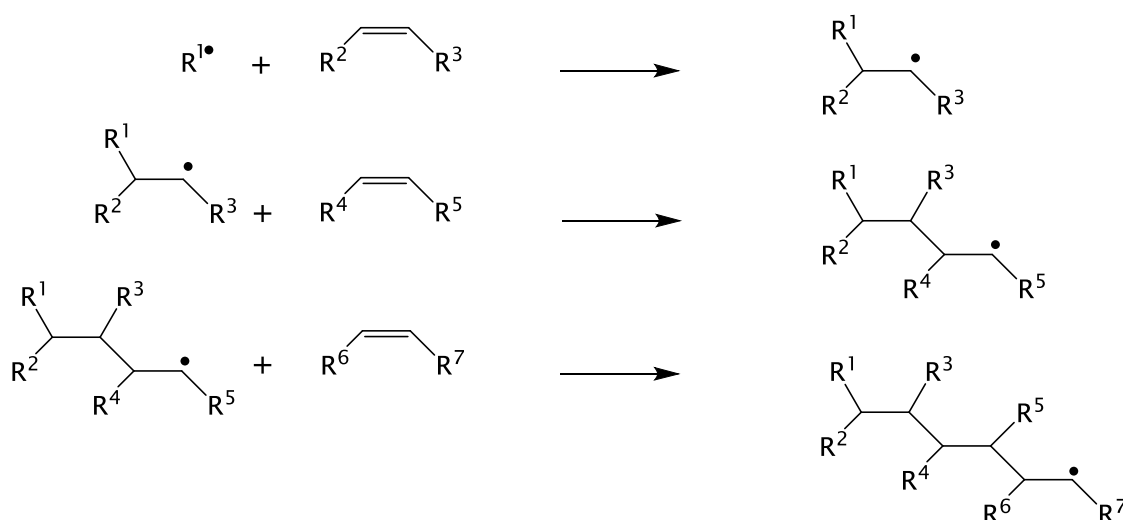
Figure 1-5   Vinyl polymerisation mechanism to form oligomeric and polymeric compounds.[47][50]

Thus, the increase in viscosity of biodiesel is a result of the formation of dimeric, oligomeric and polymeric compounds. Also, deposits in the fuel system form when the polarity and molecular weight of these compounds is high enough.[45]

1.5.3 Flash point

The flash point of a fuel is the temperature at which it will ignite when exposed to a flame or a spark.[51] The flash point of biodiesel is higher than that of diesel, improving its suitability for transport, handling and storage purposes when compared with petrodiesel.[18] The flash point is influenced by the chemical compositions of the biodiesel, including the number of double bonds and the number of carbon atoms. Each biodiesel has its own flash point, and Table 1-5 shows biodiesel has a higher flash point than diesel. Biodiesel (a mixture of CME, RME, and SME) has a flash point of more than 100 °C, while diesel has a flash point of 50-98 °C.

1.5.4 Cetane number (CN)

The cetane number (CN) is a commonly used indicator for the determination of the ignition quality of a diesel fuel. A long straight-chain hydrocarbon, hexadecane ($C_{16}H_{34}$) is the high quality standard on the CN with an assigned CN of 100. A highly branched compound, 2,2,4,4,6,8,8,-heptamethylnonane ($C_{16}H_{34}$), a compound with poor ignition quality, is the low-quality standard and has an assigned CN of 15. The two reference compounds on the CN scale indicate that CN decreases with decreasing chain length and increasing branching.[43][52]

1.5.5   Cold flow properties

The cold flow properties are considered the most important determination of a fuel when it uses in low temperatures because it influences the operation of the fuel directly in the engines at lower temperatures. Three low temperature properties must be considered, consisting of cold filter plugging point (CFPP), cloud point (CP) and pour point (PP).

1.5.5.1   Cold filter plugging point (CFPP)

The CFPP is defined as the lowest temperature at which fuel completely passes through a standardised filtration device in a specified time when cooled under certain conditions.[18] This is important as in cold temperate countries, a high cold filter plugging point will clog engines more easily. Biodiesel rich in saturated FAMEs will result in a lower CFPP whilst a higher proportion of unsaturated FAMEs will result in a higher CFPP. CME rich in saturated FAME like methyl laurate (C12:0) shows one of the lowest CFPP compared with RME and SME (see, Table 1-5).

1.5.5.2   Cloud point (CP)

The cloud point (CP) is defined as the temperature at which a cloud of wax crystals first appears when the fuel is cooled.[51] Therefore, cloud point indicates the tendency of the oil to plug filters or small orifices at cold operating temperatures.[53] Biodiesel produced from feedstocks such as rapeseed and soybean oils have a cloud point close to or below 0 °C because of the presence of saturated FAMEs like methyl palmitate (C16:0) and methyl stearate (C18:0).

1.5.5.3   Pour point (PP)

The pour point (PP) is the temperature at which the amount of wax that has come out of solution is sufficient to gel the fuel, thus it is the lowest temperature at which the fuel can flow; in other words it is a measure of the fuel gelling point. The pour point is always lower than the cloud point.

Table 1-5   Comparison of diesel and biodiesel properties from some biodiesel feedstocks[4,11,12,22,26,54–60,61,62]

Property	Types of biodiesel			
	Diesel	**CME**	**RME**	**SME**
CN (min)	45-55	42.0-59.3	52.6 -53.7	45.0-57.6
CFPP (°C)	-7	-5 to -4	-16 to -12	-5 to -3
CP (°C)	-10 to -3	0 to -3	-4 to -3	-2 to 3
PP (°C)	-20 to -25	-9 to -3	-12 to -10	-4 to -3
FP (°C)	55-98	96.0-120.5	155 to 170	69 to 178
Density (kg/m^3)	816.0-843.5	849.2–870.0	882.0-883.0	880.0-885.0
Kinematic viscosity at 40 °C (mm^2/s)	2.0–5.7	2.0-4.5	4.43 to 4.83	4.08-4.70

The blending of biodiesel with diesel is the most widely used method of improving the low temperature properties of biodiesel. The blending of biodiesel with diesel fuel improves the cloud point, the cold filter plugging point (CFPP) and the pour point.[63]

17

1.5.6 Advantages of biodiesel

The advantages of biodiesel as diesel fuel are its liquid nature portability, ready availability, renewability, higher combustion efficiency, lower sulphur and aromatic content, higher cetane number and higher biodegradability.[7][36][64][65]

1.5.7 Disadvantages of biodiesel

The major disadvantages of biodiesel as diesel fuel are its higher viscosity, lower energy content, higher cloud point and pour point, higher nitrogen oxide (NOx) emissions, lower engine speed and power, injector coking, engine compatibility, and high price.[1][27][66] There are two main problems associated with the use of biodiesel as an alternative of diesel: these are poor cold flow properties and stability.

1.6 Oxidation stability

Oxidation stability is one of the most important parameters to be considered for biodiesel and fuel. The stability of biodiesel is lower than that of petrodiesel. The number of unsaturated fatty acids found in biodiesel depends upon the parent feedstock used for biodiesel production. Most of the unsaturated fatty acids derived from vegetable oils, including rapeseed oil and soybean oil, have chemical structures with a methylene-interrupted configuration, whilst a conjugated configuration occurs very rarely in seed oils.[67] Figure 1-6 (A) shows the methylene-interrupted configuration for (9Z, 12Z)-9, 12-octadecadienoic acid (C18:2). This structure is different from an isomer having a conjugated

configuration (Figure 1 6 (B)). A conjugated configuration is more stable because of delocalisation of the pi (π) electrons, whereas in contrast, the methylene-interrupted configuration is least stable.[50]

(A) Methyl-interrupted linoleic acid
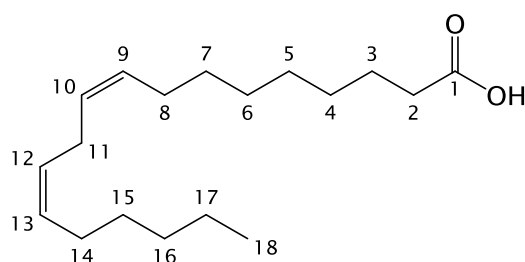
(B) Conjugated linoleic acid
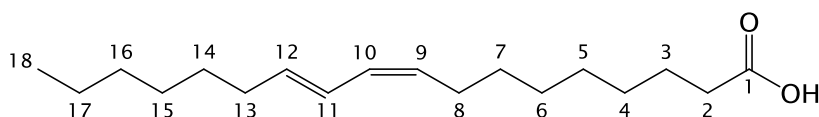
Figure 1-6   Chemical structures of octadecadienoic acid (C18:2). (A) methyl-interrupted configuration; (B) conjugated configuration.

Most *cis*-configured fatty acids are naturally occurring rather than commercially produced. Both (9*Z*, 12*Z*)-octadeca-9, 12-dienoic acid (linoleic acid) and (9*E*, 12*E*)-octadeca-9, 12-dienoic acid (linolelaidic acid) (see, Figure 1-7) are 18-carbon fatty acids with two double bonds. (9*Z*, 12*Z*)-octadeca-9,12-dienoic acid has a *cis*-double bond (hydrogen atoms are on the same side of the bond), which causes a bend in the fatty acid chain, whereas (9*E*,12*E*)-octadeca-9,12-dienoic acid has a *trans*-double bond, which straightens the fatty acid chain.[68]

(A) *cis, cis*-9, 12-octadecadienoic acid
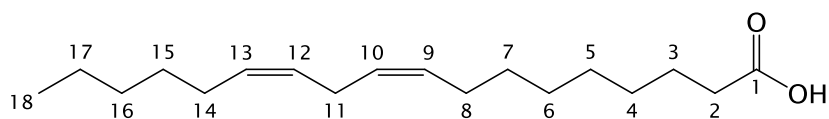
(B) *trans, trans*-9,12-octadecadienoic acid
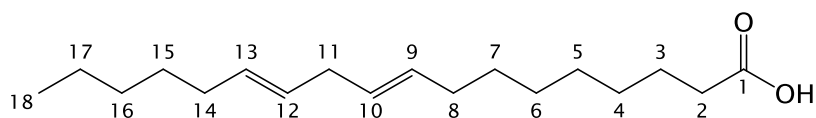
Figure 1-7   **Chemical structures of *cis* and *trans* configurations of C18:2. (A) *cis, cis*-9,12-octadecadienoic acid (linoleic acid); (B) *trans, trans*-9,12-octadecadienoic acid (linolelaidic acid).**

The structure is shown in Figure 1-8, for example, methyl linoleate (Figure 1-8 (A)) has double bonds at C-9 and C-12 that result in one bis-allylic position at C-11, whereas methyl linolenate (Figure 1-8 (B)) has double bonds at C-9, C-12 and C-15. This configuration has two bis-allylic positions at the C-11 carbon and C-14.[43][69] The bis-allylic positions are more reactive to autoxidation than allylic. The relative rate of oxidation for the methyl esters of oleic (C18:1), linoleic (C18:2), and linolenic (C18:3) acids is 1:41:98.[43]

(A) One bis-allylic

bis-allylic

allylic

(B) Two bis-allylic
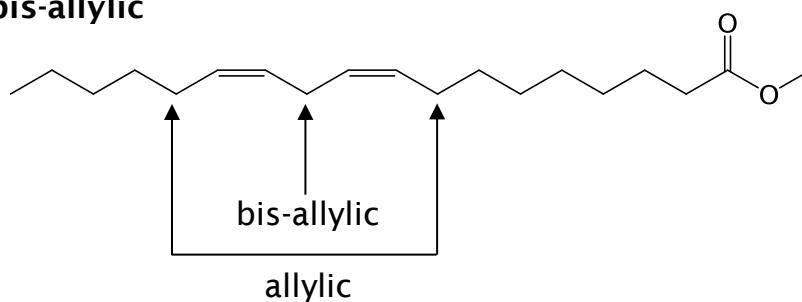
bis-allylic
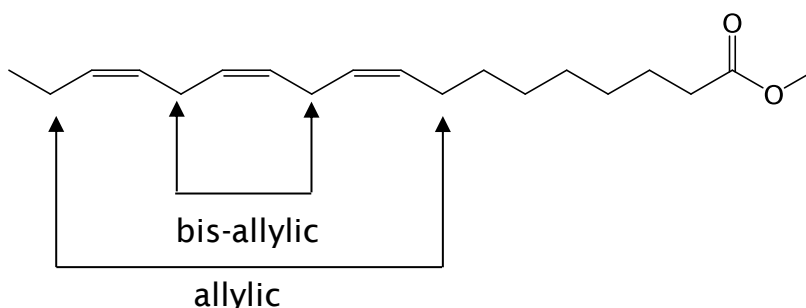
allylic

Figure 1-8   Structure of methyl linoleate (C18:2) has one bis-allylic position (A) and methyl linolenate (C18:3) has two bis–allylic positions (B).

Oxidation of biodiesel can be promoted by several factors such as accelerated temperature and contact with ambient air or light. The degradation of biodiesel can occur by one of the three following mechanisms[70]: (1) auto-oxidation or natural oxidation, (2) thermal oxidation, and (3) storage oxidation.

Auto-oxidation of biodiesel can occur from the biodiesel contact with oxygen at ambient temperature. This mechanism occurs before biodiesel combustion in an engine. Many factors affect this process including the nature of the biodiesel feedstocks, the method of biodiesel production, additives and impurities of biodiesel, as well as conditions of storage and

handling. The scheme of auto-oxidation of biodiesel is shown in Figure 1-9.

Thermal oxidation refers to the biodiesel degradation due to accelerated temperature. This mechanism is relevant to biodiesel usage because high fuel temperatures may occur in the diesel engine injection system, while uncombusted biodiesel is re-circulated through the injection fuel system and back to the fuel tank.[70]

Storage stability is the stability of the biodiesel over a long period of time. It might also involve issues of water contamination and microbial growth. Water can promote microbial growth, lead to tank corrosion and participate in the formation of emulsions, as well as cause hydrolysis or hydrolytic oxidation.[70]

Biodiesel is a mixture of fatty acid mono alkyl esters with relatively significant amounts of long-chain monounsaturated and polyunsaturated compounds, for example methyl oleate, methyl linoleate and methyl linolenate for RME. Oxidation reactions of fatty acids lead to the formation of free radicals, *cis/trans* isomerisation and free fatty acid production.

Figure 1-9 shows the three steps of oxidation reaction consist of initiation, propagation and termination.[50][69] In the initiation step, a hydrogen atom adjacent to the double bond in the unsaturated fatty acid (RH) is abstracted by initiator (I) to produce an unsaturated fatty acid free radical (R•). In the propagation step, the unsaturated fatty acid free radical (R•) reacts with oxygen (O_2) to form a peroxy radical (ROO•). The peroxy radical

(ROO•) is sufficiently reactive to rapidly abstract a hydrogen atom from another unsaturated fatty acid (RH) to form a hydroperoxide (ROOH) and a new unsaturated fatty acid free radical (R•), propagating the oxidation process.

The ROOH concentration in the initial stages rises slowly until an interval of time has elapsed. This time is known that the "Induction Period" and is analysed by the oxidation stability of the fatty oil or fatty acid methyl ester under accelerated conditions. After the initial period the concentration of ROOH increases quickly.[70] The terminal step is the end of reaction when two free radicals react to form a non-radical products.

Initiation

$$RH + I• \longrightarrow R• + HI$$

Propagation

$$R• + O_2 \longrightarrow ROO•$$

$$ROO• + RH \longrightarrow ROOH + R•$$

Termination

$$R• + R• \longrightarrow RR$$
$$ROO• + R• \longrightarrow ROOR$$
$$ROO• + ROO• \longrightarrow ROOR + O_2$$

Non-radical products

Figure 1-9   Auto-oxidation reaction.

Chapter 1: Introduction

The mechanism for the auto-oxidation is shown in Figure 1-10, using the example of the hydroperoxide formation during the auto-oxidative degradation of linoleic acid.
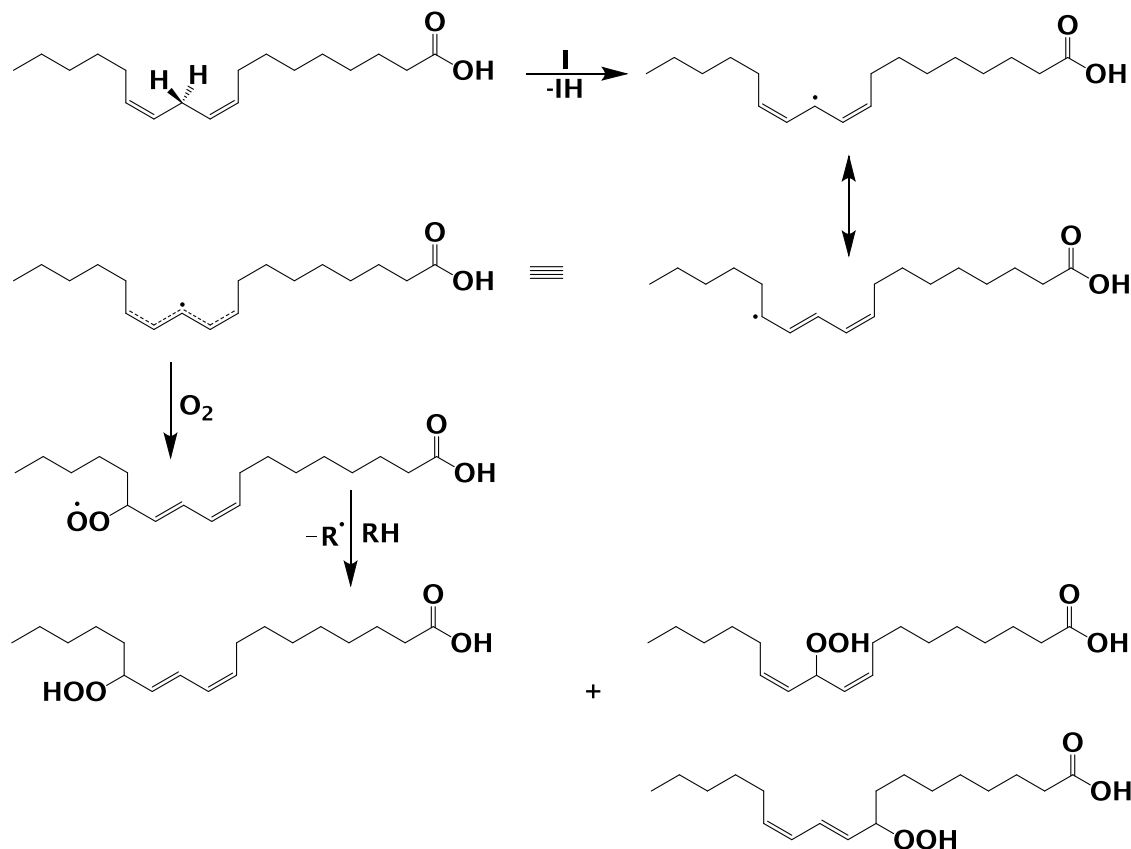
Figure 1-10   Mechanism for the auto-oxidation of linoleic acid (C18:2) leading to the formation of its hydroperoxides.[42]

1.6.1   Oxidation products

1.6.1.1   Primary oxidation compounds

Hydroperoxides are the primary products in auto-oxidation of unsaturated fatty acids. They can undergo further oxidation into a variety of volatile and non-volatile secondary products. The peroxide value (PV) is most commonly used as an indicator of oxidation progression. It is a chemical method, based on an iodimetric titration. The method measured

in milliequivalents of peroxide per kg of sample indicates the content of primary products of oxidation; hydroperoxides. Low peroxide value (PV) means high oxidation stability in biodiesel.[70] The existing analytical method is time consuming,[71] costly, and require large amounts of hazardous reagents.[72]

Normal phase high-performance liquid chromatography (NP-HPLC) coupled with an evaporative light-scattering detector (ELSD) has been used to separate the hydroperoxides formed during auto-oxidation of FAME. [73][74] NP-HPLC with ultraviolet (UV) absorbance detection at 234 nanometre (nm) has been analysed for primary oxidation products of linoleic acid and triacylglycerols and has been confirmed by fast atom bombardment (FAB)-mass spectrometry (MS) and/or nuclear magnetic resonance (NMR) spectroscopy.[75] MS and NMR spectroscopy have also been used for the analysis of hydroperoxides during auto-oxidation of methyl oleate (C18:1).[76]

1.6.1.2   Secondary oxidation compounds

Volatile organic compounds are produced during the secondary step of FAME oxidation. Once the FAME hydroperoxides are formed, they decompose to form aldehydes such as, heptanal, hexenal, heptenal, propanal, hexanal, further heptane, octane, pentane, and 2,4-heptadienal have also been detected. Figure 1-11 shows the chemical structures of some volatile compounds detected during the secondary oxidation stage. Gas chromatography-mass spectrometry (GC-MS) has also been used for

Chapter 1: Introduction

analysis of volatile organic compounds to detect and identify oxidation

products of FAME.[77][78][79]

(2*E*,4*E*)-Hepta-2,4-dienal

Nonanoic acid

Nonanal

7-oxoheptanoic acid

(*E*)-4-hydroperoxynon-2-

(*E*)-4-hydroxynon-2-

Pentane

Acetic acid

Formic acid
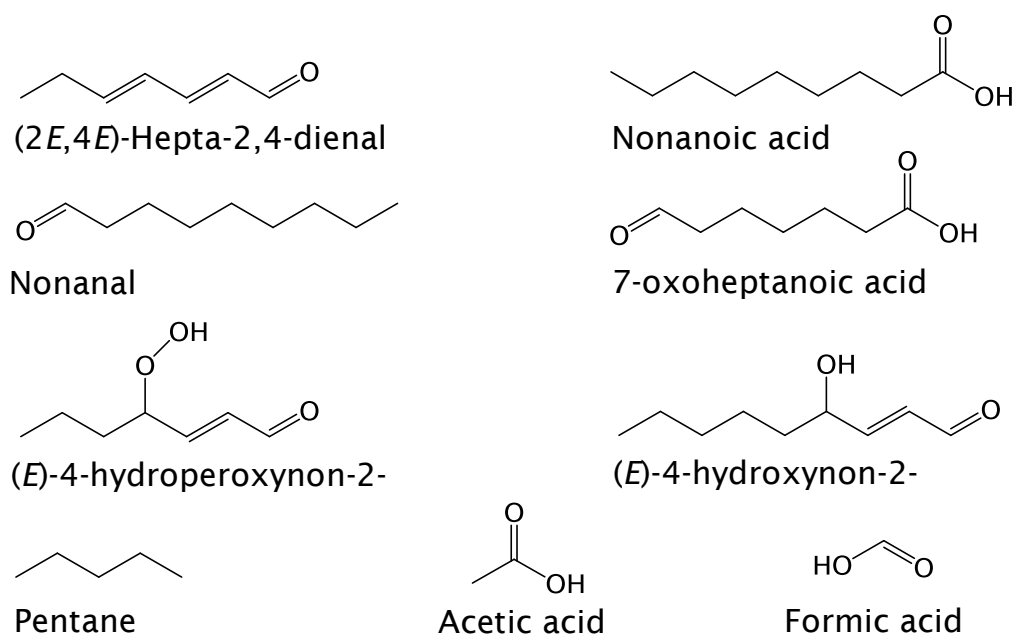
Figure 1-11   Chemical structures of oxidation products detected in biodiesel.[42]

FAME hydroperoxide decomposition and oxidative polymerisation of fatty acid chains can occur and can form high molecular weight polymers. For the isomerisation process, one of the conjugated diene groups in the chain can react with the olefinic group from the nearby fatty acid chain and can form a substituted cyclohexene ring from the Diels-Alder reaction, see Figure 1-12.[42] For example, thermal dimerisation occurs for the FAME due to the Diels-Alder reaction and forms the dimer. Figure 1-13 shows the cyclohexene ring formed from methyl linoleate (C18:2) *via* the Diels-Alder reaction.
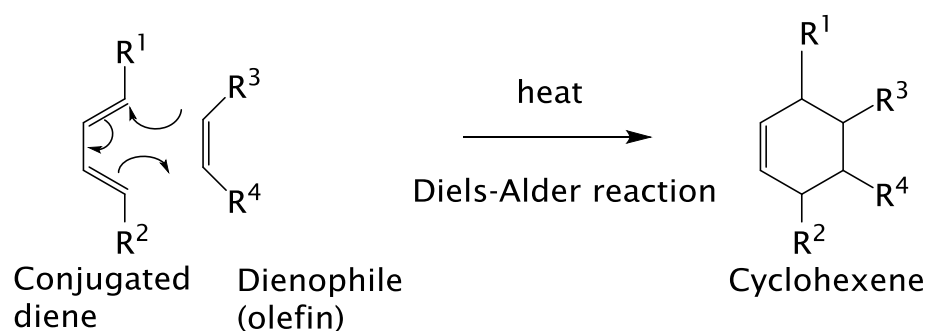
Figure 1-12   Diels-Alder reaction.[80]

(A) Conjugated linoleic acids
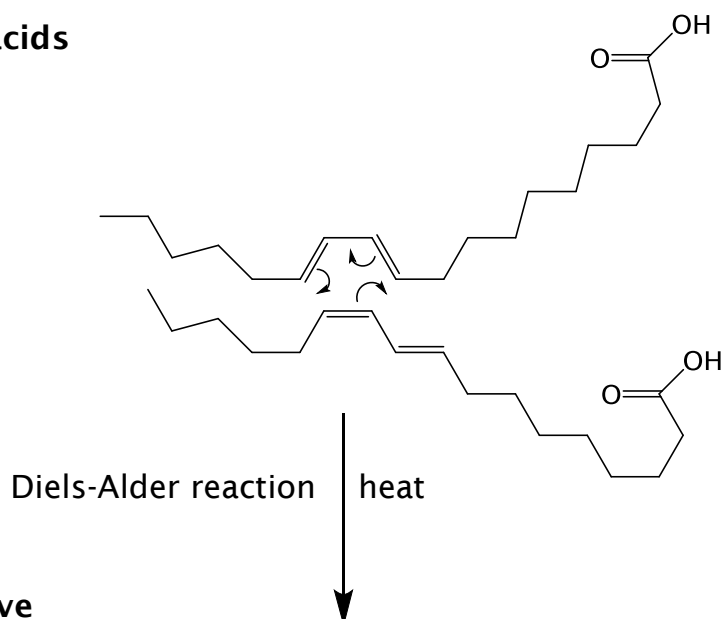
(B) Cyclohexene derivative
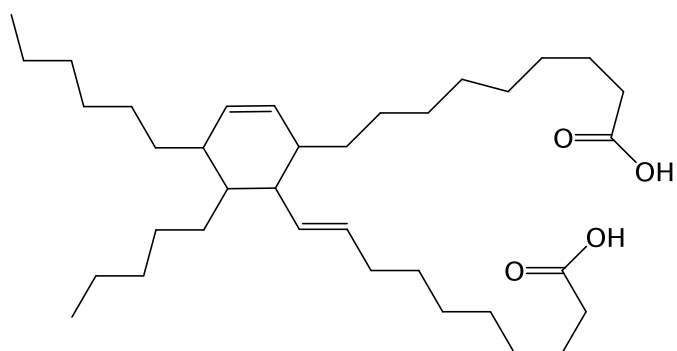
Figure 1-13   Typical structure of dimer linoleic acid formed *via* Diels-Alder reaction.[81]

Reversed phase–high performance liquid chromatography (RP-HPLC)

coupled with UV detection was used for the analysis of secondary

oxidation products, for example epoxyoctadecanoate, epoxy- and epoxyhydrooctadecennoates in methyl oleate (C18:1) and methyl linoleate (C18:2).[82][83] Easy ambient sonic-spray ionisation mass spectrometry (EASI-MS) is able to analyse the oxidation products from FAMEs.[84] Capillary gas chromatography–ion-trap mass spectrometry (GC–IT/MS) has also been used for analysis of epoxides and dimers produced from methyl oleate (C18:1 *cis* 9) and methyl elaidate (C18:1 *trans* 9).[85]

1.7   Antioxidants

Oxidation products of biodiesel may cause engine and fuel injector problems. The presence of high molecular polymerisation species can lead to deposit formation and an increase in fuel viscosity which may affect the fuel spray characteristics. Additionally, the formation of organic acids increases the total acidity of the fuel with increased risk of corrosion in vehicles' fuel distribution handling systems.

Antioxidants significantly slow down the biodiesel degradation process. Two types of antioxidants are generally known: chain breakers and hydroperoxide decomposers. The two most common types of chain breaking antioxidants are phenolic and amine-types.[86] Normally antioxidants act to inhibit the oxidation process and are well established for the use of controlling oxidation of biodiesel. For example, an antioxidant (AH) inhibits the peroxide radical (ROO•) in order to prevent it from creating another radical by the autoxidation mechanism. The related mechanism is shown in Figure 1-14.

$$AH + ROO^\bullet \longrightarrow ROOH + A^\bullet$$

$$A^\bullet + ROO^\bullet \longrightarrow ROOA$$
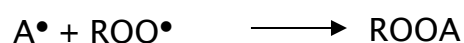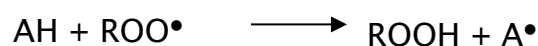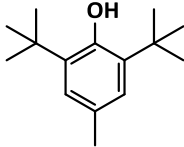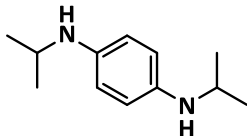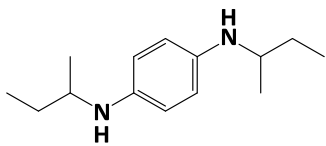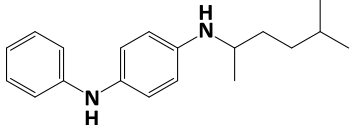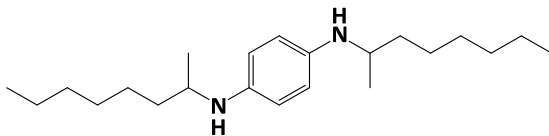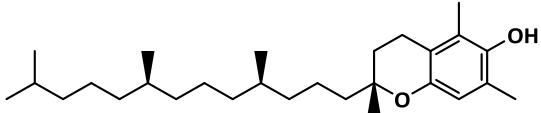
AH = Antioxidant

Figure 1-14   Antioxidant mechanism.[87]

Various types of chemicals or additives are used to improve the stability properties and enhance the performance characteristics of fuels. There are four groups of chemical stability additives: stabilisers, dispersants, chelating agents, and antioxidants. The use of antioxidant additives can inhibit or prevent the oxidation process by protecting fuels from oxidative degradation whilst also allowing the fuel to properly fulfil the requirements demanded by the industry. Fuel oxidation is initiated by free radicals, which are obtained either from combustion or from decomposition of primary oxidation products such as hydroperoxides ROOH. In the absence of antioxidants, peroxy radicals further react with additional fuel to form hydroperoxides (ROOH) and alkyl radicals ($R^\bullet$). Several types of antioxidants, derived both from natural and synthetic sources, are widely used to increase oxidative stability in fuels such as tocopherols, *N, N'*-di-*sec*-butyl-*p*-phenylenediamine, butylated hydroxyanisole (BHA), butylated hydroxytoluene (BHT), *tert*-butylhydroquinone (TBHQ), or 4,4' -methylenebis (2,6-di-*tert*-butylphenol) (MBP). Table 1-6 shows the structures, formulae and relative molecular masses of antioxidants.

Table 1-6   Structures, formulae and relative molecular masses of antioxidants

Name	Chemical structure molecular formula and monoisotopic mass
2,6-di-*tert*-butyl-4-methylphenol	 $C_{15}H_{24}O$, monoisotopic mass: 220.1827 Da
N,N´-diisopropyl-*p*-phenylenediamine	 $C_{12}H_{20}N_2$, monoisotopic mass: 192.1626 Da
N,N´-di-sec-butyl-*p*-phenylendiamine	 $C_{14}H_{24}N_2$, monoisotopic mass: 220.1939 Da
N-(1,4-dimethylpentyl)-*N'*-phenyl-1,4-benzenediamine	 $C_{19}H_{26}N_2$ monoisotopic mass:282.2096 Da
N,N'-bis(1-methylheptyl)-*p*-phenylendiamine	 $C_{22}H_{40}N_2$, monoisotopic mass:332.3191 Da
Tocopherols	 $C_{28}H_{48}O_2$, monoisotopic mass: 416.3654 Da

Several analytical methods have been reported for the investigation of antioxidants in fuels. These included spectrophotometry, liquid chromatography (LC), infrared spectroscopy and gas chromatography (GC). LC with electrochemical detection has been undertaken for monitoring

phenolic antioxidant compounds in JP 5 aviation fuels.[88] Aromatic amine antioxidants were characterised by positive-ion electrospray ionisation mass spectrometry whereas sterically hindered phenols were analysed by negative-ion electrospray ionisation mass spectrometry.

Headspace-programmed temperature vaporisation–gas chromatography–mass spectrometry (HS–PTV–GC–MS) was proposed for the detection of antioxidants (2-, 3-, and 4-*tert*-butylphenol, 2,6-di-*tert*-butylphenol, 3-*tert*-butyl-4-hydroxyanisol, 2,6-di-*tert*-butyl-4-methylphenol, 1-naphthol, and diphenylamine) in lubricants.[89] An ion trap–time-of-flight mass spectrometer (IT–TOF) interfaced with an atmospheric pressure chemical ionisation (APCI) source has also been used for determination of antioxidant *tert*-butylhydroquinone (TBHQ) doped biodiesel.[90]

The use of electrochemical oxidation has been investigated to determine whether this approach can be used to probe the role of the antioxidants BHA, BHT and TBHQ, by using a gold nanoparticle modified glassy carbon electrode (AuNPs/GCE) as the working electrode.[91] BHT content in transformer oil was investigated by both differential pulse voltammetry and linear sweep voltammetry with a glassy carbon electrode as the working electrode,[92] other samples also analysed were for BHA and TBHA in biodiesel,[93] TBHQ in biodiesel[94], and BHT in vegetable oils.[95]

1.8 Fatty acid methyl esters (FAMEs) contamination in aviation turbine fuel (AVTUR)

Biodiesel must meet the requirements of fuel standards such as ASTM D6751 or EN 14214 before it can be blended with petrodiesel. Presently, B5 (5% vol. biodiesel in petrodiesel) and B7 are allowed in ASTM D975 and EN 590, the U.S. and European diesel fuel standards, respectively.[96] The introduction of biodiesel into the fuel infrastructure has also given rise to unforeseen problems where these materials can cross-contaminate other fuel types. In the case of aviation turbine fuel (AVTUR) this is a significant issue since the international jet fuel specifications (DEF STAN 91-91) limit FAME content to less than 5 mg/kg (5 ppm w/w).[97] The polar nature of the FAMEs means that they tend to adsorb onto the metal surfaces of pipelines or containers and these materials can then be released by the AVTUR from these shared common pipelines. For example, the presence of FAME at high concentration in AVTUR or jet fuel can significantly impact the thermal stability of the fuel resulting in coking and can affect the freezing point of jet fuel leading to gelling. To avoid such issues the AVTUR must be B0, *i.e.* no biodiesel content, which is defined as less than 5 mg/kg (5 ppm) biodiesel content.

IP585/10 is the current ASTM reference method for the determination of rapeseed methyl ester (RME) in jet fuel.[98] This GC-MS method uses a 60 m polar GC capillary column to separate the FAME species (C16:0-C18:3) from the non-polar hydrocarbon matrix of the jet fuel. The total GC-MS analysis time is approximately 1 h. However, it cannot detect and quantify

all the short chain FAMEs (C8-C14), *e.g.* from coconut oil (from FAME production in the Pacific Rim region) due to co-elution of these species with the fuel matrix. Comprehensive two-dimensional gas chromatography (GC × GC) has recently been developed for analysis of trace levels of FAME in petroleum-based fuel.[99] This method can be used for the identification and determination of the individual FAME component and total FAME content; however, this specialised instrumentation is not routinely accessible. Normal phase high performance liquid chromatography (NP-HPLC) has also been used for the determination of FAME in diesel.[100] Whilst all the FAME species eluted as a single peak in the chromatogram method, this can still determine the total FAME content in diesel fuel faster than the GC method. An adapted version of IP585/10 and a novel orthogonal ultra-high performance supercritical fluid chromatography mass spectrometry (UHPSFC-MS) method have been developed and are discussed in Chapter 5.

1.9   Summary

Following of the review of literatures summarised that:

- Vegetable oils and animal fats commonly used to produce fatty acid methyl esters (FAMEs).
- Transesterification is commonly used for biodiesel production
- Biodiesel produced from a variety of feed stocks having different carbon chain length and degree of unsaturation.
- The compositional fatty acid profiles of common vegetable oils, *e.g* soy and rapeseed oils, are dominated by five fatty acid species.

consisting of palmitic acid (16:0), stearic acid (18:0), oleic acid (18:1), linoleic acid (18:2), and linolenic acid (18:3). Coconut oil is significantly different, containing large amount of lighter fatty acid species–especially lauric acid (12:0) and myristic acid (14:0).

- The physical and chemical properties of a biodiesel depend on fatty acid composition: the fatty acid chain and the fatty the degree of unsaturation.

- Some properties of biodiesel such as density, viscosity, cetane number, old filter plugging point (CFPP), cloud point (CP) and pour point (PP), related to the chemical composition of biodiesel.

- Instability of biodiesel is one of the major issues for the use of biodiesel as an alternate fuel to petrodiesel.

- Biodiesel oxidation is affected by fatty acid composition, and degree of unsaturation within the fatty acid chain.

- Hydroperoxides are the primary products in auto-oxidation of unsaturated fatty acids. They can undergo further oxidation into a variety of volatile and non-volatile secondary products.

- Decomposition of FAME hydroperoxide and oxidative polymerisation of fatty acid chains can occur and can form high molecular weight polymers leaded to the formation of insoluble compounds caused by the accumulation of gum deposits on engine system.

- Antioxidants use for improving the oxidation stability in biodiesel and fuels.

- The introduction of biodiesel as an alternate fuel to petrodiesel has also given rise to unforeseen problems where these materials can cross-contaminate other fuel types.

- A wide range of techniques can be used for analysis of oxidation products in biodiesel (see, section 1.6) and determination of biodiesel contamination in aviation turbine fuels (see, section 1.8).

Chapter 2: Instrumentation

Analysis of complex samples is typically achieved using a combination of separation science and mass spectrometry. This research is focused on the use of various types of chromatography including gas chromatography (GC), high performance liquid chromatography (HPLC) and supercritical fluid chromatography (SFC) coupled to mass spectrometry for the analysis of fatty acid methyl esters (FAMEs), FAME oxidation, and FAMEs in a complex fuel matrix. Chromatography is the technique of separating components within a mixture. It is based on distribution of an analyte between the stationary phase and the mobile phase. The stationary phase is a solid or liquid supported on a solid, whereas the mobile phase may be gas, liquid or supercritical fluid.

Mass spectrometry is used to produce gas phase ions of compounds by a variety of ionisation techniques, such as electron ionisation (EI) and electrospray ionisation (ESI), and to separate these ions according to their mass-to-charge ratio *(m/z)*. The separation of the gas phase ions in a mass spectrometer is achieved by using electric or/and magnetic fields. A mass spectrometer consists of an ion source, a mass analyser and detector. The mass analyser and detector are operated under high vacuum.

The first section of this chapter deals with the basic principles of the separation techniques including GC, HPLC, and SFC used for separation of FAMEs. Electrochemistry (EC) was used as a surrogated system for FAME oxidation. Two types of ionisation, EI and ESI, are described in detail. The combination of the separation techniques to mass spectrometry with

different types of mass analysers including single-quadrupole, hybrid quadrupole-time of flight (Q-TOF) and Fourier transform ion cyclotron resonance (FT-ICR) instruments are also described in order to understand their basic principles of operations.

2.1   Chromatography

Chromatography was originally developed by the Russian botanist, M.S.Tswett, who discovered liquid–solid adsorption chromatography in 1903 for the separation of plant pigments.[101] Tswett is generally considered as the "father of chromatography".[102] Chromatography is composed of two Greek roots, chroma (colour) and graphein (to write), and its verbatim translation means "colour writing" which refers to visualising the separated multi-coloured rings on the column.[101] Chromatography is a technique that separates the components of a mixture based on certain physical properties. All chromatography (GC, LC and SFC) requires a stationary phase and a mobile phase. Chromatography separation is based upon one of the following mechanisms: adsorption, partition, ion exchange, or size exclusion.

2.1.1   Gas chromatography (GC)

This technique was developed by A.T. James and A.J.P. Martin in 1952, from initial work describing liquid-phase partitioning by A.J.P. Martin and R.L.M. Synge in 1941.[103] GC uses a gas as the mobile phase, and the stationary phase is either a solid or a liquid. Two types of the stationary phases are gas solid chromatography (GSC) and gas liquid chromatography

(GLC) of which GLC is the most commonly used method. The mechanism of GC separation is based on a series of partition events between a carrier gas and a stationary phase. A gas chromatograph system consists of a carrier gas, an injector port, an oven, a GC column and a detector: see Figure 2-1.

A sample is injected into a heated injection port where it is volatilised, and it is carried into the column by a carrier gas. Typically, carrier gases are hydrogen (H_2), nitrogen (N_2), or helium (He). Helium is usually used as the carrier gas when the GC is coupled to a mass spectrometer. The carrier gas neither interacts with the analytes nor with the column packing material, and the column is maintained in a temperature-controlled oven. After the separation of the analytes in the GC column, components are eluted from the column and pass to a detector.
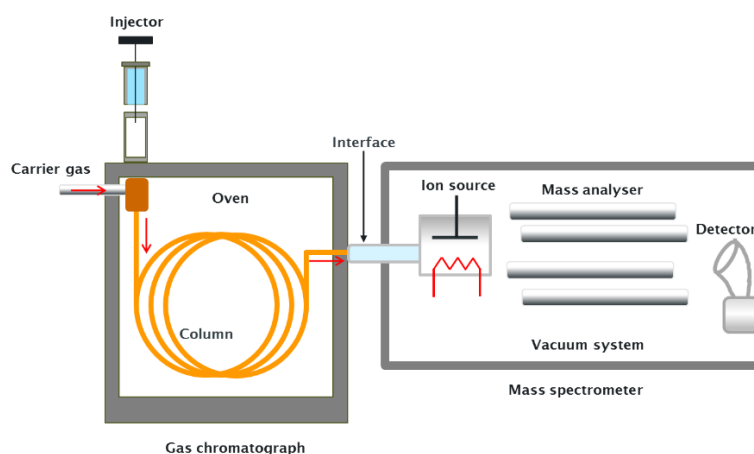
Figure 2-1   Schematic diagram of a gas chromatograph-mass spectrometer.

Chapter 2: Instrumentation

There are two primary columns used in GC. Originally the column was a tube packed with a solid support coated with the stationary liquid but most applications today use a capillary column. The capillary column is a small diameter (0.25-0.53 mm i.d.) open tube with the liquid separation phase coated on the inside of the capillary wall (typically 0.1 to 0.5 μm film thickness). The inside layer of a capillary column is the stationary phase where separation occurs.

Figure 2-2 shows a cross-section of a column containing a three-component sample (the coloured circles). When a vaporised component is transferred to the column, the analyte distributes itself between the stationary phase and the carrier gas. Analytes are separated based on solubility in the stationary phase and their boiling point. The analyte (blue circle) that shows a higher affinity for the stationary phase will move through the column more slowly than the other two (red and green circle) that have a lower affinity.
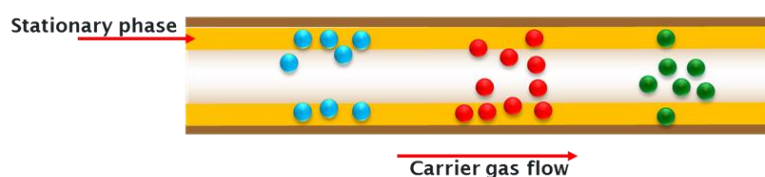
Figure 2-2   A cross section of a column showing analyte separation.

Capillary GC columns are available with a wide variety of stationary phases, *e.g.* non-polar and polar stationary phases. The selection of an appropriate GC stationary phase can be based on "like dissolved like". This means that a polar stationary phase column (*e.g.* polyethylene glycol) is used to separate polar analytes (*e.g.* alcohols) and a non-polar stationary

phase column (*e.g.* polydimethyl siloxane) is used for non-polar analytes (*e.g.* hydrocarbons), see Figure 2-3.

(A) Polar analyte interacting with a polar stationary phase
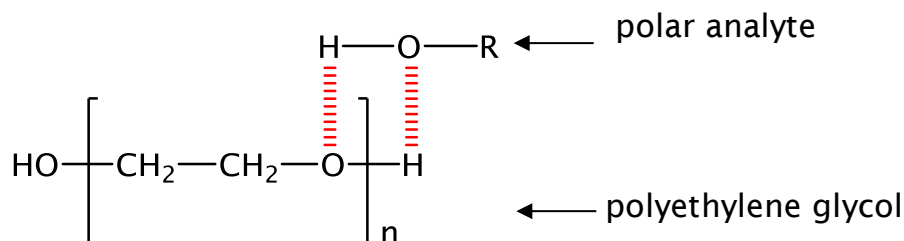
$$H\!-\!O\!-\!R \longleftarrow \text{polar analyte}$$

$$HO\!-\!\left[CH_2\!-\!CH_2\!-\!O\right]_n\!-\!H$$

$$\longleftarrow \text{polyethylene glycol}$$

(B) Non-polar analyte interacting with a non-polar stationary phase

$$CH_3\!-\!CH_2\!-\!CH_2\!-\!CH_2\!-\!CH_2\!-\!CH_3 \longleftarrow \text{non-polar analyte}$$

$$H_3C\!-\!Si(CH_3)_2\!-\!O\!-\!\left[Si(CH_3)_2\!-\!O\right]_n\!-\!Si(CH_3)_2\!-\!O\!-\!Si(CH_3)_2\!-\!CH_3$$

$$\longleftarrow \text{polydimethyl siloxane}$$

Figure 2-3   (A) Polar analyte interacting with a polar stationary phase. (B) Non-polar analyte interacting with a non-polar stationary phase.
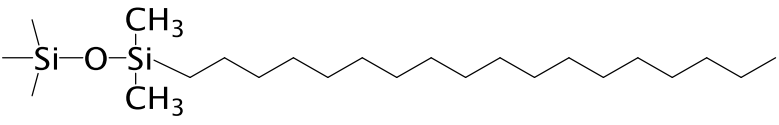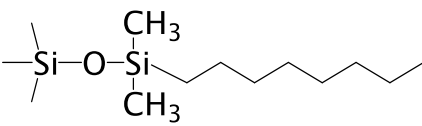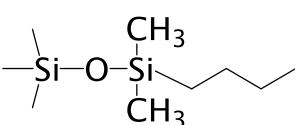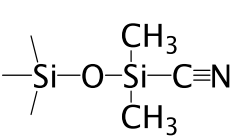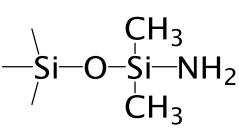
For non-polar stationary phases, analytes are separated by boiling point, while polar stationary phase analytes are separation by polar interactions with the stationary phase. However, analytes amenable to analysis by GC must be volatile and thermally stable at the temperatures used to achieve separation.

2.1.2 High performance liquid chromatography (HPLC)

HPLC was developed in the late 1960s and early 1970s.[104] HPLC is a separation technique for thermally labile compounds not amenable to separation by GC. HPLC uses a liquid mobile phase to carry the sample through the HPLC column. HPLC has four main separation methods including reversed-phase chromatography, normal-phase chromatography, ion exchange chromatography and size exclusion chromatography. The principle of reversed-phase high performance liquid chromatography (RP-HPLC) is based upon the partitioning of analytes between the mobile phase and the stationary phase. RP-HPLC is characterised by a condition in which the mobile phase used is more polar than the stationary phase.

Figure 2-4 shows the HPLC system consists of a mobile phase reservoir, a high pressure pump is used to generate the flow of the mobile phase. A sample manager or autosampler is used to introduce the sample solution into the continuous flow of mobile phase stream that transfers the sample solution into the HPLC column. A range of possible stationary phase chemistries can be used, with the most common being C18. The components in a sample mixture are separated by the column before passing through to a detector. The most commonly used stationary phases in RP-HPLC are presented in Table 2-1.

Table 2-1 **The most commonly used stationary phases in RP-HPLC**[81]

Name	Structure	
Octadecylsilane (C18)	$-\text{Si}-\text{O}-\text{Si}(\text{CH}_3)_2-(\text{CH}_2)_{17}\text{CH}_3$	
Octylsilane (C8)	$-\text{Si}-\text{O}-\text{Si}(\text{CH}_3)_2-(\text{CH}_2)_7\text{CH}_3$	
Butylsilane (C4)	$-\text{Si}-\text{O}-\text{Si}(\text{CH}_3)_2-(\text{CH}_2)_3\text{CH}_3$	Increasing polarity
Cyano	$-\text{Si}-\text{O}-\text{Si}(\text{CH}_3)_2-\text{C}\equiv\text{N}$	
Amino	$-\text{Si}-\text{O}-\text{Si}(\text{CH}_3)_2-\text{NH}_2$	

Figure 2-4   Schematic diagram of a basic HPLC system.

Two basic elution modes consisting of isocratic elution and gradient elution are used in HPLC. In isocratic elution, the composition of the mobile phase is constant during the separation of the analytes, while in gradient elution, the composition of mobile phase changes during analysis. Gradient elution is useful for the separation of analytes with a wide range of polarities. The main advantages of HPLC over GC are that the analytes are not required to have high volatility, but must be dissolved in the mobile phase. It can separate analytes over a wide range of polarity, and large molecules such as proteins, oligonucleotides and polymers are suitable for HPLC analysis.

The recent advances in technology have allowed for the development of smaller stationary phase particle size. This in turn allowed for improvements in column performance and separation efficiency through the use of higher flow rates and pressures than HPLC. The principles of this development are based on the van Deemter equation (see Equation 2-1), which is an empirical formula that defines the relationship between

linear velocity (flow rate) and the height equivalent to a theoretical plate (HETP).

$$H = A + B/\mu + C \times \mu$$ **Equation 2-1**

The van Deemter equation relates three terms: (A) eddy diffusion, (B) longitudinal diffusion, and (C) mass transfer. Figure 2-5 presents the effect of these terms. The first term, eddy diffusion (A) relates to a component of the sample which can travel by one of many paths through the column. These many paths arise because of inhomogeneity and variation in the particle size of packing material in the column. The effect of multiple paths causes the broadening of the analyte band as it moves through the column. Laminar and non-laminar flow profiles in the column also tends to produce a broader band of analyte molecules. The second term, longitudinal diffusion (B) depends on mobile phase velocity. Diffusion along the length of the column leads to peak broadening. Normally, molecules diffuse from regions of high concentration to regions of low concentration. Longitudinal diffusion has a large effect at low mobile phase flow whereas high mobile phase velocity will decrease the effect of peak broadening. Mass transfer (C) is the movement of an analyte between the mobile and stationary phases. This effect may be decreased by reducing the particle size of the column packing material.
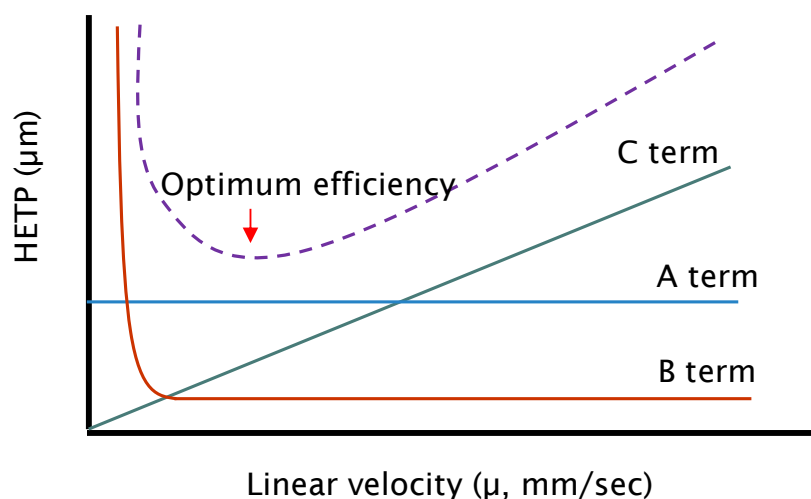
Figure 2-5   Van Deemter plot showing the effect of eddy diffusion, longitudinal diffusion and mass transfer.

In recent years, the development of sub-2 µm particles presented a significant advance. Reducing the stationary-phase particle size to less than 2 µm, not only improved efficiency but the efficiency does not diminish at increased eluent flow rates or linear velocities, see Figure 2-6.
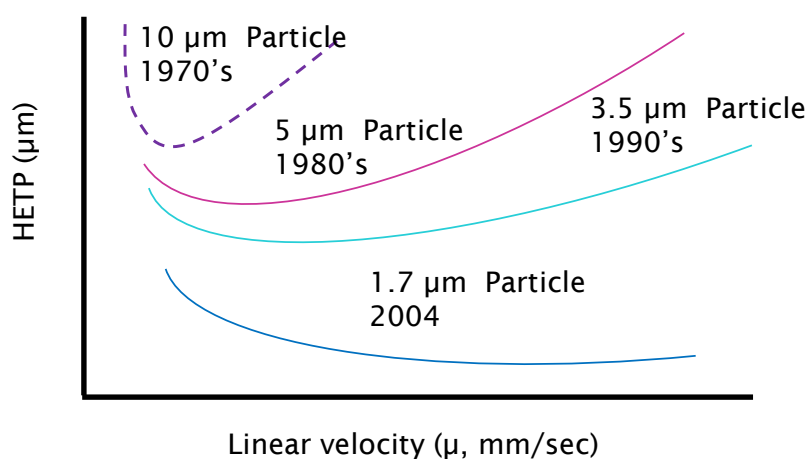
Figure 2-6   Van Deemter plot showing the development of particle sizes over the last three decades.

In 2004, Waters introduced ultra-high performance liquid chromatography UHPLC which they termed UPLC®.[106] UHPLC operates at high pressures, up to 1030 bar (15,000 psi), for delivering mobile phase which increases throughput, and improves resolution whilst decreasing analysis time. Conventional HPLC methods can readily be transferred to UHPLC methods.

2.1.3 Supercritical fluid chromatography (SFC)

In 1962, the first introduction of SFC was proposed by Klesper *et al.*[107] SFC can be considered as an intermediate technique between gas and liquid chromatography. SFC is an analytical technique which uses supercritical fluids as the primary mobile phase. A supercritical fluid occurs when the temperature and pressure of a substance are increased above its critical temperature and pressure.[108] At the region above the critical temperature and pressure, a substance cannot be classified as either a gas or a liquid because it has properties of both; therefore a substance is called a supercritical fluid.

Consequently, a supercritical fluid has a greater diffusion coefficient and lower viscosity and surface tension than a liquid solvent, which leads to a more favourable mass transfer. A comparison of the properties of gas, liquid and supercritical fluid is shown in Table 2-2. The advantage of supercritical fluids over liquid phases rest with improved mass transfer process because of lower fluid viscosities and higher diffusivities.

Table 2-2   **Comparison of the properties of liquids, gases and supercritical fluid[109]**

State of substance	Density (g cm^{-3})	Diffusion (cm^2 s^{-1})	Viscosity (g cm^{-1} s^{-1})
Gas	10^{-3}	10^{-1}	10^{-4}
Supercritical fluid	0.1-1.0	10^{-4}-10^{-3}	10^{-4}-10^{-3}
Liquid	1	$<10^{-5}$	10^{-2}

Supercritical fluid CO_2 (scCO_2) is the most widely used as mobile phase in SFC because CO_2 is low critical pressure and temperature[110], non-toxic, non-flammable, easy to handle, chemical inert, and inexpensive.[110][111] The critical pressure and critical temperature of scCO_2 are 31 °C and 73 bar, respectively.[112][113] The supercritical fluid region for carbon dioxide is illustrated in the phase diagram in Figure 2-7.
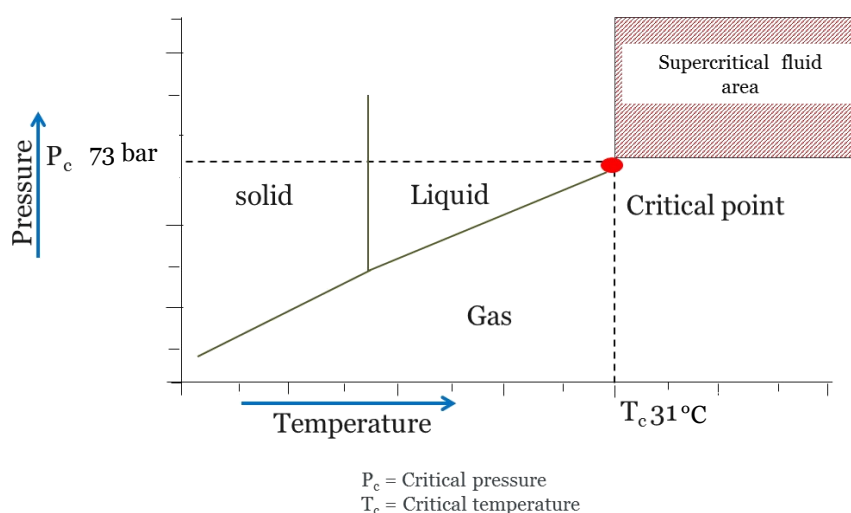
Figure 2-7   **Schematic diagram of *p-T* phase diagram of CO_2.**

In 2012, a new generation of SFC instrumentation, ultra-performance convergence chromatography (UPC^2) was developed by Waters to enable the use of sub-2 μm particle size stationary phases. The schematic diagram of the UPC^2-MS system is shown in Figure 2-8. UPC^2 has be shown to be a rapid, reliable, and cost-effective chromatographic separation method, and can be regarded as the surrogate of normal phase HPLC and is complementary to reversed phase HPLC.[114] Coupling of UPC^2 to a mass spectrometer *via* an atmospheric pressure ionisation source affords a highly sensitive and selective detector that is effective for compound identification and quantification.
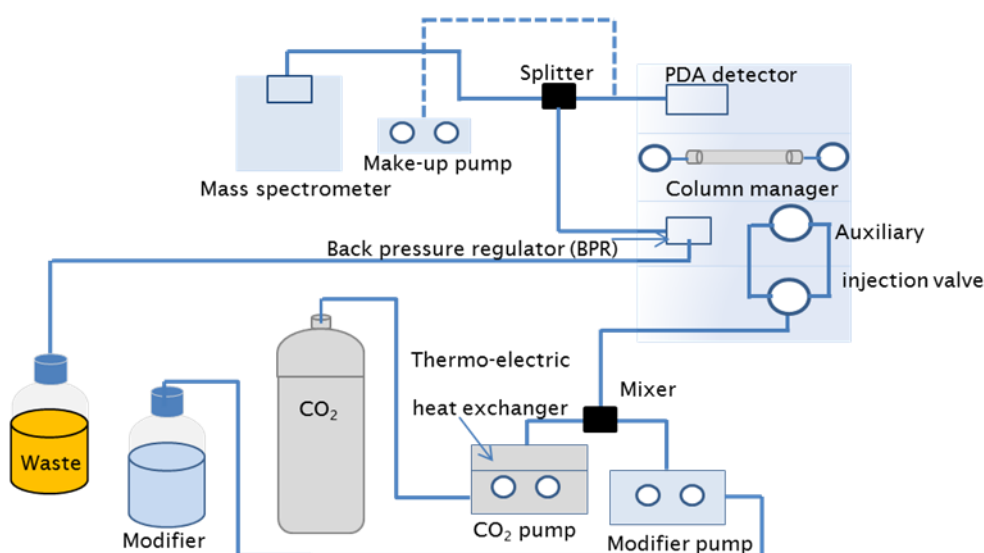
Figure 2-8   Schematic diagram of the UPC^2-MS.

2.1.4   Basic chromatography properties

Chromatographic development methods refer to the selection of conditions which provide an acceptable parameters of given analytes. Some basic chromatography parameters are considered, such as resolution

Chapter 2: Instrumentation

(R_s), peak tailing and peak symmetry. Resolution (R_s) is a measure of how well two peaks are separated from each other. It is calculated as the difference in retention time of two eluting peaks divided by the average width of the two peaks at the baseline. The most common formula (Equation 2-2) for measuring resolution (R_s) uses the half-height method:

$$Rs = 2(t2 - t1)/1.7(w_{0.5,\ 1} - w_{0.5,\ 2})$$ **Equation 2-2**

Where t_1 and t_2 are the retention times of the two peaks of interest, and $w_{0.5,1}$ and $w_{0.5,2}$ are the peak widths measured at half height.[115][116]

Peak tailing and asymmetry factors were considered in order to choose optimum conditions for chromatography. A peak is decided as tailing if its asymmetry is greater than an acceptable value of 1.2-1.5.[115] Figure 2-9 and Figure 2-10 are shown calculation of peak tailing and peak asymmetry factors.
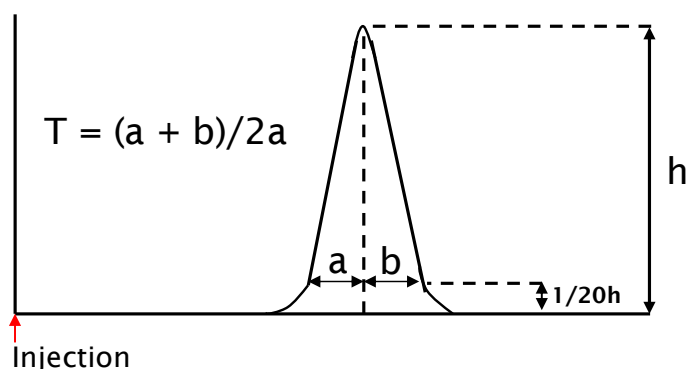
Figure 2-9 Calculation of tailing factor.

Where T is tailing factor (measured at 5% of peak height), b is distance from the point at peak midpoint to the trailing edge, and a is distance from the leading edge of the peak to the midpoint.
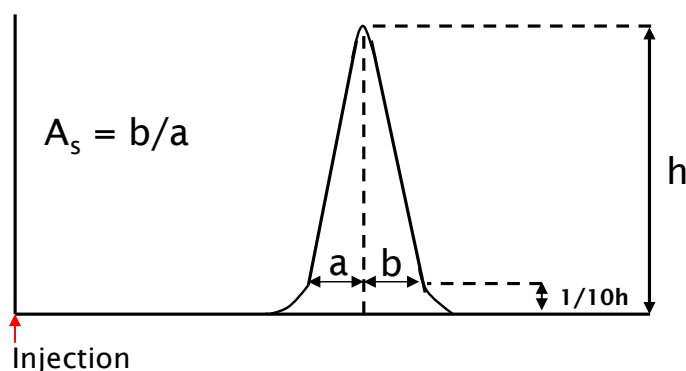
Figure 2-10   Calculation of asymmetry factor.

Where A_s is peak asymmetry factor, b is distance from the point at peak midpoint to the trailing edge (measured at 10% of peak height), a is distance from the leading edge of peak to the midpoint (measured at 10% of peak height).

2.2   Electrochemistry (EC)

In 1971, the first report of the use of a coupling of electrochemistry with mass spectrometry was developed by Bruckenstein and Gadde.[117] An electrochemical reaction is based on applying a potential between a working electrode and an auxiliary electrode. The μ-PrepCell operates in a three-electrode configuration, see Figure 2-11. The working potential is set between the working electrode and the auxiliary electrode (AUX). The auxiliary electrode is kept at a precisely defined reference electrode

51

potential by means of the so-called voltage clamp. This is an electronic

feedback circuit that compensates for polarisation effects at the

electrodes. At the working electrode, which is kept at virtual ground, the

electrochemical reaction takes place, *i.e.* electrons are transferred at the

working electrode. This results in an electrical current to the current-to-

voltage (I/E).
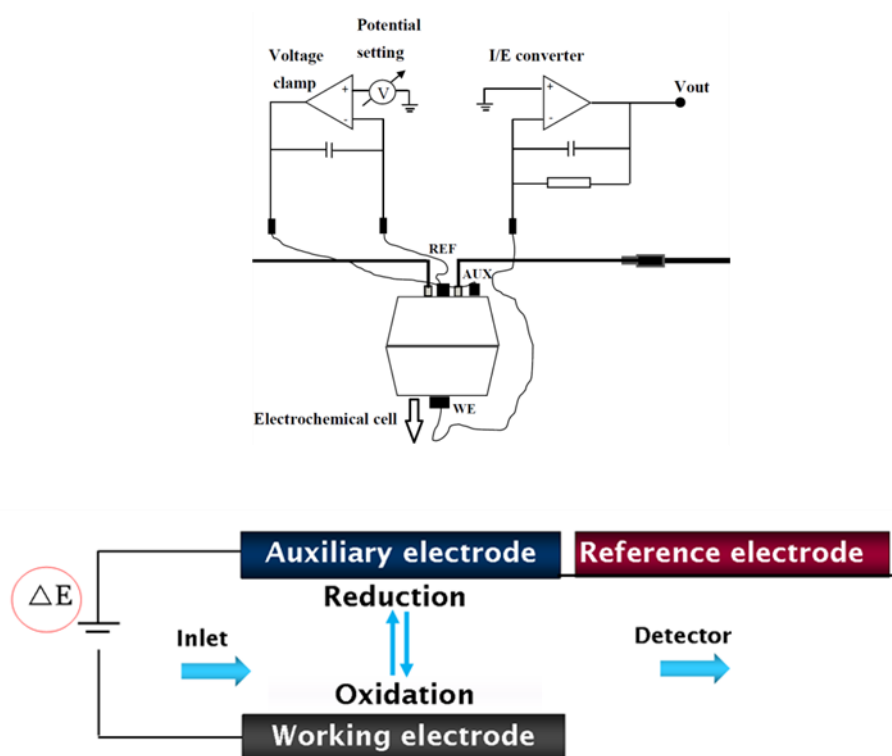
Figure 2-11   Schematic drawing of an electrochemical cell showing a three-electrode configuration showing electrochemical reaction take place on the electrochemical cell.

Electrode potential facilitates electrochemical reactions. At low potential there is no reaction, while higher potential oxidation occurs (Figure 2-12).
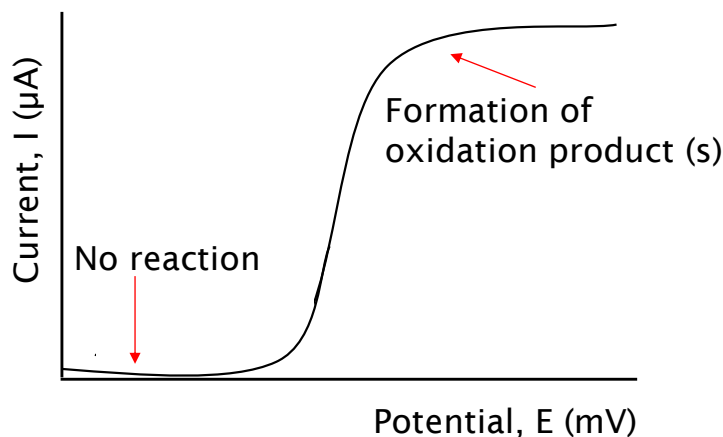
Figure 2-12   Role of electrode potential.

The μ-PrepCell™ combined with the ROXY™ Potentiostat (Antec) can be used to generate metabolites of drugs, similar to those generated during *in vivo* metabolic processes, in a shorter time (seconds *vs.* days or weeks) without separation of the components.[118]

2.3   Mass spectrometry

The mass spectrometer is designed to separate gas phase ions according to their mass-to-charge ratio (*m/z*). The separation of gas phase ions occurs in the mass analyser under high vacuum conditions and is based on the interaction of the ions with electric and/or magnetic fields, detected and this signal is transferred to the data system. Generally, the mass spectrometer consists of the following components; sample introduction, ion source, mass analyser, ion detection system and data

processing unit. Figure 2-13 shows the basic components of a mass

spectrometer, an interface is required to remove the solvent and produce

gas phase ions. For atmospheric pressure ionisation (API) solvent

elimination and ionisation occur in the source at atmospheric pressure as

is shown in Figure 2-13 (A). In electron ionisation (EI) though, the solvent

elimination and ionisation steps are separated (see Figure 2-13 (B)).

(A) Atmospheric pressure ionisation (API)
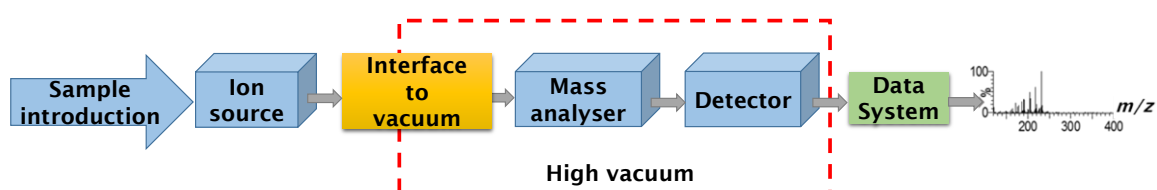
(B) Electron ionisation (EI)
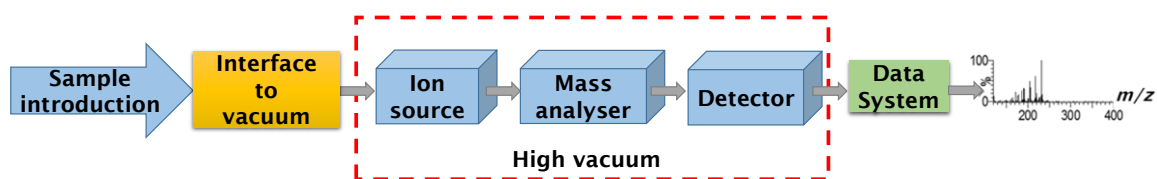
Figure 2-13   Block diagrams for mass spectrometer. (A) Atmospheric pressure ionisation (API); (B) electron ionisation (EI).

2.3.1   Ionisation

A variety of ionisation techniques are used for mass spectrometry.

The selection of the most suitable ionisation technique depends on the

nature of a sample.

2.3.1.1   Electron ionisation (EI)

Electron ionisation (EI) is widely used to ionise and fragment analyte molecules before being directed towards the mass analyser. A typically EI source consists of an ionisation volume, filament, collector, magnetic field, repeller, accelerating potential, and a focusing lens is shown Figure 2-14.

The EI process occurs under a high vacuum (10^{-4}-10^{-6} mbar).[119]The gaseous analyte molecules enter the ionisation volume where they interact with a beam of highly energetic electrons (usually 70 eV) that have been accelerated by a potential difference of 50-70 volts.[119] The electron beam emitted is produce by a heated filament which is typically made from rhenium or tungsten.[120] A magnetic field is produced by a set of small permanent magnets and helps to focus the electron beam.[119][121] In order to eliminate the possibility of ion loss due to collision and subsequent neutralisation with the walls of the ion source, the ions are pushed out after production by applying a positive potential to the repeller electrode/plate. The positive ions formed are expelled from the ionisation volume pass through a series of electrostatic lenses that focus the ions into a tight beam and direct them towards the mass analyser.
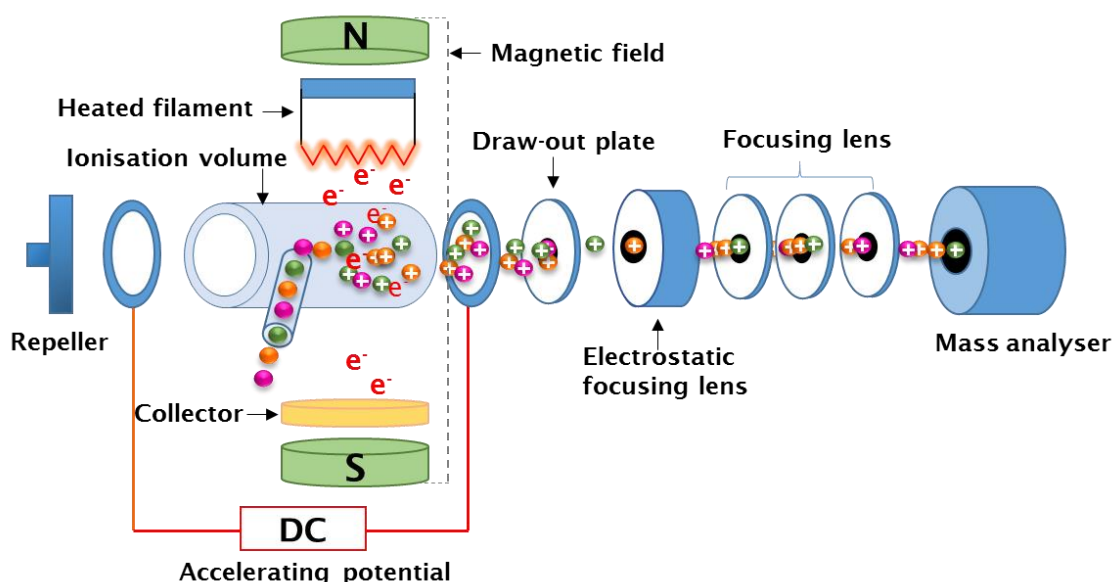
Figure 2-14   Schematic drawing of an EI ion source adapted from http://www.chromacademy.com/Electron_Ionization_for_GC-MS.[121]

In the EI process, if the electron interacts with the gaseous molecules of the analyte, the energy transferred usually exceeds the ionisation energy (IE) of the molecule.[120] Ionisation takes place by ejection of a valence electron to produce a molecular ion (M$^{+\bullet}$), positive radical ion is shown in Equation 2-3. The electrons do not "impact" molecules and hence the term electron impact ionisation is deprecated.[122]
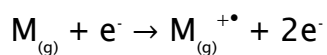
$$M_{(g)} + e^- \rightarrow M_{(g)}^{+\bullet} + 2e^-$$ **Equation 2-3**

Removal of a valence electron from a molecule can occur at a σ bond, a π bond, or at a lone electron pair.[120] The order of ease with which electrons are lost under electron ionisation conditions is lone pair > π-bonded pair > σ-bonded pair.[123] Research in the field reported that most

organic compounds will have an ionisation energy approximately 5-20 eV

[120][122][124] ; however, EI spectra are almost always acquired at 70 eV.

Figure 2-15 shows electron energy versus ion production at low energies; 10 eV to approximately 15 eV. This is the threshold region (A region) in which the EI process for most organic compounds happens. As the electron energy increases, the production of fragment ions becomes important (B region). The plateau of the curve at ~70 eV indicates that small variations in the electron energy have negligible effects on ion production or the pattern of the spectrum (C region). Under the mass spectrometer conditions at 70 eV, for every 1,000 molecules entering the ionisation volume, only one ion is produced.[122][124] Reproducibility of fragmentation patterns is achieved and allows comparison of mass spectra obtained from different mass spectrometers or from mass spectral databases.[120][124]
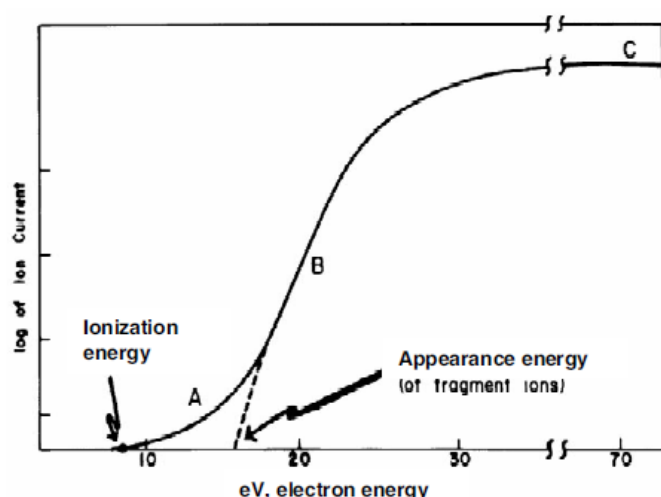
Figure 2-15   Relationship between ion production and energy (electron volts) of ionising electrons: A, threshold region, principally molecular ions produced; B, production of fragment ions becomes important; C, routine operation, mostly fragment ions. Reproduced with permission. Copyright John Wiley and Sons.[124]

Moreover, the 70 eV EI is referred to as a "hard" ionisation because it usually produces extensive fragmentation of the analyte.[125] The EI fragmentation pattern is very useful since it provides structural information for elucidation of known and unknown compounds.[126][127] This ionisation technique is gas-phase ionisation. It is used for analysing non-to medium-polarity, non-ionic compounds with a molecular weight up to 1,000 Da.[120] However, the EI process is limited to analytes that are sufficiently volatile and thermally stable.

2.3.1.2   Electrospray ionisation (ESI)

ESI is one type of atmospheric pressure ionisation (API) and widely used for the analysis of large molecules (*e.g.* proteins, peptides, oligonucleotides) and small polar organic molecules. It is highly compatible with non-volatile compounds, thermally labile analytes found in the liquid or aqueous phase, making it ideal for coupling to separation techniques such as LC. Fenn and co-workers[128] were the first to successfully couple the ESI source to a mass spectrometer based on the theory originally described by Dole *et al.* in 1968.[129]

The basic principle of the electrospray process is the transfer of analyte ions, found in the condensed phase (solution), into the gaseous phase [128] before they are subjected to mass analysis. The production of gas phase ions in ESI can be divided into three major steps[128][129][130]: (1) production of charged droplets at the electrospray capillary tip; (2) shrinkage of the charged droplets; (3) production of gas phase ions from these droplets.

A sample solution flows through a capillary tip towards the mass spectrometer inlet, which is held at a potential difference to the capillary tip. For positive ion electrospray, the capillary tip is the positive electrode (anode) and the sampling cone is the negative electrode (cathode) (Figure 2-16). Under these conditions, the electrospray system can be considered as an electrochemical cell. The oxidation reaction occurs at the capillary tip and a reduction reaction occurs at the sampling cone.[131] The applied high electric field at the capillary tip causes charge separation because the

electric field penetrates the solution.[129][130] The electric field will be strongest near the edges of the capillary tip. The polarisation of the solution near the meniscus of the solution leads to accumulation of positive ions near the surface of the meniscus and negative ions drift away from the liquid surface towards the capillary. The polarisation causes a distortion of the meniscus into a cone shape which is called "Taylor cone".[128]
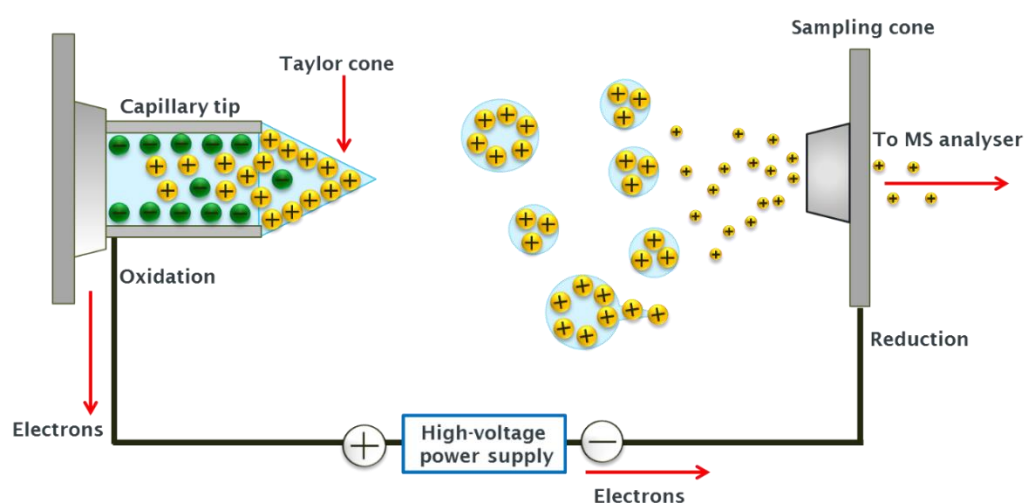
Figure 2-16   **Schematic of electrochemical process of ESI.**

At a specific electric field strength, the cone is not stable and a fine jet is emitted from the Taylor cone tip. The repulsion between the charges on the jet leads to the formation of charged solvent droplets. They are sprayed into the desolvation space towards the sampling cone of the mass spectrometer. The droplets shrink by solvent evaporation and leads to decrease of the droplet radius but their total charge amount remains constant. Solvent evaporation is achieved by increasing the temperature of ambient air within the ionisation chamber and using a desolvation gas

which is introduced coaxially to the flow of the aqueous phase. The decrease in the droplet radius leads to an increase in the surface charge density.

This, in turn, leads to an increase in the repulsion between the charges at the surface, until the electrostatic repulsion force becomes equal to the surface tension of the liquid. This condition is expressed by Rayleigh's stability limit where the charged droplet is unstable and undergoes fission into smaller droplets. The process is known as "Coulombic fission or Coulombic explosion".[131]

Two different models, the charge residue model (CRM) and the ion evaporation model (IEM), have been proposed for the production of gas phase ion from small charged droplets with a radius of around 10 nm. The first model is the CRM has been described by Dole and co-workers.[129–133] The CRM proposes that the gas phase ions produce from the evaporation of solvent from small droplets which contain only one ion.[131][133][134]

Thomson and Iribarne proposed a different model, the IEM. The model predicts that when solvent evaporation and Coulombic fission have reduced the size of the charged droplets to around 10 nm in diameter, direct emission of ions to the gas phase will occur (as shown in Figure 2-17).[129][130][133] The ion evaporation model replaces Coulomb fission by removing charge. In general, the IEM is considered in the process of gas phase ion production for high analytes, whereas the CRM is considered for high weight analytes such as proteins.
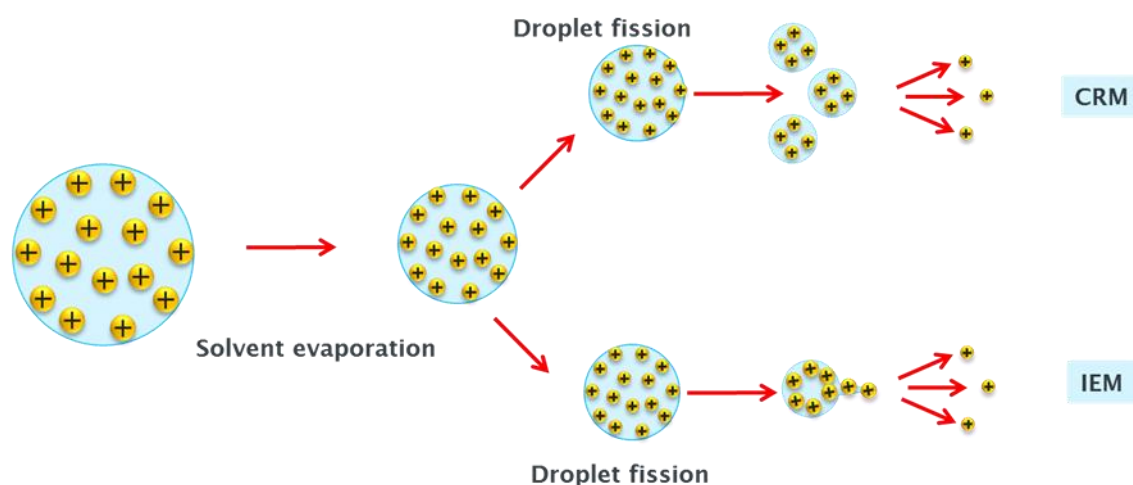
Figure 2-17 Schematic of the two models for gas-phase ion production by ESI: the charge residue model (CRM) and the ion evaporation model (IEM).

2.4 Mass analyser

After the gas-phase ions are produced, they are accelerated into the mass analyser which is the heart of the mass spectrometer. The mass analyser separates these ions according to their mass-to-charge ratio *(m/z)*. Mass analysers use electric and/or magnetic field(s) to exert a force on the ions. The relationship between force, mass, and the applied fields can be described by Newton's second law (Equation 2-4) and Lorentz force law (Equation 2-5) which are a fundamental basis for mass analysers.

$$F = ma$$ **Equation 2-4**

$$F = e\,(E + v \times B)$$ **Equation 2-5**

Where F is the force applied to the ion, m is the mass of the ion, a is the acceleration, E is the electric field, B is the magnetic field, v is velocity, and q is electric charge.

From Newton's second law, the force causes ions to accelerate depending on the mass of the ion, and the Lorentz force law dictates that the applied force is also dependent on the ionic charge. These two basic principles help to understand that mass spectrometers separate ions according to their *m/z* rather than by their mass alone. There are many types of mass analysers, including quadrupole (Q), time-of-flight (TOF), Fourier transform ion cyclotron resonance (FT-ICR), quadrupole time-of-flight (Q-TOF). They all operate on the same basic principles. Some characteristics for measuring the performance of a mass analyser are mass range, mass accuracy and mass resolution. Mass range is the difference between the highest and lowest *m/z* which a mass analyser can measure. Mass accuracy is the accuracy of *m/z* measured by the mass analyser. It is the difference between the theoretical *m/z* (exact mass) and the measured *m/z* (accurate mass), see Equation 2-6. Mass accuracy can be given as absolute mass accuracy and expressed in milli *m/z* units (mDa):

$$\Delta m/z = m/z\ (measured) - m/z\ (theoretical)$$ **Equation 2-6**

However, it is often given as relative mass accuracy and expressed in part per million (ppm), (see Equation 2-7).

$$\frac{m/z\ (\text{measured}) - m/z\ (\text{theorectical})}{m/z\ (\text{theorectical})} \times 10^6$$ **Equation 2-7**

Resolving power in mass spectrometry is defined as the ability of an instrument or measurement procedure to distinguish between two peaks.[135]

2.4.1.1   Quadrupole (Q) mass analyser

The principle of the quadrupole mass analyser was first described by Paul and Steinwedel in the 1950s.[122][136] The quadrupole consists of a set of four parallel electrodes, ideally of hyperbolic cross section (Figure 2-18(A) or circular cross section (Figure 2-18 (B)).

(A) Quadrupole with hyperbolic cross section
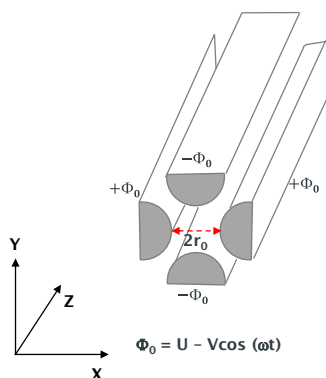
(B) Quadrupole with circular cross section
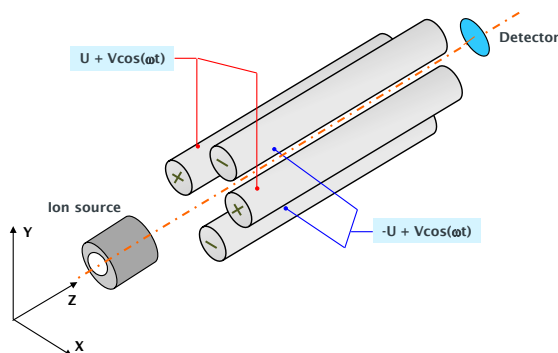
Figure 2-18   Schematic of quadrupole mass filter with a hyperbolic cross section (A) and a circular cross section (B), showing the potential applied to the two pairs of electrically connected rods; the rods space is $2r_0$ at the closest.

For commercial instruments circular cross section quadrupoles are preferred due to the simplicity of construction and cost.[137][138] However, if circular cross section rods are used an approximate quadrupole field

similar to the ideal hyperbolic field can be obtained if the radius (r) of the circular electrodes is related to the quadrupole field radius (r_0) by the following Equation 2-8.[137]

$$r = 1.148r_0$$ **Equation 2-8**

In the quadrupole mass analyser, the two pairs of opposite rods are connected electrically. Two voltages, a direct current (DC) and an alternating current (RF), are applied to each pair of rods. For a positive ion, the x direction corresponds to the positive electrode and the y direction corresponds to the negative electrode (see, Figure 2-18). The quadrupole mass analyser uses electric fields to separate ions according to their *m/z* ratios as they travel along the central z axis of the four parallel rods. The electric potential of the quadrupole is given by Equation 2-9:

$$\Phi(x,y) = [(U + V\cos(\omega t)]\frac{(x^2 - y^2)}{r_0^2}$$ **Equation 2-9**

where Φ is the potential applied to the rods, x and y are the distances along the given coordinate axes, r_0 is the distance from the centre axis to the surface of any electrode, so-called, "field radius";[139] ω is the angular frequency ($2\pi f$) of the applied AC waveform, U is DC potential and V is the magnitude (zero-to-peak amplitude) of the RF voltage.

The potential is zero at the centre of the quadrupole and increases quadratically away from the centre-line. The ions accelerated along the z axis enter the space between the quadrupole rods and keep their velocity along the z axis. The motion of an ion with mass m and charge e within the quadrupole can be described by Newton's second law, F = ma.

An ion having an amplitude greater than r_0, is considered to have an unstable trajectory through the mass analyser. This will cause it to collide with the rods and be neutralised and not detected. Conversely, an ion trajectory is considered "stable" if the amplitude is less than r_0. The ion will pass through the quadrupole and eventually reach the detector.[138][140] Stable and unstable trajectories of ions in a quadrupole mass analyser are shown in Figure 2-19.

⊕ Ion with a stable trajectory
● Ion with an unstable trajectory
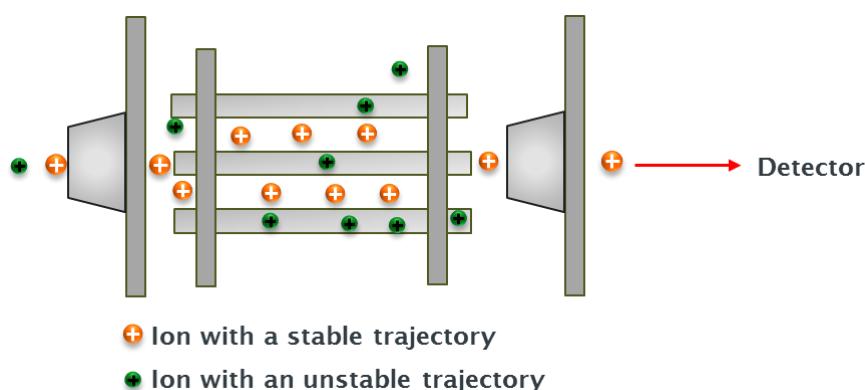
Figure 2-19   Schematic diagram of a quadrupole mass analyser showing ions with a stable and unstable trajectory.

Mathieu provided the equations of motion for an ion of mass m and charge e in the electric field of a quadrupole (see, Equation 2-10 to Equation 2-13). Two factors, a and q, are of importance to describe the stable trajectory of the ion.

$$\frac{d^2u}{d\xi^2} + (a_u - 2q_u cos2\xi)u = 0 \qquad \textbf{Equation 2-10}$$

$$\xi = \ \omega t/2 \qquad \textbf{Equation 2-11}$$

$$a_u = \frac{8eU}{mr_o{}^2\omega^2} \qquad \textbf{Equation 2-12}$$

$$q_u = \frac{4eV}{mr_o{}^2\omega^2}$$
Equation 2-13

where u is displacement (x or y), ξ is a dimensionless modified time parameter, e is the charge on the electron and m is the mass of the ion, r_0 is the distance from the centre axis to the surface of any electrode. ω is the angular frequency ($2\pi f$) of the applied ac waveform. U is direct potential and V is the magnitude (zero-to-peak amplitude) of the RF voltage.

Considering the Equations 2-11 and Equation 2-12, the a term has related to the DC voltage (U) and the q terms has related to the RF voltage (V). Combination of the stability for ion motion in the x and y directions are given by the following equation (see, Equation 2-14).

$$a_u = a_x = -a_y \; and \; q_u = q_x = -q_y$$
Equation 2-14

Figure 2-20 shows the stability diagram for the x and y motions in a linear quadrupole.[138] The shaded area in all of the regions that correspond to a stable trajectory.
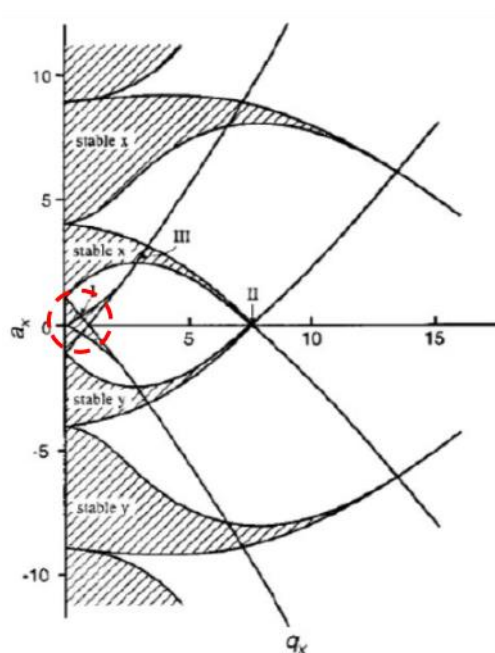
Figure 2-20   Regions of stability for the x and y motions in a linear quadrupole, expressed in terms of a_x and q_x. Reproduced from Douglas (2009)[138] with permission. Copyright John Wiley and Sons.

Most commercial instruments generally operate in the first region[138][140][141] labelled as I (red circle) in the Mathieu diagram. In practice, the mass filtering of the quadrupole is typically controlled by the DC (U) and RF (V) voltages. The expanded view of the first stability region is presented in Figure 2-21, which shows substitutions for the Mathieu parameters a and q to convert as a function of U-V values for three different m/z ($m_1 < m_2 < m_3$). Ions of different m/z have parameters that appear on the same "operating or scan line" defined by the $2U/V$ ratio or equivalently the a/q ratio. The operating line can be located just below the tip of the first stability region. The U and V voltages are then changed together, keeping a constant ratio, ions of increasing mass will reach the

tip of the stability region in order of their mass and will be transmitted sequentially to produce a mass spectrum.

The mass resolution of a quadrupole can be altered by changing the ratio of DC (U) to RF voltage (V) to change the slope of the scan line. Decreasing the slope of the mass scan line reduces its resolution. If a quadrupole is operated with a constant ratio U/V the resolution will be constant across a mass scan. It is more common to operate a quadrupole so that the peak width is constant across a spectrum.
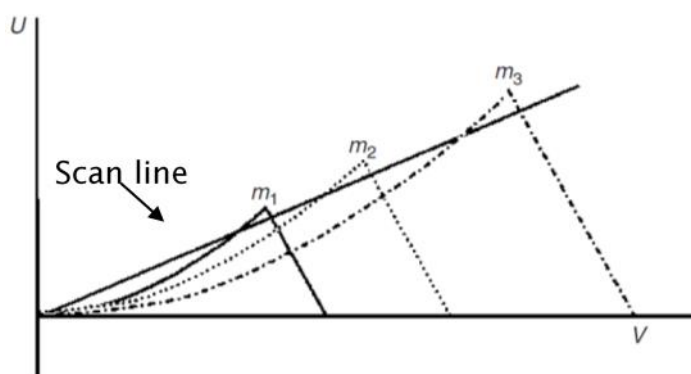
Figure 2-21 **Stability regions as a function of U and V for ions with different masses ($m_1 < m_2 < m_3$). Changing U linearly as a function of V obtain a straight operating line. Reproduced with permission. Copyright John Wiley and Sons.**

Quadrupole mass analysers are now widely used for combined GC-MS and LC-MS instruments. However, quadrupole instruments are generally limited to unit mass resolution and have a low mass range in the order of up to *m/z* 4000.[120]

2.4.1.2   Time of flight (TOF) mass analyser

The first concept of TOF mass analyser was described by Stephens in 1946.[142] In 1955, a linear TOF was designed by Wiley and McLaren and became the first commercial instrument.[143] The principle of linear TOF analysers involves measuring the time required for an ion to travel from an ion source to a detector. The TOF analyser separates ions according to their velocities when they move in a free-field region that is called a flight tube.[143]

Figure 2-22 shows the schematic representation of a linear TOF mass analyser. Ions having different masses produced at the same time in an ion source and then the ions are accelerated along towards the flight tube by electric field. The ions obtain the same kinetic energy, but they have different masses.
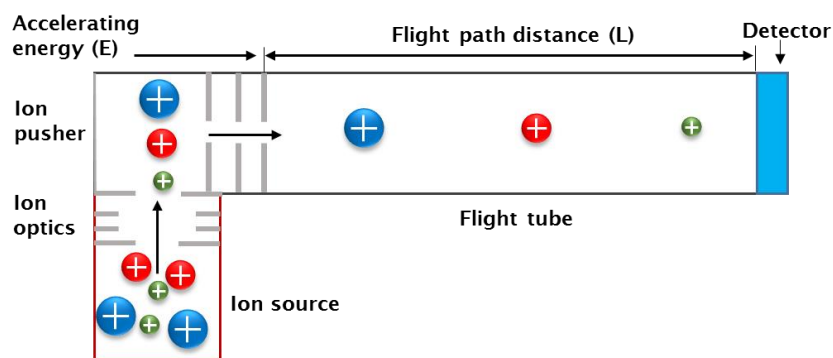
Figure 2-22   **Schematic of a linear TOF mass analyser, where the blue red and green circles represent ions of different masses, each with a single charge. While ions travelling along the field-free path (d), they are dispersed in time. Smaller ions arrive the detector first.**

When the ions leave from the acceleration region, they enter a field-free region where they are separated according to their velocities, before arriving at the detector. In linear TOF mass analyser, an ion with mass m and total charge $q = ze$ is accelerated by a potential V_s. It electric potential energy E_{el} is converted into kinetic energy E_k, see Equation 2-15.

$$E_k = \frac{mv^2}{2} = qVs = zeVs = Eel \qquad \textbf{Equation 2-15}$$

The velocity of the ion leaving the source is given by rearranging the Equation 2-16 as:

$$v = \left(\frac{2zeVs}{m}\right)^{1/2} \qquad \textbf{Equation 2-16}$$

The ion travels in a straight line at constant velocity to the detector. The time t needed to cover the distance L before reaching the detector is given by the following equations:[122][124]

$$t = \frac{L}{v} = L\left(\frac{m}{2zeVs}\right)^{1/2}$$

$$t^2 = \frac{m}{z}\left(\frac{L^2}{2eVs}\right) \qquad \textbf{Equation 2-17}$$

The Equation 2-17 shows that the lower the mass of an ion, the faster it will reach the detector. The advantage of a TOF analyser is that theoretically there is no limit to the upper *m/z* value that can be detected.[122][124] The resolution in TOF is derived from the relationship between *m/z* and flight time. Therefore, the resolution is given by Equation 2-18.

$$R = \frac{m}{\Delta m} = \frac{t}{2\Delta t}$$ **Equation 2-18**

Where m and t are the mass and flight time of the ion. Δm and Δt are the peak widths measured at the the 50% on the mass and time scale, respectively. L is the flight tube length.

The disadvantage of a linear TOF analyser is low mass resolution and, subsequently, poor mass accuracy. Since the resolution in a TOF is related to the flight time and the flight tube, one solution to improve resolution and sensitivity is to use a long flight tube with a length of 1-2 m and an acceleration voltage of at least 20 kV.[122] Resolution in a TOF can be improved using, delayed extraction, orthogonal acceleration, and a reflectron.[143] In this section, the reflectron is discussed in detail.

The reflector TOF was proposed for the first time by Mamyrin *et al.* in 1973.[144] The reflectron acts as an ion mirror by deflecting the ions and then sending them back through the flight tube. It consists of a grid electrodes or ring electrodes which are located behind the free-field drift tube opposite the ion source.

Figure 2-23 shows a reflectron-TOF mass analyser. Two ions of the same *m/z* that have different kinetic energies. The ion with more kinetic energy and more velocity and the ion with lower kinetic energy enter into the reflectron and continue reducing velocity until their kinetic energy reaches zero. At this point, the ions are pushed from the reflectron in the opposite direction by the electric field. The ion with more kinetic energy and more velocity will enter faster and deeper into the reflectron that

spend more time within the reflectron than the less energetic ion. Then, the faster ion will reach the detector at the same time as the initially slower ion with the same *m/z*. The reflectron compensates for the kinetic energy distribution by correction in time of flight. In this way, the reflectron increases the flight path without increasing the dimension of the mass spectrometer. The reflectron then improves mass resolution compared to a linear TOF.
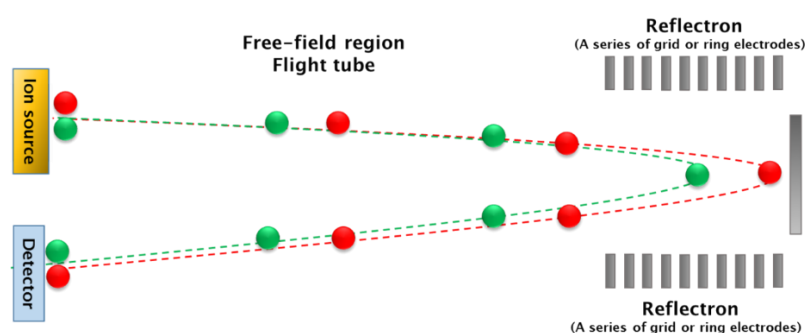
Figure 2-23   Scheme of a reflector TOF-mass analyser showing two ions with the same *m/z* but different kinetic energies. Higher kinetic energy (red circle) and lower kinetic energy (green circle) ions. The ions reach the detector at the same time because of the correction time they spend in the reflectron.

2.4.1.3   Fourier transform-ion cyclotron resonance mass analyser (FT-ICR MS)

The theory of cyclotron resonance was first described by Lawrence in the 1930s.[145] In 1978, Comisarow and Marshall developed FT-ICR and constructed the first FT-ICR MS instrument. All FT-ICR MS instruments consist of four common main components: a superconductive magnet, an analyser cell, an ultrahigh vacuum system and a data acquiring system.[146][145] The first component is a magnet, which can be either a

permanent magnet, an electromagnet or a superconducting magnet. The superconducting magnets usually used for FT-ICR MS have field strengths ranging from 3 to 9.4 Tesla (T).[145] Currently (2015), a 21 T magnet is the largest magnet that has been used for FT-ICR MS experiments.[147] The performance of the FT-ICR MS improves as the magnetic field strength increases. The second component is a ICR analyser cell, where ions are trapped, exposed to the magnetic field, forced into their cyclotron motion, analysed, and detected.[145][146] Various ICR analyser cell with different geometries were designed.[148] The simplest analyser cells (cubic and cylindrical) are shown in Figure 2-24. The cell consists of six plate electrodes, two perpendicular to the magnetic field and the other four arranged in such a way as to form a closed cube or cylinder. Ions enter the cell through an opening in one of the perpendicular trapping plates.
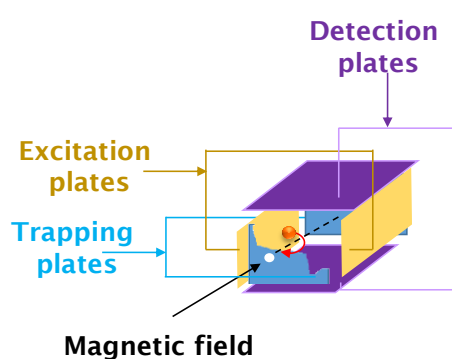
(A) Cubic analyser cell   **(B) Closed cylindrical analyser cell**
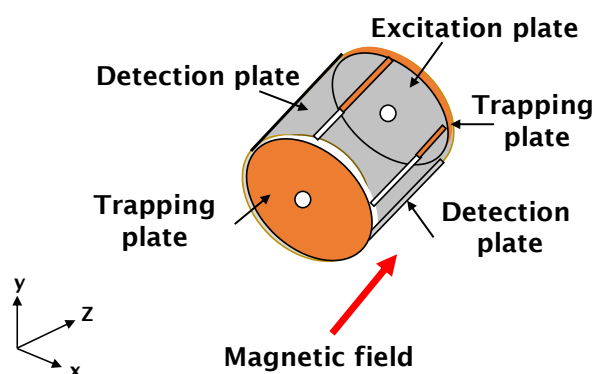
Figure 2-24   Schematic diagram of a cubic analyser cell (A); a closed cylindrical analyser cell (B).

Ions are trapped and stored in the cell by applying a small voltage (typically +/- 1–2 V, depending on the polarity of the ions)[149] to the trapping plates. The ions in the analyser cell are exposed to the strong magnetic field and undergo motion in a plane perpendicularly to the magnetic field, named "cyclotron motion". In a magnetic field (B), ions of charge (q) and velocity (v) experience the Lorentz force F which is given by Equation 2-19. The Lorentz force is a "centripetal" force and is counterbalanced by the "centrifugal" force (F), (see, Equation 2-20) and defined by the ion mass m, the ions velocity (v_{xy}) in the x-y-plane and the orbital radius (r).[122][150]

$$F = q\,v\,B \qquad \text{Equation 2-19}$$

$$F = \frac{mv^2}{r} \qquad \text{Equation 2-20}$$

Movement of ions parallel to the magnetic field is not influenced by this field. Each ion rotates with its frequency in respect to its (m/q), the so-called "cyclotron frequency". Thus positive-charged ions rotate counter clockwise and negative ions rotate clockwise, (see Figure 2-25).

(A) Magnetic force acting on a positive ion
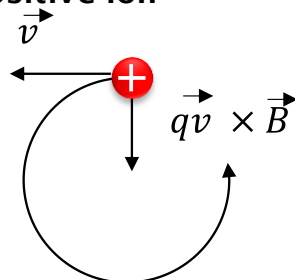
(B) Magnetic force acting on a negative ion
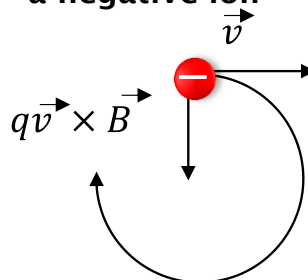
Figure 2-25   Ion cyclotron. Magnetic force acting on a positive ion (A) and negative ion (B), each with velocity, v, subjected to a magnetic field, B, direct in plane of the paper. The path of an ion moving in the plane of the paper is bent into a circle by the inward-directed Lorentz magnetic force produced by a magnetic field directed perpendicular to the plane of the paper. Note that positive and negative ions orbit in opposite senses.[150][151]

The ion stabilises on the trajectory resulting from the balance of Equation 2-19 and Equation 2-20, as shown in Equation 2-21.

$$qvB = \frac{mv^2}{r} \quad qB = \frac{mv}{r}$$ **Equation 2-21**

The ion completes a circular trajectory of $2\pi r$ with a specific frequency, thus the angular velocity ω is given by Equation 2-22.

$$\omega = 2\pi v = \frac{q}{m}B$$ **Equation 2-22**

The cyclotron frequency is related to the *m/z* of the ion and is given by Equation 2-23.

$$\omega = 2\pi v_c = \frac{v}{r} = \frac{q}{m}B$$ **Equation 2-23**

Then, ions with different *m/z* can be analysed, detected, and separated by way of their different cyclotron frequencies. Ions with the

same m/z have the same cyclotron frequency but different energies and then different velocities in their orbits and different radii. The potential change between the detection plates can be measured as a function of time and it is from here that the raw data comes, known as a ''transient'' or ''time-domain'' data. It should be noted that the ions repeatedly pass by the detector plates for the duration of the acquisition time, as non-destructive detection is employed. It is therefore necessary to extract data about the different ion packets. This is done through usage of the mathematical procedure known as a ''Fourier transform'' (FT) where frequency information is obtained from time-domain data.

When ions are trapped in the analyser cell the radius of the cyclotron orbits is too small to be detectable, hence the ions must be excited into coherent motion by applying a radio frequency (RF) potential to two excitation plates. As a result, the ion spirals outward when its cyclotron frequency is in resonance with the frequency of the applied RF potential.[145]

The third component is the ultrahigh vacuum system, and a pressure of 10^{-9} to 10^{-10} mbar is required in FTICR-mass spectrometry. This high vacuum is provided by turbo molecular pumps or cryogenic pumps.[145] The last component is a data system including a frequency synthesiser, which is used to process and analyse the data. Following excitation, ions of the same mass-to-charge ratio go through cyclotron motion as an "ion packet". When the ion packet passes by the detection plates, "image current"[149] is induced in the two plates by attraction (positive ion

detection) or repulsion (negative ion detection). Detection of the ions occur

as the ion packets travel past two detection plates because the potential

change between the detection plates can be measured as a function of

time, known as a "transient" or "time-domain". The signal is then converted

from the time-domain to the frequency-domain by Fourier transform (FT).

The frequency spectrum is converted into a mass spectrum, which is later

calibrated by applying a calibration formula derived from the cyclotron

equation.[145] Figure 2-26 shows a basic FT-ICR MS with a cubic cell.

Presently, FT-ICR MS is the most powerful commercially available

instrument in terms of mass accuracy and resolution.[152]
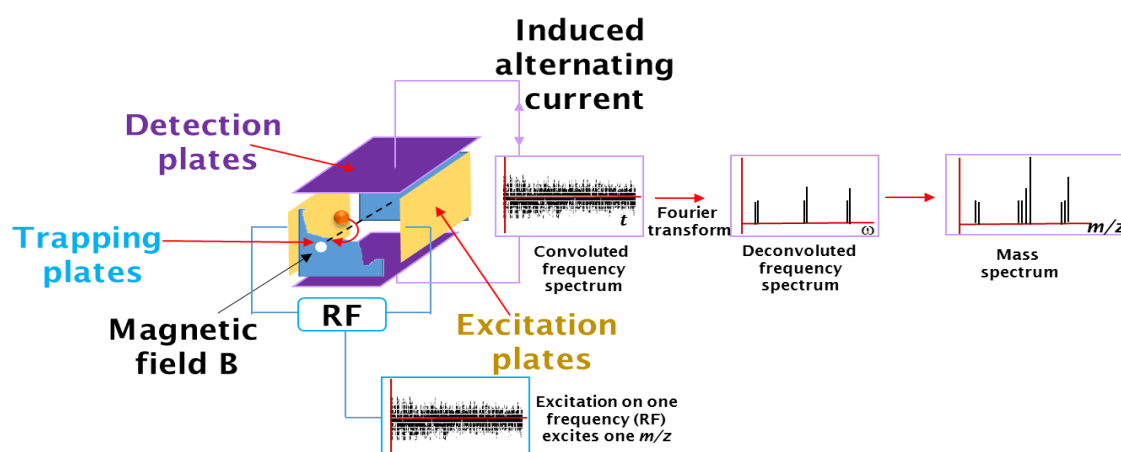
Figure 2-26   Schematic drawing of a FT-ICR MS showing in a cubic cell.

2.4.1.4 Tandem mass spectrometry

Tandem mass spectrometry, mass spectrometry/mass spectrometry, requires to combine at least two stages of mass analysers often referred to as MS1 and MS2, respectively. MS/MS (Figure 2-27) consists of several sequential processes: ionisation of sample molecules, mass selection of parent ions, collision induced dissociation (CID) of the parent ions with neutral gas (*e.g.* N_2, Ar) molecules to produce ions, mass analysis and detection of these product ion.[153] Basically, there are two types for MS/MS: MS/MS in space and MS/MS in time. For MS/MS in space, uses two mass analysers combined in tandem. These processes occur sequentially in separate regions[153][154], for example, QqQ, TOF-TOF and QTOF.[120]
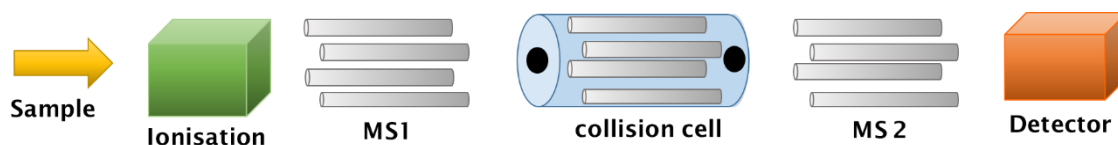
Figure 2-27   Schematic diagram of triple quadrupole mass analyser.

2.4.1.5 Quadrupole-Time of flight mass analyser

The Q-TOF tandem mass spectrometer can be explained in the simplest way as a triple quadrupole with the last quadrupole section replaced by a TOF analyser. The development and commercialisation of the hybrid quadrupole-TOF (QTOF) mass spectrometer used a similar approach to oa-TOF. A schematic representation of a Q-TOF is shown in Figure 2-28.
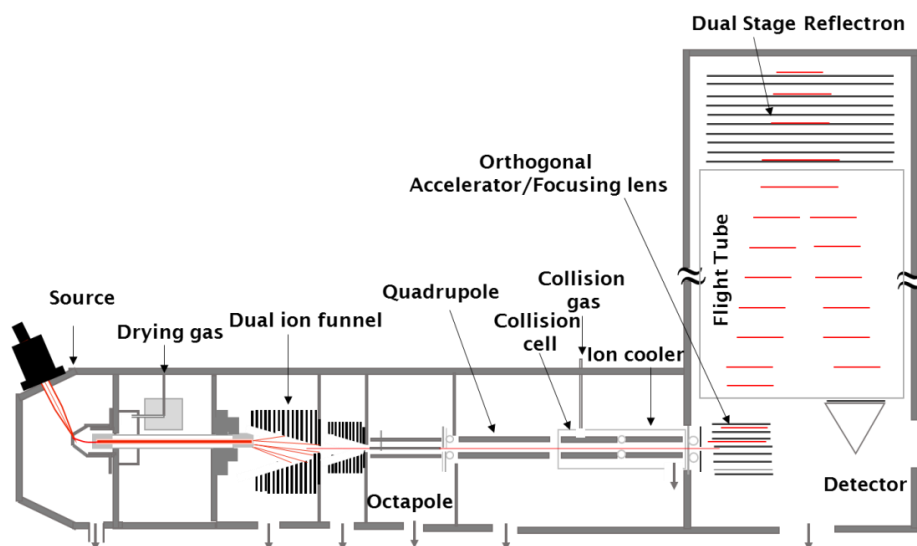
Figure 2-28   Schematic representative of Q-TOF.

2.5   Summary

In this project, the main aspect was the application of chromatography, electrochemistry, and mass spectrometry to the analysis of fuels. The objectives of this chapter were:

- To understand the basic concepts of separation sciences techniques (GC, HPLC, SFC and EC), the principles of EI and ESI and also various mass analysers including quadrupole (Q), TOF-MS, FT-ICR MS and MS/MS.
- To know how hyphenation in mass spectrometry, GC–MS, HPLC–MS, UHPLC–MS, UHPSFC–MS and EC–MS, works and what it can do as a powerful tool for the research.

The summary of the key points of this chapter are:

- GC is suitable for volatile analytes and thermal stability, whilst HPLC is amenable for non-volatile or thermally labile analytes.

- SFC uses supercritical fluid CO_2 ($scCO_2$) as mobile phase which the properties of $scCO_2$ have liquid like diffusivity and gas like viscosity.

- SFC is an intermediate between GC and HPLC that uses for analytes cannot resolve by either GC and HPLC.

- The introduction of UHPLC and UHPSFC utilise sub-2 particle size stationary phases for improving the analytical tool both separation resolution and speed.

- EC coupling to MS has been used for monitoring and investigating oxidation process in a shorter time (seconds *vs.* days or weeks).

- Electron ionisation is gas-phase ionisation which it is used for analysing non-to medium-polarity, non-ionic compounds with a molecular weight up to 1,000 Da. However, the EI process is limited to analytes that are sufficiently volatile and thermally stable.

- ESI is one type of atmospheric pressure ionisation (API) and widely used for the analysis of large molecules. It is highly compatible with non-volatile compounds, thermally labile analytes.

- Coupling of chromatography to mass spectrometry to allow compound identification.

Chapter 3:   Experimental details

3.1   Chemicals

Methyl oleate (C18:1), methyl linoleate (C18:2), methyl linolenate (C18:3), methyl heptadecanoate (C17:0), 2,6-di-*tert*-butyl-4-methylphenol (BHT) and sodium formate were purchased from Sigma-Aldrich (Gillingham, UK). Methanol (MeOH), acetonitrile (ACN), isopropanol (IPA), water (LC-MS grade), hexane (HPLC grade) and dodecane (99% pure) were purchased from ThermoFisher Scientific (Loughborough, UK). Food grade carbon dioxide was purchased from BOC Special Gases (Manchester, UK). Formic acid was purchased from Riedel-de Haën (Seelze, Germany). Internal standard (methyl heptadecanoate, d_{33}), rapeseed methyl ester (RME), soy methyl ester (SME), coconut methyl ester (CME) and fresh and aged fuel samples were supplied by BP (Pangbourne, UK). Aviation fuel was obtained from Air BP UK Ltd and the Energy Institute.

3.2   Experimental details for Chapter 4

3.2.1   Electrochemistry-mass spectrometry (EC-MS)

The EC system was the ROXY potentiostat (Antec, Zoeterwoude, ARC Sciences, Hampshire, UK) equipped with the μ-PrepCell™. In the μ-PrepCell™ a three-electrode configuration is used, *i.e.* a working electrode, a HyREF palladium-hydrogen (Pd/H_2) reference, and titanium an auxiliary electrode. Glassy carbon (GC) and magic diamond (MD) working electrodes were compared. The MD electrode consisted of an ultra-thin film of doped

diamond material deposited on a Si wafer. A working standard solution of individual FAMEs (1 µg/mL) passed through the electrochemical cell at a flow rate of 10 µL/min using a Harvard syringe pump (ARC Sciences, Hampshire, UK). The working electrode size was 30 × 12 mm with the effective spacer thickness of approximately 50 µm corresponding to a cell volume of 11 µL. The working electrode potential was applied in the range 0 to 2.5 or 3 V (depending on the working electrode used) to determine optimal conditions for generation of oxidation products. The EC system was controlled by Antec Dialogue software. The instrumental set-up of the ROXY EC system is shown in Figure 3-1.
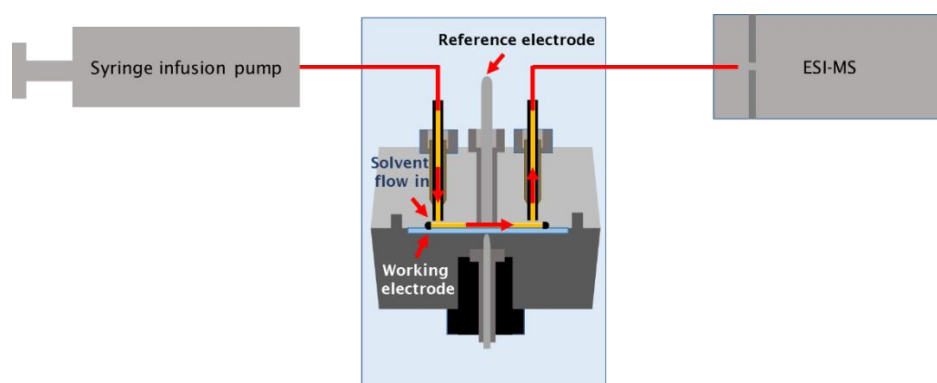
Figure 3-1   Schematic drawing of the µ-PrepCell in a ROXY EC system.

The outlet of the EC cell was directly coupled to a quadrupole-time of flight-mass spectrometer (maXis Q-TOF MS) (Bruker Daltonics). Positive ion ESI mass spectra were recorded using the following parameters: capillary voltage, -4000 V; nebuliser pressure, 1.0 bar; drying gas flow rate, 4.0 L/min; drying gas temperature, 200 °C; funnel RF, 200 Vpp; ISCID energy, 30 eV; quadrupole ion energy, 4.0 eV; mass range *m/z* 50-1200.

Acquisition and analysis of data were controlled by Compass

DataAnalysis™ software version 4.0.

3.2.2 High performance liquid chromatography-mass spectrometry (HPLC-MS)

The HPLC-MS analysis was performed using an Agilent 1050 Series

HPLC coupled to a VG platform LCZ quadrupole mass spectrometer and

positive ion ESI data were acquired. The chromatographic separation was

performed using an XBridge C18 column (2.1 × 50 mm, 5 μm) at column

temperature of 40 °C. Mobile phase A consisted of water with 0.1% formic

acid (v/v), and mobile phase B consisted of methanol with 0.1% formic acid

(v/v). The HPLC gradient conditions are shown in Table 3-1. The injection

volume was 2 μL and the UV was set at a wavelength of 254 nm.

Positive ion ESI mass spectra were recorded using the following

parameters: capillary voltage, 3.5 kV; cone voltage, 30 V; extractor, 3 V;

source block temperature, 80 °C; desolvation temperature, 120 °C;

desolvation gas flow, 3.6 L/h; mass range m/z 120–600; scan duration,

1 s. Samples were analysed and data processed using Masslynx v 3.5

(Waters).

Table 3-1   HPLC gradient conditions for separation of FAMEs and their oxidation products

Time (min)	Mobile phase A %	Mobile phase B %	Flow rate (mL/min)
0.00	80	20	0.5
2.00	80	20	0.5
12.00	0	100	0.5
16.00	0	100	0.5
16.01	80	20	0.5
20.00	80	20	0.5

3.2.3   Ultra high performance liquid chromatography-mass spectrometry (UHPLC-MS)

UHPLC–MS analysis was performed using an ACQUITY UPLC™ H-Class (Waters, Wilmslow, UK) consisting of ACQUITY UPLC™ binary solvent manager and ACQUITY UPLC™ sample manager. An Acquity UPLC® BEH C18 column (2.1 mm × 50 mm, 1.7 μm) (Waters, Hertfordshire, UK) was used for separation. The column temperature was 40 °C. Mobile phase A consisted of water with 0.1% formic acid (v/v), and mobile phase B consisted of methanol with 0.1% formic acid (v/v). The UHPLC gradient conditions are shown in Table 3-2. The injection volume was 2 μL and the UV was set at a wavelength of 254 nm. The UHPLC system was coupled to a Xevo TQD tandem quadrupole mass spectrometer (Waters) equipped with an orthogonal Z-spray™ electrospray ionisation (ESI) source was used for detection of oxidation products of FAMEs. Positive ion ESI mass spectra were recorded using the following parameters: capillary voltage, 3.3 kV; cone voltage, 25 V; source temperature, 150 °C; desolvation temperature,

350 °C; desolvation gas flow, 700 L/h; mass range *m/z* 150–1000; scan duration, 0.1 s.

Table 3-2   UHPLC gradient conditions for separation of FAMEs and their oxidation products

Time (min)	Mobile phase A %	Mobile phase B %	Flow rate (mL/min)
0.00	80	20	0.6
1.00	80	20	0.6
4.00	0	100	0.6
5.30	0	100	0.6
7.00	80	20	0.6

3.2.4   Ultra high performance supercritical fluid chromatography-mass spectrometry (UHPSFC-MS)

The UHPSFC-MS system used was an Acquity ultra-performance convergence chromatograph (UPC[2]), (Waters, Wilmslow, UK) consisting of a binary solvent pump, an autosampler, a column oven and a backpressure regulator. The separations were performed using an Acquity UPC[2] BEH column (2.1 mm × 100 mm, 1.7 μm). The mobile phase consisted of (A) supercritical fluid CO_2 (scCO_2) and (B) methanol as organic modifier at a flow rate of 1.5 mL/min The gradient conditions are shown in Table 3-3. The column temperature and backpressure regulator (BPR) were set at 45 °C and 105 bar, respectively. The injection volume was 2 μL and methanol with 1% formic acid (v/v) used as make-up flow at a flow rate of 0.45 mL/min. The UHPSFC system was coupled to a single quadrupole mass spectrometer (SQD2) (Waters, Wilmslow, UK), and positive ion ESI mass

spectra were recorded using the following parameters: capillary voltage, 3.6 kV; cone voltage, 30 V; extractor voltage, 3 V; source temperature, 150 °C; desolvation temperature, 600 °C; desolvation gas flow, 1000 L/h; mass range m/z 110–600; scan duration, 0.1 s. Acquisition and data processing achieved using MassLynx™ version 4.1.

Table 3-3   UHPSFC gradient conditions for separation of FAMEs and their oxidation products

Time (min)	Mobile phase A %	Mobile phase B %	Flow rate (mL/min)
0.00	100	0	1.5
2.00	99	1	1.5
3.00	90	10	1.5
5.30	100	0	1.5

3.2.5   Gas chromatography-mass spectrometry (GC-MS)

70eV electron ionisation (EI) mass spectra were recorded using a Trace GC-MS (Thermo Finnigan, Manchester, UK) equipped with an Innowax capillary column (J & W Scientific, Berkshire, UK), 60 m × 0.25 mm i.d., 0.50 μm film thickness or HP Innowax capillary column, 30 m × 0.25 mm inner diameter, 0.25 μm film thickness. The stationary phase used was 100% polyethylene glycol (PEG). One μL samples were introduced *via* a splitless injector at a temperature of 240 °C. The oven temperature programme used was 40 °C for 4 min, ramped at a rate of 5 °C /min up to 240 °C for 16 min. Helium (He) was used as carrier gas at a constant flow rate of 1 mL/min The detector voltage was applied at 350 V. Positive ion EI mass spectra were recorded using the following parameters: mass range

m/z 20-510; scan rate, 2 scans/s. Each FAME component and their oxidation products was identified by comparison of the EI mass spectrum with a NIST Mass Spectral Library. Xcalibur™ software was used for control of the GC–MS and data acquisition.

3.2.6 Infusion Fourier transform ion-cyclotron resonance mass spectrometry (infusion FT-ICR MS)

Infusion FT-ICR MS measurements were performed using a 4.7 Tesla (T) Solarix mass spectrometer (Bruker Daltonics, UK). ESI infusion was performed using a syringe pump (Hamilton, UK) with the samples solution in methanol at a concentration of 1 mg/mL. The instrument was calibrated using a standard solution of diphenhydramine (monoisotopic mass: 255.1623 Da), oxybutynin (monoisotopic mass: 357.2304 Da), terfenadine (monoisotopic mass: 471.3137 Da), reserpine (monoisotopic mass: 608.2734 Da), erythromycin (monoisotopic mass: 733.4612 Da) and gramicidin_S (monoisotopic mass: 1140.7059 Da) mixed at a concentration of 1 µg/mL per component.

Positive ion ESI mass spectra were recorded using the following parameters: capillary voltage, -4 kV; drying gas flow rate, 4.0 L/min; drying gas temperature, 200 °C; mass range *m/z* 150–1500. Instrument control, data acquisition and handling were performed with Compass solariX control (Bruker Daltonics). For tandem mass spectrometry, the instrument was calibrated using a 1 µg/mL solution of reserpine (monoisotopic mass: 608.2734 Da). The collision energy was adjusted between 15-25 eV.

3.3 Analysis of antioxidant in fuels

2,6-Di-*tert*-butyl-4-methylphenol (BHT), (10 mg) was dissolved in methanol (10 mL) to give a stock solution of 1 mg/mL and then diluted to 10 µg/mL in methanol with 10% water (v/v) that was used as a standard solution.

3.3.1 Sample preparation

The aged samples were heated to 120 °C for 16 h. Each sample was diluted in methanol with 10% water (v/v) to give a final concentration of 1 µg/mL and analysed by EC-MS.

3.4 Experimental details for Chapter 5

3.4.1 Coconut methyl ester (CME) and rapeseed methyl ester (RME) stock solution preparation

Preparation of the stock solutions followed the defined protocol of IP585/10. Coconut and rapeseed FAME were used (covering a range of C8:0 to C18:3). 0.0100 g ± 0.0001 g of CME and RME respectively were dissolved in hexane to give a total mass of 10 g ± 0.05 g, *i.e.* standard solutions of 1000 mg/kg. These solutions were then diluted by a factor of two to give the nominal working solutions (500 mg/kg).

3.4.2 Calibration solution preparation

Calibration standards were prepared containing nominally 2, 4, 6, 8, 10, 20, 40, 60, 80 and 100 mg/kg of each FAME using volumetric dilution

of the working solution (500 mg/kg) in hexane and included a 10 μL aliquot of an internal standard solution (1,000 mg/L).

3.4.3   Internal standard solution preparation

Methyl heptadecanoate, C17:0 or methyl heptadecanoate, d_{33} (0.0100 g ± 0.0001g) was dissolved in hexane or dodecane (10 mL) to give a 1000 mg/L solution.

3.4.4   Sample preparation

AF-1 is a kerosene grade aviation fuel and this was used as a surrogate matrix for the standard solutions. A nominal 1000 mg/kg stock solution of CME and RME respectively was prepared by mixing each FAME (0.0100 g ± 0.0005 g) with AF-1 to give a total mass of 10 g ± 0.05 g. The samples were further diluted with AF-1 to give final solutions of 5 mg/kg CME or RME respectively. Commercially doped samples of AVTUR with FAME were supplied by the Energy Institute, and these samples were used neat and analysed by UHPSFC-MS and GC-MS respectively.

3.4.5   Gas chromatography-mass spectrometer (GC-MS)

Electron ionisation mass spectra (70 eV) were recorded using a TRACE GC-MS (Thermo Finnigan, Manchester, U.K.) equipped with an Innowax capillary column (J & W Scientific, Berkshire, U.K.), 60 m × 0.25 mm inner diameter, 0.50 μm film thickness, as demanded by IP585/10, the international reference method. One μL injections were made *via* a

splitless injector at a temperature of 260 °C. The oven temperature

programme used was 150 °C for 5 min, ramped at a rate of 12 °C/min to

200 °C for 17 min, then ramped at a rate of 3 °C/min to 252 °C, and held

at the final temperature for 6.5 min. Helium was used as the carrier gas at

a constant flow rate of 1 mL/min. Mass spectra were acquired between

m/z 20 and 510 at a scan rate of 2 scans/s. Each FAME component was

identified by comparison of the EI mass spectrum with a National Institute

of Standards and Technology (NIST) Mass Spectral Library. Xcalibur,

version 1.1, was used for control of the GC-MS and data acquisition.

3.4.6   High performance liquid chromatography-mass spectrometry (HPLC-MS)

The HPLC-MS system was described in 3.2.2. The mobile phase A

consisted of water with 0.1% formic acid (v/v), and mobile phase B

consisted of methanol with 0.1% formic acid (v/v). The HPLC gradient

conditions for analysis of FAMEs in AVTUR are shown in Table 3-4.

Table 3-4   The HPLC gradient conditions for analysis of FAMEs in AVTUR

Time (min)	Mobile phase A %	Mobile phase B %	Flow rate (mL/min)
0.00	30	70	0.3
10.00	0	100	0.3
16.00	0	100	0.3
16.01	30	70	0.5
20.00	30	70	0.5

3.4.7   Ultra high performance liquid chromatography-mass spectrometry (UHPLC-MS)

The UHPLC-MS system was described in section 3.2.3.The mobile phase A consisted of water with 0.1% formic acid (v/v), and mobile phase B consisted of methanol with 0.1% formic acid (v/v). The UHPLC gradient conditions for analysis of FAMEs in AVTUR are shown in Table 3-5. Methanol 10 mM sodium formate (HCOONa) was used as additive solvent at a flow rate of 50 µL/min.

Table 3-5   **The UHPLC gradient conditions for analysis of FAMEs in AVTUR**

Time (min)	Mobile phase A %	Mobile phase B %	Flow rate (mL/min)
0.00	30	70	0.6
2.50	0	100	0.6
3.00	0	100	0.6
4.00	30	70	0.6
5.00	30	70	0.6

3.4.8   Ultra high performance supercritical fluid chromatography-mass spectrometer (UHPSFC-MS)

Chromatography was performed using an Acquity ultra-performance convergence chromatograph (UPC[2]) (Waters, Wilmslow, UK) with CO_2 as the supercritical fluid. Different sub-2 µm particle size 3 mm × 100 mm packed columns (including BEH, HSS C18 SB, BEH-amide and HSS cyano) were investigated with a variety of organic modifiers (including methanol, acetonitrile, isopropanol and methanol with 25 mM ammonium acetate). The injection volume was 2 µL and samples were eluted at a flow rate of 1.5 mL/min. The column temperature was optimised in the range of 35-50 °C. The $scCO_2$ back pressure of the system was optimised and set to 105 bar. Methanol with 1% formic acid (v/v) was used as make-up flow at a flow rate of 0.45 mL/min.

Positive ion ESI mass spectra were recorded using a single quadrupole mass spectrometer (SQD2) (Waters, Manchester, UK) with the following conditions: capillary voltage 3.6 kV; cone voltage 30 V; extractor 3.0 V;

source temperature 150 °C; desolvation temperature 600 °C; desolvation

gas flow 1000 L/h; mass range of *m/z* 110–600; scan duration time of

0.1s providing 37.38 data points per peak and acquisition and data

processing achieved using MassLynx™ version 4.1.

3.4.8.1 Stationary phase

Four different UPC^2 stationary phase columns: Acquity BEH, Acquity

BEH-amide (100 mm × 3.0 mm, 1.7 µm), Acquity HSS cyano, Acquity HSS

C18 SB (100 mm × 3.0 mm, 1.8 µm) were obtained from Waters (Elstree,

UK). The chemical structure of all columns is represented in Figure 3-2.
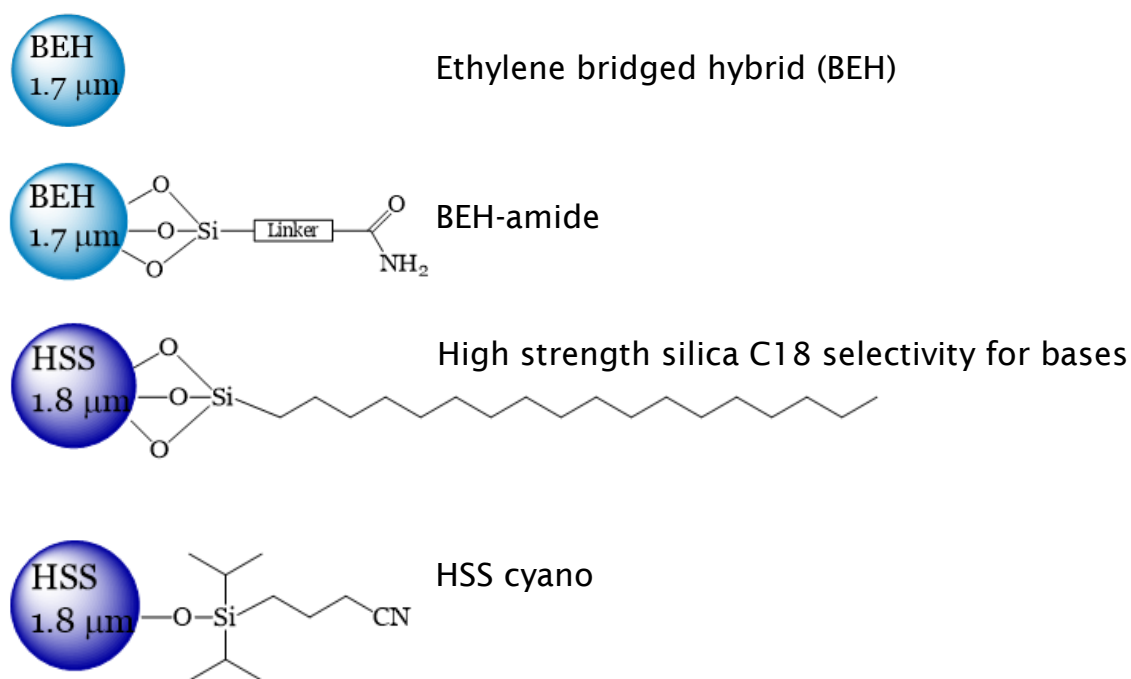
Figure 3-2 Chemical structure of the stationary phases used.

3.4.9 High performance liquid chromatography (HPLC)- Microsaic miniaturised mass spectrometer

The miniaturised MS system used was a HPLC (Agilent 1100 Series) coupled to a Microsaic miniaturised MS (Microsaic 4000 MiD®) (Microsaic Systems plc, Surrey, UK). The HPLC gradient conditions are shown in Table 3-6. The injection volume was 5 μL.

Table 3-6   The HPLC gradient conditions for analysis of FAMEs in AVTUR

Time (min)	Mobile phase A %	Mobile phase B %	Flow rate (mL/min)
0.00	30	70	1.0
10.00	0	100	1.0
16.00	0	100	1.0
16.01	30	70	1.0
20.00	30	70	1.0

Positive ion ESI mass spectra were recorded using the following parameters: capillary voltage, 850 V; vacuum interface voltage, 50 V; tube lens voltage, 10 V; plate lens voltage, 5 V; ion guide voltage, 1 V; mass range m/z 50–800. Samples were analysed and processed using Masscape® software.

Chapter 4:   Analysis of FAMEs oxidation

Biodiesel is a mixture of fatty acid methyl esters having different molecular structures with varying chain lengths, and levels of unsaturation. It is generally recognised that the following chemical aspects can have an impact on the oxidation stability of biodiesel. The oxidation process changes the physical chemistry properties of the fuel, and also forms the undesirable compounds. The primary compounds formed during the oxidation process are hydroperoxides.

For soy methyl ester (SME) and rapeseed methyl ester (RME), methyl oleate (C18:1), methyl linoleate (C18:2), and methyl linolenate (C18:3) are the three main unsaturated fatty acids undergoing degradation.

For example, methyl oleate (C18:1), initial hydrogen abstraction in the initiation reaction of auto-oxidation occurs at the allylic carbon-8 and carbon-11 to give two delocalised three-carbon allylic radicals (see, Figure . The further reaction with oxygen (O_2) forms a mixture of four allylic hydroperoxides containing the hydroperoxy groups on carbons 8, 9, 10 and 11.[155]
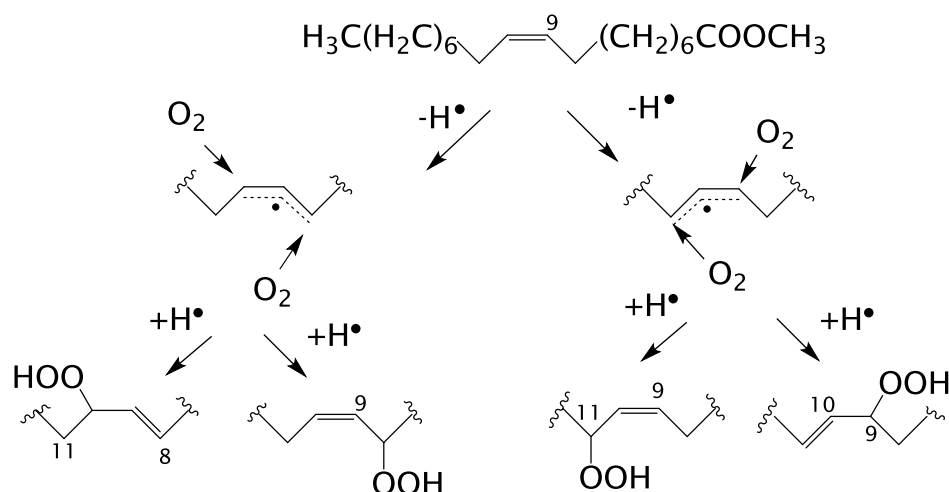
Figure 4-1   Mechanism of hydroperoxides formation in auto-oxidation of methyl oleate (C18:1).[155]

For methyl linoleate (C18:2) with two double bounds separated by a methylene group, hydrogen abstraction is more favoured because there is a methylene group that is doubly activated by two adjacent double bonds. Hydrogen abstraction takes place at the carbon-11 position, giving rise to a hybrid pentadienyl radical effectively stabilised by resonance, which reacts with oxygen at the carbon-9 and carbon-13 positions to produce a mixture of two major conjugated diene 9- and 13-hydroperoxides, see Figure 4-2 and Figure 4-3 for methyl linoleate (C18:2) methyl linolenate (C18:3), respectively.
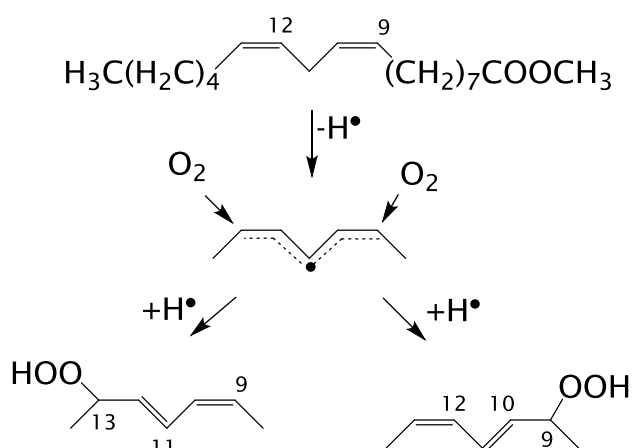
Figure 4-2   Mechanism of hydroperoxides formation in auto-oxidation of methyl linoleate (C18:2).[155]
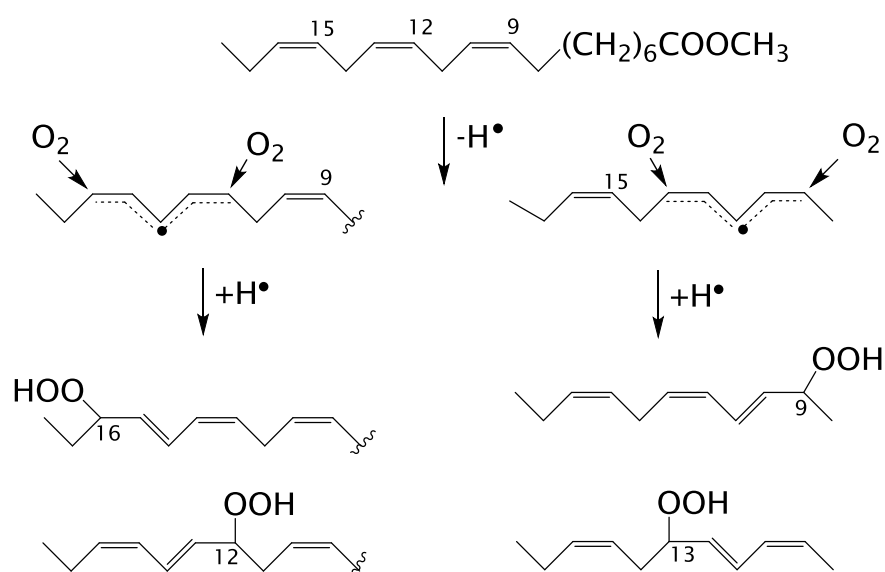
Figure 4-3   Mechanism of hydroperoxides formation in auto-oxidation of methyl linolenate (C18:3).[155]

The isomeric structures of hydroperoxides formed in the auto-oxidation of methyl oleate (C18:1), methyl linoleate (C18:2), and methyl linolenate (C18:3) are shown in Table 4-1. Methyl oleate (C18:1) and

methyl linolenate (C18:3) give four hydroperoxides by auto-oxidation, only

two hydroperoxides from methyl linoleate (C18:2).[78][156]

Table 4-1   Hydroperoxides positional isomers of methyl oleate (C18:1), methyl linoleate (C18:2) and methyl linolenate (C18:3) by auto-oxidation[78][156]

Fatty acid methyl ester	Hydroperoxides positional isomers of FAMEs
Systematic name: Methyl (9*Z*)-9 octadecenoate Common name: Methyl oleate (C18:1)	8-OOH, 9-OOH, 10-OOH, 11-OOH
Systematic name: Methyl (9*Z*,12*Z*)-9,12-octadecadienoate Common name: Methyl linoleate (C18:2)	9-OOH, 13-OOH
Systematic name: Methyl (9*Z*,12*Z*,15*Z*)-9,12,15-octadecatrienoate Common name: Methyl linolenate (C18:3)	9-OOH, 13-OOH, 12-OOH, 16-OOH

Hydroperoxides usually decompose and crosslink to form various

secondary oxidation products including aldehydes, ketones, epoxides,

hydroxy compounds, oligomers and polymers. The oxidation products

formed may cause damage to engines, such as corrosion of the metal

parts of the systems, degradation of the physical properties of the

elastomers, and blockage in the fuel injection nozzles and filters. The

decomposition pathway of hydroperoxides is a homolytic cleavage

between oxygen and the oxygen bond to give an alkoxy and hydroxyl

radicals.[157,158] The alkoxy radical then undergoes homolytic β-scission of

the carbon-carbon bond and formed oxo-compounds and saturated or unsaturated alkyl radicals.[157,158] This mechanism leads to the formation of a major of the volatile compounds.

Currently, the standard reference method EN 14112 is the Rancimat method which is an accelerated oxidation test that directly measures oxidation stability of FAMEs.[159] This method measures the induction period (IP), which is determined when a rapid increase in the volatile secondary oxidation products is seen and can produce chemicals such as formic acid. In advanced steps of the oxidation process, both volatile and non-volatile compounds can be formed. However, this method does not provide detailed information about the oxidation products. The evaluation of the oxidation products formed from biodiesel usually requires the application of more than one analytical method.

GC-MS has been successfully used to identify volatile oxidation products during biodiesel storage.[160–163]Due to the limited thermal stability of non-volatile compounds, GC-MS is not an appropriate technique for the analysis of the non-volatile products formed in biodiesel. Alternatively, HPLC can be used to separate these oxidation products. Normal phase HPLC-UV methods have been used to detect the conjugated diene structure of the oxidation products of linoleic acid (C18:2).[75][164] Due to the absence of conjugated double bonds, oxidation compounds of oleic acid (C18:1) cannot be detected in the NP-HPLC-UV analysis.[74]

NP-HPLC coupled to two detectors in series, UV and evaporative light scattering detector (ELSD) has been used for successful analysis of

oxidation products of FAME.[73,74] Moreover, non-volatile oxidation products can be detected by mass spectrometry which is a universal detector and provides very sensitive detection. In fuel samples, the oxidation products may be present at low concentrations which can be detected by MS. In addition, MS detection has the advantage that it can provide structural information and determine the elemental composition of the analytes detected.

NP-HPLC-MS using positive ion ESI source has also been used for analysis of non-volatile oxidation products of lipid.[165] Additionally, RP-HPLC thermospray-mass spectrometry (RP-HPLC–TSP-MS) has been used for detection of oxidation products of polyunsaturated-fatty acids.[166] HPLC–tandem mass spectrometry (HPLC-QqQ-MS) was used to identify and quantify the nonpolar aldehydes/ketones in oxidised oil samples.[167] Easy ambient sonic-spray ionisation mass spectrometry (EASI-MS) has been also used for monitoring oxidation of biodiesel.[84][168][169]

The objectives of this project are to separate and identify the oxidation products formed during the oxidation process of rapeseed methyl ester (RME) and soy methyl ester (SME) samples under auto-oxidation conditions compared to accelerated oxidation using electrochemistry-mass spectrometry (EC-MS). The aim is to develop methods including EC-MS, infusion electrospray ionisation-mass spectrometry (ESI-MS), ultra high performance supercritical fluid chromatography-mass spectrometry (UHPSFC-MS), high performance liquid chromatography-mass spectrometry (HPLC-MS), ultra high performance

liquid chromatography-mass spectrometry (UHPLC-MS), ultra high performance liquid chromatography-high resolution mass spectrometry (UHPLC-HR MS) methods with different mass spectrometers such as single quadrupole (SQ), quadrupole-time of flight (Q-TOF) and Fourier transform-ion cyclotron resonance (FT-ICR) for the separation and the identification of the oxidation species.

4.1 Oxidised FAMEs using the electrochemical cell

Here the performance of magic diamond (MD) and glassy carbon (GC) electrodes were investigated. The effect of different electrode potentials on the oxidation of FAMEs was also studied. The oxidation products occurring at the electrode surfaces were monitored by ESI-QTOF MS.

4.1.1 The performance of magic diamond (MD) and glassy carbon (GC) working electrodes

The same selected potential of 2.5 V was applied to the MD and GC electrodes to generate oxidation products of C18:1, C18:2 and C18:3 FAME. An example of extracted ion current chromatogram (EICC) of *m/z* 317 corresponding to the sodiated methyl linoleate (C18:2) is shown in Figure 4-4 (A). The signal intensity of the ion at *m/z* 317 from the GC electrode falls to 50% of its initial value while the MD electrode falls to 0% of its initial value. The range of oxidation products formed on the GC and MD electrodes at EC cell potential off and EC potential on is presented in Figure 4-4 (B) to Figure 4-4 (E).
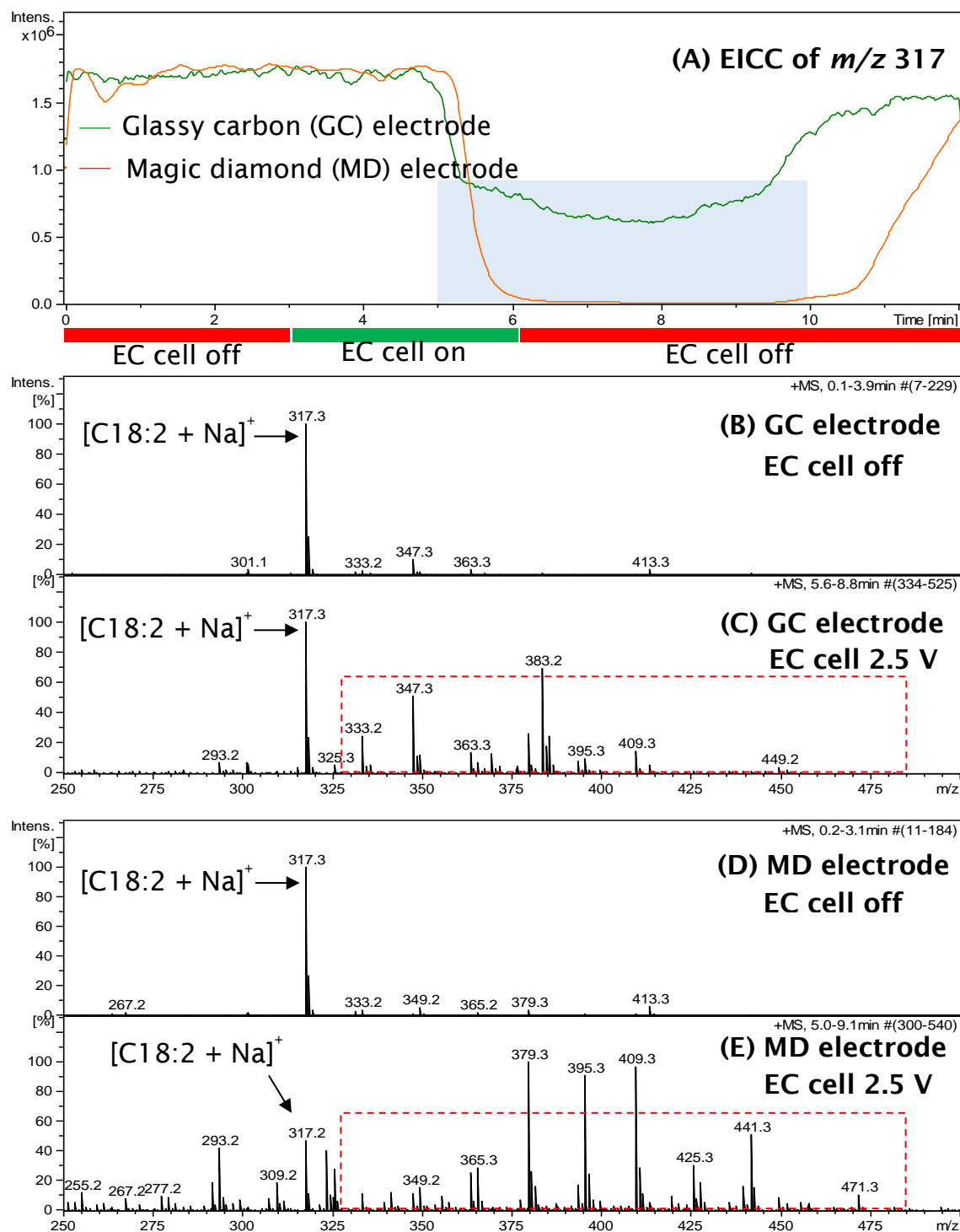
Figure 4-4   (A) EICCs of C18:2 (*m/z* 317) at EC cell on potential of 2.5 V applied on the GC and MD electrodes. (B) to (E) showing ESI mass spectra corresponding to the blue area from (A).

The presence of products with a mass increase of 16 Da compared to $[C18:2 + Na]^+$ indicates the formation of oxygenated compounds *via* addition of an oxygen (O) atom to the structure of the FAME, but at an unknown location within the molecule, though expected to initially be at a site of unsaturation.

The same potential (2.5 V) was applied to both electrodes for generation of oxidation products of C18:1 and C18:3. Figure4-5 compares the number of oxidised C18:1, C18:2 and C18:3 compounds formed on the MD and GC electrodes. The results indicated that the gross amount of the oxidation products formed using the MD electrode was much higher than when the GC electrode was used.
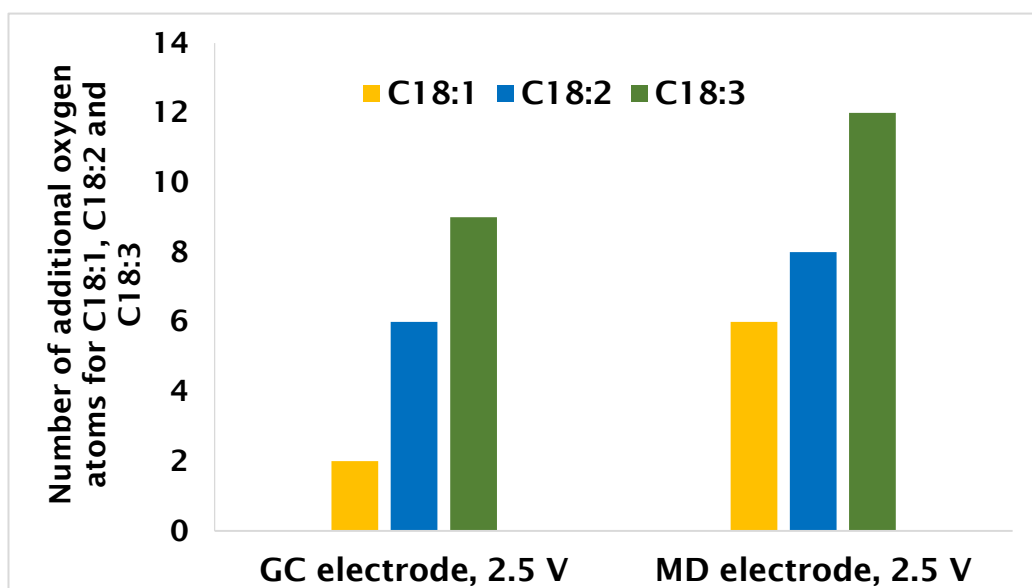
Figure 4-5   Comparison of number of additional oxygen atoms for C18:1, C18:2 and C18:3 from the GC and MD working electrodes at the EC cell potential of 2.5 V.

4.1.2 The effect of working electrode potential on FAMEs oxidation

Different EC cell potentials between 0.5-2.5 V and 0.5-3.0 V were applied to the GC and the MD working electrodes, respectively. C18:2 was used to determine the optimal potential for maximal conversion. The EICCs of the sodiated C18:2 molecule (m/z 317) were compared under varying potentials applied to the MD working electrode as shown in Figure 4-6. The signal intensity of C18:2 reduced with higher potentials, a significant drop in response is observed after 2.0 V. A potential increase in the electrochemical cell leads to oxidised C18:2 and results in a decrease in signal of the ion corresponding to the parent compound (m/z 317). The maximal conversion of C18:2 occurred at 3.0 V for the MD working electrode and led to a gradual decrease of sodiated C18:2 signal to zero. Oxidation potentials of 3.0 V and 2.5 V were the optimal potentials for the MD and GC working electrodes, respectively and so were used to generate the oxidation products of C18:1, C18:2 and C18:3.
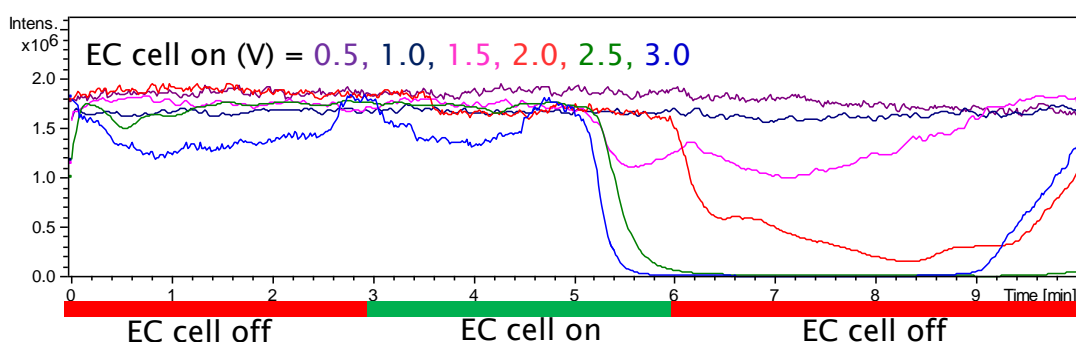
Figure 4-6 **EICCs of sodiated C18:2 (*m/z* 317) at different potentials applied using the MD working electrode, EC cell 0.5 V (purple), EC cell 1.0 V (blue), EC cell 1.5 V (pink), EC cell 2.0 V (red), EC cell 2.5 V (green), and EC cell 3.0 V (light blue).**

Examples of mass spectra of sodiated C18:2 at different potentials of 0, 1.0, 2.0 and 3.0 V for MD working electrode are presented in Figure 4-7. Oxidation products of C18:2 were not observed if the EC cell potential was off (Figure 4-7 (A)). The drop of response of the parent compound C18:2 (sodiated C18:2; m/z 317) in Figure 4-7 is attributed to the oxidation of C18:2 in the EC cell as indicated by the presence of oxidation products in the respective mass spectra with a mass increase of 16 Da in series, for instance, m/z 333, 349 and 365.

When potentials greater than 2.0 V were applied, a progressive decrease of the parent compound signal with a related increase of the $[C18:2 + Na + n16]^+$ products was observed (see Figure 4-7 (D)).

(A) MD electrode, EC cell off
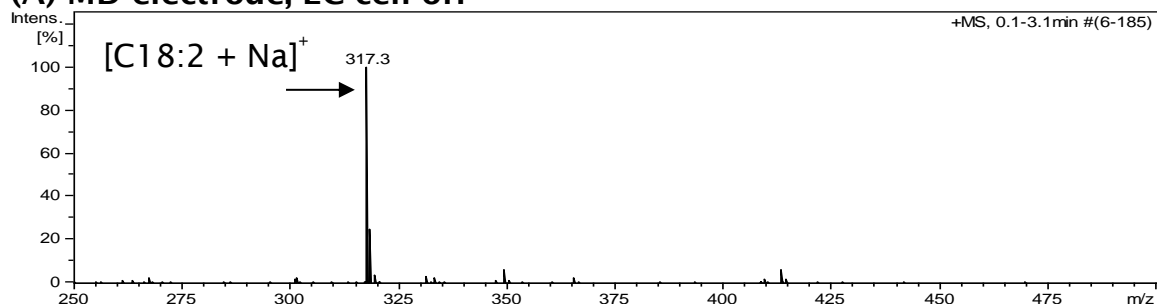
(B) MD electrode, EC cell 1.0 V
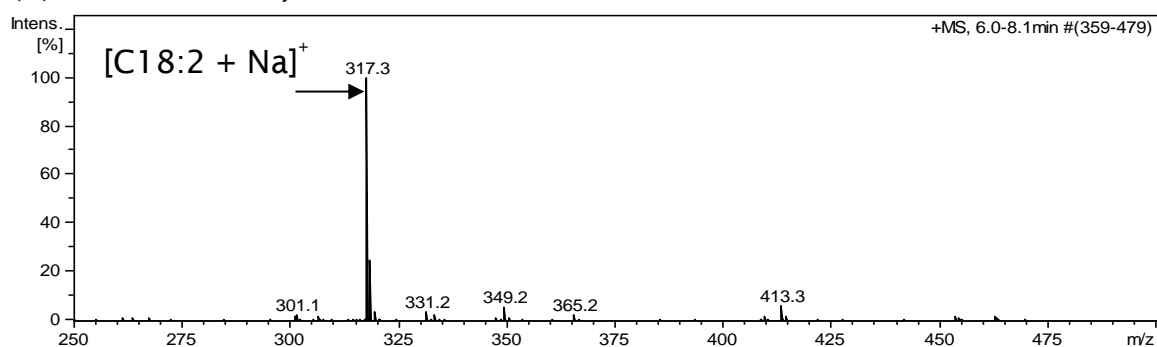
(C) MD electrode, EC cell 2.0 V
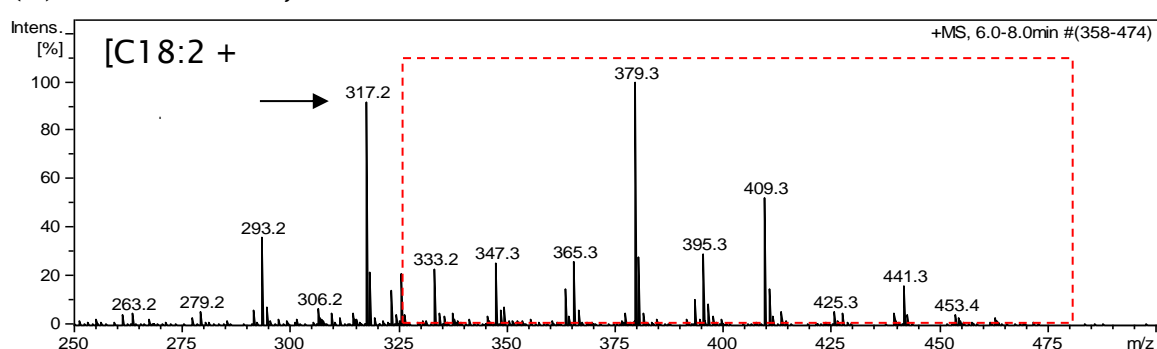
(D) MD electrode, EC cell 3.0 V
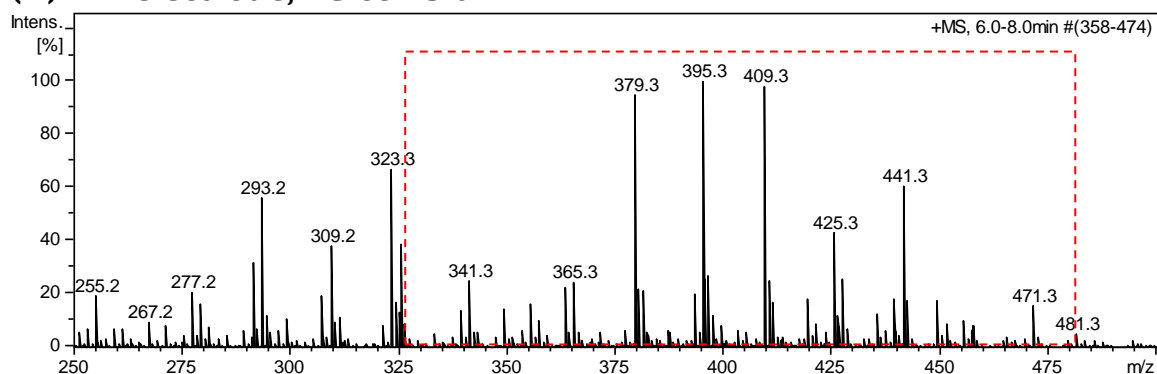
Figure 4-7   ESI mass spectra of C18:2 and its oxidation products obtained (in the red line boxes) at the different potentials applied to the MD working electrode.

In all cases, the products formed in the EC cell showed an increase in mass by 16 Da indicating that the addition of an oxygen atom occurs somewhere in the FAMEs. The examples of EICCs and mass spectra of sodiated C18:1, C18:2 and C18:3, together with their oxidation products formed during the electrochemical process are shown in Figure 4-8 to Figure 4-10. The number of oxidation products increased in the order C18:1 < C18:2 < C18:3 for both MD and GC electrodes.

(A) EICCs of *m/z* 319 and 349
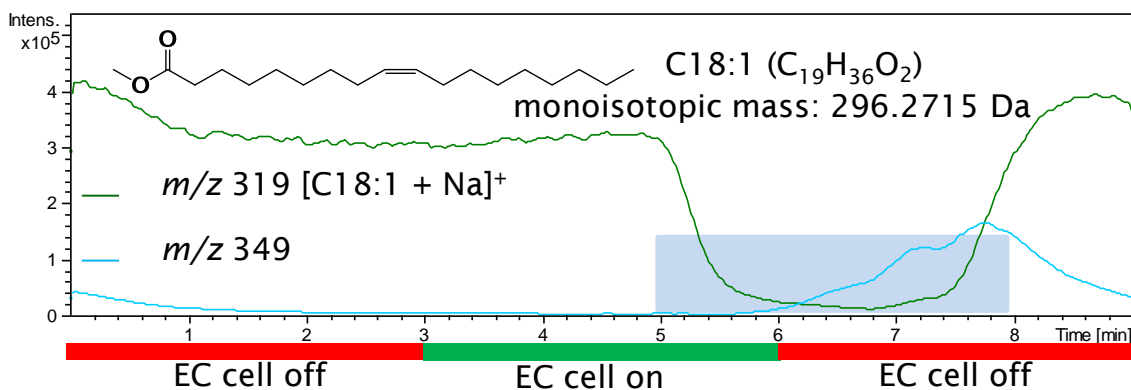
(B) ESI-MS mass spectra, MD electrode, EC cell on 2.5 V
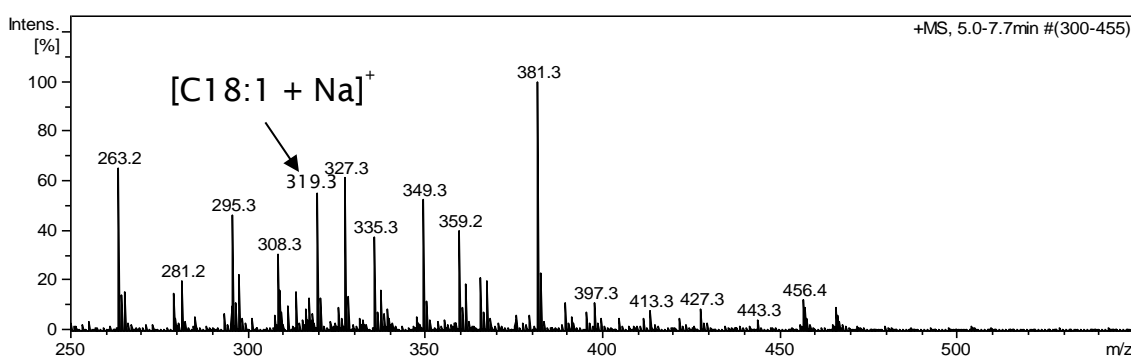
Figure 4-8 **(A) EICCs of sodiated C18:1 (*m/z* 319) and its oxidation product (*m/z* 349) using the MD working electrode, EC cell potential of 3.0 V. (B) positive ion ESI mass spectra corresponding to the blue area (A) showing the ion values (in the red line box) occurred in the EC cell on.**

(A) EICCs of *m/z* 317 and 379

EC cell off   EC cell on   EC cell off
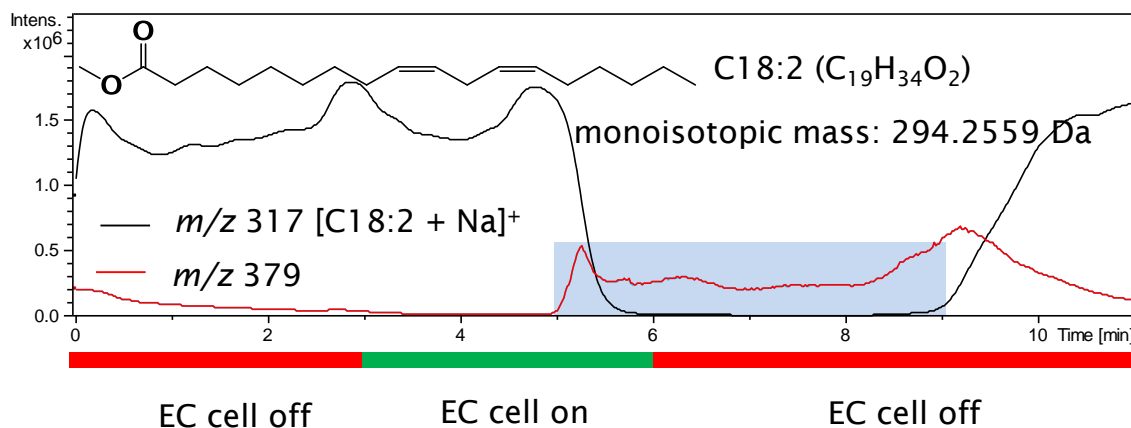
(B) MD electrode, EC cell on 2.5 V
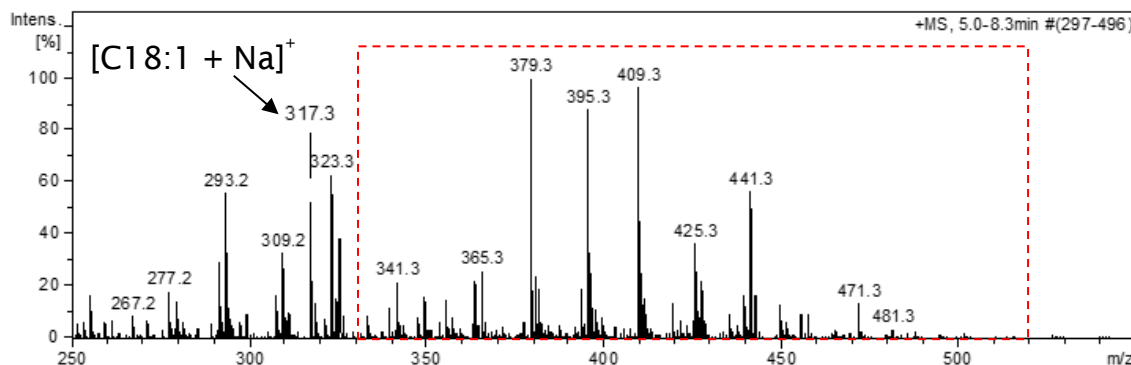
Figure 4-9   **(A) EICCs of sodiated C18:2 (*m/z* 317) and its oxidation product (*m/z* 379) using the MD working electrode, at the EC cell potential of 3.0 V. (B) positive ion ESI mass spectra corresponding to the blue area (A) showing the ion values (in the red line box) occurred in the EC cell on.**

(A) EICCs of *m/z* 315 and 393
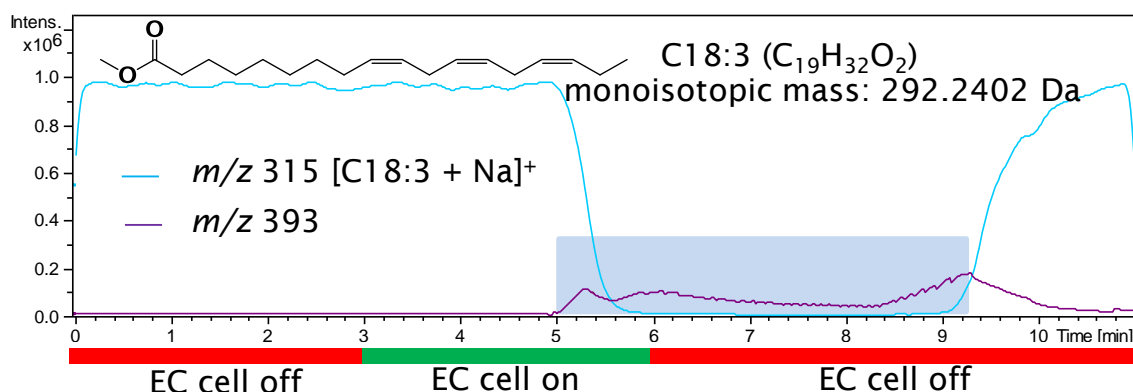
(B) MD electrode, EC cell on 2.5 V
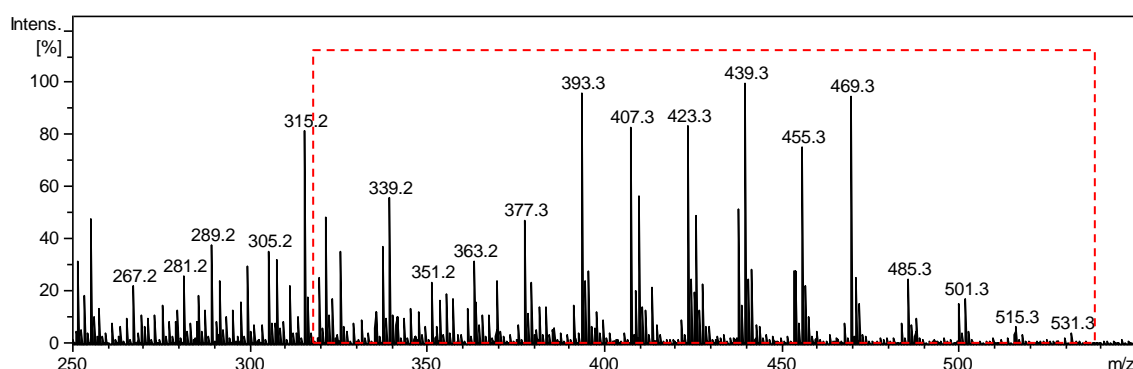
Figure 4-10   (A) EICCs of sodiated C18:3 (*m/z* 315) and its oxidation product (*m/z* 393) using the MD working electrode, the EC cell potential of 3.0 V. (B) Positive ion ESI mass spectra corresponding to the blue area (A) showing the ion values (in the red line box) occurred in the EC cell on.

4.1.3   Electrochemical oxidation of RME and SME samples

Electrochemical (EC) oxidation has been used as a surrogate system for inducing and monitoring oxidation for rapeseed methyl ester (RME) and soy methyl ester (SME). This was performed by applying the optimal potentials for the formation of oxidation products using both GC (2.5 V) and MD (3.0 V) working electrodes (see, Figure 4 11 to Figure 4 14) show mass spectra of RME and SME samples correspond to without and with

Chapter 4: Analysis of FAME oxidation

potential applied to the GC and MD electrodes. The mass spectra of RME and SME with the EC cell potential off shows the major ions of m/z 315 [C18:3 + Na]$^+$, 317 [C18:2 + Na]$^+$ and 319 [C18:1 + Na]$^+$ which are identical to the ESI-MS profiles of RME and SME. The ions of m/z 331/333/335/, m/z 347/349/351, m/z 361/363/365, m/z 379 $etc.$, with low intensity were also observed when the EC was cell off (see, Figure 4-11 (A), Figure 4-12 (A), Figure 4-13 (A) and Figure 4-14 (A)). This occurred as a result of oxidation of RME and SME under auto-oxidation, due to the RME and SME samples being kept for over one year prior to this analysis.

Figure 4-11 (B), Figure 4-12 (B), Figure 4-13 (B), and Figure 4-14 (B) show the results obtained when the following potentials were applied to the EC cell 2.5 V (GC working electrode) and 3.0 V (MD working electrode) for the RME and SME samples. The same ions of m/z 331/333/335/, m/z 347/349/351, m/z 361/363/365, m/z 379, $etc.,$ and new m/z values were also observed (m/z 377/379, m/z 391/393/395, m/z 407/409, m/z 423/425/427, m/z 437/439/441, m/z 453/455, m/z 469, m/z 483,485, m/z 499, 501, and m/z 515 compared to the EC cell off.

(A) RME, GC electrode, EC cell off
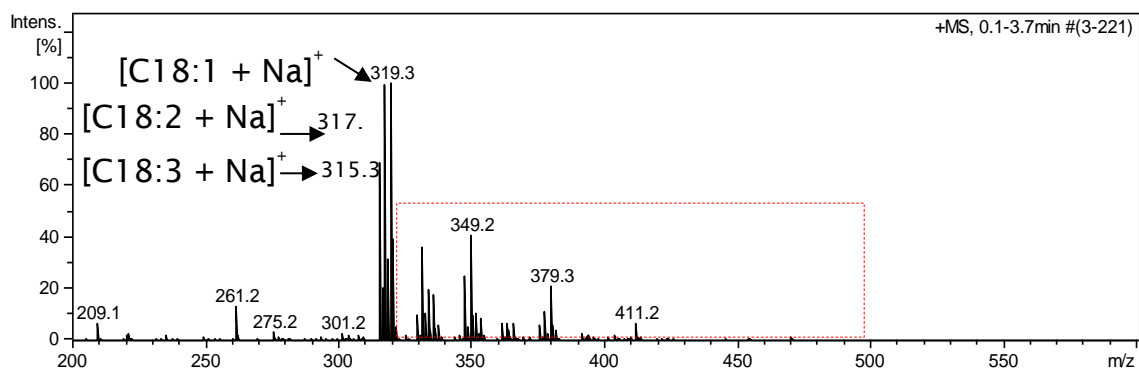
(B) RME, GC electrode, EC cell 2.5 V
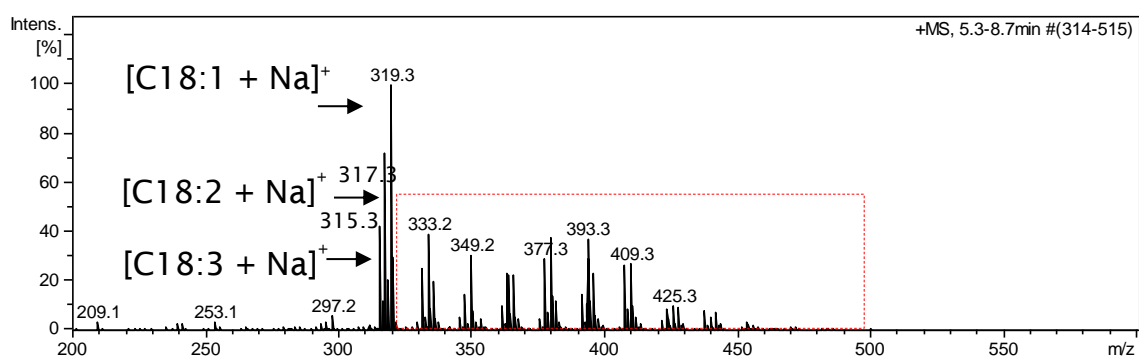
Figure 4-11   Positive ion ESI mass spectra of rapeseed methyl ester (RME) and its oxidation products (in the red line boxes) using the GC working electrode. (A) EC cell potential off, (B) EC cell potential of 2.5 V.

(A) RME, MD electrode, EC cell off
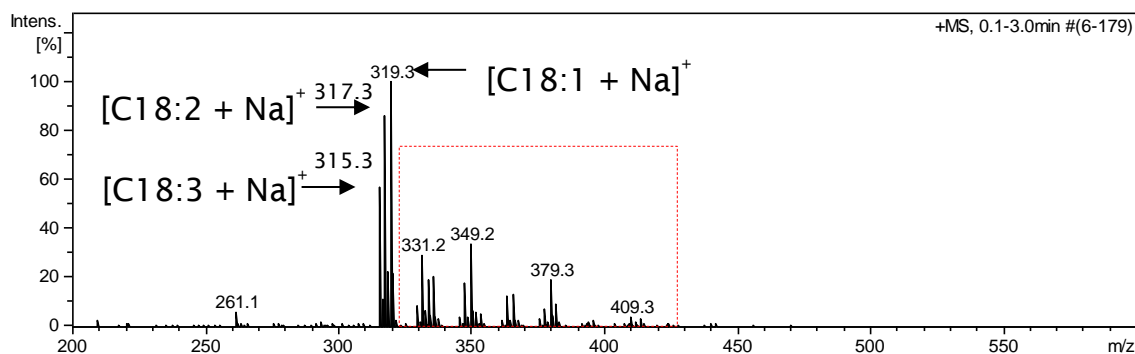
(B) RME, MD electrode, EC cell 3.0 V
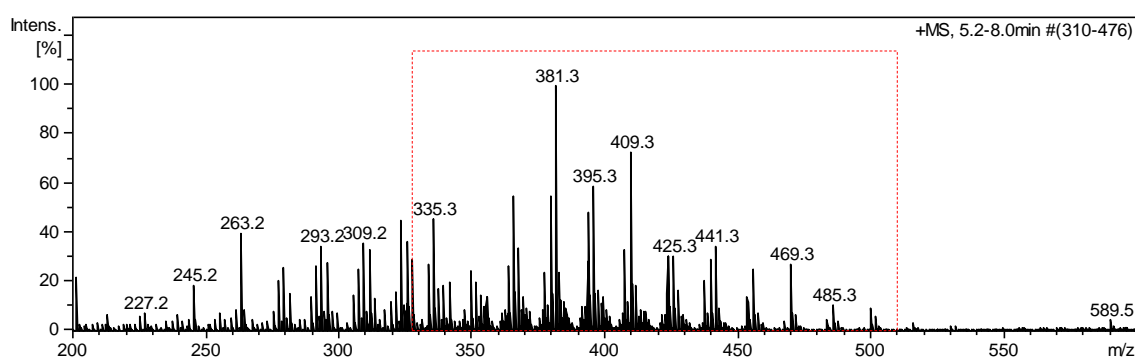
Figure 4-12   Positive ion ESI mass spectra of rapeseed methyl ester (RME) and its oxidation products (in the red line boxes) using the magic diamond (MD) working electrode. (A) at the EC cell potential off, (B) at the EC cell potential of 3.0 V.

(A) SME, GC electrode, EC cell off
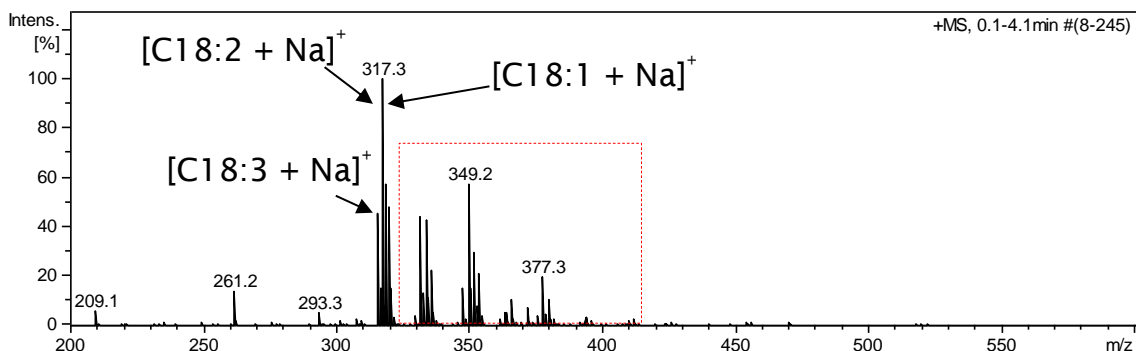
(B) SME, GC electrode, EC cell 2.5 V
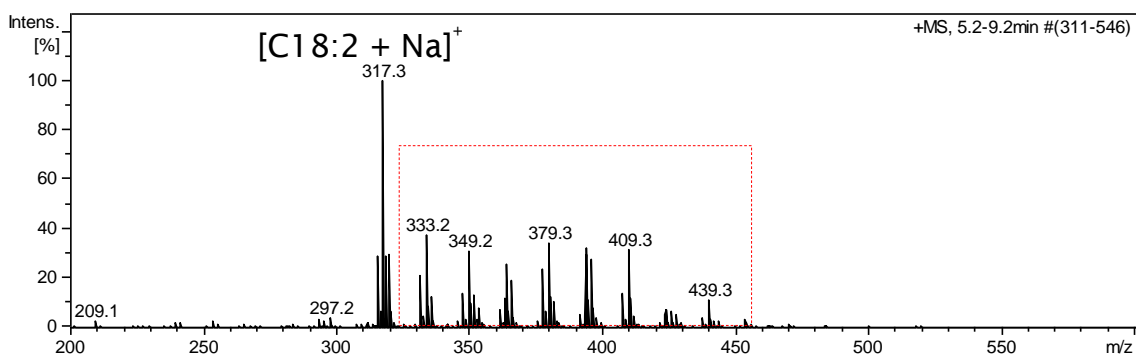
Figure 4-13   Positive ion ESI mass spectra of soy methyl ester (SME) and its oxidation products (in the red line boxes) using the glassy carbon (GC) working electrode. (A) At the EC potential off, (B) at the EC cell potential of 2.5 V.

(A) SME, GC electrode, EC cell off
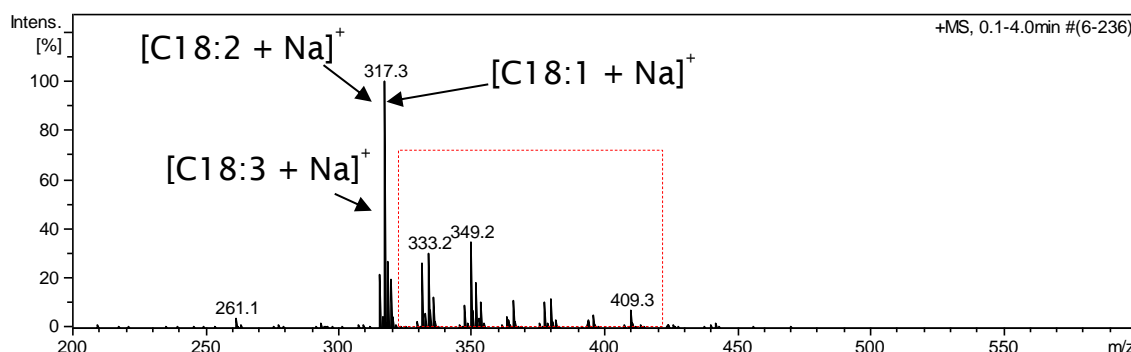
(B) SME, GC electrode, EC cell 2.5 V
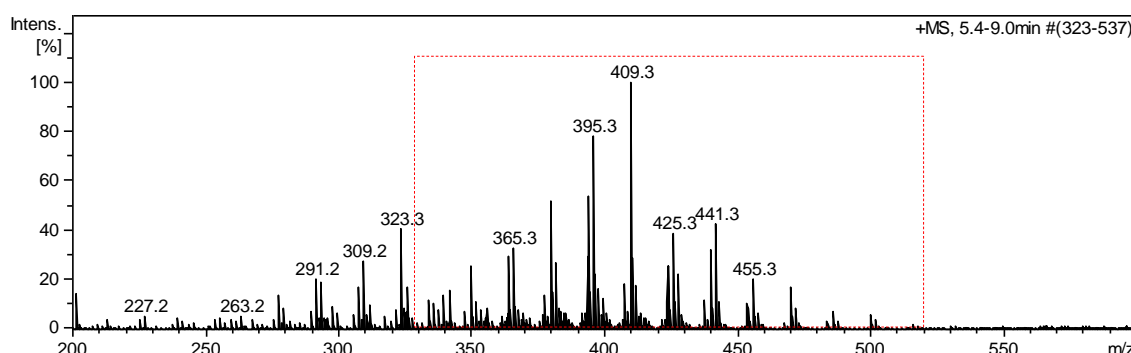
Figure 4-14   Positive ion ESI mass spectra of soy methyl ester (SME) and its oxidation products (in the red line boxes) using the MD (A) at the EC cell potential off, (B) at the EC potential of 2.5 V.

As expected from the results obtained in electrochemical cell of RME and SME, the ions of *m/z* 333, 333 and 335 [FAME + O + Na]$^+$ were detected by ESI-MS and estimated as epoxide-FAME or hydroxyl-FAME or keto-FAME. They have been identified as oxidation products of the autoxidised FAME.[170][171] The ions of *m/z* 347, 349, 351 correspond to [FAME + 2(O) + Na]$^+$, they were expected as hydroperoxides of FAMEs, which are primary oxidation products of methyl linolenate (C18:3), methyl linoleate (C18:2) and methyl oleate (C18:1), respectively. They have been found in oxidised biodiesel and analysed by ambient-ionisation mass

spectrometry.[168][169] The ions of *m/z* 361, 363 and 365 that probably correspond to [FAME + 3 (O) + Na]$^+$. The ion of *m/z* 379 expected as [FAME + 4(O) + Na]$^+$ that the ion may be hydroperoxy-cyclic peroxides of FAME[83] or dihydroperoxides FAME.[168] These compounds have been reported from autoxidised methyl linoleate (C18:2).[83] Other ions of *m/z* 391/393/395, *m/z* 407/409, *m/z* 423/425/427, *m/z* 437/439/441, *m/z* 453/455, *m/z* 469, *m/z* 483/485, *m/z* 499/501, and *m/z* 515 were also observed in EC cell for RME and SME samples.

In summary, the electrochemical oxidation has been applied for the investigation and monitoring of FAME oxidation in a very short time period (~10 min) compared to storage stability (over one year).[172] The magic diamond (MD) working electrode was investigated as the working electrode in comparison to the glassy carbon (GC) working electrode. The ions at *m/z* 331, 333 and 335 estimated as epoxide-FAME or hydroxyl-FAME or keto-FAME. The ions of *m/z* 347, 349, 351 correspond to [FAME + 2(O) + Na]$^+$, they were expected as hydroperoxides of FAMEs, which are primary oxidation products of methyl linolenate (C18:3), methyl linoleate (C18:2) and methyl oleate (C18:1), respectively. The ions of *m/z* 361, 363 and 365 that probably correspond to [FAME + 3 (O) + Na]$^+$. The ions of *m/z* 379 may correspond to bis-hydroperoxides. Increasing the oxidation potential of the GC working electrode up to 2.5 V generated oxidation products of C18:1, C18:2 and C18:3 with addition of oxygen (O) atom up to +2(O), +6(O), and +9(O) atoms respectively, while the maximum number of additional oxygen atoms for C18:1, C18:2 and C18:3 was +8(O), +10(O),

and +14(O) respectively, from the MD working electrode at 3.0 V. For all experiments, the intensity of parent compounds (C18:1, C18:2, C18:3) was clearly reduced upon EC oxidation, whereas the *m/z* of oxidation products, for example *m/z* 331/333/335/, *m/z* 347/349/351, *m/z* 361/363/365, *m/z* 379, *etc.*, increased with increased EC potential. Both the working electrodes were well suited for generating FAME oxidation products with the MD working electrode affording higher oxidation products *cf.* the GC working electrode. The oxidation potentials increased in the order methyl esters of C18:3 < C18:2 < C18:1 for both MD and GC working electrodes.

4.2   Analysis of FAMEs oxidation using UHPSFC-MS

The aim of the this work was to develop and optimise UHPSFC-MS for separation of the different groups of oxidation products formed during FAMEs oxidation. Positive ion ESI source coupled to a single quadrupole mass spectrometry was used to identify the different groups of oxidation products present. FAMEs and their oxidation products were separated using an Acquity UPC^2 BEH column (2.1 mm × 100 mm, 1.7 μm) with a gradient elution of organic modifier (0-10% methanol) within 5 min

Figure 4-15 shows the separation of non-oxidised FAMEs, eluted between retention times of 0.95–1.25 min, whereas expected oxidised FAME species eluted between retention times of 2.28-3.32 min. The elution order of unsaturated FAMEs on a polar column depends on the chain lengths and the number of double bonds in the fatty acid chain. The retention times (t_R) of methyl oleate (C18:1) (t_R = 0.95), methyl linoleate

(C18:2) (t_R = 1.08) and methyl linolenate (C18:3) (t_R = 1.25), increased with increasing number of double bonds. These results suggest a strong interaction between the unsaturated groups and silanols on the surface of the stationary phase.[173] The positive ion ESI mass spectra of methyl oleate (C18:1), methyl linoleate (C18:2) and methyl linolenate (C18:3) were detected as protonated molecules $[M + H]^+$ at *m/z* 297, 295, and 293 and sodiated molecules $[M + Na]^+$ at *m/z* 319, 317, and 315 for C18:1, C18:2, and C18:3, respectively.
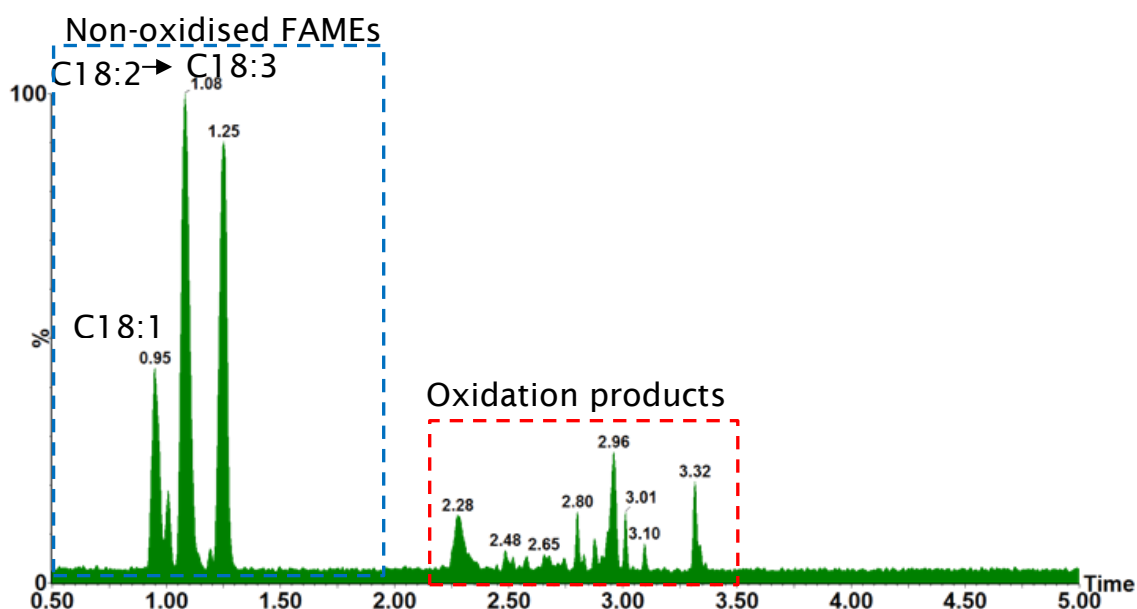
Figure 4-15   Base peak ion current chromatograms (BPICCs) of rapeseed methyl ester (RME) and the oxidation products using UHPSFC-MS analysed using the BEH column 1.7 μm 3 mm × 100 mm. Chromatographic conditions: scCO$_2$ pressure 105 bar; column temp 45 °C; gradient 0-10% MeOH in CO$_2$ at 1.5 mL/min in 5 min.

Chapter 4: Analysis of FAME oxidation

As expected, the oxidation products are oxygenated compounds by the addition of oxygen atoms to FAME molecules as [FAME + nO]. The sequential elution order of oxidation products from a silica column are according to polarity, the more polar oxidation products were strongly retained on the silica column. The addition of one oxygen atom to FAME [FAME + 1(O) + Na]$^+$ such as epoxy, keto and hydroxyl-FAMES are eluted earlier than an increasing number of oxygen atoms such as [FAME +2(O) + Na]$^+$ such as hydroperoxides. These show the oxidation products of FAMEs functionalised with one, two, three and four oxygen atoms (see, Figure 4-16).

(A)

Methyl *cis*-9,10-epoxystearate

(B)

Methyl (9E,11E)-13-oxooctadeca-9,11-dienoate

(C)

Methyl (9E,11E)-13-hydroxyoctadeca-9,11-dienoate

(D)

Methyl (9E,11E)-13-hydroperoxyoctadeca-9,11-dienoate
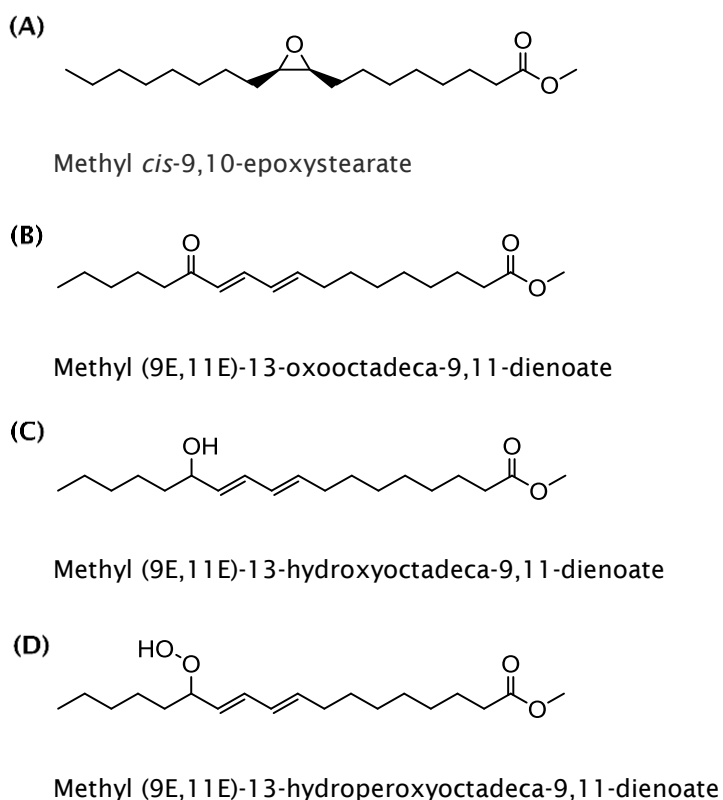
Figure 4-16   Chemical structures of some oxidation products of FAMEs, showing the addition of one oxygen atom to FAME, and (D) two oxygen atoms to FAME.

Reconstructed ion current chromatograms of *m/z* 335 (FAME + 1(O) + Na]+,

m/z 349 [FAME + 2(O) + Na]+, *m/z* 365 [FAME + 3(O) + Na]+ and *m/z* 379

[FAME+ 4(O) + Na]+ are shown in Figure 4-17. A single quadrupole mass

spectrometry cannot distinguish between the same molecules that have

the same molecular mass (isobaric compounds).
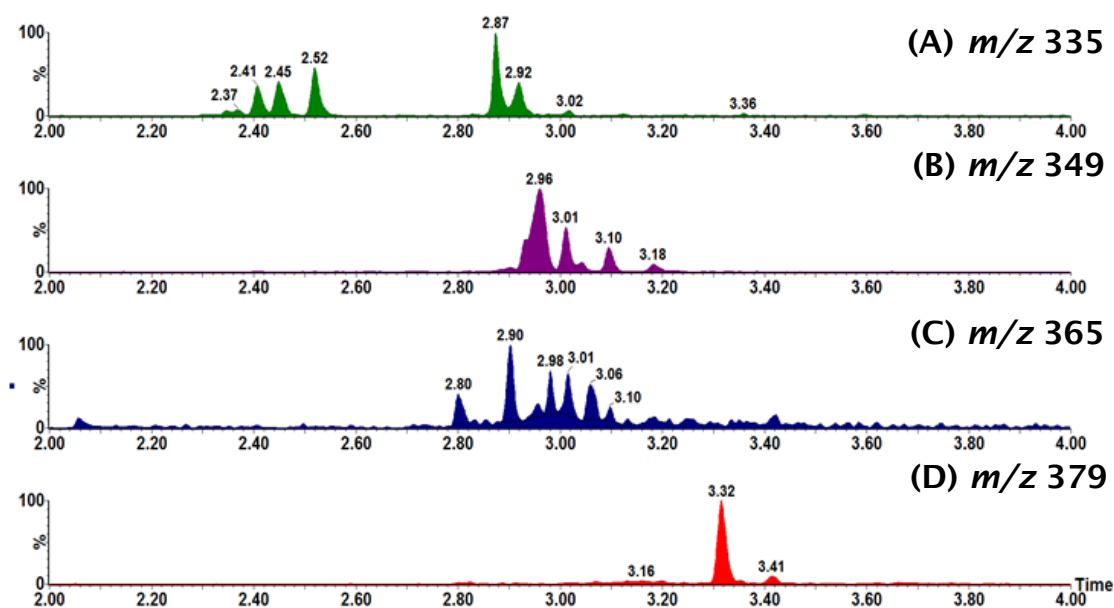
**Figure 4-17   RICCs of *m/z* 335 (FAME + 1(O) + Na]+ (A); *m/z* 349 [FAME
+ 2(O) + Na]+ (B); *m/z* 365 [FAME + 3(O) + Na]+ (C) and *m/z* 379
[FAME + 4(O) + Na]+ (D).**

Figure 4-18 (A) shows the chromatograms of isobaric compounds,

which have different retention time (t_R) of 2.96, 3.01, 3.10 and 3.18 min

respectively. Focusing on Figure 4-18 (B)-(E) which show the RICCs of the

ion at *m/z* 349 show the presence of four peaks each showing similar

mass spectra.
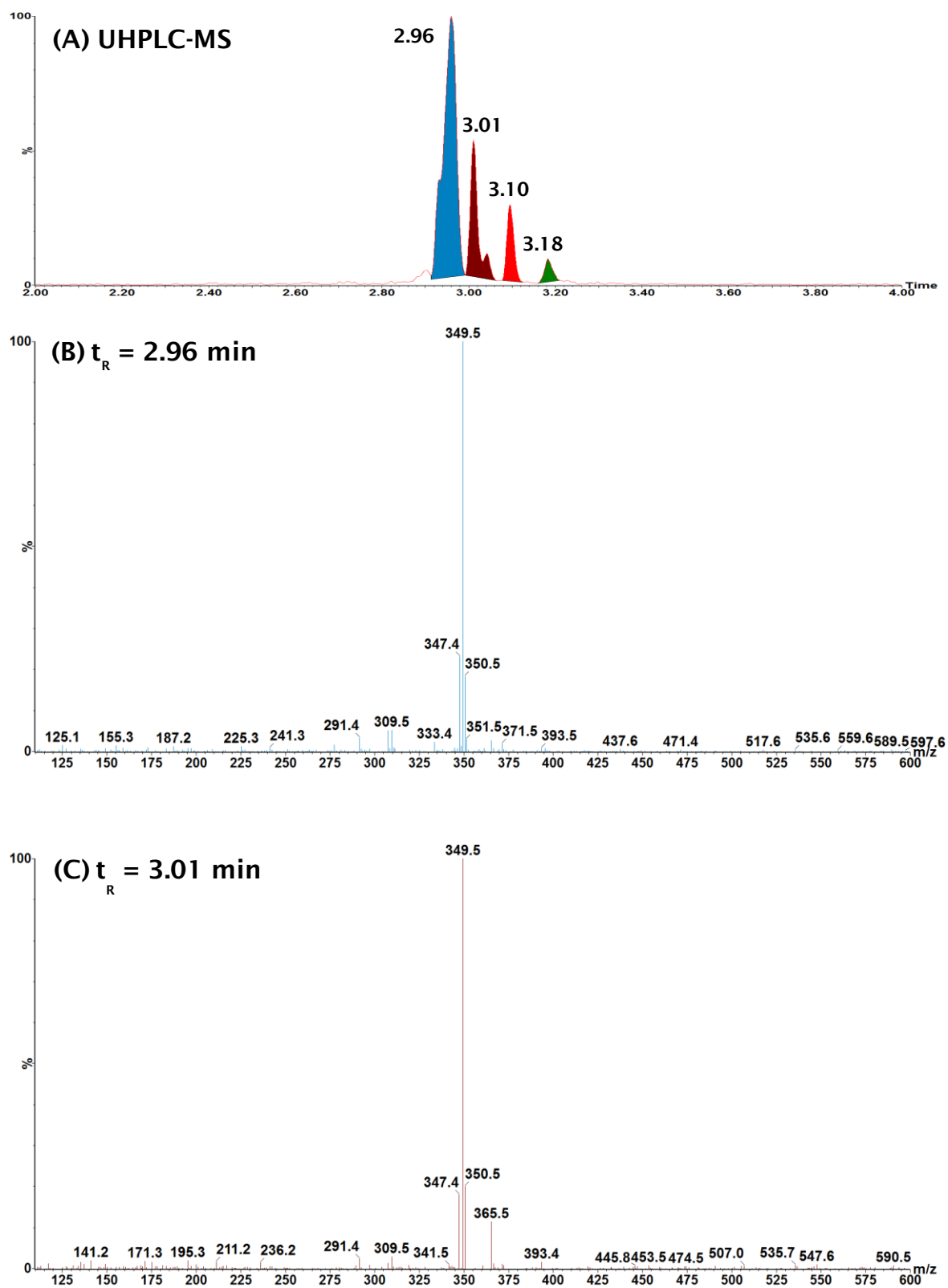
Figure 4-18   Continued overleaf
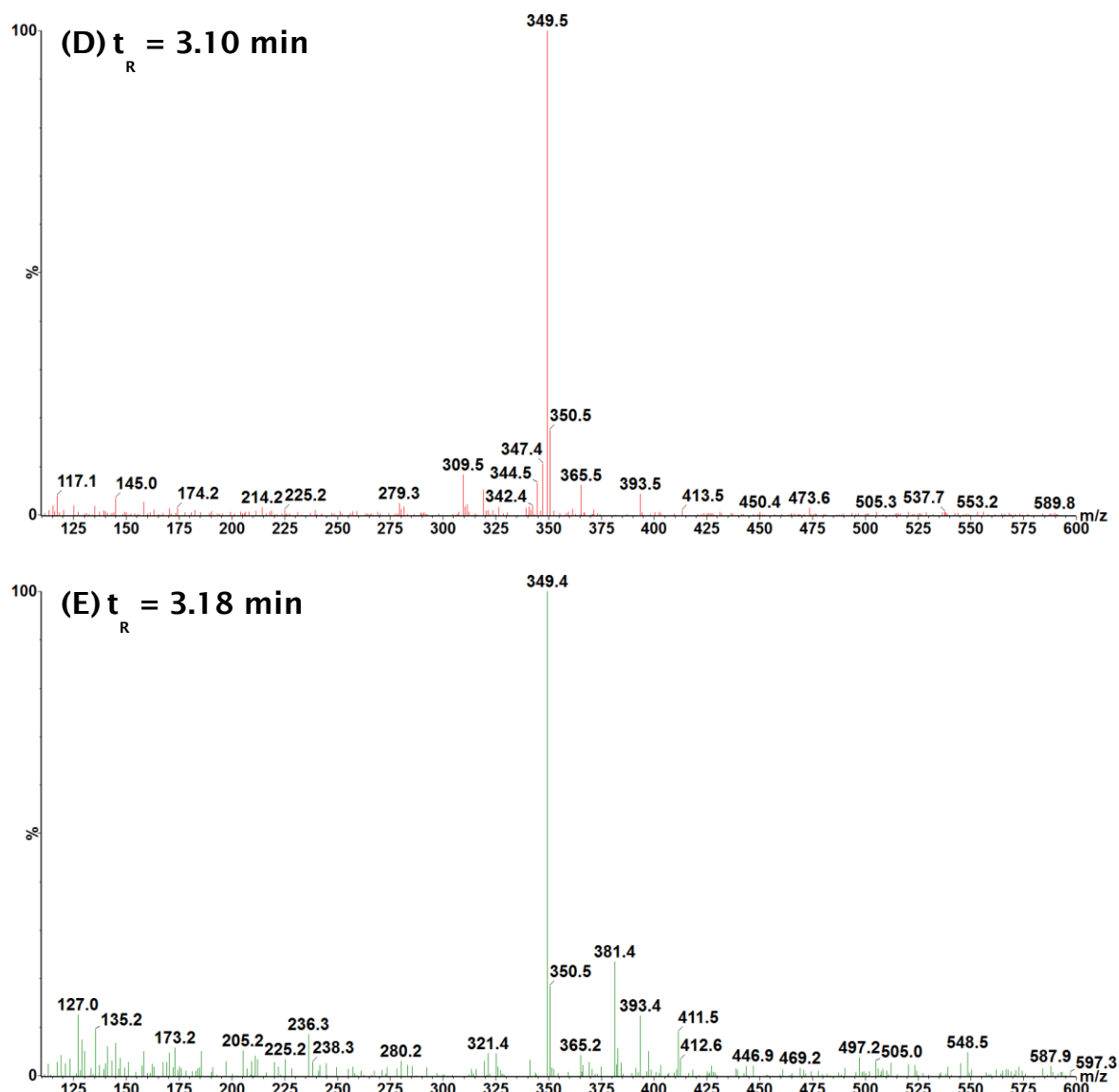
Figure 4-18   UHPLC-MS of FAMEs and oxidation products, showing (A) RICC of *m/z* 349 of four isobaric compounds; (B) ESI mass spectrum at t$_R$ 2.96 min; (C) ESI mass spectrum at t$_R$ 3.01 min; (D) ESI mass spectrum at t$_R$ 3.10 min; (E) ESI mass spectrum at t$_R$ 3.18 min.

This UHPSFC-MS method can clearly separate oxidation products from parent molecules. The oxidised FAMEs species that contain one or more oxygen atoms can be easily detected. However, the limitation of the single quadrupole mass spectrometer is that it is a low resolution instrument and

cannot identify oxidation products that have the same nominal mass. However, high resolution mass spectrometers with high mass accuracy are required in order to positively distinguish between the compounds with the same nominal mass but different exact masses, for example, *m/z* 349 $[C_{19}H_{32}O_4 + Na]^+$ and *m/z* 349 $[C_{21}H_{41}O_2 + Na]^+$.

4.3 Analysis of FAMEs oxidation using HPLC-MS and UHPLC-MS

The aim of this work was to develop a RP-HPLC-MS method and transfer the developed method to UHPLC-MS for separation of the different groups of oxidations formed during FAMEs oxidation. Positive ion ESI source coupled to a single quadrupole mass spectrometry was used to identify the different groups of products present. Initially, a RP-HPLC-MS method was optimised to allow separation of the different groups of oxidation products formed in biodiesel samples. The optimised HPLC conditions for the gradient elution separation of FAMEs and their oxidation products were initially achieved using a XBridge C18 column (2.1 × 50 mm, 5 µm) with a 20-100% linear gradient of methanol 0.1% v/v formic acid, and the total analysis time was 20 min. The developed HPLC method transferred to UHPLC-MS by using an Acquity UPLC® BEH C18 column (2.1 mm × 50 mm, 1.7 µm).

The gradient elution can be separate the group of non-oxidised FAMEs and oxidised FAMEs. Three major peaks in the chromatograms at t_R 13.63, 13.89, and 14.20 min, respectively were detected as $[C18:3 + Na]^+$ ion at *m/z* 315, $[C18:2 + Na]^+$ ions at *m/z* 317 and $[C18:1 + Na]^+$ ion at

m/z 319 , respectively, (see, Figure 4-19 (A)). These compounds correspond to non-oxidised FAMEs. FAME with a greater degree of unsaturation eluted earlier than less unsaturated ones with the same carbon length. Peaks in the retention time region of 12.33-13.19 min and 14.58–14.95 min obtained from HPLC-MS (see, Figure 4-19 (A)) and 4.23– 4.67 min, and 5.08 – 5.45 min obtained from UHPLC-MS (see, Figure 4-19 (B)) are oxidation products of FAMEs. The major peaks of oxidation product at t_R 12.64 min (Figure 4-19 (A)) and at t_R 4.34 min (Figure 4-19 (B)) were detected as ion of *m/z* 349 which correlated to [FAME + 2(O) + Na]$^+$.
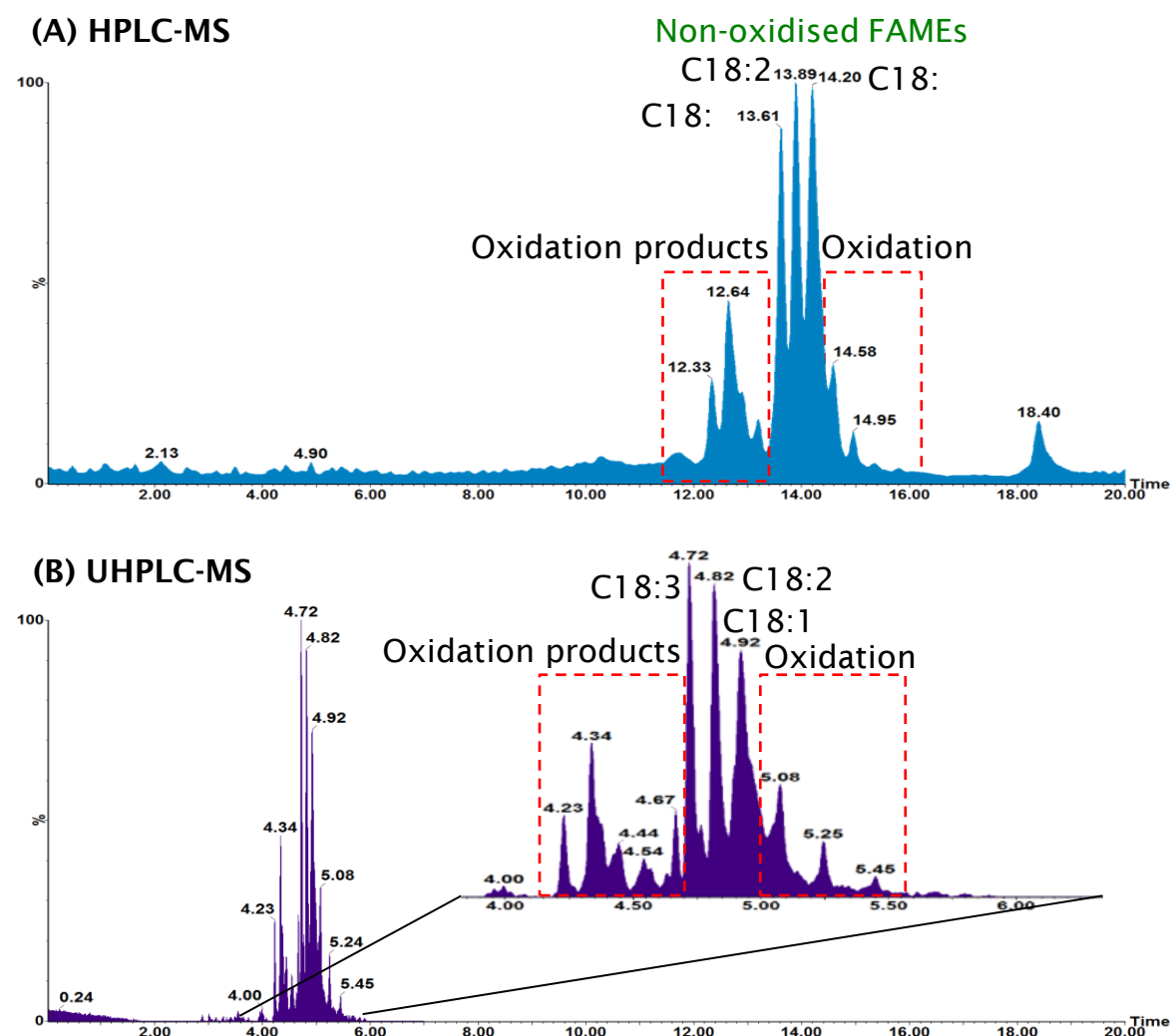
Figure 4-19 **TICCs of RME and oxidation products using (A) HPLC-MS and (B) UHPLC-MS.**

Similarly the elution of FAMEs and oxidation products were obtained by the HPLC and UHPLC methods. In this application, significant improvement in resolution, sensitivity, and analysis time were achieved by using UHPLC for separation of non-oxidised FAMEs and various groups of oxidation products. Figure 4-20 shows RICCs of m/z 335 (FAME + 1(O) + Na]+, m/z 349 [FAME + 2(O) + Na]+, m/z 365 [FAME + 3(O) + Na]+ and m/z 379 [FAME+ 4(O) + Na]+ using HPLC-MS (traces A) and UHPLC–MS (traces B).
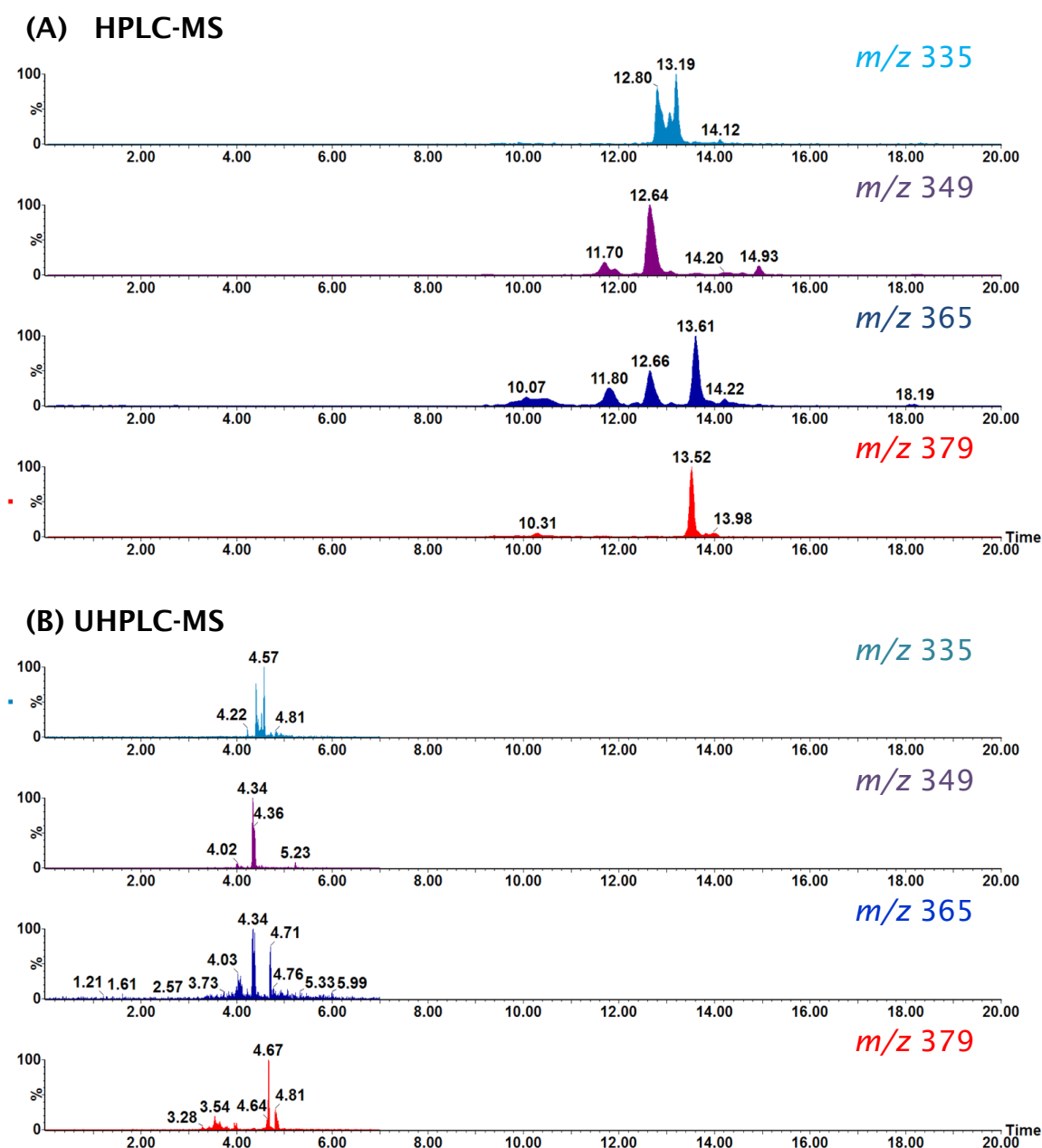
Figure 4-20 Comparison of RICCs of oxidation products of auto-oxidised RME using HPLC-MS (traces A) and UHPLC–MS (traces B). *m/z* 335 (FAME + 1(O) + Na]+ (light blue), *m/z* 349 [FAME + 2(O) + Na]+ (purple), *m/z* 365 [FAME + 3(O) + Na]+ (blue) and *m/z* 379 [FAME + 4(O) + Na]+ (red).

4.3.1 Comparison of UHPSFC-MS and UHPLC-MS

Figure 4-21 compares the separation of FAMEs and oxidation products from the auto-oxidised RME sample. In UHPLC-MS, the groups of oxidised FAME species eluted before the groups of non-oxidised ones, obviously due to their higher polarities contrast to UHPSFC-MS. The UHPSFC-ESI/MS method is suitable for the separation of non-volatile oxidation products of FAMEs from parent molecules.

Table 4-2 presents the oxidation produces detected in auto-oxidised RME using the three different methods (HPLC-MS, UHPL-MS and UHPSFC-MS). Similar results the oxidised FAMEs species that contain one or more oxygen atoms can be easily detected by using both techniques. For HPLC-MS, UHPSFC-MS and UHPLC-MS provided a total analysis time of 22.34 min, 6.11 min and 8.32 min, respectively including equilibration time.

(A) UHPLC-MS
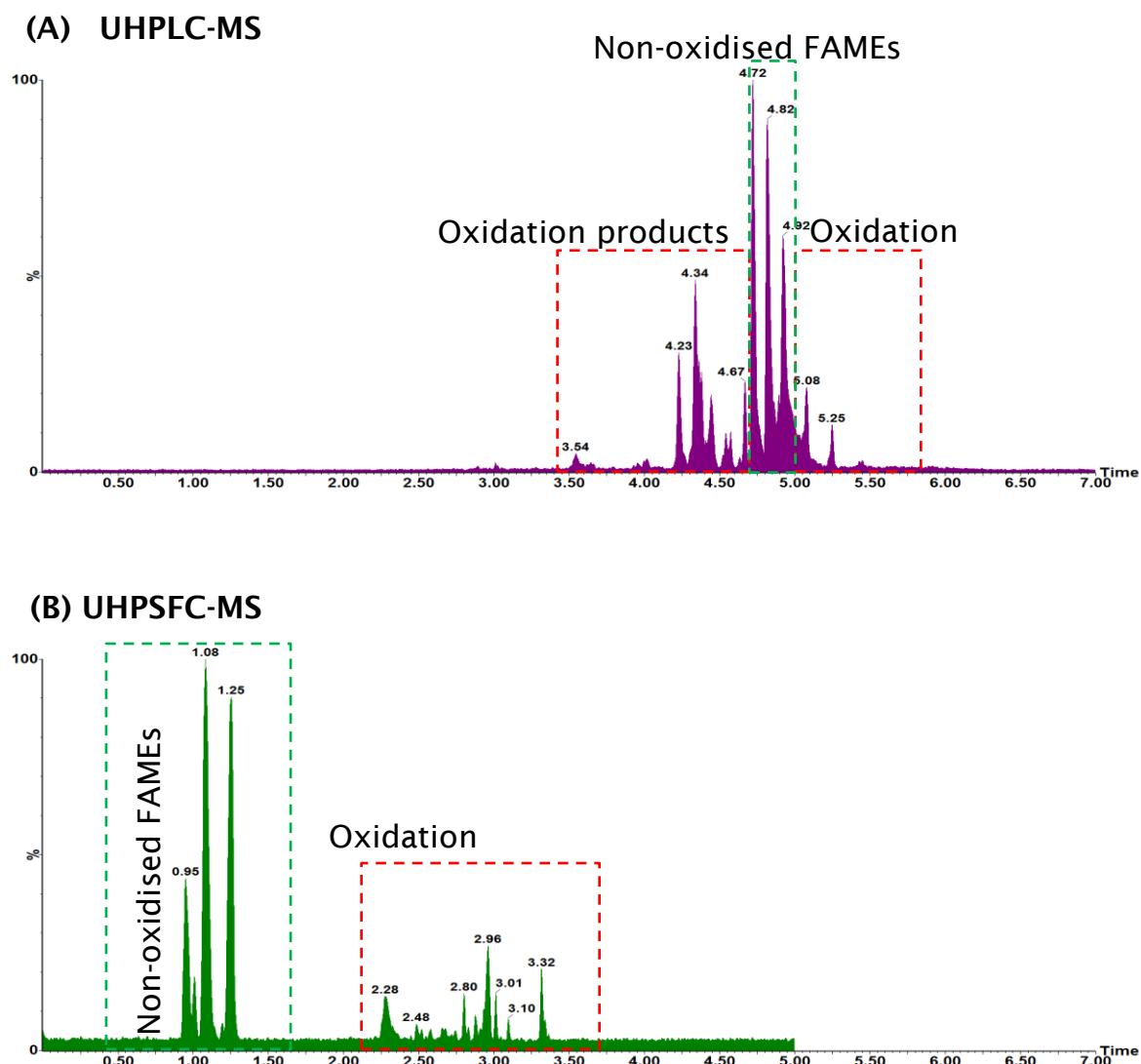
(B) UHPSFC-MS

Figure 4-21   Comparison of BPICCs of the RME sample obtained from (A) UHPLC-MS using the BEH C18 column (2.1 mm × 50 mm, 1.7 μm), and (B) UHPSFC-MS using the BEH column (2.1 mm × 100 mm, 1.7 μm).

Table 4-2   Comparison of HPLC-MS, UHPLC-MS and UHPLC-MS for the analysis of auto-oxidised RME sample

HPLC-MS		UHPLC-MS		UHPSFC-MS	
t_R (min)	*m/z*	t_R (min)	*m/z*	t_R (min)	*m/z*
12.33	347.2	4.23	347.1		
12.62	349.2	4.34	349.1	2.48	331.5
12.91	351.2	4.44	351.2	2.52	335.5
13.19	377.2	4.54	377.2	2.80	363.5
13.61	315.2	4.67	379.2	2.87	351.5
13.90	317.2	4.72	315.2	2.96	349.5
14.18	319.2	4.82	317.2	3.01	349.5
14.58	347.2	4.92	319.2	3.10	349.5
14.95	375.3	5.08	347.2	3.31	379.5
		5.25	375.2		

The UHPSFC-MS method can clearly separate oxidation products from non-oxidised FAMEs. This method provided faster analysis time with lower organic solvent consumption when compared to the HPLC-MS and UHPLC-MS methods. The UHPSFC-MS can be considered as a suitable technique to overcome the separation of non-oxidised FAMEs and oxidised FAMEs with similar chemical structures when it cannot be separated with HPLC-MS or UHPLC-MS methods. However, the limitation of the single quadrupole mass spectrometer is that it is a low resolution instrument and cannot identify compounds that have the same nominal mass. For example, RICC at *m/z* 349 showed more than one peak by using single quadrupole MS (UHPLC-MS and UHPSFC-MS).

4.4   Analysis of FAMEs oxidation using UHPLC-HR MS

Accurate mass measurement for the determination of elemental formula of oxidation products of RME and SME was determined by coupling of ultra-high-performance liquid chromatography (UHPLC) with a quadrupole-time of flight mass spectrometry (Q-TOF). The mass accuracy can be used to identify unknown compounds and differentiate isobaric compounds (different compounds with the same nominal mass but different elemental composition, and thus, different exact masses).

Figure 4-22 and Figure 4-23 show the BPICCs of RME and SME samples, respectively which are oxidised to different extents due to length of storage. The elution order and profiles of oxidised and non-oxidised FAMEs are similar to those in HPLC-MS and UHPLC-MS. Peaks at retention times of 5.0-5.2 min showed non-oxidised FAMEs, which correspond to C18:3, C18:2, and C18:1, respectively. The chromatograms show similarities in the eluting peak profiles; however, there are some differences in peaks at t_R 4.8 min in the chromatograms of 5.5-year-old biodiesels, RME (Figure 4-22 (B)) and SME (Figure 4-23 (B)).

The peaks at t_R 4.8 min of the chromatograms Figure 4-22 (B) and Figure 4-23 (B) presents at a higher intensity than that of the chromatogram of 1.5-year-old biodiesels, RME (Figure 4-22 (A)) and SME (Figure 4-23 (A)).

(A) 1.5-year-old RME
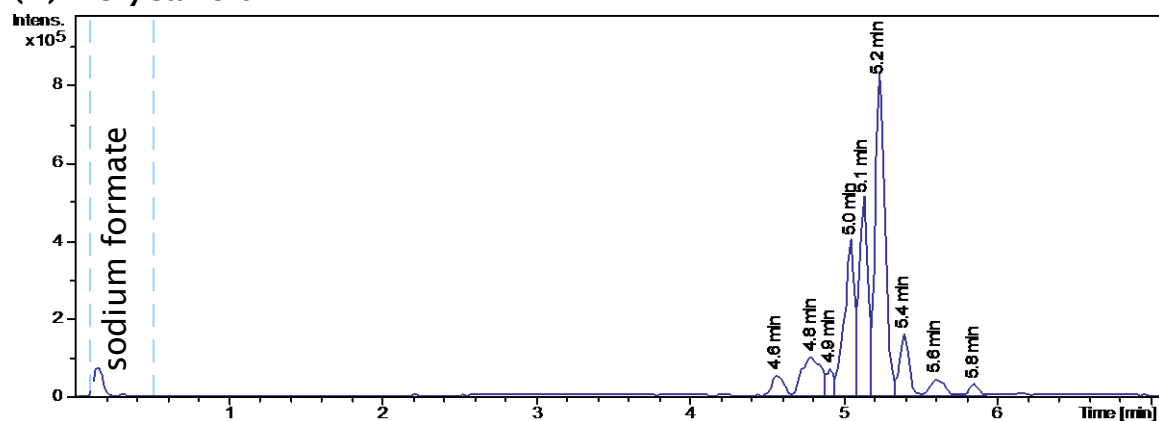
(B) 5.5-year-old RME
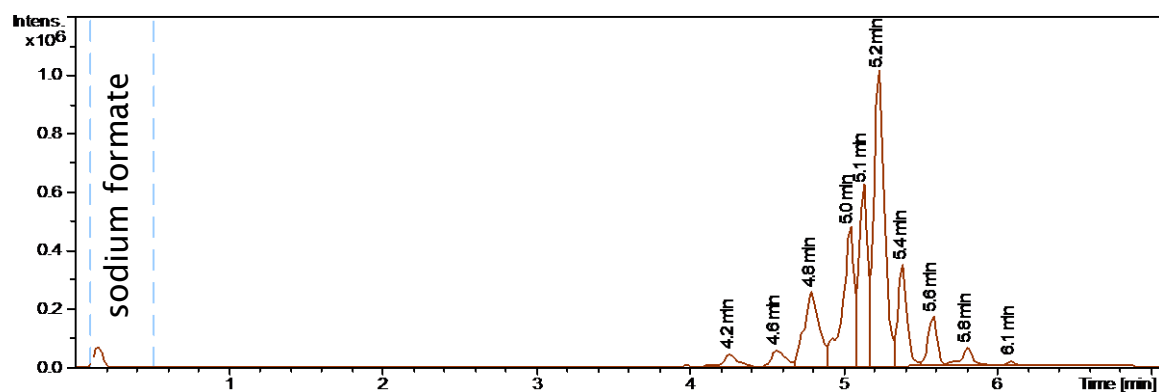
Figure 4-22 BPICCs of non-oxidised and oxidised rapeseed methyl ester (RME) at different time storage. (A) 1.5-year-old RME, (B) 5.5-year old RME.

The peak at t_R 4.8 min in all chromatograms (Figure 4-22 and Figure 4-23) was detected as ion of *m/z* 349.2347 $[C_{19}H_{34}O_4Na]^+$ with a 0.9 ppm error that is corresponds to methyl linoleate (C18:2) with the addition of two oxygen atoms, $[C18:2 + 2(O) + Na]^+$, this is the same species observed in the HPLC-MS, UHPLC-MS and UHPSFC-MS experiments. RICCs of *m/z* 347 $(FAME + 2(O) + Na]^+$, *m/z* 349 $[FAME + 2(O) + Na]^+$, *m/z* 351 $[FAME + 2(O) + Na]^+$ are shown in Figure 4-24.

(A) 1.5-year-old SME
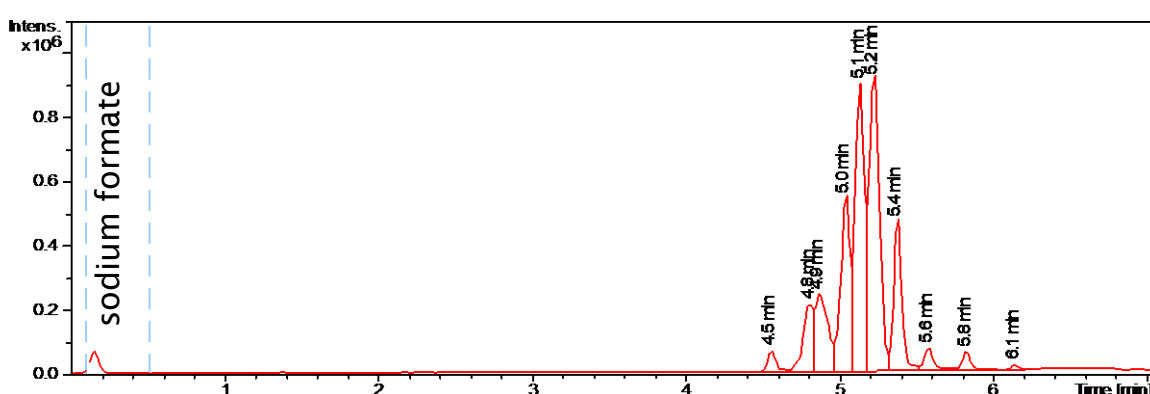
(B) 5.5-year-old SME
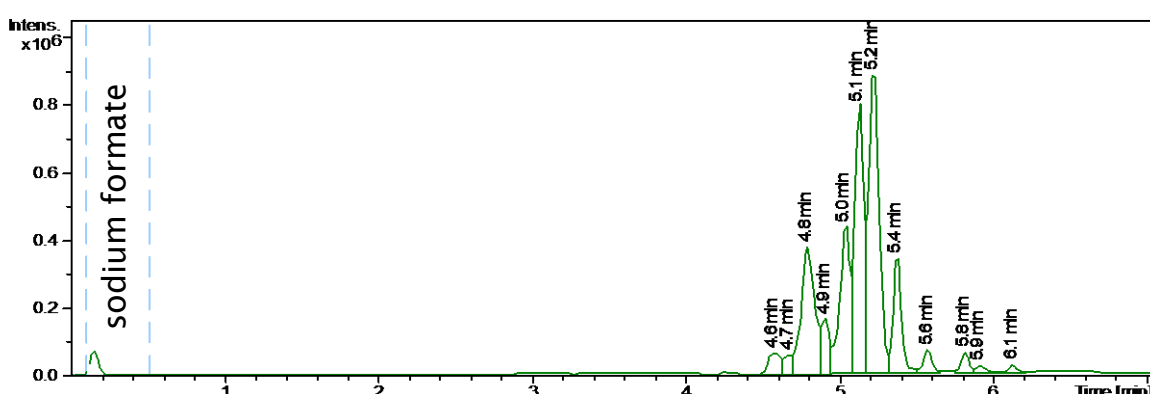
Figure 4-23   **BPICCs of non-oxidised and oxidised soy methyl ester (SME) at different time storage. (A) 1.5-year-old SME, (B) 5.5-year-old SME.**
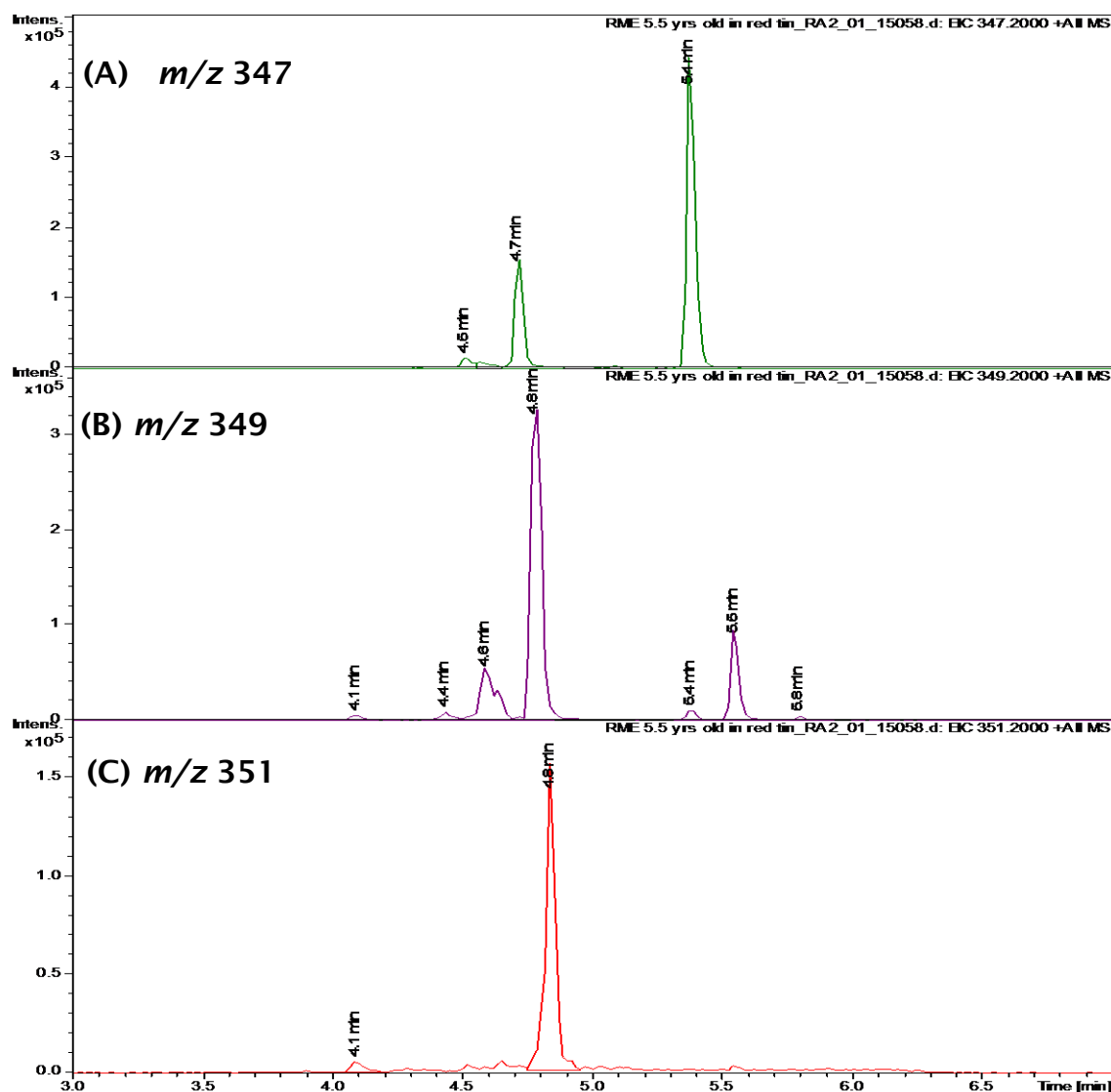
Figure 4-24   RICCs of *m/z* 347 (A), *m/z* 349 (B), and *m/z* 351 (C) of 5.5-year-old rapeseed methyl ester (RME).

The mass spectra are shown Figure 4-25 which related to RICCs of the compounds with the same nominal mass. Peak at t_R 4.7 min was detected as ion of *m/z* 347.2187 $[C_{19}H_{32}O_4 + Na]^+$ whilst peak at t_R 5.4 min was detected as ion of *m/z* 347.2917 $[C_{21}H_{40}O_2 + Na]^+$.
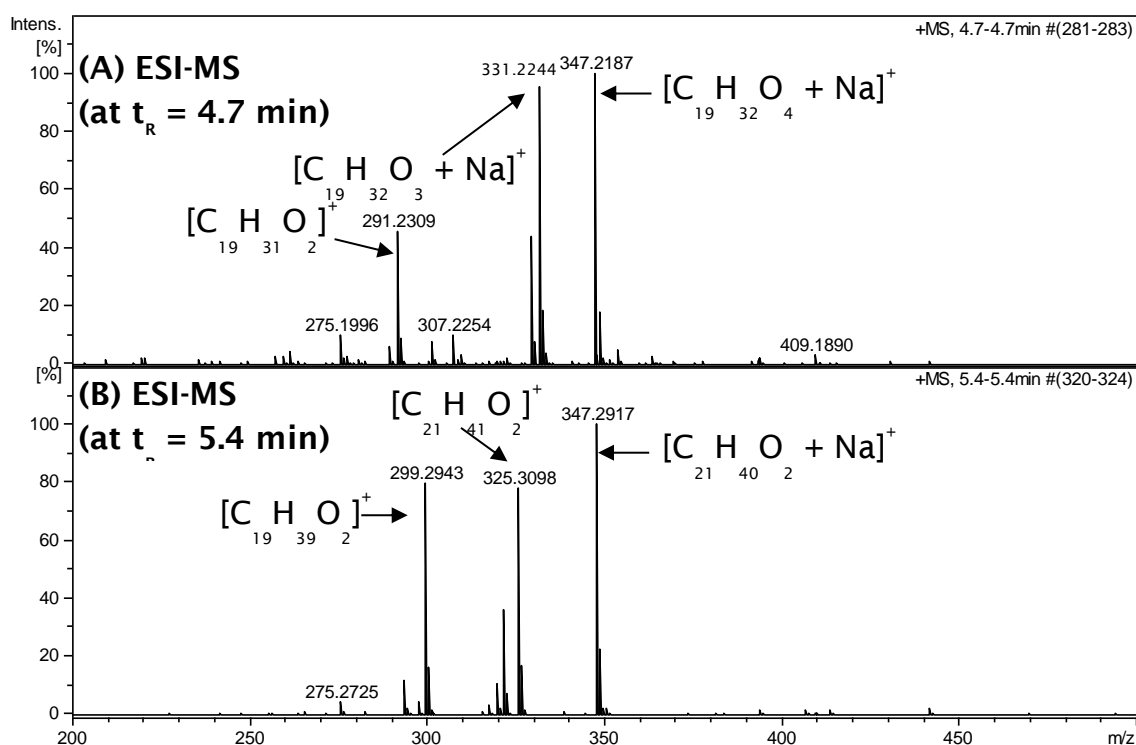
Figure 4-25 Positive ion ESI mass spectra corresponding to the chromatograms (Figure 4-24 (A) *m/z* **347, peak at t$_R$ 4.7 min (A), peak at t$_R$ 5.4 min.**
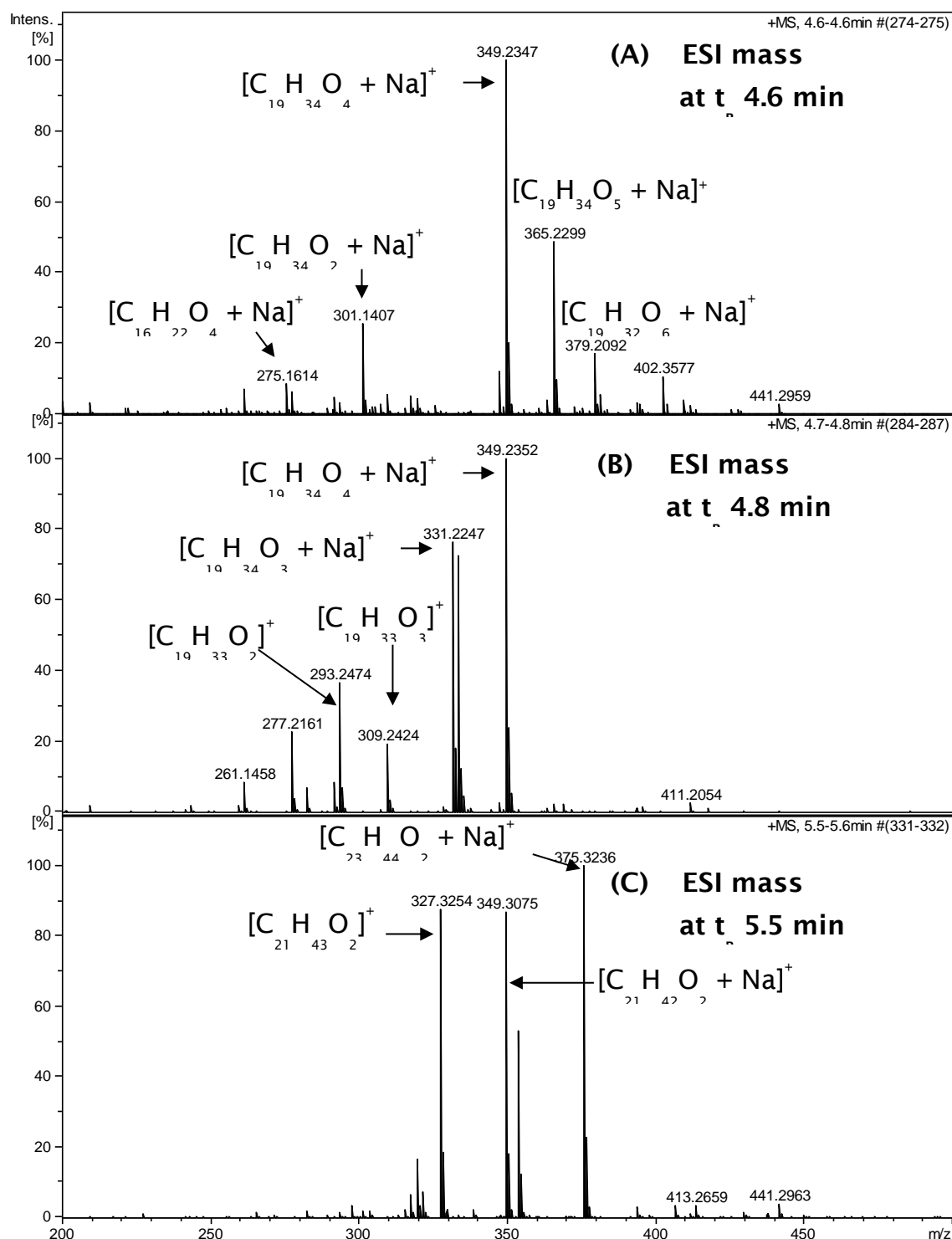
Figure 4-26 Positive ion ESI mass spectra corresponding to the chromatograms (Figure 4-24 (B)), peak at t_R 4.6 min (A), peak at t_R 4.8 min (B), and peak at t_R 5.5 min (C).

The use of accurate mass measurement is shown to be essential for distinguishing the mass spectra of the oxidised FAMEs. UHPLC-QTOF MS, the accurate mass data are shown in Table 4-3.

Table 4-3   **Accurate mass measurement results for compounds found in rapeseed methyl ester (RME) and soy methyl ester (SME) samples**

Peak t_p (min)	Measured mass	Theoretical mass	Error (ppm)	Elemental composition
4.2	379.2088	379.2091	0.7	$C_{19}H_{32}NaO_6$
	363.2131	363.2131	2.9	$C_{19}H_{32}NaO_5$
	317.2442	317.2442	2.7	$C_{19}H_{34}NaO_2$
4.6	379.2087	379.2091	1.1	$C_{19}H_{32}NaO_6$
	365.2300	365.2298	0.3	$C_{19}H_{34}NaO_5$
	349.2348	349.2349	0.3	$C_{19}H_{34}NaO_4$
	301.1406	301.1410	1.3	$C_{16}H_{22}NaO_4$
	275.1612	275.1618	2.0	$C_{15}H_{24}NaO_3$
	261.1453	261.1461	3.1	$C_{14}H_{22}NaO_3$
4.8	349.2351	349.2349	0.5	$C_{19}H_{34}NaO_4$
	333.2399	333.2400	0.4	$C_{19}H_{34}NaO_3$
	331.2245	331.2244	0.2	$C_{19}H_{32}NaO_3$
	309.2422	309.2428	0.8	$C_{19}H_{33}O_3$
	293.2473	293.2475	0.7	$C_{19}H_{33}O_2$
	277.2160	277.2162	0.7	$C_{18}H_{29}O_2$
	261.1457	261.1461	1.5	$C_{14}H_{22}NaO_3$
5.0	315.2287	315.2292	2.3	$C_{19}H_{32}NaO_2$
	293.2466	293.2475	2.9	$C_{19}H_{33}O_2$
	261.2199	261.2189	3.7	$C_{16}H_{30}NaO_2$
	243.2097	243.2107	4.3	$C_{18}H_{27}$
5.2	319.2610	319.2608	0.9	$C_{19}H_{36}NaO_2$
	297.2788	297.2788	0.1	$C_{19}H_{37}O_2$
	265.2523	265.2526	1.2	$C_{18}H_{33}O$
	247.2416	247.2420	1.6	$C_{18}H_{31}$

Table 4-3 (Continued) accurate mass measurement results for compounds found in RME and SME samples

Peak t_p (min)	Measured mass	Theoretical mass	Error (ppm)	Elemental composition
5.4	347.2923	347.2923	1.0	$C_{21}H_{40}NaO_2$
	325.2103	325.3101	0.7	$C_{21}H_{41}O_2$
	321.2773	321.2764	0.6	$C_{19}H_{38}NaO_2$
	299.2944	299.2945	0.2	$C_{19}H_{39}O_2$
	293.2835	293.2839	1.2	$C_{20}H_{37}O_2$
5.6	375.3234	375.3234	0.1	$C_{23}H_{44}NaO_2$
	353.3414	353.3414	0.0	$C_{23}H_{45}O_2$
	349.3074	349.3077	0.8	$C_{21}H_{42}NaO_2$
	327.3253	327.3258	1.3	$C_{21}H_{43}O_2$
5.8	609.4845	609.4853	1.4	$C_{38}H_{66}NaO_4$
	441.2970	441.2975	1.1	$C_{26}H_{42}NaO_4$
	403.3547	403.3547	0.2	$C_{25}H_{48}NaO_2$
	381.3728	381.3727	0.3	$C_{25}H_{49}O_2$
	377.3389	377.3390	0.4	$C_{23}H_{46}NaO_2$
	355.3568	355.3571	0.8	$C_{23}H_{47}O_2$
	319.2603	319.2608	1.4	$C_{19}H_{36}NaO_2$
	317.2443	317.2451	2.4	$C_{19}H_{34}NaO_2$
	315.2287	315.2295	2.3	$C_{19}H_{32}NaO_2$

4.5 Analysis of FAMEs oxidation using infusion FT-ICR MS

Ultra-high resolution and accuracy mass spectrometry, Fourier transform ion cyclotron resonance mass spectrometry (FT-ICR MS), allows for the identification of complex organic mixtures without the need for any prior extraction or separation steps. Infusion FT-ICR MS was applied for monitoring auto-oxidised RME, auto-oxidised-SME and their oxidation products. Oxidation products of $[M + nO + Na]^+$ at *m/z* 333, 349, 365, 379 and 381 (*n*=1, 2, 3 and 4, respectively were observed in the period of time between sample monitoring, it can be seen that the signal intensity of oxidation products, for example *m/z* 349 $[C_{19}H_{34}O_4 + Na]^+$ and *m/z* 379, $[C_{19}H_{32}O_6 + Na]^+$ significantly increased for the both biodiesels (5.5 year old RME and SME) as represented in Figure 4-26 (B) and (D).
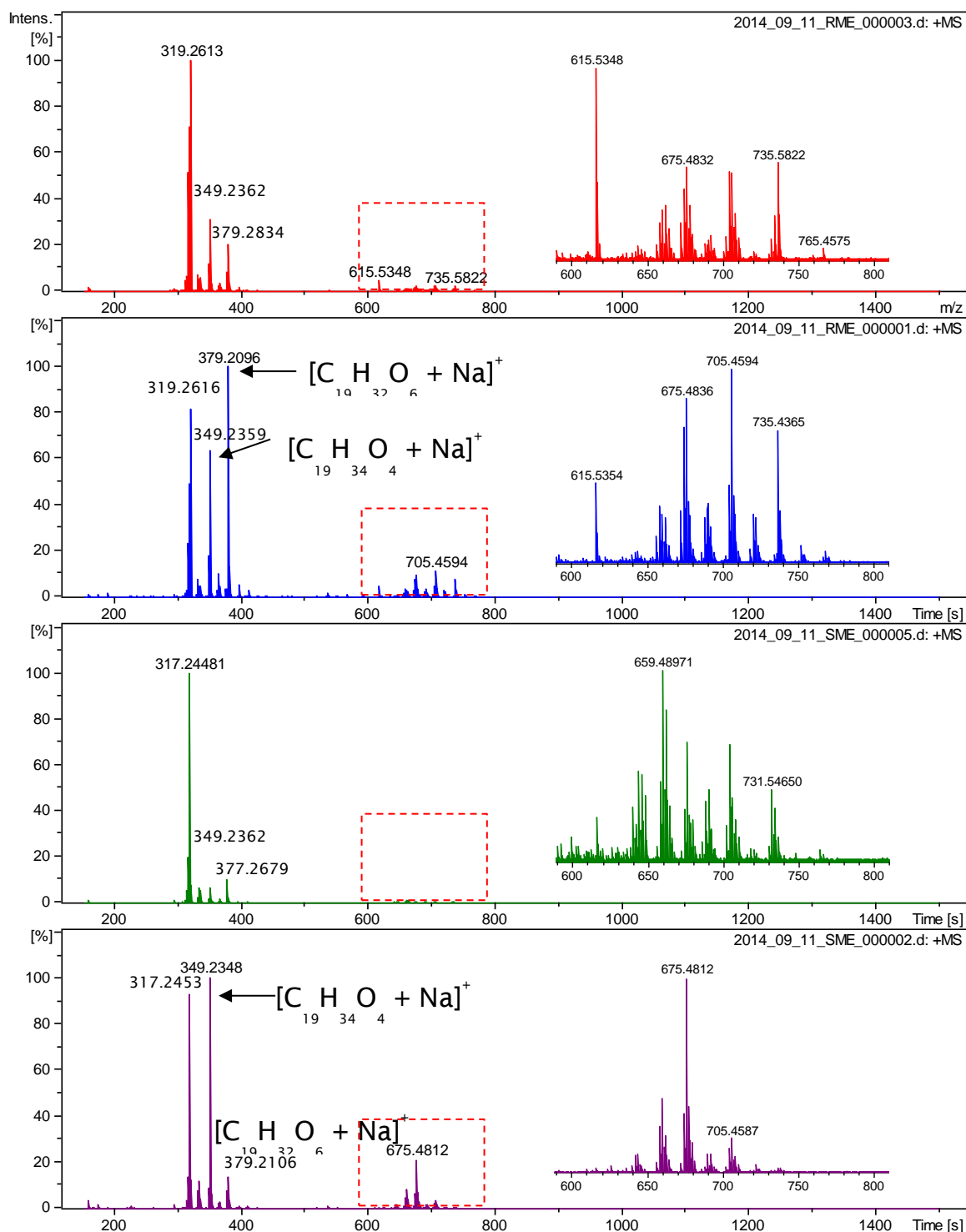
Figure 4-27 Representative of positive ion ESI mass spectra of non-oxidised and oxidised FAMEs at different time storage. (A) 1.5 year old RME, (B) 5.5 year old RME, (C) 1.5 year old SME, and (D) 5.5 year old SME. Inserts show expansion of *m/z* region of the analyte ions.

The elemental formula for these oxidised FAMEs were determined by infusion FT-ICR MS, example data are shown in Figure 4-28 below, though it must be noted that direct introduction of the sample does not afford any information for structural isomers.
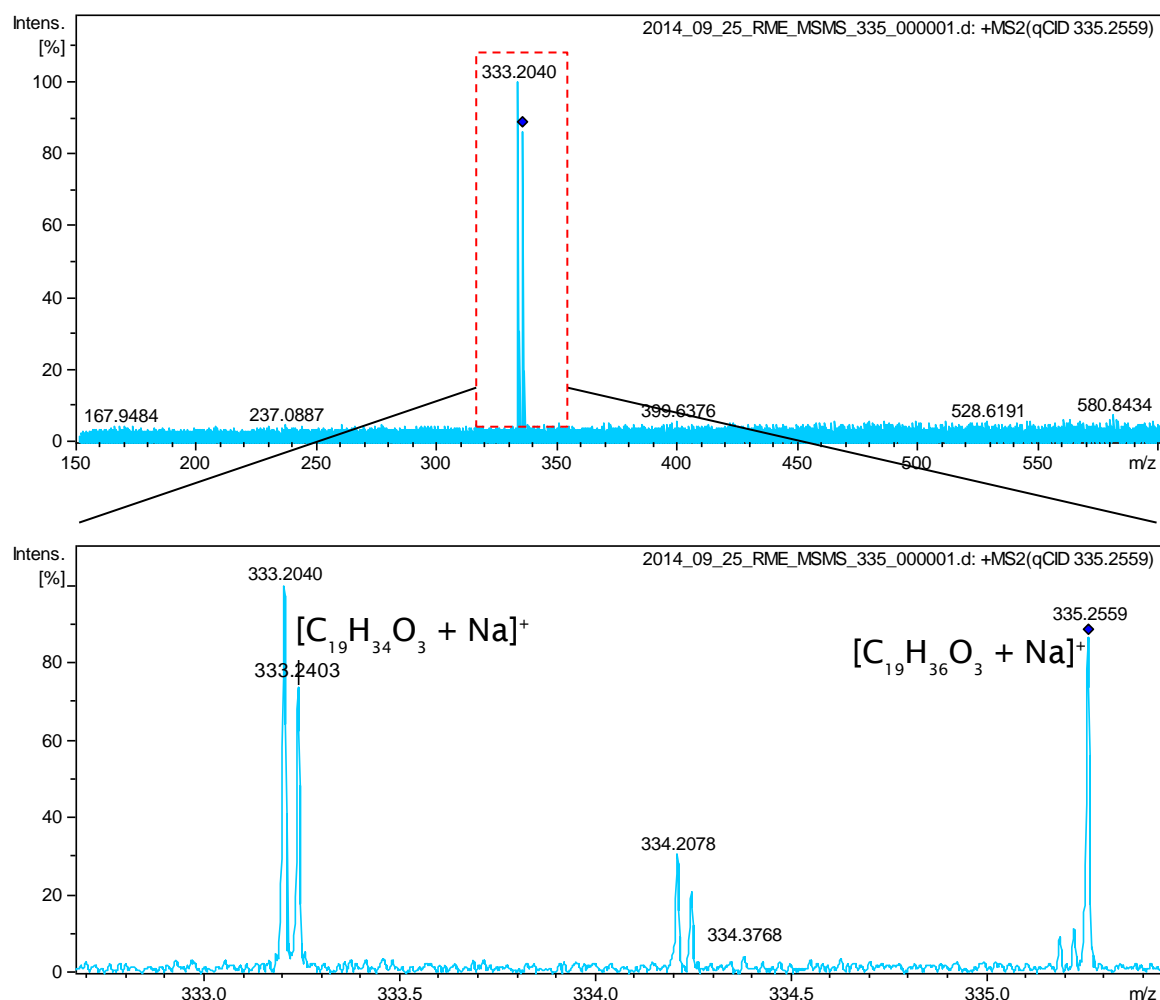
Figure 4-28   **Example of positive ion ESI mass spectra using infusion FT-ICR MS/MS.**

Chapter 4: Analysis of FAME oxidation

This shotgun analysis approach shows the presence of oxygenated species up to O (6 oxygen atoms) of the ion at *m/z* 411.1999 [$C_{19}H_{32}O_8$ + Na]$^+$ with a 2.6 ppm error. The other oxygenated species formed in auto-oxidised RME and auto-oxidised SME sample analysed using infusion FT-ICR MS are shown in Table 4-4.

Table 4-4   FAMEs auto-oxidation series detected in RME and SME samples using positive ion ESI-FT-ICR MS

Measured mass	Error (ppm)	Elemental composition
331.2244	1.3	$C_{19}H_{32}O_3Na$
333.2400	0.9	$C_{19}H_{34}O_3Na$
347.2193	2.2	$C_{19}H_{32}O_4Na$
349.2349	2.7	$C_{19}H_{34}O_4Na$
353.2662	3.2	$C_{19}H_{38}O_4Na$
361.1985	4.9	$C_{19}H_{30}O_5Na$
379.2091	3.7	$C_{19}H_{32}O_6Na$
381.2248	3.7	$C_{19}H_{34}O_6Na$
411.1990	2.6	$C_{19}H_{32}O_8Na$

4.6 Comparison of oxidised FAMEs in EC cell and auto-oxidised FAMEs

A comparison of the oxidation products of FAMEs (RME and SME) formed in EC cell and auto-oxidation shows in Figure 4-29 and Figure 4-30. On-line EC-ESI MS data show similarity with auto-oxidation. As examples, the ions of m/z 331/333/335 correlating to [FAME + 1(O) + Na]$^+$, m/z 349 correlating to [FAME + 2(O) + Na]$^+$, m/z 363/365 correlating to [FAME + 3(O) + Na]$^+$, and m/z 379 correlating to [FAME + 4(O) + Na]$^+$ observed in EC cell and auto-oxidation conditions. EC cell produced higher quantities of oxidation species than auto-oxidation. The use of EC cell is very beneficial tool in the rapid investigation of the oxidation products. The EC system could be coupled to HPLC for separation of oxidation product before MS analysis or collection and injection into tandem MS.

(A) RME oxidised in EC cell
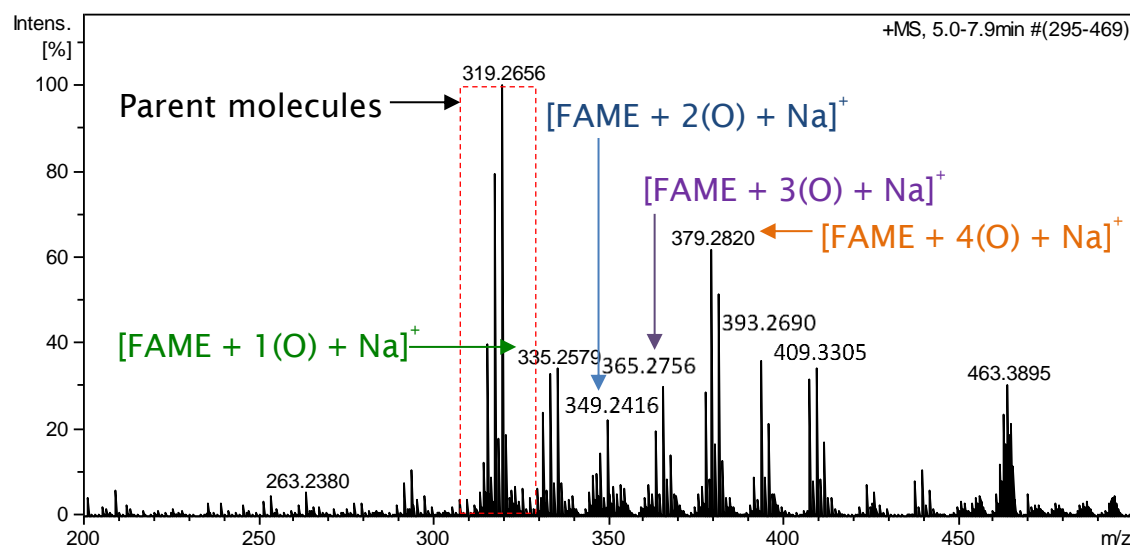
(B) Auto-oxidised RME
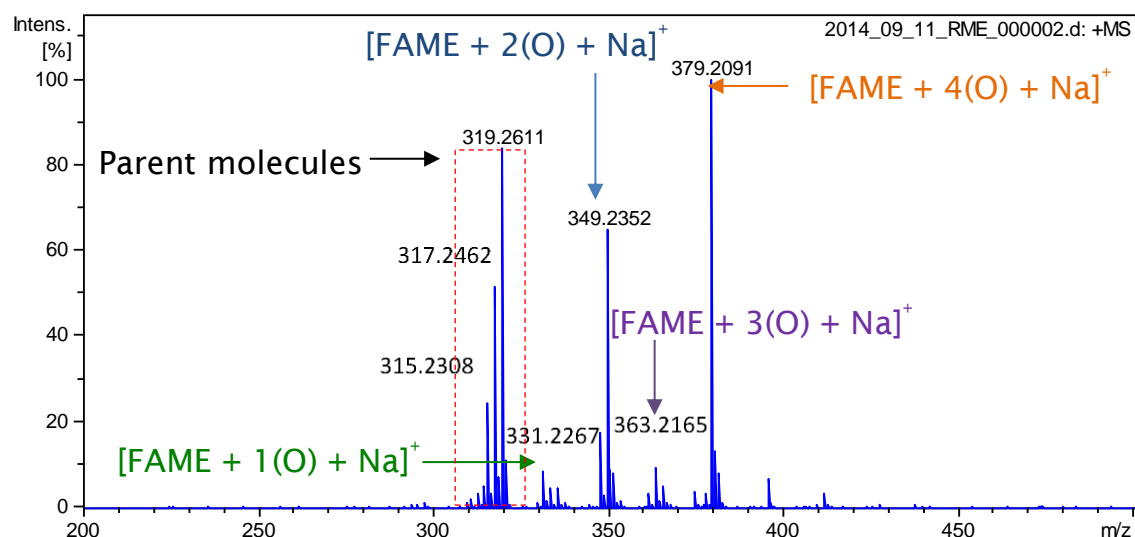
Figure 4-29   Comparison of oxidation product of rapeseed methyl ester (RME) formed in the on-line EC-ESI MS using the magic diamond working electrode at EC potential 2.0 V (A); auto-oxidation of RME analysed using infusion FT-ICR MS.

144

(A) SME oxidised in EC cell
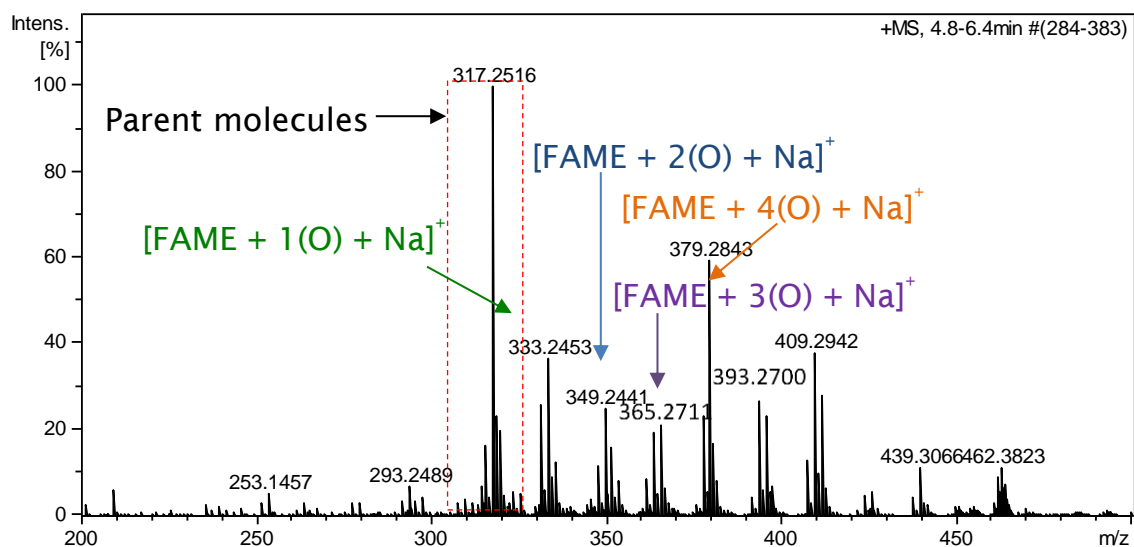
(B) Auto-oxidised SME
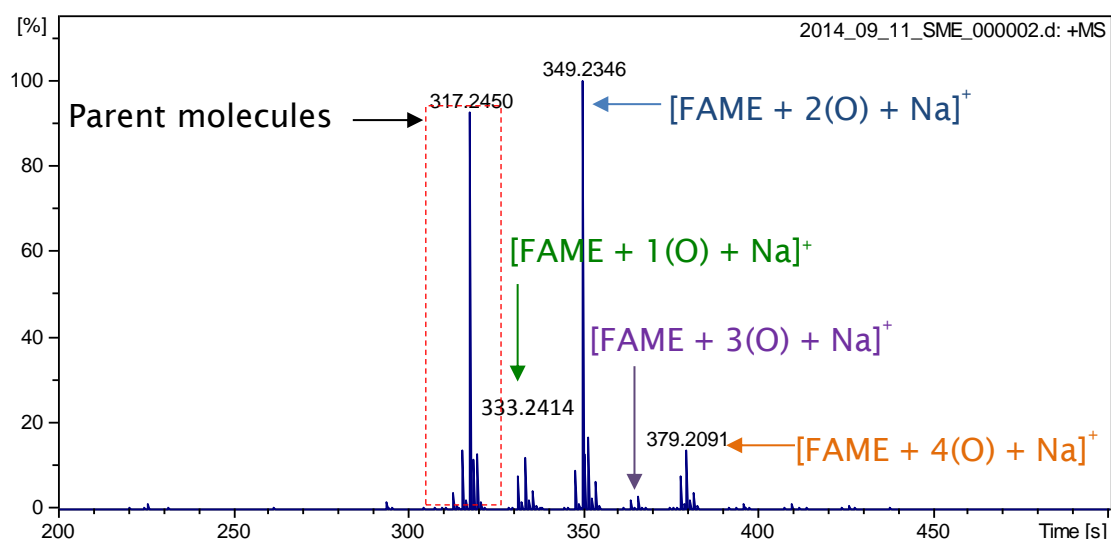
Figure 4-30   Comparison of oxidation product of soy methyl ester (SME) formed in the on-line EC-ESI MS using the magic diamond working electrode at EC potential 2.0 V (A); auto-oxidation of SME analysed using infusion FT-ICR MS.

Electrochemistry coupled on-line to ESI-MS shows a great promise for accelerated oxidation studies but further work structural identify of these species will be required. This could not be undertake because the Roxy EC system was only available for a three-month evaluation study.

4.7 Structural suggestion of oxidation products of FAMEs

Auto-oxidised of fatty acid methyl esters (FAMEs) provides a complex mixture of oxidation products. HPLC-MS, UHPLC-MS, UHPSFC-MS, UHPLC-HR MS and high-resolution and high-accuracy FT-ICR-MS were applied to analyse and identify oxidation products of auto-oxidised rapeseed methyl ester (RME) and soy methyl ester (SME) samples. In this section, the related results from HPLC-MS, UHPLC-MS, UHPSFC-MS, UHPLC-HR MS and high-resolution and high-accuracy FT-ICR-MS linked with the literatures to propose and suggest chemical structures of auto-oxidation products of FAMEs.

The ion of *m/z* 331 was identified by high resolution and FT-ICR MS that it corresponds to $C_{19}H_{32}O_3Na$ [FAME + 1(O) + Na]$^+$. It could be methyl 9,10-epoxyoctadecenoate and other epoxy monoenes including: 8,9-epoxy, 10,11-epoxy and 11,12-epoxyepoxyoctadecenoate.[82] These oxidation products have been identified by HPLC of auto-oxidised methyl linoleate.[82] The chemical structure of oxidation products corresponding the ion of *m/z* 331.2244 $[C_{19}H_{32}O_3Na]^+$ is shown in Table 4-5.

Table 4-5   Expected chemical structure of oxidation product FAMEs corresponding to *m/z* 331.2244 [C$_{19}$H$_{32}$O$_3$Na]$^+$

FT-ICR MS data: *m/z* 331.2244

Formula: C$_{19}$H$_{32}$O$_3$Na

Expected chemical structure:
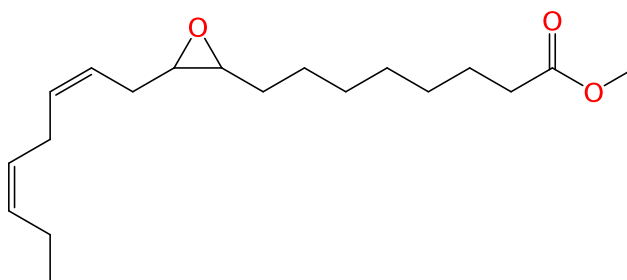
Systematic name: Methyl 9,10-epoxy-12*Z*,15*Z*-octadecadienoate

Formula: C$_{19}$H$_{32}$O$_3$

Exact mass: 308.2351 Da

The ions of *m/z* 347.2193 [C$_{19}$H$_{32}$O$_4$Na]$^+$ and 349.2349 [C$_{19}$H$_{34}$O$_4$Na]$^+$ were identified by FI-ICR MS and UHPLC-HR MS. They correspond to [FAME + 2 (O) + Na]$^+$ that expected as epoxyhydroxy-FAMEs. These compounds have been reported as secondary oxidation products from auto-oxidised methyl linolenate (C18:2) and analysed by HPLC.[83] Chemical structures of oxidation products corresponding to *m/z* 347.2193 [C$_{19}$H$_{32}$O$_4$Na]$^+$ and 349.2349 [C$_{19}$H$_{34}$O$_4$Na]$^+$ are shown in Table 4-6 and Table 4-7.

Table 4-6   Expected chemical structures of oxidation product FAMEs corresponding to m/z 347.2193[$C_{19}H_{32}O_4Na$]$^+$

FT-ICR MS data:	*m/z* 347.2193

Formula:	$C_{19}H_{32}O_4Na$

Expected chemical structure:
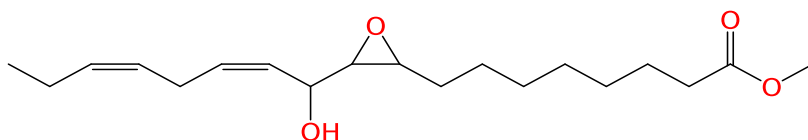
Systematic name:	Methyl 9-epidioxy-16-hydroperoxy-9,11-octadecadienoate

Formula:	$C_{19}H_{32}O_4$

Exact mass:	324.2301 Da

Table 4-7   Expected chemical structures of oxidation product FAMEs corresponding to m/z 349.2349 [$C_{19}H_{34}O_4Na$]$^+$

FT-ICR MS data:	*m/z* 349.2349

Formula:	$C_{19}H_{34}O_4Na$

Expected chemical structure:
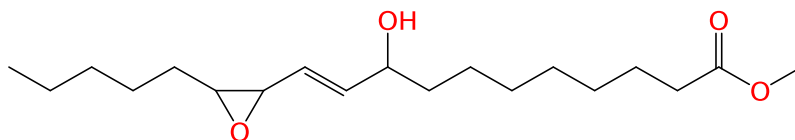
Systematic name:	Methyl 9-hydroxy-12,13-epoxy-10-octadecenoate

Formula:	$C_{19}H_{34}O_4$

Exact mass:	326.2457 Da

The ion of *m/z* 379 was detected for the autoxidised rapeseed methyl

ester (RME) and soy methyl ester (SME) samples by UHPLC-HR MS and FT-

ICR MS. The ion of *m/z* 379.2091 $[C_{19}H_{32}O_6Na]^+$ corresponds to [FAME +

4(O) + Na]$^+$. It could be hydroperoxy-cyclic peroxides-FAME or

dihydroperoxides-FAME. These compounds have been identified as major

secondary products in autoxidised methyl linolenate (C18:3) and

dihydroperoxides as minor products.[83] Then, high-resolution and high-

accuracy FT-ICR-MS data supported the previous results obtained by

UHPLC-MS, UHPSFC-MS and EC-MS. Table 4-8 to Table 4-12 show structures

of oxidation products and some isomers corresponding to *m/z* 379.2091

$[C_{19}H_{32}O_6Na]^+$.

Table 4-8   Expected chemical structures of oxidation product FAMEs corresponding to *m/z* 379.2091 $[C_{19}H_{32}O_6Na]^+$
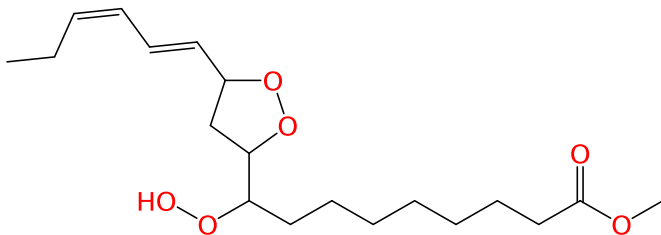
FT-ICR MS data:	*m/z* 379.2091
Formula:	$C_{19}H_{32}O_6Na$

Expected chemical structure

Systematic name:	methyl 9-hydroperoxy-10,12-epidioxy-13,15-octadecadienoate
Formula:	$C_{19}H_{32}O_6$
Exact mass:	356.2199 Da

Table 4-9   Expected chemical structures of oxidation product FAMEs corresponding to *m/z* 379.2091 [$C_{19}H_{32}O_6Na$]⁺

FT-ICR MS data: *m/z* **379.2091**

Formula: $C_{19}H_{32}O_6Na$

Expected chemical structure:
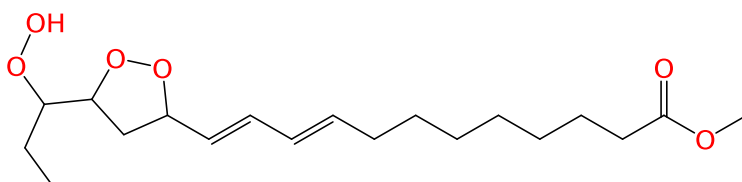
Systematic name: Methyl 13,15-epidioxy-16-hydroperoxy-9,11-octadecadienoate

Formula: $C_{19}H_{32}O_6$

Exact mass: 356.2199 Da

Table 4-10   Expected chemical structures of oxidation product FAMEs corresponding to *m/z* 379.2091 [$C_{19}H_{32}O_6Na$]⁺

FT-ICR MS data: *m/z* **379.2091**

Formula: $C_{19}H_{32}O_6Na$

Expected chemical structure:
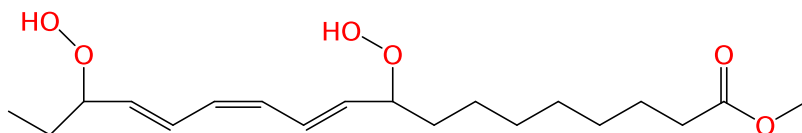
Systematic name: Methyl 9,16-dihydroperoxy-10*E*, 12*Z*, 14*E*-octadecadienoate

Formula: $C_{19}H_{32}O_6$

Exact mass: 356.2199 Da

Table 4-11   Expected chemical structures of oxidation product FAMEs corresponding to m/z 379.2091 $[C_{19}H_{32}O_6Na]^+$

FT-ICR MS data:	m/z **379.2091**

Formula: $C_{19}H_{32}O_6Na$

Expected chemical structure:
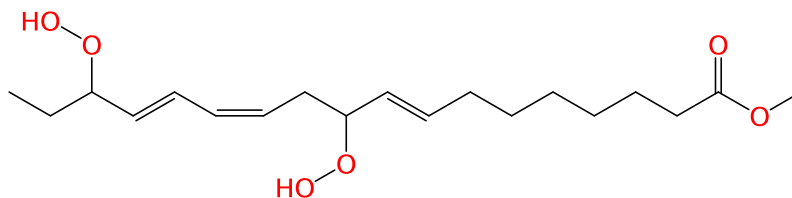
Systematic name: Methyl 10,16-dihydroperoxy-8E,12Z,14E-octadecatrienoate

Formula: $C_{19}H_{32}O_6$

Exact mass: 356.2199 Da

Table 4-12   Expected chemical structures of oxidation product FAMEs corresponding to m/z 379.2091 $[C_{19}H_{32}O_6Na]^+$

FT-ICR MS data:	m/z **379.2091**

Formula: $C_{19}H_{32}O_6Na$

Expected chemical structure:
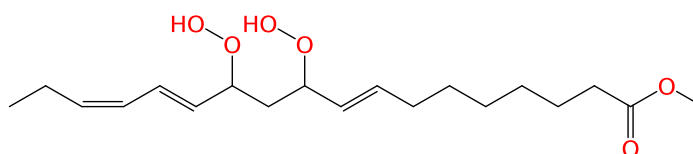
Systematic name: Methyl 10,12-dihydroperoxy-8E,13E,15Z-octadecatrienoate

Formula: $C_{19}H_{32}O_6$

Exact mass: 356.2199 Da

Chapter 4: Analysis of FAME oxidation

High-resolution and high-accuracy FT-ICR-MS data for the ion of *m/z* 411 indicated that it corresponds to $C_{19}H_{32}O_8Na$. It could probably be hydroperoxy cyclic peroxides and its isomer. This compounds have been reported as secondary oxidation product from methyl linolenate.[174] The structures of *m/z* 411.1990 $[C_{19}H_{32}O_8Na]^+$ are shown in Table 4-13 and Table 4-14.

Table 4-13   Suggestion structures of *m/z* 411.1990 $[C_{19}H_{32}O_8Na]^+$

FT-ICR MS data: *m/z* 411.1990

Formula: $C_{19}H_{32}O_8Na$

Expected chemical structure:
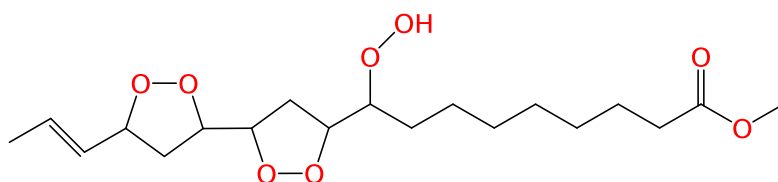
Systematic name: Methyl-10,12,13,15-bisepidioxy-9-hydroperoxy-16-octadecenoic acid

Formula: $C_{19}H_{32}O_8$

Exact mass: 388.2097 Da

Table 4-14   Suggestion structures of *m/z* 411.1990 [C$_{19}$H$_{32}$O$_8$Na]$^+$

FT-ICR MS data: *m/z* 411.1990

Formula: C$_{19}$H$_{32}$O$_8$Na

Expected chemical structure:
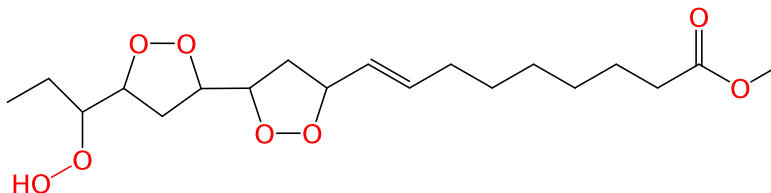
Systematic name: Methyl-10,12,13,15-bisepidioxy-16-hydroperoxy-8-octadecenoic acid

Formula: C$_{19}$H$_{32}$O$_8$

Exact mass: 388.2097 Da

The structures shown for the ions measured are postulated from literatures. Further research in this area and undertaking tandem MS and HPLC-MS/MS studies would help confirm these suggested assignments but this was beyond the time constraints of this project.

4.8   Analysis of FAMEs and oxidation products of FAMEs using GC-MS

GC-EI MS was used for monitoring RME and SME profiles under auto-oxidation. The C18 series consists of C18:1, C18:2 and C18:3 that are specific for monitoring because they contain the different numbers of double bonds which are sensitive to oxidation. Figure 4-31 shows TICC of RME and SME profiles.
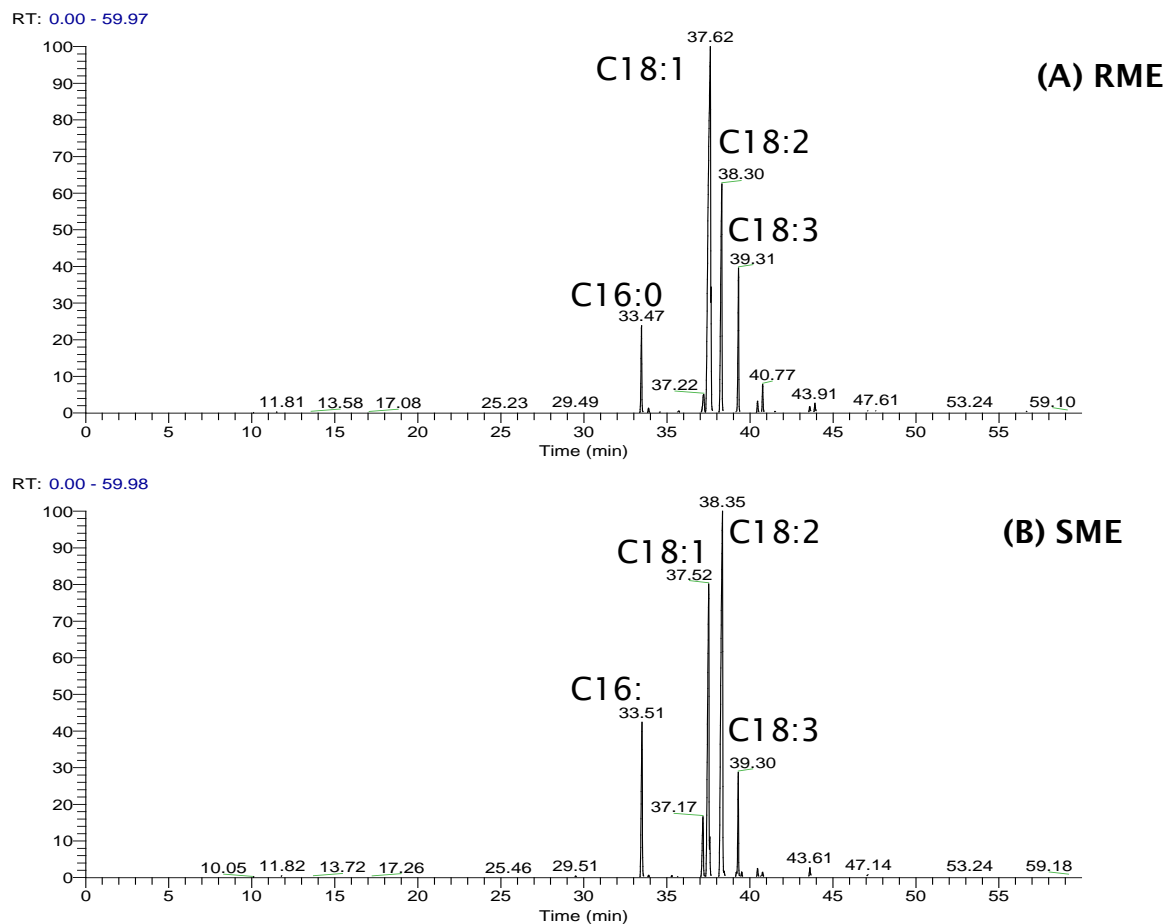
Figure 4-31   GC-MS of RME (A) and SME (B). Column: HP Innowax capillary column, 30 m × 0.25 mm inner diameter, 0.25 μm film thickness. Oven temp.: initial temp. of 40 °C, hold for 4 min, ramp at 5 °C/min until 240 °C, and hold for 16 min.

Figure 4-32 shows two volatile oxidation products, 2,4-decadienal and methyl 9-oxononanoate which were detected in both auto-oxidised RME and auto-oxidised SME using GC-MS. 2,4-Decadienal was present in higher intensity in the auto-oxidised SME samples than that in the auto-oxidised RME samples. The oxidation product, 2,4-decadienal, was suggested that and used as an indicator to determine the degree of the oxidation of oils.[158]

(A) 2,4-Decadienal
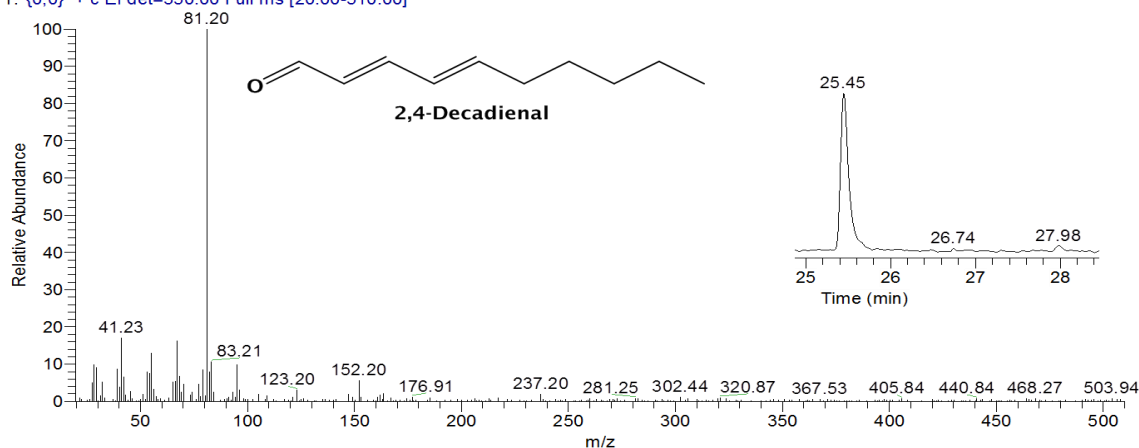
(B) Methyl 9-oxononanoate
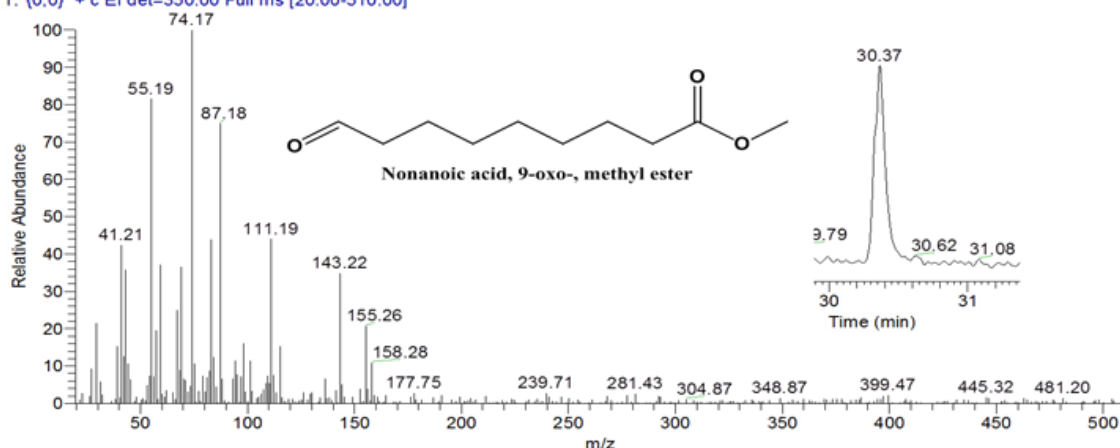
Figure 4-32   70 eV EI mass spectra of the volatile oxidation compounds detected in the auto-oxidised RME sample. (A) 2,4-decadienal and (B) methyl 9-oxononanoate.

Major peaks identified in both the auto-oxidised RME and SME samples correspond to 2,4-decadienal formed by decomposition of 9-hydroperoxides of methyl linoleate, whereas methyl 9-oxononanoate decomposed from a mixture of hydroperoxides of C18:1, C18:2 and C18:3.[78]

4.9   Analysis of antioxidants in fuels using electrochemistry-mass spectrometry (EC-MS)

Presently, the investigations for analysing fuel oxidative stability requires long timeframes (days) due to the inherent stability of most gasoline fuels. This poses challenges for timely and cost effective methods for screening fuel anti-oxidants. The present study aims to develop the EC as screening test and mass spectrometry (MS) as screening test method for anti-oxidants used in a fuel, and to identify components that can potentially lead to other potential issues by using mass spectrometry.

Electrochemical (EC) oxidation has been also used as a surrogate system for investigation of anti-oxidation degradation in hydrocarbon matrices. The use of anti-oxidant can inhibit or prevent the oxidation process by protecting fuels from oxidative degradation that lead to gum formation. The effect of anti-oxidant present in the electrochemical cell was performed by using the GC electrode as working electrode. Figure 4-33 shows electrochemical reaction of BHT. Initial experiments were undertaken to follow the oxidation of the anti-oxidants.
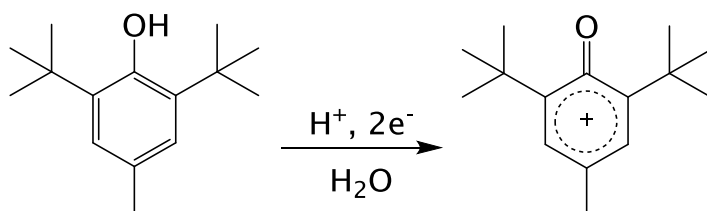
Figure 4-33   Electrochemical reaction mechanisms of BHT.[91]

Various potentials at 1.0, 1.5, 2.0 and 2.5 V were applied to the glassy carbon (GC) working electrode. Positive and negative ion ESI mass spectra were acquired with the EC cell at potential off (no voltage applied) and the EC cell at potential on (voltage applied). 2,6-Di-*tert*-butyl-4-methylphenol (BHT) was chosen as the test compound. BHT contains a phenolic group, which is preferential formed [M - H]- ion. The deprotonated molecule [M - H]- of BHT (*m/z* 219) was observed.

The extracted ion current chromatograms (EICCs) of *m/z* 219 [M - H]-, 235 [M + O - H]- and 251 [M + 2(O) - H]- obtained from the EC cell off and EC cell on at 1.0 V shown in Figure 4-34 and mass spectra of BHT without a voltage applied and with a voltage applied at 1.0 V and 2.0 V for GC are presented in Figure 4-35. The major signals observed were [M - H]- (*m/z* 219) which is the starting compound, ions of *m/z* 235 and 251which are expected oxidation products [M + *n*O - H]- where *n*=1 and 2. The maximum number of additional oxygen atoms produced by increasing the potential in the glassy carbon (GC) working electrode to generate oxidation products of BHT was 2(O). The developed screening method was applied for the analysis of the antioxidant in gasoline samples.

Reference gasoline composition consists of linear paraffins (*n*-pentane, *n*-heptane), branched paraffins (isopentane, isooctane, cyclic paraffins (cyclopentane, cyclohexane), aromatics (benzene, toluene), olefins (2-methyl-2-butene, cyclopentene) oxygenated (ethanol, MTBE).[175]
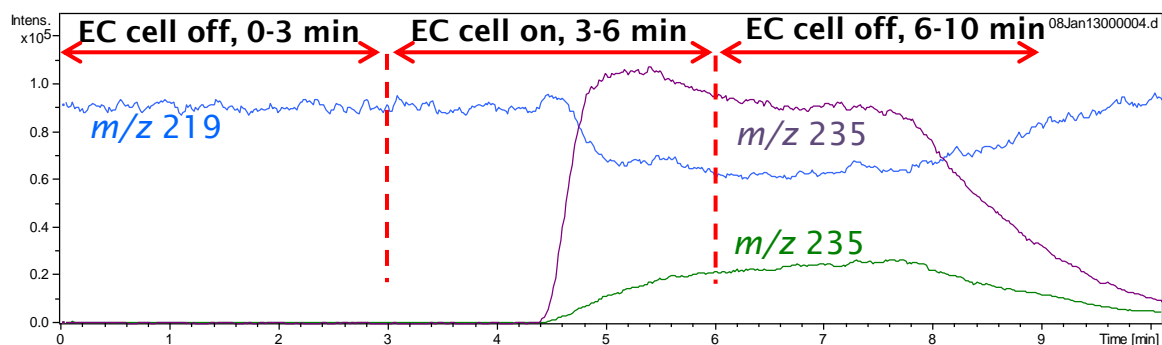
Figure 4-34   EICCs of *m/z* 219 (blue line), 235 (Byzantium line), and 251 (green line) obtained from the glassy carbon (GC) working electrode at EC cell the potential of 1.0 V.
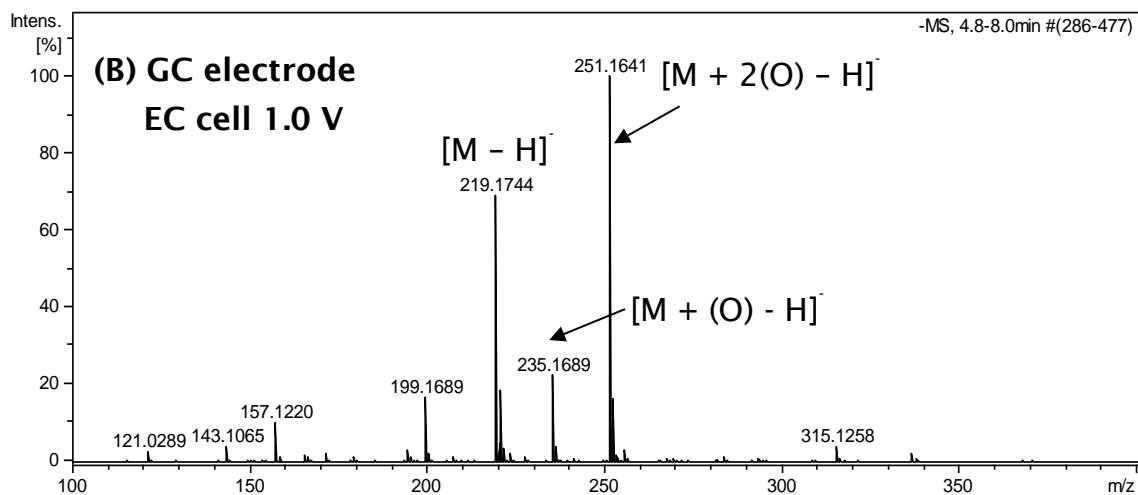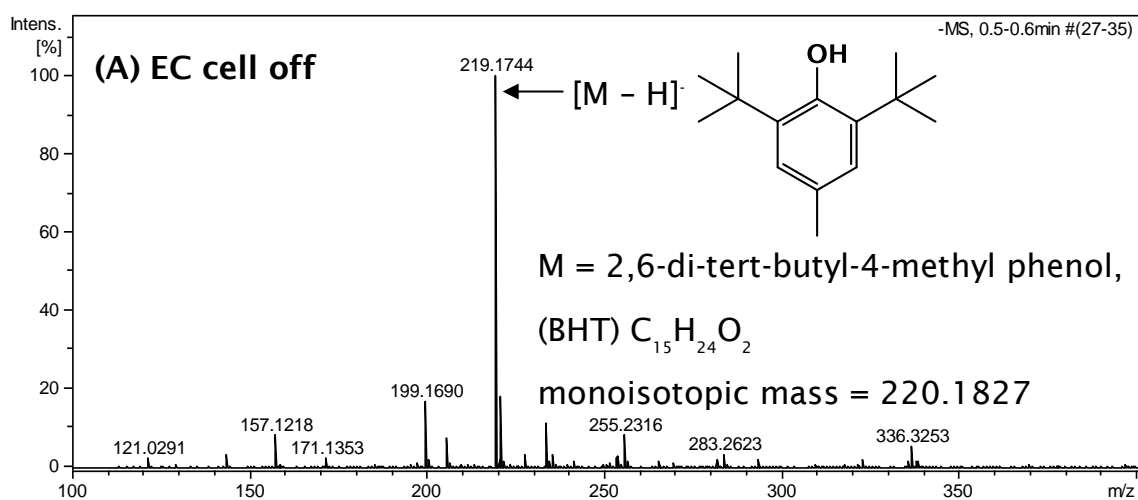
Figure 4-35   Continued overleaf
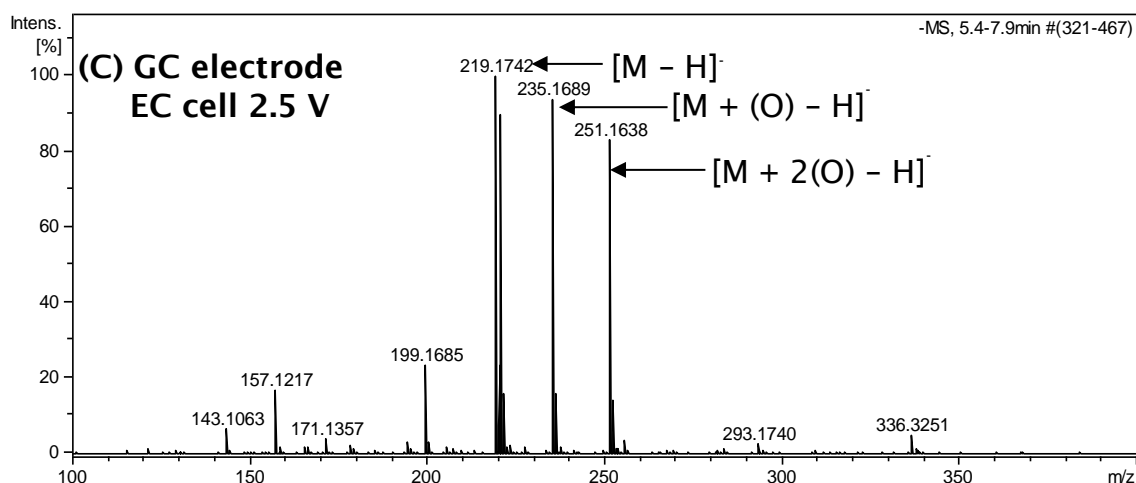
Figure 4-35   Negative ion ESI Mass spectra of 2,6-di-*tert*-butyl-4-methylphenol (BHT) BHT at different EC potentials applied to the glassy carbon (GC) working electrode. (A) EC cell the potential off, (B) EC cell the potential of 1.0 V and (C) EC cell the potential of 2.5 V.

Antioxidant in the fuel samples were determined by electrochemical (EC) using the glassy carbon (GC) working electrode, example data are shown in Figure 4-36 and Figure 4-37 below.
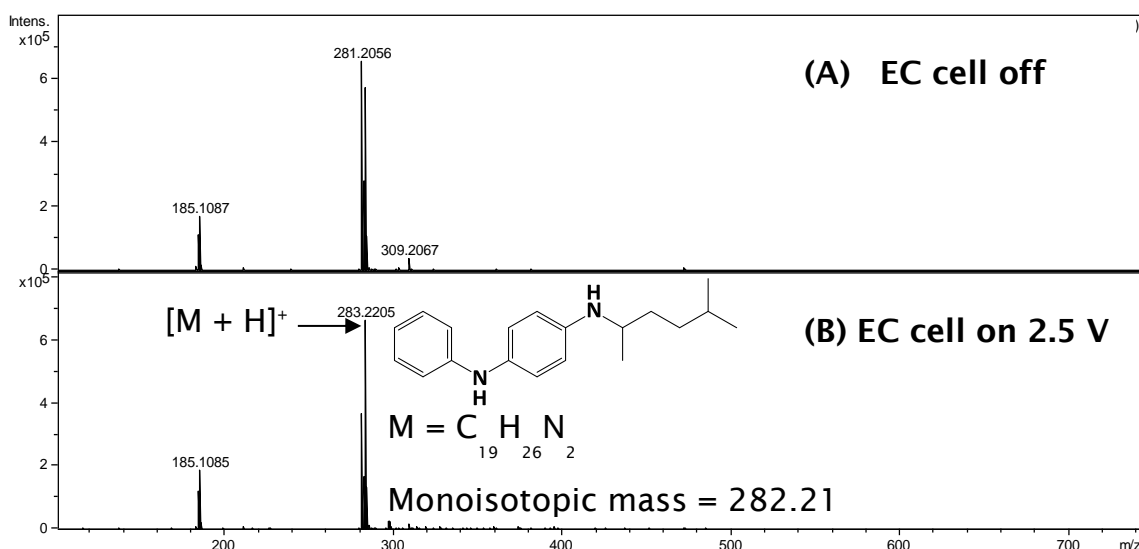
Figure 4-36 Positive ion ESI-MS of *N*-(1,4-dimethylpentyl)-*N*-phenyl-1,4-benzenediamine in the fuel. (A) EC cell the potential off; (B) EC cell the potential of 2.5 V.
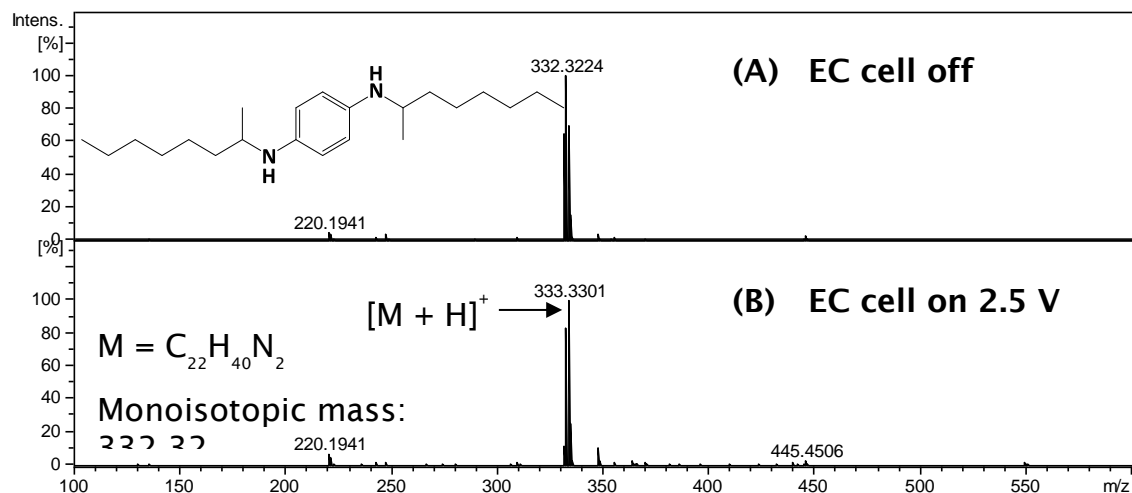
Figure 4-37 Positive ion ESI-MS of *N,N'*-di (2-octanyl)-1,4-benzenediamine in the fuel. (A) EC cell the potential off; (B) EC cell the potential of 2.5 V.

4.10 Summary

The objectives of this project were to separate and identify the oxidation products formed during the oxidation process of RME and SME samples under auto-oxidation conditions compared to accelerated oxidation using on-line EC-ESI MS.

The summarised of this chapter were the following as:

- Coupling of electrochemistry to the electrospray ion source of the mass spectrometer typical oxidation products were observed in minutes compared to months/years for the auto-oxidation process.

- The efficiency of GC and MD working electrodes was compared. Oxygenated species for C18:1, C18:2 and C18:3 with up to +2(O), +6(O), and +9(O), (2.5 V, GC) and +6(O), +8(O), and +12(O) (3.0 V, MD) respectively were observed.

- The potentials of oxidation increased in the order methyl esters of C18:3 < C18:2 < C18:1 for both MD and GC electrodes. The primary oxidation products, hydroperoxides, in the auto-oxidation of unsaturated fatty acid methyl ester (C18:1, C18:2, C18:3) can undergo further oxidation to produce numerous volatile and non-volatile secondary oxidation products.

- The volatile oxidation products, *e.g.* 2,4-decadienal and methyl 9-oxo-nonanoate were observed in auto-oxidation of RME and SME samples analysed by GC-MS.

- HPLC-ESI MS, UHPLC-ESI MS and UHPSFC-ESI MS can be used for the separation of non-volatile of the oxidation products.

- UHPSFC-ESI MS method is better than HPLC-ESI MS and UHPLC-ESI MS methods, can clearly separate oxidation products from parent molecules.

- The elemental formula for these auto-oxidised FAMEs were determined by UHPLC-Q-TOF MS and infusion FT-ICR MS. The presence of oxygenated species up to O (6 oxygen atoms) for the ion at *m/z* 411.1999 $[C_{19}H_{32}O_8 + Na]^+$ with a 2.6 ppm error was observed. It expected as the hydroperoxy bis-cyclic peroxides from auto-oxidised methyl linolenate. The structures shown (see, section 4.7) for the ion measured are postulated from literatures.

Chapter 4: Analysis of FAME oxidation

- On-line EC-ESI MS data show similarity with auto-oxidation, however, EC cell produced higher quantities of oxidation species than auto-oxidation.

- Online-EC-ESI MS shows a great promise for accelerated oxidation studies but further work structural identify of these species will be required.

Chapter 5:   Analysis of FAMEs in AVTUR

Presently, biodiesel has already been utilised successfully in worldwide as alternative fuel to fossil diesel fuel. The distribution of the individual FAMEs in pure biodiesel (B100) depends on the original feedstock. B100 can be used directly or blended with diesel at different ratios (*i.e.* B5 and B20) as a transportation fuel. Biodiesel is usually commercially blended with petrodiesel, *e.g.,* EN590 in the U.K., where petrodiesel incorporates 5% biodiesel.[176] The presence of FAMEs, in AVTUR is increasing concern. FAME can adhere onto surfaces of transmission pipelines and storage tanks. Use of these shared pipelines can lead to FAMEs contamination of AVTUR. At high concentrations FAMEs impact on the thermal stability and freezing point of AVTUR which can lead to engine operational problems. Freezing point of jet A 1 is -47 °C[177] while freezing point of biodiesel is -5 °C.[178]

Despite the rapidity and simplicity of spectroscopic and direct injection ESI-MS methods, chromatographic methods are required to separate FAMEs from a complex mixture of hydrocarbons in AVTUR. NP-HPLC with two detectors connected in series: ultraviolet-diode array detector (UV-DAD) followed by reflective index detector (RID) can be used for the determination of FAME in diesel fuels. This method can separate all the FAME components as a single peak obtained using NH_2 HPLC column.[179] GC-MS methods are mostly used for the determination of FAME content in diesel fuels. The single column GC often involves a complex sample preparation procedure, such as extraction and derivatisation, to

eliminate the interference of some blend components. The analysis is time-consuming and tedious, especially when applied to determine the FAME content in diesel fuel.

The existing ASTM GC-MS reference method (IP585/10) quantifies rapeseed methyl ester (RME, mainly C16 and C18 species)[98], but not low carbon number FAMEs from coconut oil (C8-C14), a feedstock used in the Pacific region. However, determining low levels of FAMES with gas chromatography is difficult due to the thousands of hydrocarbons found in AVTUR.[99] Comprehensive two-dimensional gas chromatography (GC×GC) has been shown to be an effective approach for the characterisation of petroleum-based fuels such as gasoline and diesel.[180][181] Comprehensive Two-dimensional gas chromatography (GC x GC) offers a powerful way to determine ppm level FAME content in the presence of bulk hydrocarbon material

The objective of this project was to quantify all of the RME (C16:0-C18:3) and the short-chain chain FAMEs (C8-C14), *e.g.*, from coconut oil FAMEs in AVTUR at the 5 mg/kg (5 ppm, w/w) level. The aim was to develop methods including GC-MS, HPLC-MS, UHPLC-MS and UHPSFC-MS methods and to compare them to the existing reference GC-MS method for the determination of low-carbon-number FAMEs.

5.1 Analysis of FAMEs in AVTUR using GC-MS

For these initial experiments, compositional profiles of FAMEs from two different feedstock types were analysed using a 30 m polar column using the GC-MS conditions that were developed in our laboratory and the results are shown in Figure 5-1. The major components of rapeseed methyl ester (RME) are unsaturated methyl esters, consisting of a series of C18 compounds with C18:1 > C18:2 > C18:3 > C18:0. Coconut methyl esters (CME) contains mostly saturated fatty acid methyl esters and the dominant component is C12:0.
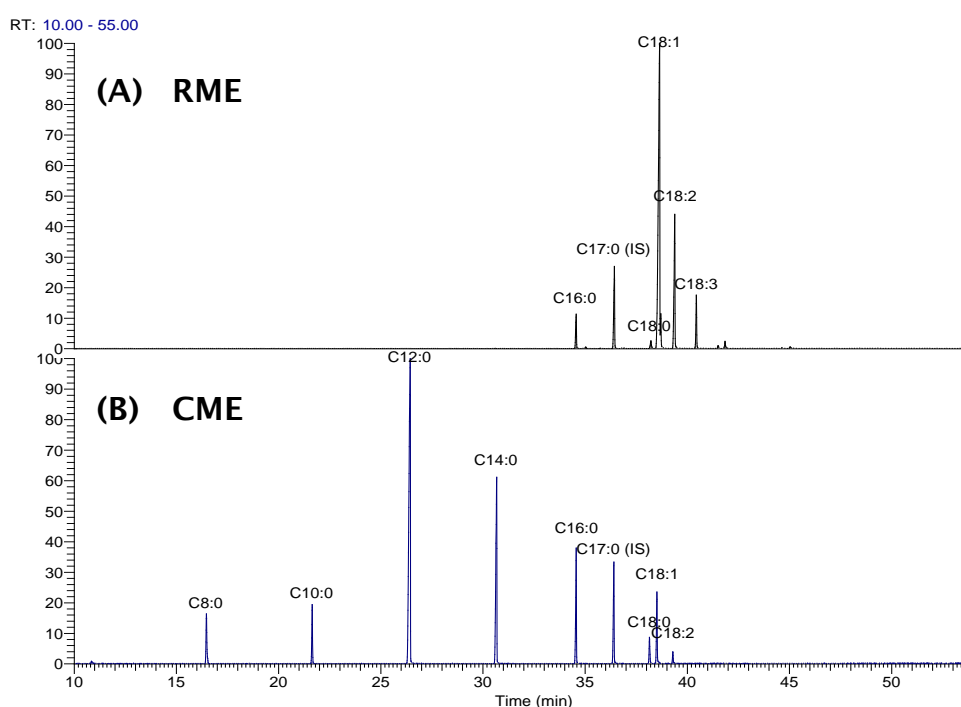
Figure 5-1   **TICCs of RME (A) and CME (B) using HP Innowax capillary column, 30 m × 0.25 mm i.d. 0.25 µm film thickness. Oven temp: Initial temp 40 ºC and hold 4 min, ramp at 5 ºC/min until 240 ºC hold for 16 min.**

Initially CME was analysed using the 60 m column, the GC-MS conditions which were set following the IP 585/10 method, see experiment section 3.3.5. The initial column temperature was set to 150 °C with constant carrier gas flow rate of 0.6 mL/min, and a 20 min solvent delay time. A reconstructed ion current chromatogram (RICC), *m/z* 74, is shown in Figure 5-2. The limitation of this method is that it cannot detect all the short chain FAMEs (C8-C12), which are the major components of CME. The GC-MS conditions were proposed in the IP 585/10 method which was developed by the Energy Institute for the determination rapeseed methyl esters (RME) (C16:0 to C18:3) in AVTUR, IP585/10.
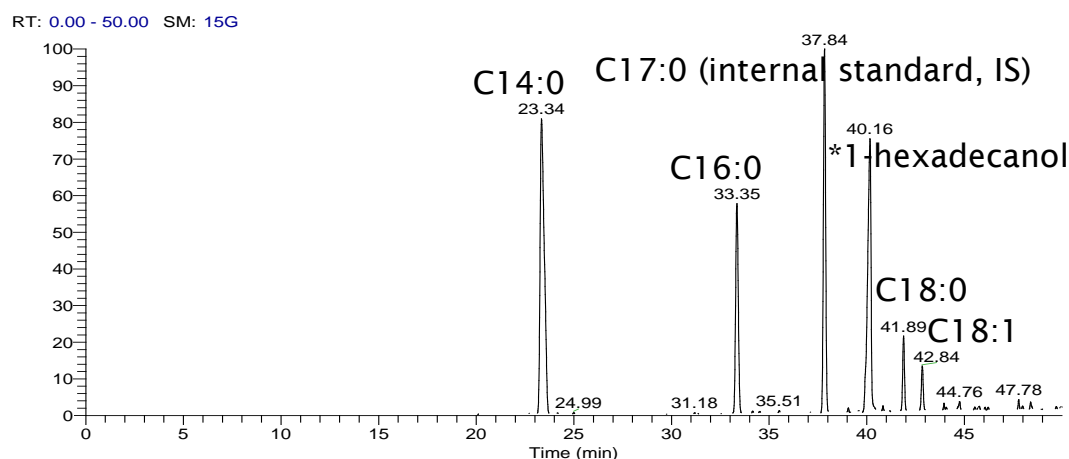
Figure 5-2   **RICC of *m/z* 74 of CME at 100 ppm in n-dodecane using an Innowax 60 m × 0.25 mm 0.5 μm film, carrier gas flow rate 0.6 mL/min and initial temp. at 150 °C for 5 min, ramped at a rate of 12 °C/ min up to 200 °C for 17 min, then ramped 3 °C/min up to 252 °C and hold for 6.5 min, solvent delay time: 20 min.**

In this work a GC-MS method was required for separation, detection and quantification of short chain FAMEs, for example, C12:0 and C14:0 from coconut methyl ester (CME) that adhered to the method described in IP585/10 where these species are present in AVTUR.

5.1.1 Revised IP 585/10, the reference GC-MS method

The requirements of the EI were that any new method for the analysis of the short chain methyl esters (CME) should be closely related to the existing reference method (IP/585/10). One microliter of samples were introduced *via* a splitless injector at a temperature of 260 °C. The oven temperature programme used was 150 °C for 5 min, ramped at a rate of 12 °C/min up to 200 °C for 17 min, then ramped at a rate of 3 °C/min up to 252 °C and held at the final temperature for 6.5 min, column flow rate was 1.0 mL/min and a 10 min solvent delay time. Figure 5-3 shows RICCs of *m/z* 74, 87 of CME.
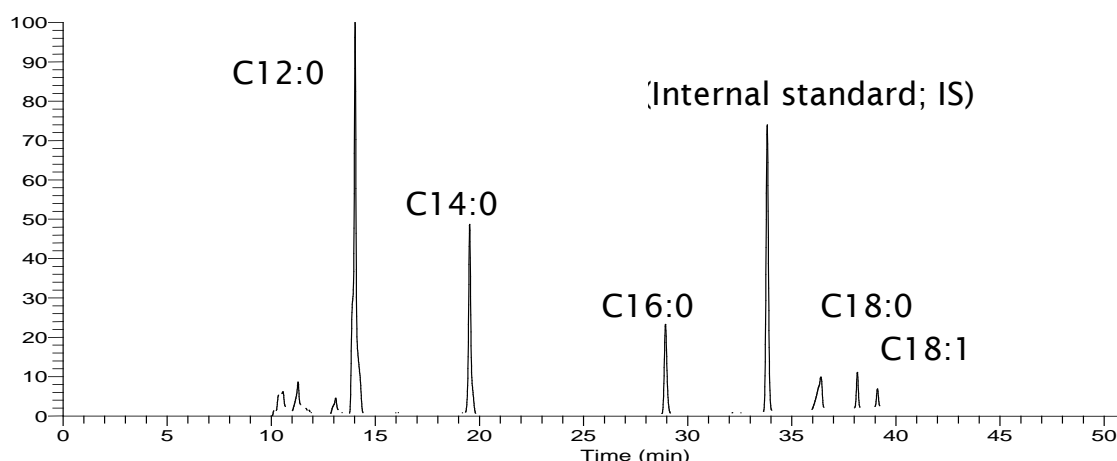
Figure 5-3 **RICCs of *m/z* 74, 87 of CME at 100 ppm in n-dodecane using an Innowax 60 m × 0.25 mm 0.5 μm film, constant carrier gas flow rate 1.0 mL/min and initial column temperature at 150 °C for 5 min, ramped at a rate of 12 °C/min up to 200 °C for 17 min, then ramped at a rate of 3 °C/min up to 252 °C and held at the final temperature for 6.5 min, solvent delay time 10 min.**

Electron ionisation (EI) mass spectra for each FAME component are shown in Figure 5-4. The fragmentations of FAMEs in 70 eV EI-MS provided very useful information in the mass spectrum of each FAME component to

identify saturated and unsaturated FAMEs. The base peaks in mass spectra of straight-chain methyl esters in the C_6-C_{26} range arise from β-cleavage with transfer of a γ-hydrogen atom, resulting in the formation of an ion *m/z* 74 (see, Figure 5.4). This process is named as the McLafferty rearrangement.[182]
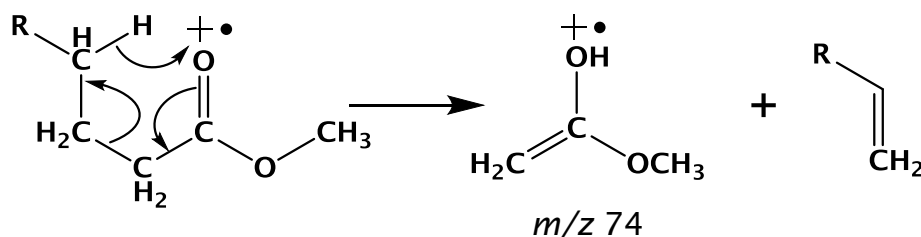
Figure 5-4   Formation of *m/z via* McLafferty rearrangement.

Saturated FAMEs are dominated by the ion at *m/z* 74 $[CH_2C(OH)OCH_3]^{+\cdot}$ (Figure 5-5 (A)) from the McLafferty rearrangement. Losses of aliphatic radicals produces a series of ions, $[(CH_2)_nCO_2CH_3]^+$, where *m/z* 87 is the maximum intensity. The significant ions in monoenes of FAME are a series of ions, $[C_nH_{2n}-1]^+$ and the base peak is *m/z* 55 $[C_4H_7]^+$ (Figure 5-5 (B)). FAME or methylene-interrupted obtain a series of $[C_nH_{2n-3}]^+$, *m/z* 67 is usually the base peak (Figure 5-5 (C)). In addition, in spectra of with trienes the series with molecular formula $[C_nH_{2n-5}]^+$ are dominant, *m/z* 79 $[C_6H_7]^+$ (Figure 5-5 (D)) is usually the base peak.
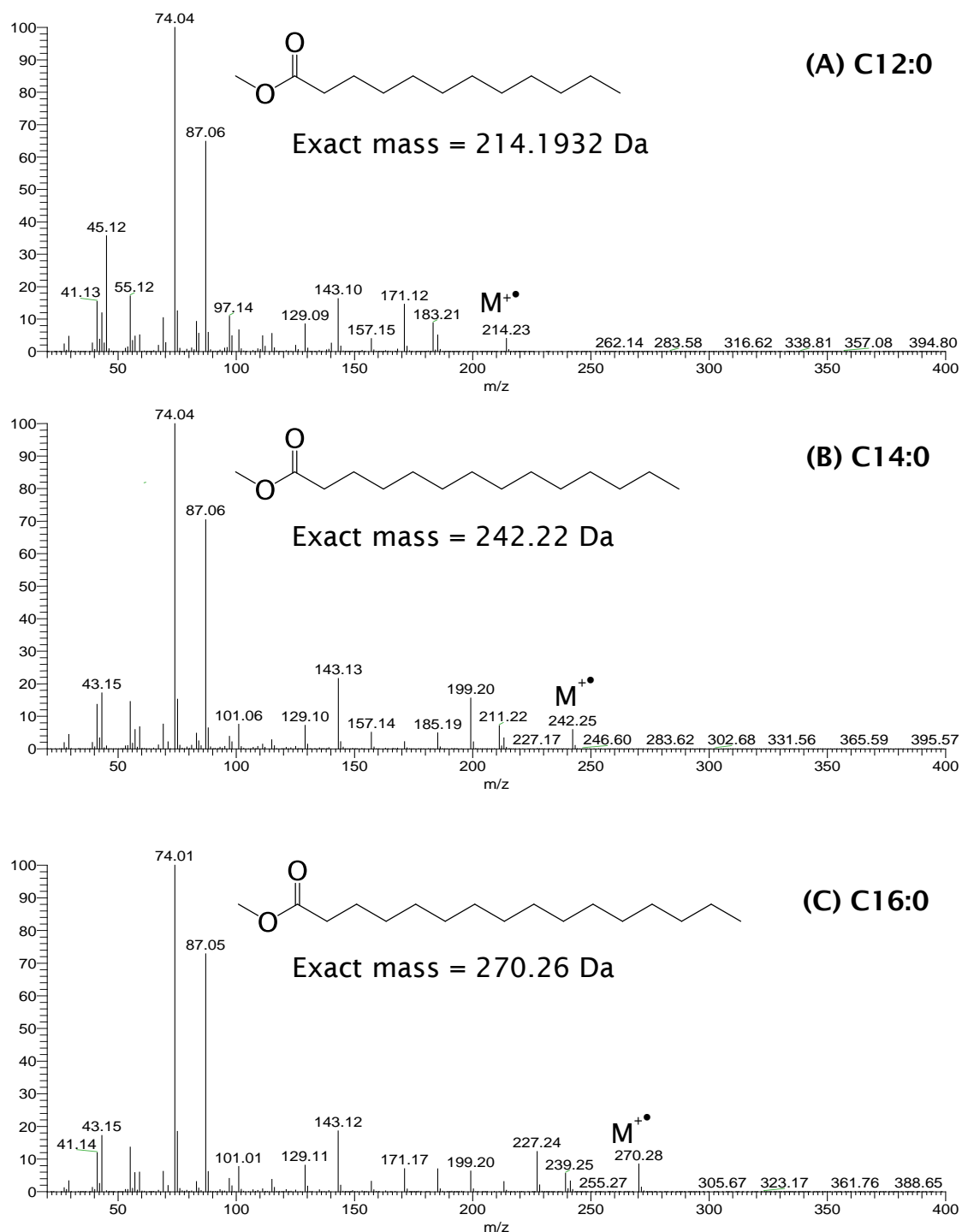
(A) C12:0

Exact mass = 214.1932 Da

(B) C14:0

Exact mass = 242.22 Da

(C) C16:0

Exact mass = 270.26 Da

Figure 5-5   **Continued overleaf**
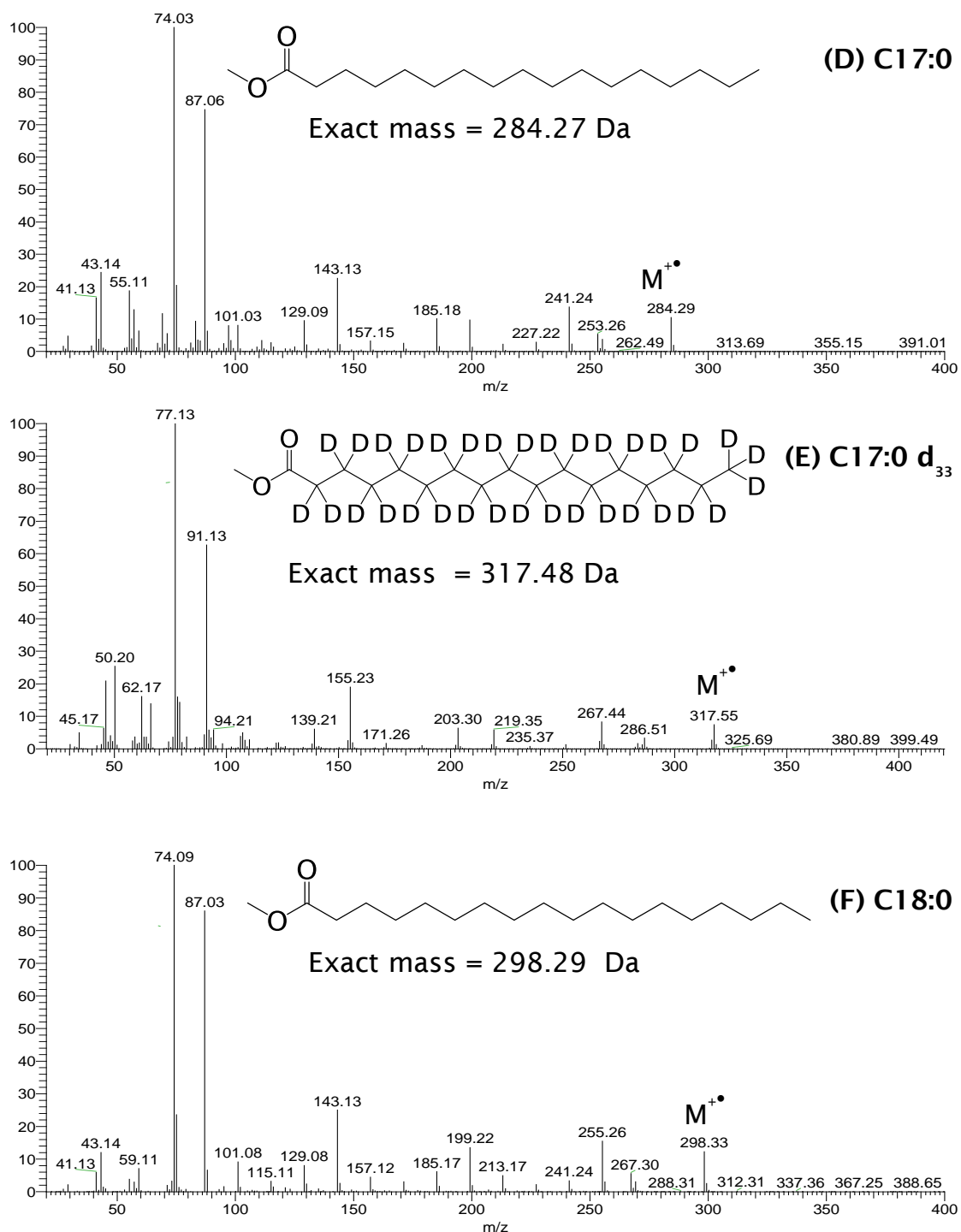
Figure 5-5   Continued overleaf
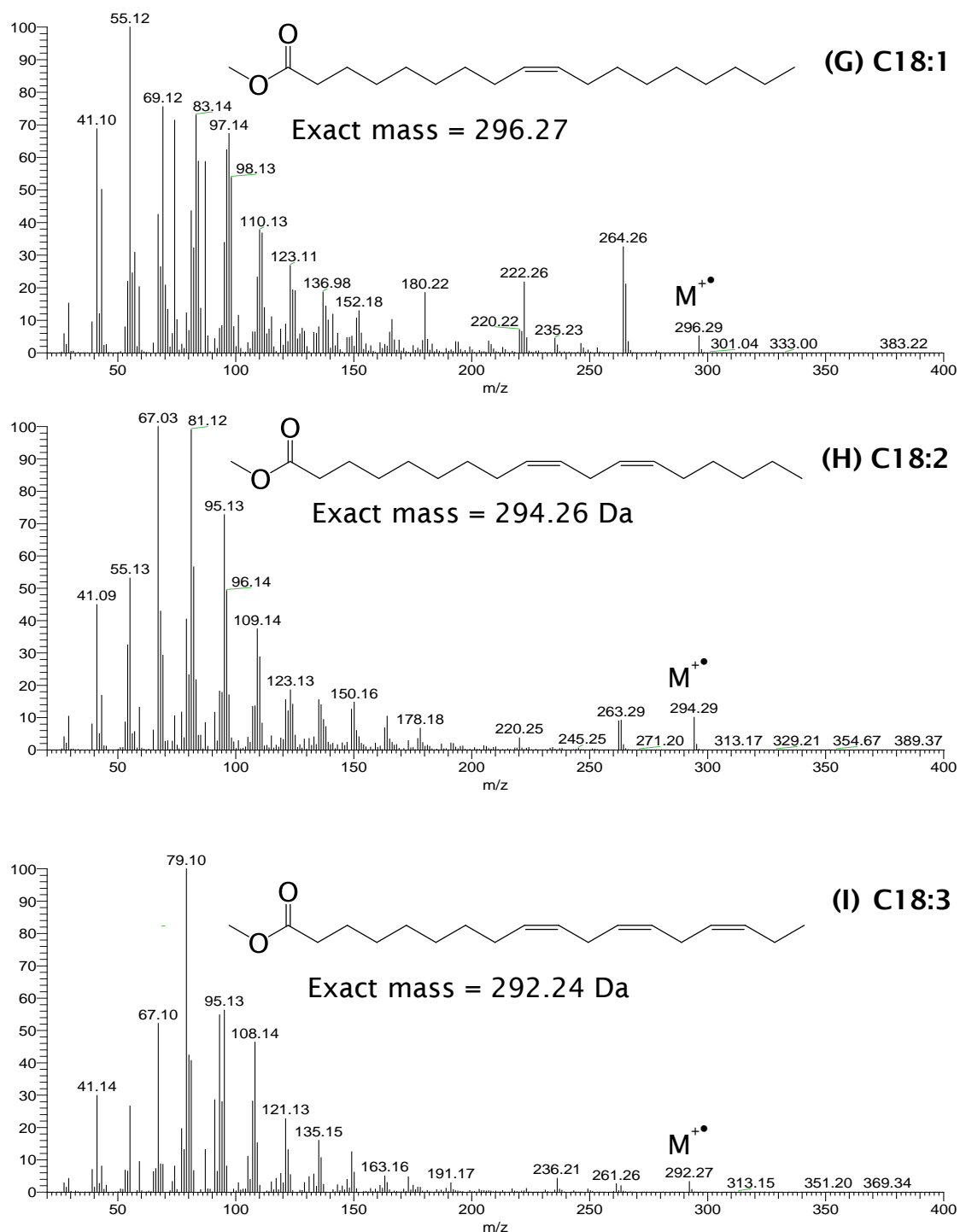
Figure 5-5 70eV EI-MS of each FAMEs: (A) C12:0, (B) C14:0, (C) C16:0, (D) C17:0, (E) C17:0 d$_{33}$, (F) C18:0, (G) C18:1, (H) C18:2 and (I) C18:3.

Chapter 5: Analysis of FAMEs in AVTUR

Due to natural background of high end naphtha components present in the fuel, complete separation of the FAMEs from these materials is difficult. Selected-ion monitoring (SIM) and reconstructed ion current chromatograms (RICCs) from scan data were considered. Factors considered when selecting which ions to monitor using SIM were (i) the ions at high mass are usually molecular ions (ii) the quantitative ion is generally the most abundant ion (iii) the qualifier is the second most abundant ions which show uniqueness.[183][184]

Figure 5-6 to Figure 5-12 show a linear dynamic range for RME and CME in n-dodecane. The detection of individual FAME and total FAMEs for 0–150 mg/kg. A 10 ppm of methyl heptadecanoate (C17:0) was used as the internal standard. Peak areas, relative to the internal standard, of the RICCs of selected ions of each FAME species were plotted versus the FAME concentration. The ions to be used for quantification of FAME species are shown in Table 5-1 to Table 5-2. Excellent linearity was achieved in all cases with a linear correlation (R^2) higher than the required value for FAMEs in AVTUR, IP585/10 ($R^2 = 0.9850$).[98]
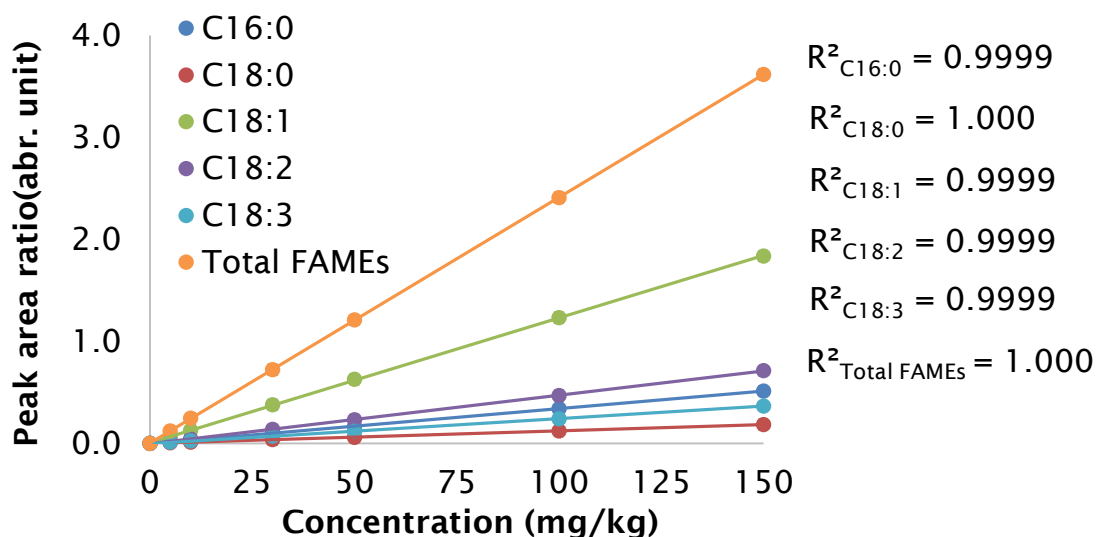
Figure 5-6 Internal calibration curve of RME in n-dodecane by using base peak ions, *m/z* 74 for C16:0, C18:0 and *m/z* 55, 67, 79 for C18:1, C18:2 and C18:3, respectively. Number of replicate measurements = 3.
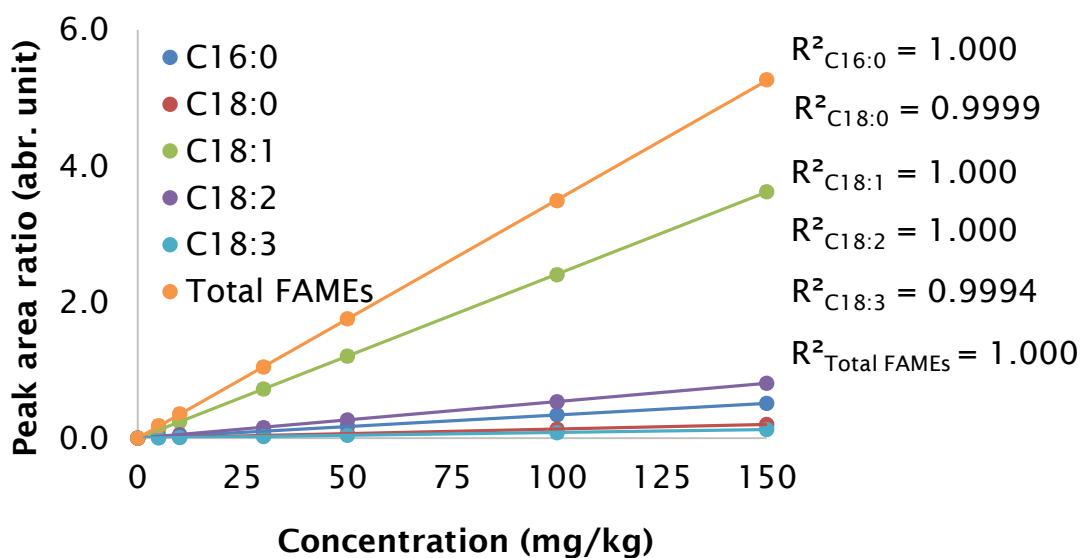
Figure 5-7 Internal calibration curve of RME in n-dodecane by using RICCs followed the IP 585/10 method.[91] RICCs *m/z* 227, 239, 270, 27 for C16:0, *m/z* 255, 267, 298 for C18:0, *m/z* 264, 265, 296 for C18:1, *m/z* 262, 263, 264, 294, 295 for C18:2, *m/z* 236, 263, 292, 293 for C18:3. Number of replicate measurements = 3.

$R^2_{C16:0} = 1.000$

$R^2_{C18:0} = 0.9999$

$R^2_{C18:1} = 0.9999$

$R^2_{C18:2} = 0.9999$

$R^2_{C18:3} = 0.9989$

$R^2_{Total\ FAMEs} = 1.000$
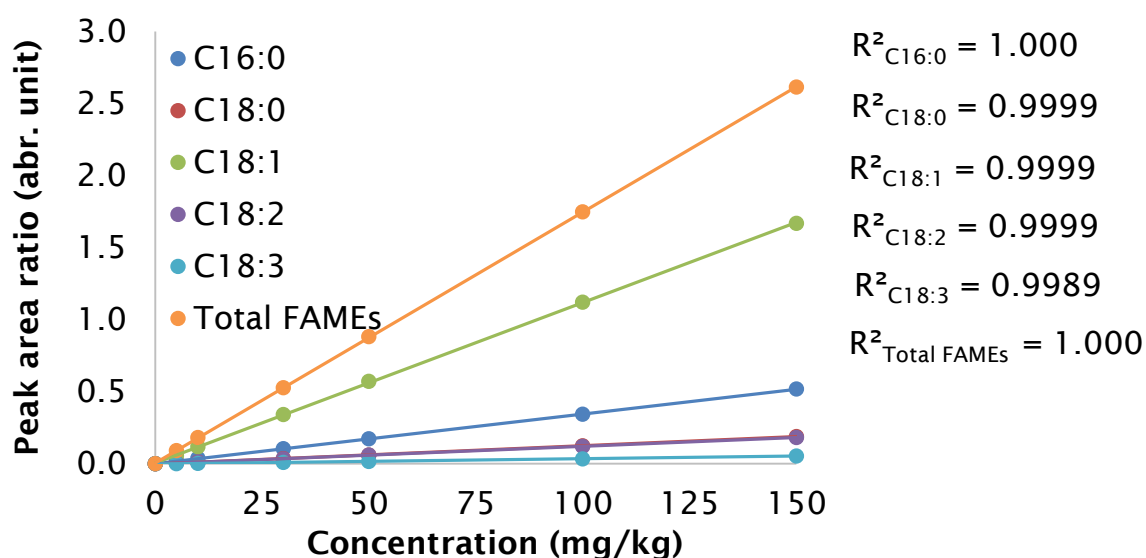
Figure 5-8 Internal calibration curve of RME in n-dodecane by using RICCs *m/z* 74, 87, 227, 239, 270, 27 for C16:0, *m/z* 74, 87, 255, 267, 298 for C18:0, *m/z* 55, 264, 265, 296 for C18:1, *m/z* 67, 262, 263, 264, 294, 295 for C18:2, *m/z* 79, 236, 263, 292, 293 for C18:3. Number of replicate measurements = 3.

$R^2_{C16:0} = 0.9992$

$R^2_{C18:0} = 0.9991$

$R^2_{C18:1} = 0.9990$

$R^2_{C18:2} = 0.9995$

$R^2_{C18:3} = 0.9995$

$R^2_{Total\ FAMEs} = 0.9992$
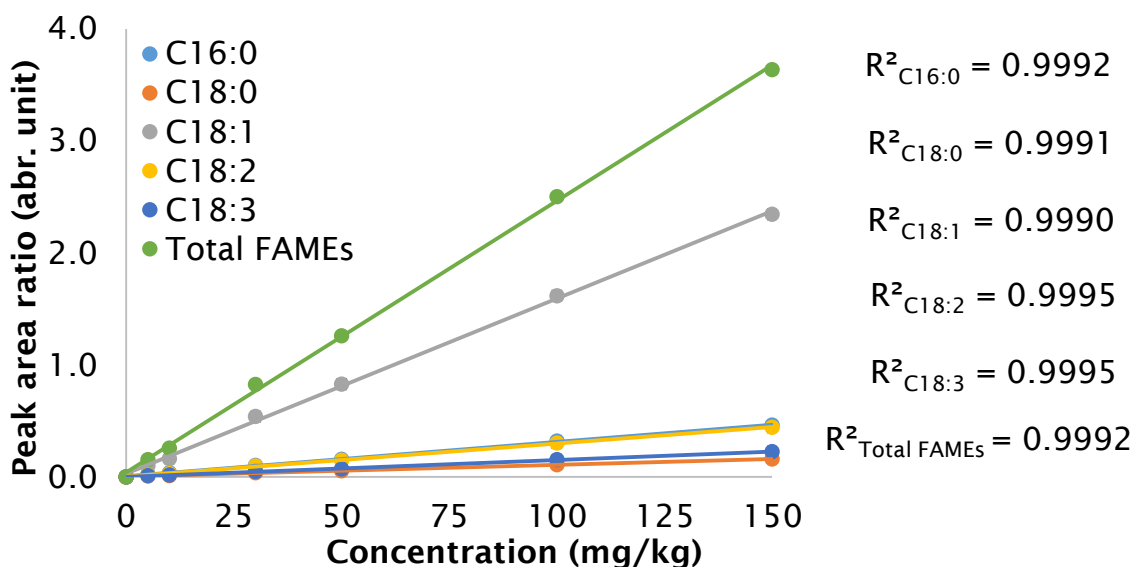
Figure 5-9 Internal calibration curve of RME in n-dodecane by using SIM ions *m/z* 74, 79, 81, 87, 227, 239, 270, 271 for C16:0, *m/z* 74, 79, 81, 87, 255, 267, 298 for C18:0, *m/z* 55, 74, 79, 81, 87, 264, 265, 296 for C18:1, *m/z* 67, 74, 79, 81, 87, 262, 263, 264, 294, 295 for C18:2 and *m/z* 74, 79, 81, 87, 236, 263, 292, 293 for C18:3. Number of replicate measurements = 3.

Table 5-1   **Summarised R^2 of RME acquisition in RICCs and SIM data**

RME	Selected ions	Calibration equation (y = mx + b)	R^2
C16:0	*m/z* 74	y = 0.0034x - 0.0014	0.9999
	m/z 227, 239, 270, 271	y = 0.0034x + 0.0020	1.000
	m/z 74, 87, 227, 239, 270, 271	y = 0.0034x + 0.0019	1.000
	SIM ions: *m/z* 74, 79, 81, 87, 227, 239, 270, 271	y = 0.0031x + 0.0057	0.9992
C18:0	*m/z* 74	y = 0.0012x + 0.0005	1.000
	m/z 255, 267, 298	y = 0.0013x + 0.0009	0.9999
	m/z 74, 87, 255, 267, 298	y = 0.0013x - 0.0005	0.9999
	SIM ions: *m/z* 74, 79, 81, 87, 255, 267, 298	y = 0.0011x + 0.0022	0.9991
C18:1	*m/z* 55	y = 0.0122x + 0.0071	0.9999
	m/z 264, 265, 296	y = 0.0241x + 0.0011	1.000
	m/z 55, 264, 265, 296	y = 0.0156x + 0.0279	0.9999
	SIM ions: *m/z* 55, 74, 79, 81, 87, 264, 265, 296	y = 0.0156x + 0.0279	0.9990
C18:2	*m/z* 67	y = 0.0048x – 0.0024	0.9999
	m/z 262, 263, 264, 294, 295	y = 0.0054x - 0.0014	1.000
	m/z 67, 262, 263, 264, 294, 295	y = 0.0030x + 0.0022	0.9995
	SIM ions: *m/z* 67, 74, 79, 81, 87, 262, 263, 264, 294, 295	y = 0.0030x + 0.0022	0.9995

Table 5-1   (continued) Summarised R² of RME acquisition in RICCs and SIM data

RME	Selected ions	Calibration equation (y = mx + b)	R^2
C18:3	*m/z* 79	y = 0.0024x - 0.0007	0.9999
	m/z 236, 263, 292, 293	y = 0.0008x - 0.0006	0.9994
	m/z 79, 236, 263, 292, 293	y = 0.0015x + 0.0012	0.9995
	SIM ions: *m/z* 74, 79, 81, 87, 236, 263, 292, 293	y = 0.0015x + 0.0012	0.9995
Total FAMEs	a	y = 0.0241x + 0.0034	1.000
	b	y = 0.0350x + 0.0019	1.000
	c	y = 0.0174x + 0.0054	1.000
	c	y = 0.0242x + 0.0391	0.9992

Note: a = total FAMEs from summed area of RICCs using base peak ion of each FAME component (*m/z* 74 for C16:0, C18:0, *m/z* 55 for C18:1, *m/z* 67 C18:2 and *m/z* 79 for C18:3).

b = total FAMEs from summed area of RICCs using selected ions following IP585/10[98] SIM ions for each FAME components

c = total FAMEs from summed area of RICCs using selected ions following IP585/10[98] and *m/z* 74 for C16:0, C18:0, *m/z* 55 for C18:1, *m/z* 67 C18:2 and *m/z* 79 for C18:3)

d = total FAMEs from summed area of SIM ions

$R^2_{C12:0} = 0.9997$

$R^2_{C14:0} = 0.9998$

$R^2_{C16:0} = 0.9999$

$R^2_{C18:0} = 0.9998$

$R^2_{C18:1} = 0.9994$

$R^2_{Total\ FAMEs} = 0.9998$
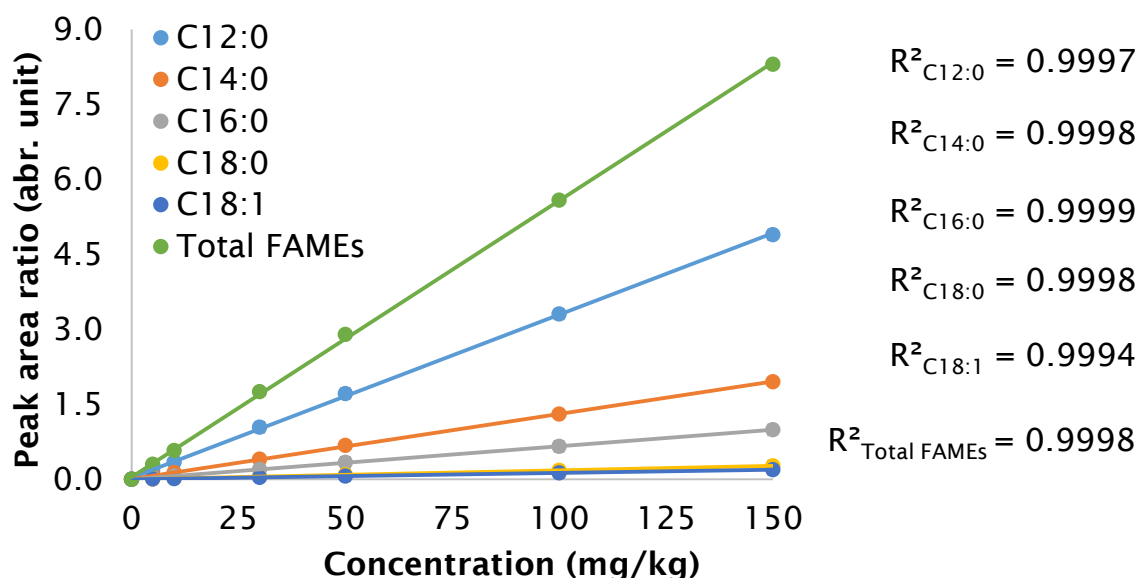
Figure 5-10   Internal calibration curve of CME in n-dodecane by using base peak ions, *m/z* 74 for C12:0, C14:0, C16:0, C18:0 and *m/z* 55 and 67 for C18:1 and C18:2, respectively. Number of replicate measurements = 3.

$R^2_{C12:0} = 0.9997$

$R^2_{C14:0} = 0.9997$

$R^2_{C16:0} = 0.9998$

$R^2_{C18:0} = 0.9999$

$R^2_{C18:1} = 1.000$

$R^2_{Total\ FAMEs} = 0.9997$
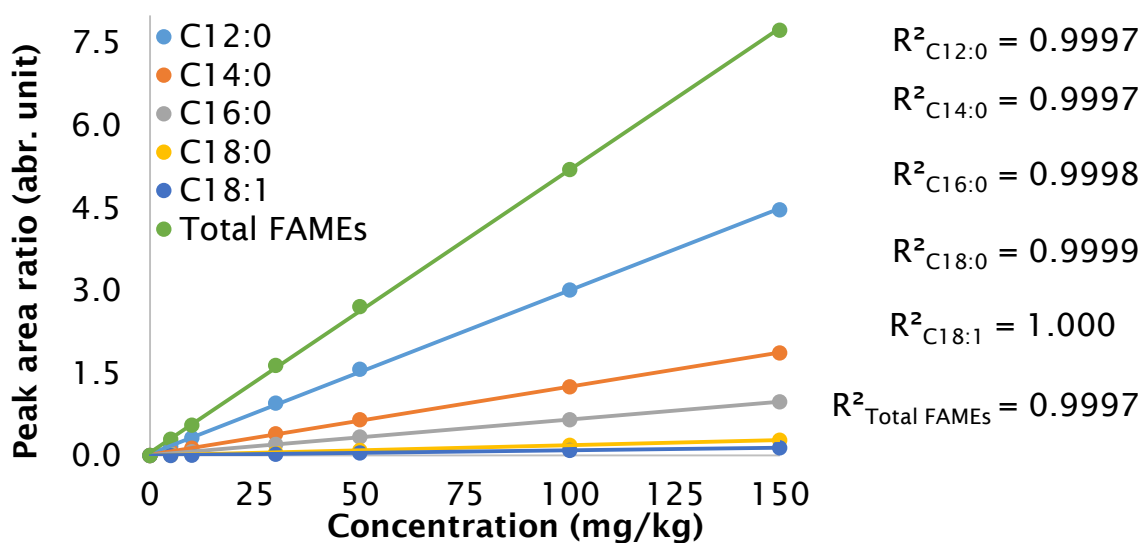
Figure 5-11   Internal calibration curve of CME in n-dodecane by using RICCs *m/z* 74, 87, 214 for C12:0, *m/z* 74, 87, 242 for C14:0, *m/z* 74, 87, 270 for C16:0, *m/z* 74, 87, 298 for C18:0, *m/z* 55, 74, 87, 296 for C18:1. Number of replicate measurements = 3.
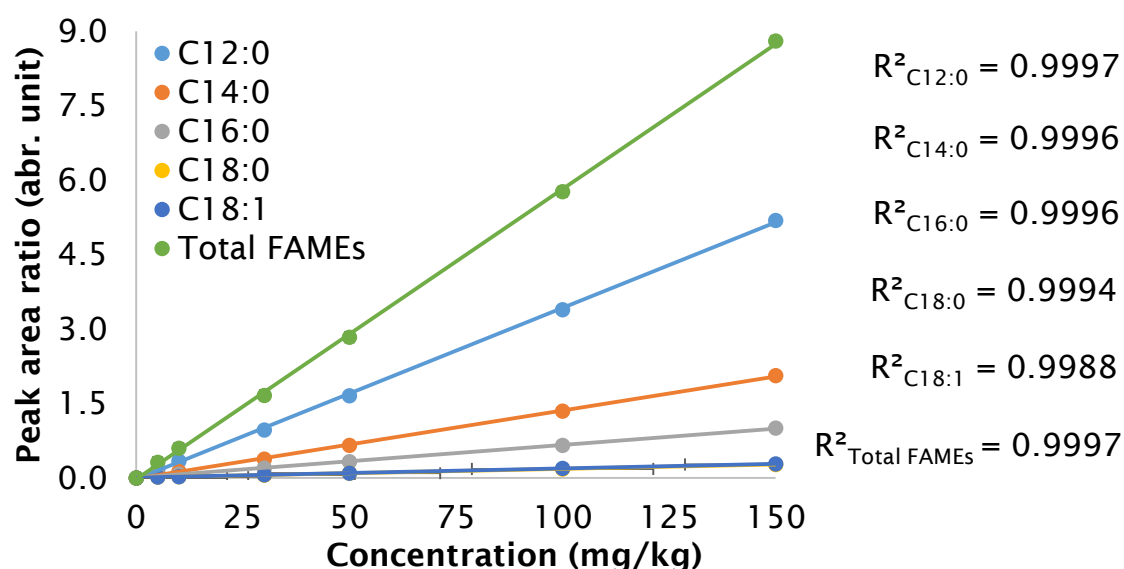
Figure 5-12   Internal calibration curve of CME in n-dodecane by using SIM ions *m/z* 74, 79, 81, 87, 171, 183, 214 for C12:0, *m/z* 74, 79, 81, 87, 199, 211, 242 for C14:0, *m/z* 74, 79, 81, 87, 227, 239, 270, 271 for C16:0, *m/z* 74, 79, 81, 87, 255, 267, 298 for C18:0, *m/z* 55, 74, 79, 81, 87, 264, 265, 296 for C18:1. Number of replicate measurements = 3.

Table 5-2   (continued) Summarised R^2 of CME acquisition in RICCs and SIM data

FAMEs from CME	Selected ions	Calibration equation (y = mx+b)	R^2
C12:0	*m/z* 74	y = 0.0326x + 0.0338	0.9997
	m/z 74,87, 214	y = 0.0297x + 0.0336	0.9997
	SIM ions: *m/z* 74, 79, 81, 87, 171, 183, 214	y= 0.0345x - 0.0273	0.9997
C14:0	*m/z* 74	y = 0.0130x + 0.0093	0.9998
	m/z 74,87, 242	y = 0.0124x + 0.0155	0.9997
	SIM ions: *m/z* 74, 79, 81, 87, 199, 211, 242	y = 0.0137x - 0.0137	0.9996
C16:0	*m/z* 74	y = 0.0066x + 0.0027	0.9999
	m/z 74,87, 270	y = 0.0065x + 0.0069	0.9998

Table 5-2   **(continued) Summarised R^2 of CME acquisition in RICCs and SIM data**

FAMEs from CME	Selected ions	Calibration equation (y = mx+b)	R^2
	SIM ions: *m/z* 74, 79, 81, 87, 227, 239, 270, 271	y = 0.0066x + 0.0060	0.9996
C18:0	*m/z* 74	y = 0.0018x + 0.0015	0.9998
	m/z 74, 87, 298	y = 0.0019x + 0.0010	0.9999
	SIM ions: *m/z* 74, 79, 81, 87, 255, 267, 298	y = 0.0018x + 0.0046	0.9994
C18:1	*m/z* 55	y = 0.0013x + 0.0029	0.9994
	m/z 55, 74, 87, 296	y = 0.0010x - 0.0006	1.000
	SIM ions: *m/z* 55, 74, 79, 81, 87, 264, 265, 296	y = 0.0019x + 0.0067	0.9988
Total FAMEs	a	y = 0.0553x + 0.0501	0.9998
	b	y = 0.0514x + 0.0564	0.9997
	c	y = 0.0585x - 0.0237	0.9997

Note: a = total FAMEs from summed area of RICCs using base peak ion of each FAME component (*m/z* 74 for C12:0, C14:0, C16:0, C18:0 and *m/z* 55 for C18:1).

b = total FAMEs from summed area of RICCs 74, 87, base peak ions and $M^{+\bullet}$c = total FAMEs from summed area of SIM ions

The revised the IP585/10 provided satisfied to achieve a satisfactory separation of the all FAME components in n-dodecane. However, when FAME in a spiked AVTUR sample is directly injected on the GC column then the matrix of the fuel can impact on the FAME peaks, causing some of them to have slightly longer retention times, as presented in Figure 5-13.

Chapter 5: Analysis of FAMEs in AVTUR

The retention time of earlier eluted peaks have a slightly longer shift when the matrix effect was present. The retention times of C14:0 and C16:0 in AVTUR are estimated 0.16 and 0.08 minutes longer when compared to the retention time in n-dodecane, but the retention shifted. Especially, the peaks of C12:0 and C14:0 in the chromatograms Figure 5-13 (B) co-eluted with the fuel matrix. Retention times of C17:0, C18:0 and C18:1 were not significantly shifted.
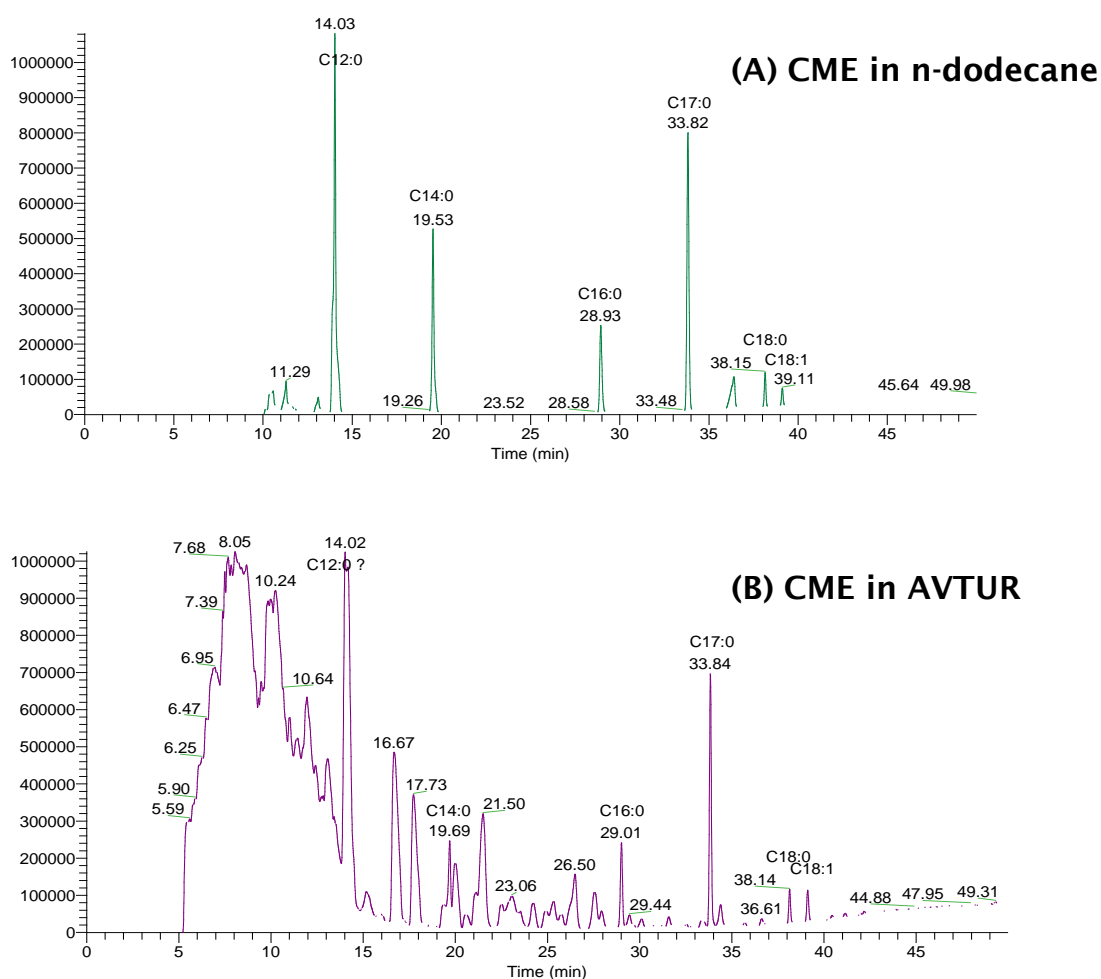
Figure 5-13   Comparison of the retention times obtained by injection coconut methyl ester (CME) in n-dodecane (A) and spiked CME in AVTUR.

Matrix effects were studied by comparing the response from FAMEs in AVTUR with FAMEs in n-dodecane. The sensitivity difference between solvent (n-dodecane) calibration and the fuel matrix calibration is shown in Figure 5-14. The plots of CME, *i.e.* C12:0 in n-dodecane and spiked CME in AVTUR. The response of C12:0 in AVTUR was higher than that in n-dodecane as a result of matrix-induced enhancement. Whereas the response of C14:0 in the AVTUR was lower than that in the fuel matrix as a result of matrix-induced diminishment.

(A) C12:0 in AVTUR and n-dodecane
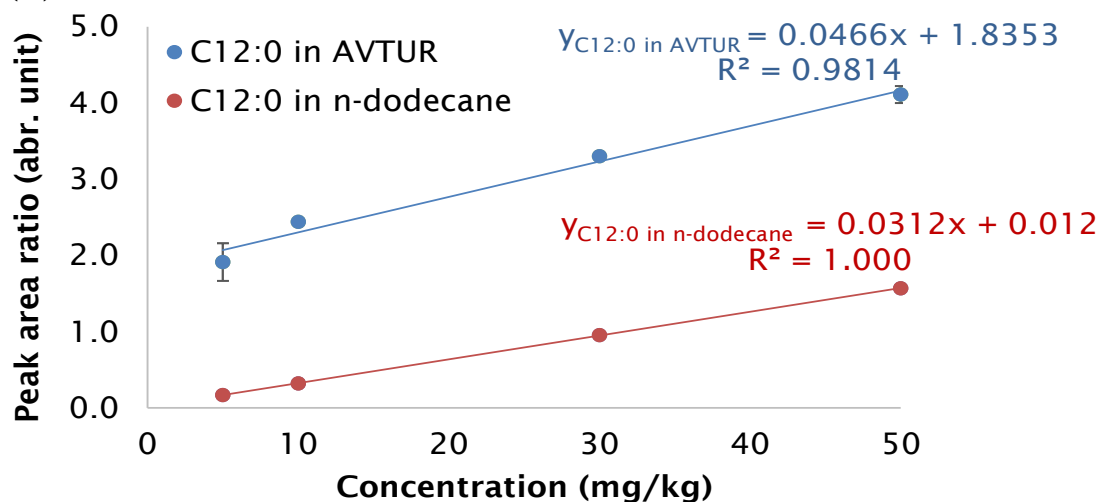
(B) C14:0 in AVTUR and n-dodecane
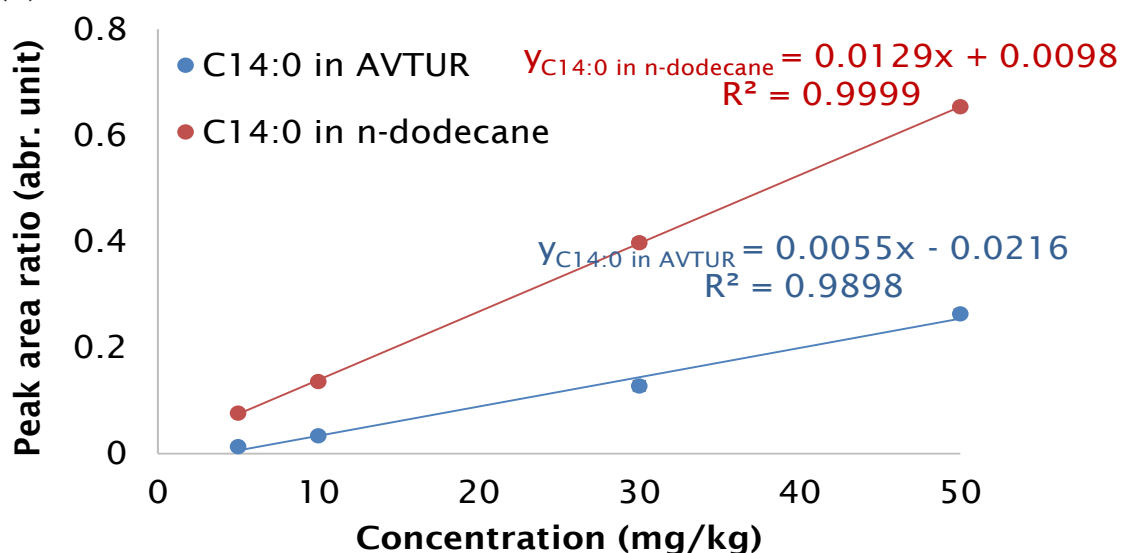
Figure 5-14   Comparison of calibration curve of C12:0 (A) and C14:0 (B) in n-dodecane (red) and CME in AVTUR (blue) lines, in the range of 5-50 mg/kg.

Then, matrix interference can be caused by C12:0 and C14:0 co-eluting in the fuel samples leading to false positive/negative identification. This results in a lower or higher signal, which affects the accuracy of the

quantitative analysis. To achieve a satisfactory separation of C12:0 and C14:0 from the fuel matrix the GC-MS conditions required adaptation.

5.1.2   New GC-MS method

The oven temperature programme used was 130 °C for 5 min, ramped at a rate of 2 °C/min to 240 °C for 5 min. The GC-MS conditions were applied to analyse C12:0 surrogate CME 100 mg/kg in AVTUR. Figure 5-15 shows the peak of C12:0 is completely separated from the fuel matrix background (see, Figure 5-15 (B)). Whereas, the peak of C12:0 in the chromatograms (A) co-eluted with naphthalene, the fuel matrix obtained from the GC-MS conditions which revised IP/585 method.

(A) Revised IP 585/10 method
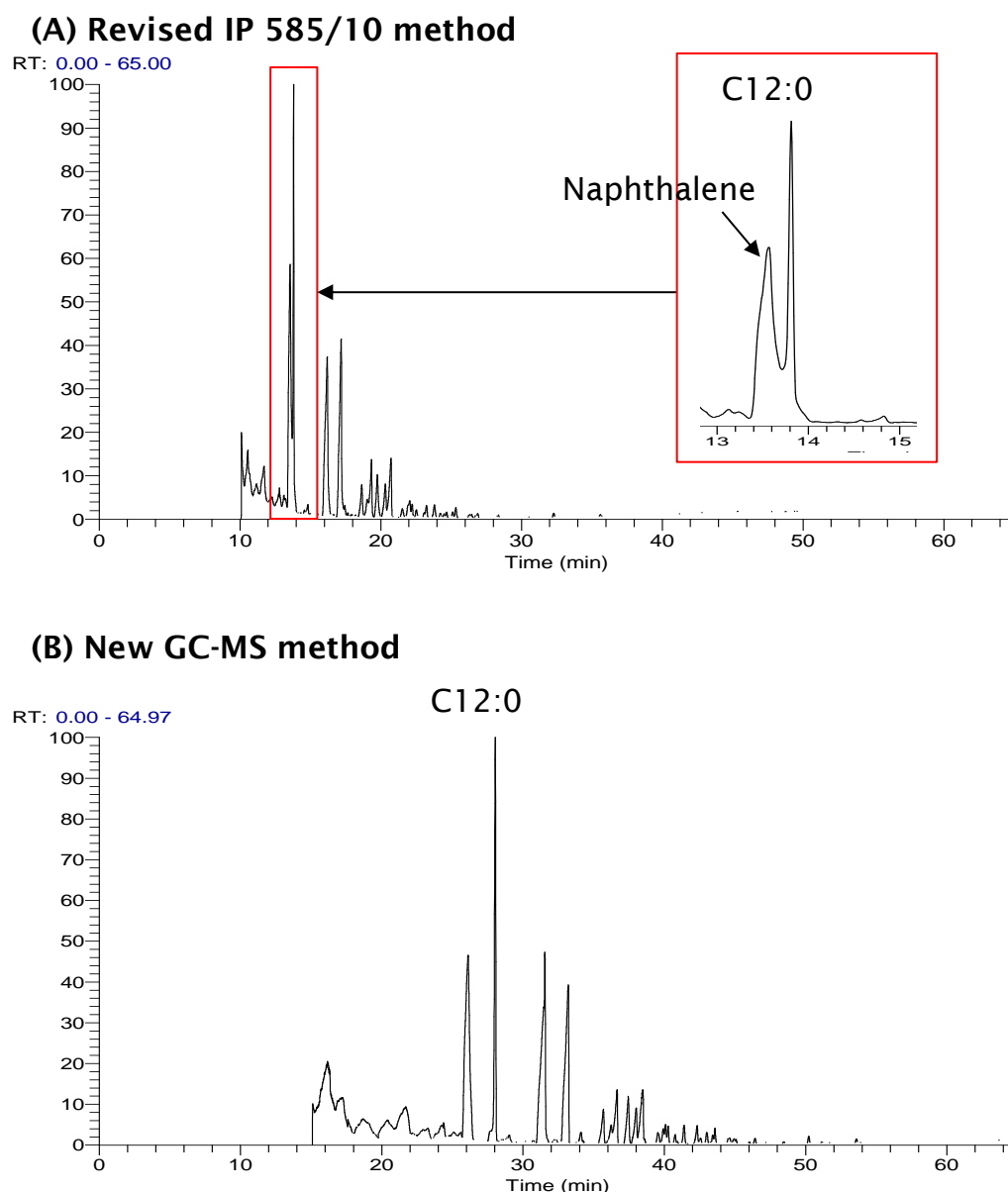
(B) New GC-MS method

Figure 5-15   Comparison of RICCs *m/z* 74, 87 and 214 of 100 mg/kg
of CME in AVTUR analysed using HP-Innowax 60 m × 0.25 mm
id × 0.5 µm film thickness with two different GC-MS methods.
(A) Revised IP 585/10, initial temp. 150 °C hold for 5 min, 12
°C/min to 200 °C for 17 min, 3 °C/min to 252 °C for 6.5 min;
(B) New GC-MS method, initial temp. 130 °C hold for 5 min, 2
°C/min to 240 °C for 5 min.

Figure 5 16 shows mass spectra corresponding to the peak of C12:0 which was obtained from two different GC-MS methods. The mass spectrum of the peak of C12:0 obtained from the revised IP 585/10 methods which interfered with the mass spectrum of naphthalene (*m/z* 128) (see Figure 5-16), while the mass spectrum of the peak C12:0 obtained from the adapted GC-MS method which shows no interference of *m/z* 128 (see, Figure 5-17).
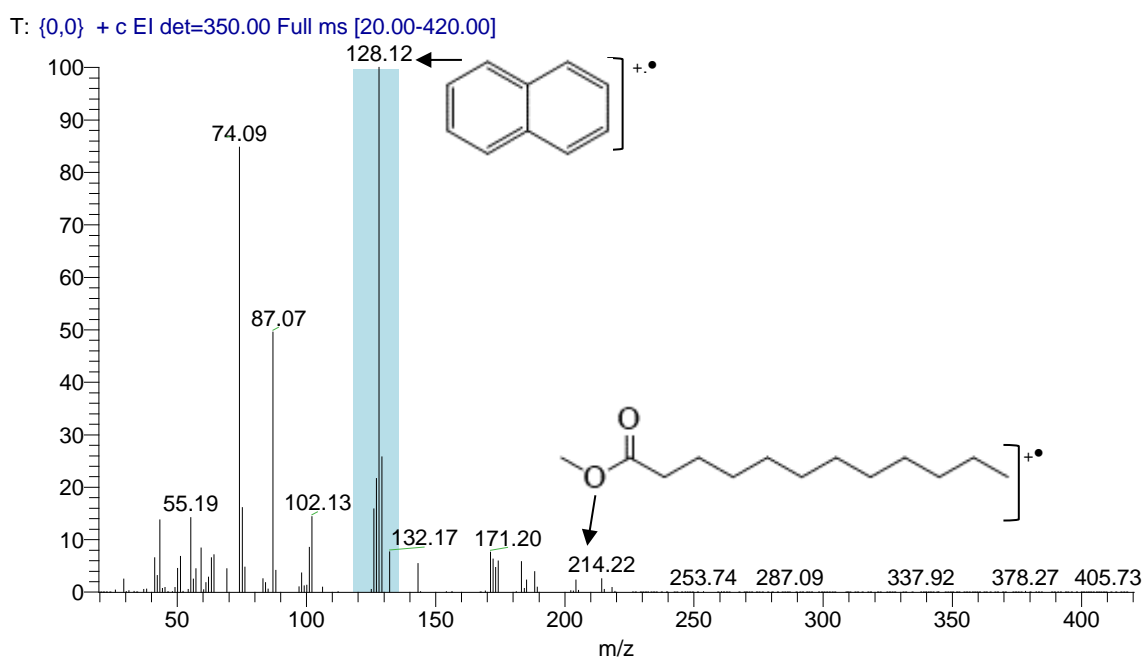
Figure 5-16   EI mass spectra of C12:0 corresponding to Figure 5-15. (A) mass spectrum of the peak of C12:0 obtained from the revised IP 585/10 method.

T: {0,0} + c EI det=350.00 Full ms [20.00-420.00]
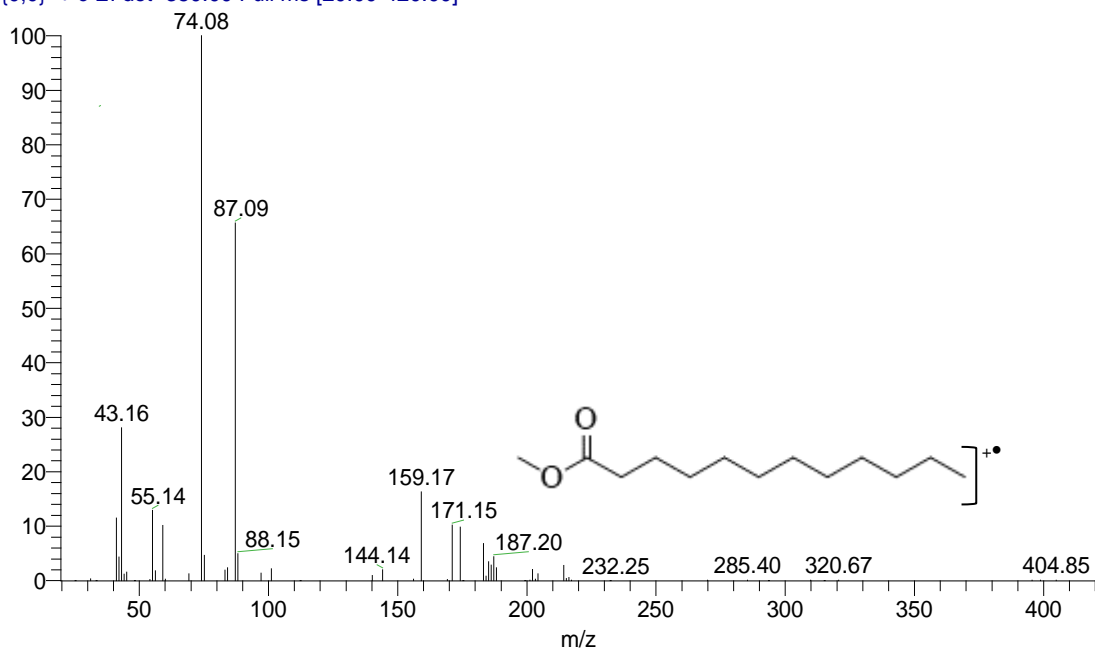
Figure 5-17   EI mass spectra of C12:0 corresponding to Figure 5-15. (B) mass spectrum of the peak of C12:0 obtained from from the new GC-MS method showing no interfering ions from naphthalene.

To compare the performance of the both GC-MS methods for determination of FAMEs contamination in AVTUR, the methods were applied to analyse the twenty commercially doped samples of AVTUR with FAME supplied by the Energy Institute. The linearity of each GC-MS method was determined by analysis of n-dodecane solutions of standard RME and CME (0.0-150 mg/kg), see Figure 5-18 and Figure 5-19. A total of 10 ppm of methyl heptadecanoate-d_{33} (C17:0 (-d_{33})) was used as the internal standard. Peak areas, relative to the internal standard, the RICCs of each FAMEs species C12:0 (*m/z* 74, 87, 171, 183, 214), C14:0 (*m/z* 74, 87, 199, 211, 242), C16:0 (*m/z* 74, 87, 227, 239, 270, 271), C17:0 (d_{33}) (*m/z* 317), C18:0 (*m/z* 74, 87, 255, 267, 298), C18:1 (*m/z* 55, 74, 87, 264,

265, 296), C18:2 (*m/z* 67, 74, 87, 262, 263, 264, 294, 295) and C18:3

(*m/z* 79, 87, 236, 263, 292, 293).

(A) RME

$y_{\text{Total FAMEs from RME, included low } m/z \text{ less than 100}} = 4.0995x - 4.5645$
$R^2 = 0.9931$

$y_{\text{Total FAMEs from RME, excluded low } m/z \text{ less than 100}} = 0.5442x - 0.7943$
$R^2 = 0.9930$

(B) CME

$y_{\text{Total FAMEs from CME, included low } m/z \text{ less than 100}} = 5.8204x + 3.4019$
$R^2 = 0.9991$

$y_{\text{Total FAMEs from CME, excluded low } m/z \text{ less than 100}} = 0.6985x + 0.1567$
$R^2 = 0.9977$
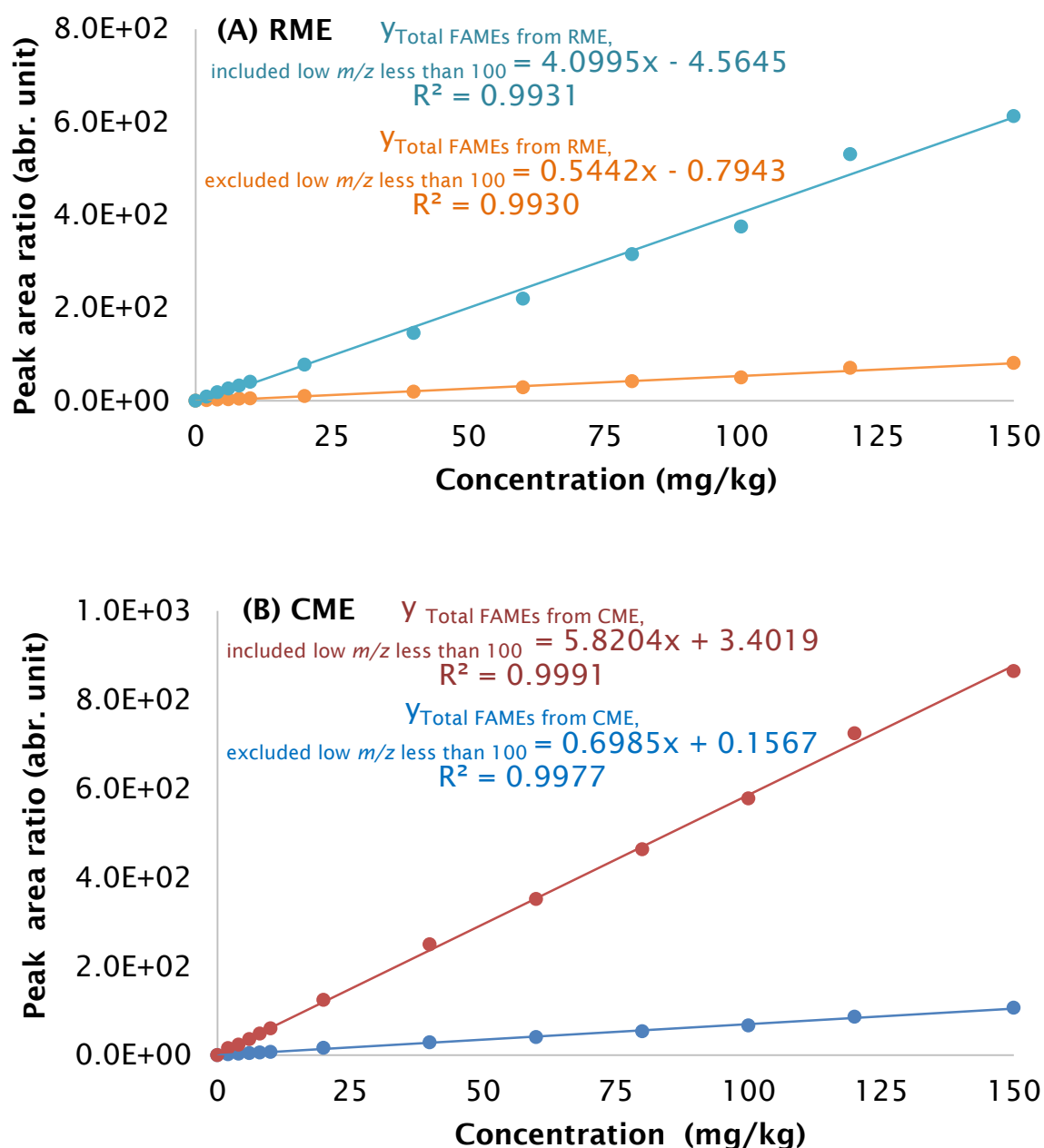
Figure 5-18   Internal calibration curve of RME (A) and CME (B) in n-dodecane by using ions less than *m/z* 100. 227, 239, 270, 271. GC-MS conditions analysed using HP-Innowax 60 m × 0.25 mm id × 0.5 µm film thickness initial temp. 150 °C hold for 5 min, 12 °C/min to 200 °C for 17 min, 3 °C/min to 252 °C for 6.5 min.

(A) RME

$y_{\text{Total FAMEs from RME, included low } m/z \text{ less than 100}} = 4.6676x - 6.7893$

$R^2 = 0.9937$

$y_{\text{Total FAMEs from RM, excluded low } m/z \text{ less than 100}} = 0.602x - 0.9839$

$R^2 = 0.9924$

(B) CME

$y_{\text{Total FAMEs from CME, included low } m/z \text{ less than 100}} = 6.343x + 0.0418$

$R^2 = 0.9967$

$y_{\text{Total FAMEs from CME, excluded low } m/z \text{ less than 100}} = 0.6983x - 0.2862$

$R^2 = 0.9964$
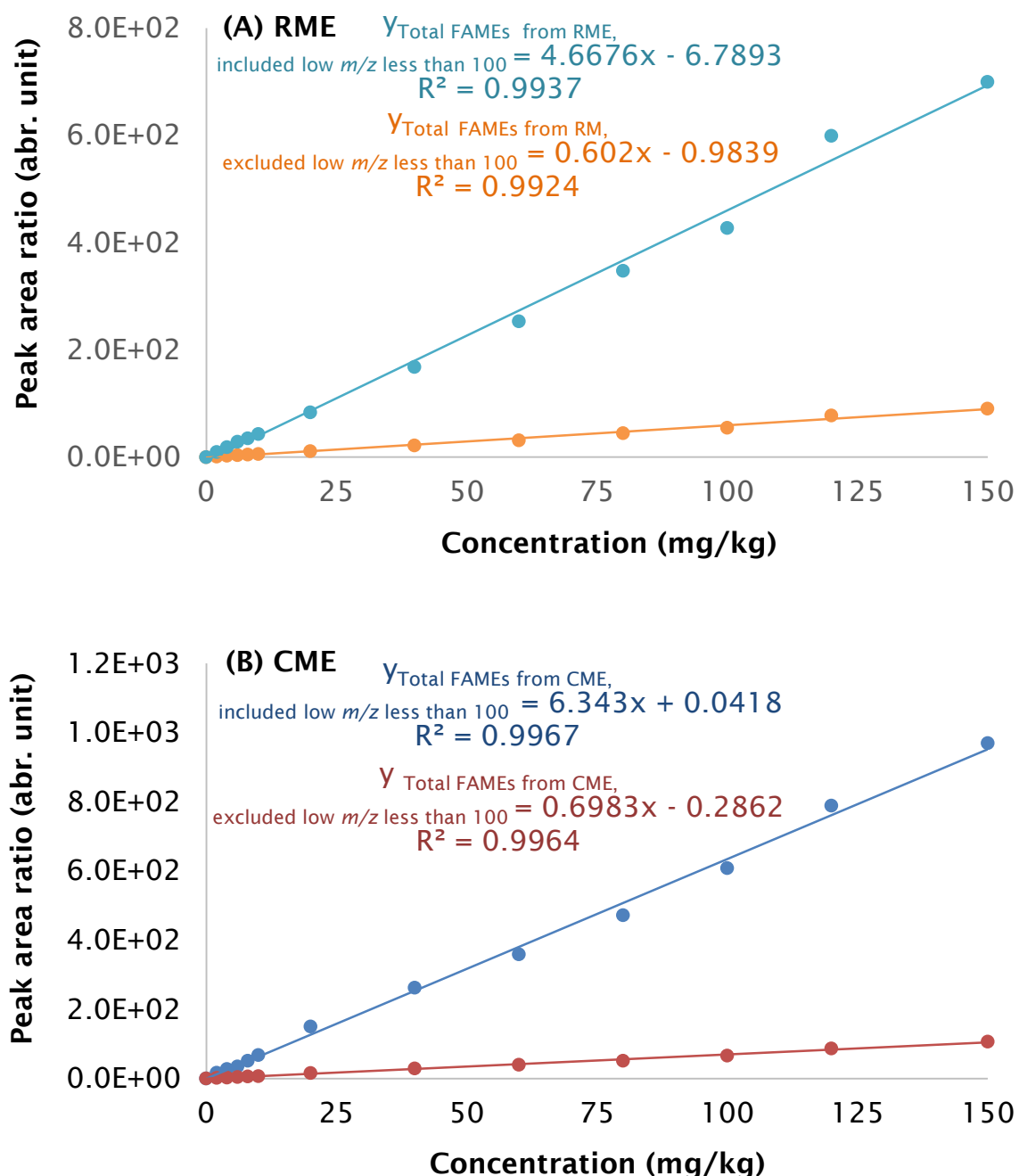
Figure 5-19 **Internal calibration curve of RME (A) and CME (B) in n-dodecane by using ions less than *m/z* 100. GC-MS conditions analysed using HP-Innowax 60 m × 0.25 mm i.d. × 0.5 μm film thickness, initial temp. 130 °C hold for 5 min, 2 °C/min to 240 °C for 5 min.**

Table 5-3 and Table 5-4 show the results of commercially doped samples of AVTUR with using the revised IP 585/10 method and the new GC-MS method.

188

Table 5-3   The results of analysis of commercially doped samples of AVTUR with using the revised IP 585/10 method

No.	Sample name	Result (mg/kg)	
		Incl. ions $< m/z$ 100	Excl. ions $< m/z$ 100
1	AF1 SDA 5mg/L	0.0	0.0
2	AF5 Mixed FAME 5mg/kg	18.9	14.3
3	AF1 CME 5mg/kg	0.0	0.0
4	AF1 Mixed FAME 5mg/kg	6.8	5.2
5	AF1 MDA 5.7mg/L	0.0	0.0
6	AF1 FS11 0.15% vol	0.0	0.0
7	AF1 DF LI Ester 10mg/kg	0.0	0.0
8	AF1 DF LI Acid 10mg/kg	0.0	0.0
9	AF1 Jet LI 23mg/L	0.0	0.0
10	AF1 A0 24mg/L	0.0	0.0
11	AF3 Mixed FAME 30mg/kg	30.1	21.0
12	AF4 Mixed FAME 30mg/kg	38.0	26.4
13	AF3 Mixed FAME 100mg/kg	137.2	100.3
14	AF1 Mixed FAME 100mg/kg	161.4	114.4
15	AF4 Mixed FAME 100mg/kg	116.4	84.6
16	AF1 CME 100mg/kg	92.0	70.0
17	AF5 Mixed FAME 100mg/kg	108.1	81.3
18	AF1 CNI 125mg/kg	0.0	0.0
19	AF5 Mixed FAME 150mg/kg	141.0	97.8
20	AF1 Mixed FAME 150mg/kg	205.5	148.9

Table 5-4   The results of analysis of commercially doped samples of AVTUR with using the new GC-MS method

No.	Sample name	Result (mg/kg)	
		[a]Incl. ions < *m/z* 100	[b]Excl. ions < *m/z* 100
1	AF1 SDA 5mg/L	0.0	0.0
2	AF5 Mixed FAME 5mg/kg	18.5	13.9
3	AF1 CME 5mg/kg	3.8	2.3
4	AF1 Mixed FAME 5mg/kg	5.8	4.8
5	AF1 MDA 5.7mg/L	0.0	0.0
6	AF1 FS11 0.15% vol	0.0	0.0
7	AF1 DF LI Ester 10mg/kg	0.0	0.0
8	AF1 DF LI Acid 10mg/kg	0.0	0.0
9	AF1 Jet LI 23mg/L	0.0	0.0
10	AF1 A0 24mg/L	0.0	0.0
11	AF3 Mixed FAME 30mg/kg	26.5	20.8
12	AF4 Mixed FAME 30mg/kg	31.8	24.0
13	AF3 Mixed FAME 100mg/kg	101.7	74.5
14	AF1 Mixed FAME 100mg/kg	149.9	103.2
15	AF4 Mixed FAME 100mg/kg	129.5	87.4
16	AF1 CME 100mg/kg	99.8	105.9
17	AF5 Mixed FAME 100mg/kg	113.9	78.5
18	AF1 CNI 125mg/kg	0.0	0.0
19	AF5 Mixed FAME 150mg/kg	123.8	86.8
20	AF1 Mixed FAME 150mg/kg	186.5	131.9

Note: The results obtained from using the new developed GC-MS method with the following conditions: 60 m × 0.25 mm inner diameter, 0.50 μm film thickness; the oven temperature program used was 130 °C for 5 min, ramped at a rate of 2 °C/min to 240 °C, and held at the final temperature for 5 min[a] = the selected ions to be used for detected quantification.

Neither of the revised IP585/10 and the new GC-MS methods appears to give good quantitative results, particularly when short chain FAME is present. The revised IP585/10 method is being tested for robustness by the Energy Institute with the aim of undergoing a full round-robin study later in 2015. Given the difficulties outlined above with the GC-MS methods alternative approaches were explored.

5.2   Analysis of FAMEs in AVTUR using HPLC-MS

Gradient elution reversed-phase HPLC was coupled with ESI-MS for the separation of FAMEs. The different proportions of mobile phases were studied. Increasing the proportion methanol 0.1% formic acid in the mobile phase has an effect on unsaturated C18 FAMEs retention because of the change in the mobile phase polarity. The elution order of FAMEs on a C18 stationary phase column depends on the extent of unsaturation C18:3. Containing more double bonds than C18:2 and C18:1 eluted sooner. Peak asymmetry factors were considered in order to choose optimum conditions for HPLC.

A peak is considered as tailing if its asymmetry is greater than a value of 1.2-1.5. The unsaturated FAMEs were eluted from the C18 column with acceptable peak symmetry (A_s of 1.43 - 1.55) and baseline separation using a high proportion of organic mobile phase (70% mobile phase B), see Table 5-5 and Figure 5-20. Starting at a high % organic modifier to save analysis time as all FAME components were eluted very quickly.

Table 5-5   The results of peak asymmetry at different ratios of mobile phases

	Peak asymmetry		
Mobile phase composition	**C18:1**	**C18:2**	**C18:3**
80% A 20% B	1.91 (24.75)	2.10 (7.87)	2.38 (6.99)
70% A 30% B	1.83 (15.75)	1.93 (6.66)	2.02 (26.49)
60% A 40% B	1.71 (4.22)	2.86 (19.39)	1.94 (21.57)
50% A 50% B	1.79 (10.66)	1.67 (8.66)	1.56 (10.82)
40% A 60% B	1.80 (25.94)	1.58 (15.86)	1.61 (6.67)
30% A 70% B	1.55 (13.47)	1.46 (4.95)	1.43 (4.64)
20% A 80% B	1.75 (14.29)	1.36 (11.09)	1.44 (15.15)

Note: A= 0.1% (v/v) formic acid in water and B = 0.1% (v/v) formic acid in methanol. The value in a bracket () is standard deviation (SD) from number of replicate measurements = 3.
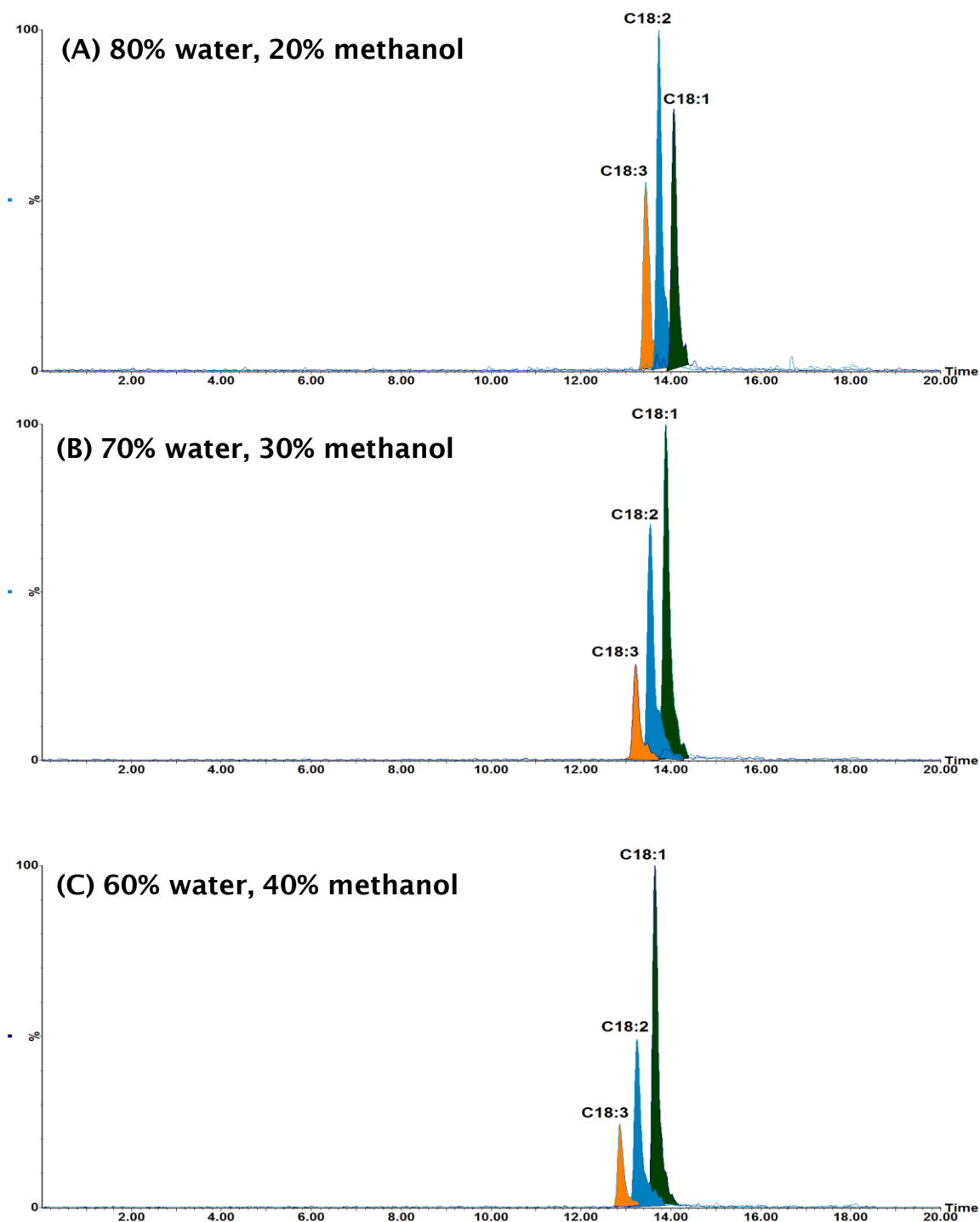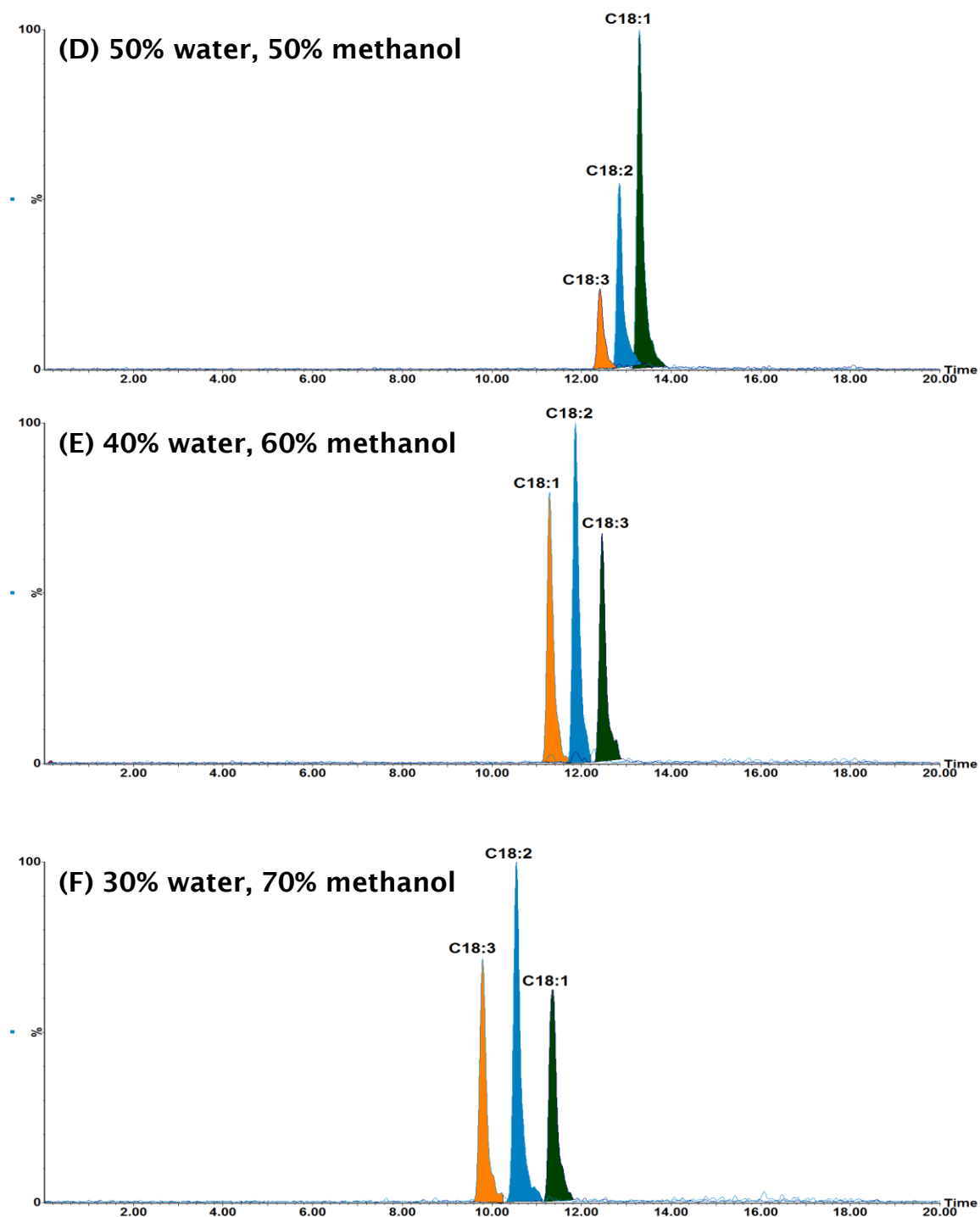
Figure 5-20 RICCs of standard C18:1(*m/z* 319), C18:2 (*m/z* 317) and C18:3 (*m/z* 315) in methanol showing the separation of C18:1, C18:2 and C18:3 using HPLC-MS at the different mobile phase ratios. (Continued overleaf)

Figure 5-20   RICCs of standard C18:1(m/z 319), C18:2 (m/z 317) and C18:3 (m/z 315) in methanol showing the separation of C18:1, C18:2 and C18:3 using HPLC-MS at the different mobile phase ratios. (continued overleaf)

(G) 20% water, 80% methanol
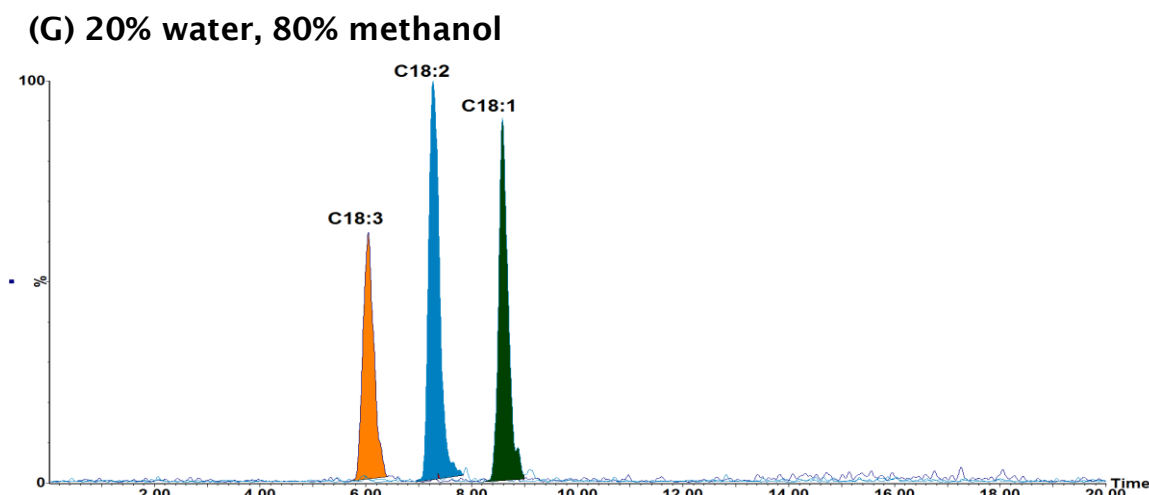
Figure 5-20 **RICCs of standard C18:1(*m/z* 319), C18:2 (*m/z* 317) and C18:3 (*m/z* 315) in methanol showing the separation of C18:1, C18:2 and C18:3 using HPLC-MS at the different mobile phase ratios.**

5.3 Analysis of FAMEs in AVTUR using ultra high performance liquid chromatography-mass spectrometry (UHPLC-MS)

In this study, HPLC-MS conditions were transferred to the UHPLC method. Figure 5-21 shows the typical chromatograms of unsaturated C18 FAMEs originally obtained using an XBridge C18 column 5 μm, 2.1 × 50 mm and further transferred to UHPLC with an ACQUITY UPLC® BEH C18 column 1.7 μm, 1.7 × 50 mm. The HPLC separation was performed in 20 minutes and efficiency transferred to UHPLC in 5 min. Comparison of this UHPLC method with the HPLC method for FAME in AVTUR shows a 4 fold improvement in analysis time.
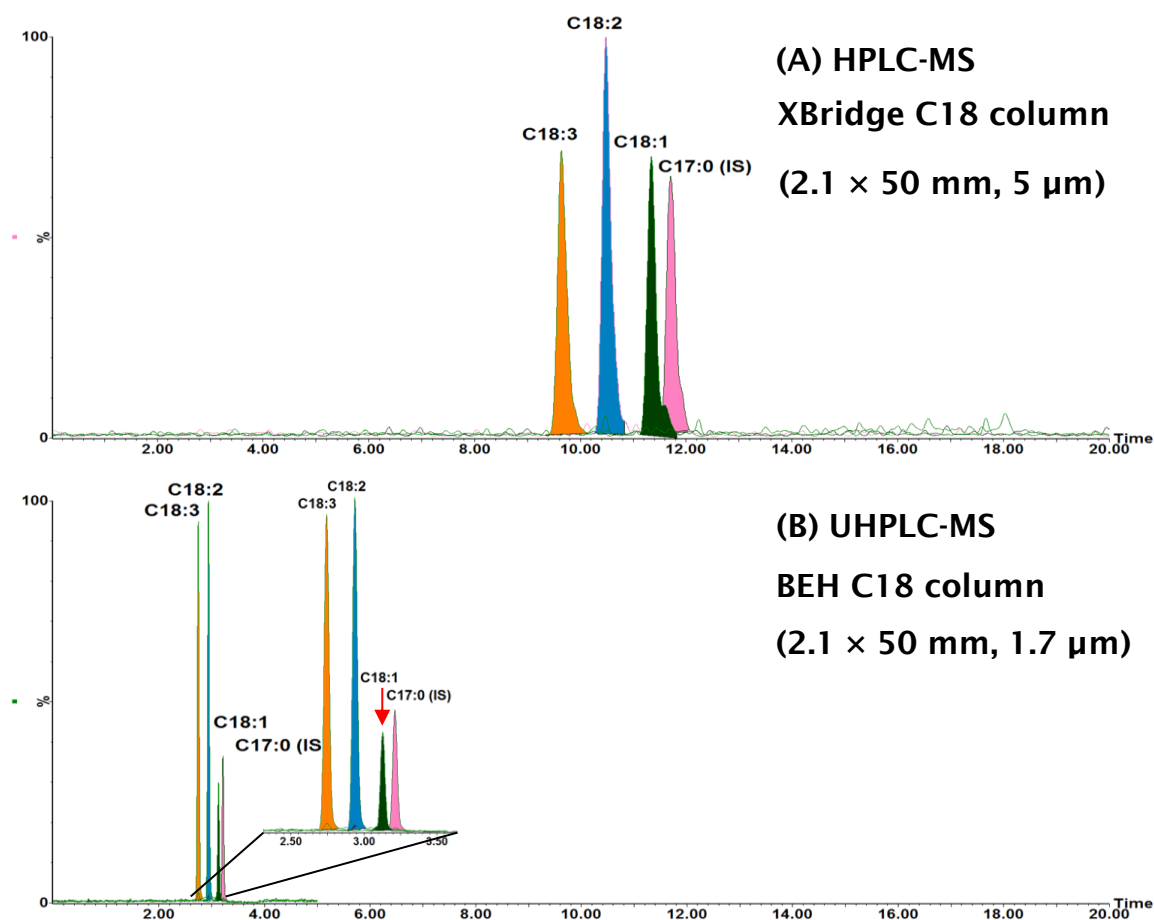
Figure 5-21   Comparison of the separation of standard FAMEs (C18:1, C18:2 and C18:3) in MeOH using (A) HPLC-MS using an XBridge C18 column (2.1 × 50 mm, 5 μm) and (B) UHPLC-MS using a BEH C18 column (2.1 × 50 mm, 1.7 μm), showing RICCs of _m/z_ 319 [C18:1 + Na]⁺, _m/z_ 317 [C18:2 + Na]⁺, _m/z_ [C18:3 + Na]⁺ and _m/z_ 307 [C17:0 + Na]⁺. Insert shows expansion of the chromatograms of the analytes.

The developed UHPLC-MS method was applied for the separation the shorter chain methyl esters _e.g._ coconut methyl ester (CME) in methanol, see Figure 5-22. The UHPLC-MS method can clearly separate the C8-C18 FAMEs from CME in methanol. When introduction CME into the fuel matrix, the short chain methyl esters (C8:0 to C14:0) eluted in the same chromatographic space as the fuel matrix, see Figure 5-23. However, the developed UHPLC-MS can be used for the separation of RME (C16:0 to C18:3) at the 5 mg/kg level in AVTUR, see Figure 5-24.
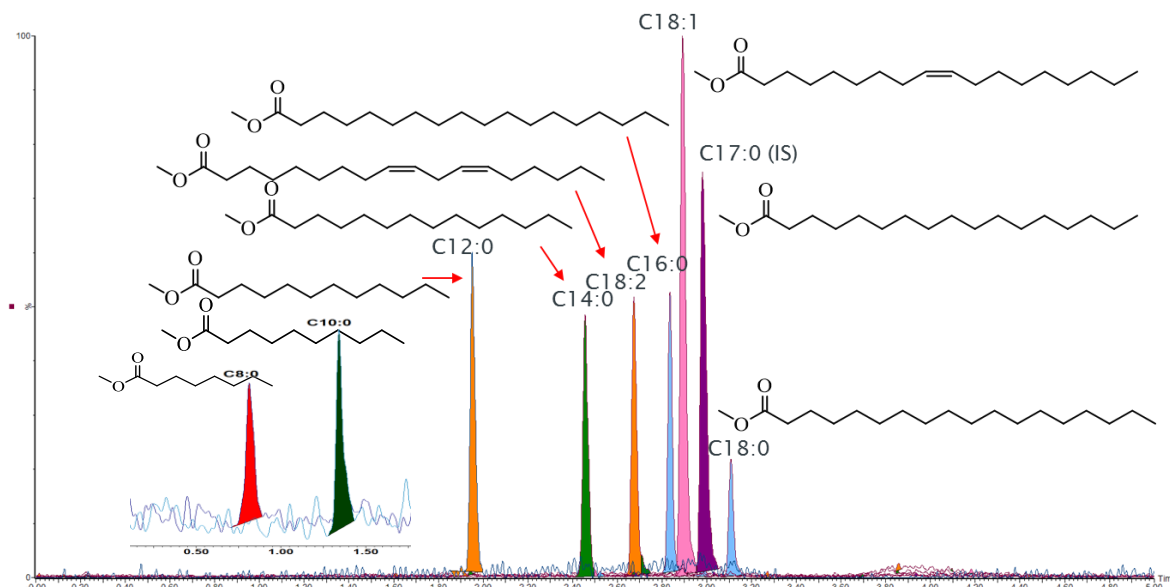
Figure 5-22 RICCs of CME in methanol using the UHPLC-MS method showing RICCs of *m/z* 159 [C8:0 + H]⁺, *m/z* 187 [C10:0 + H]⁺, *m/z* 215 [C12:0 + H]⁺, *m/z* 243 [C14:0 + H]⁺, *m/z* 271 [C16:0 + H]⁺, *m/z* 299 [C18:0 + H]⁺, *m/z* 319 [C18:0 + Na]⁺ and *m/z* 317 [C18:1 + Na]⁺. Insert shows expansion of the chromatograms of C8:0 and C10:0.
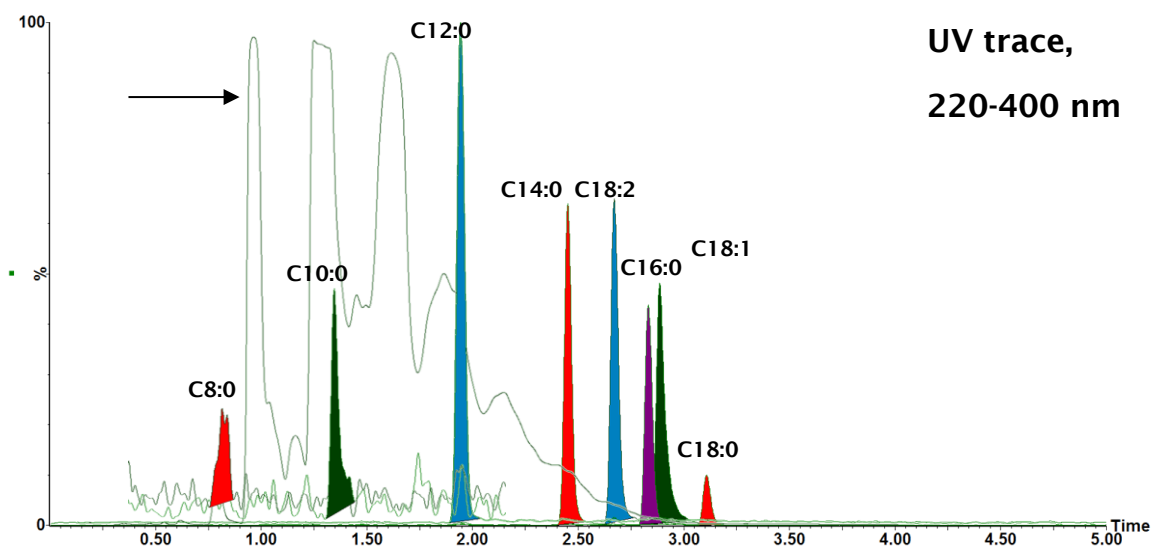
Figure 5-23 Chromatograms of AVTUR from UV trace (green line) and standard CME in methanol showing the shorter chain methyl esters (C8:0 to C10:0) eluted in the same chromatographic space as the fuel matrix, C12:0 and C14: 0 are still co-eluting with the fuel matrix.
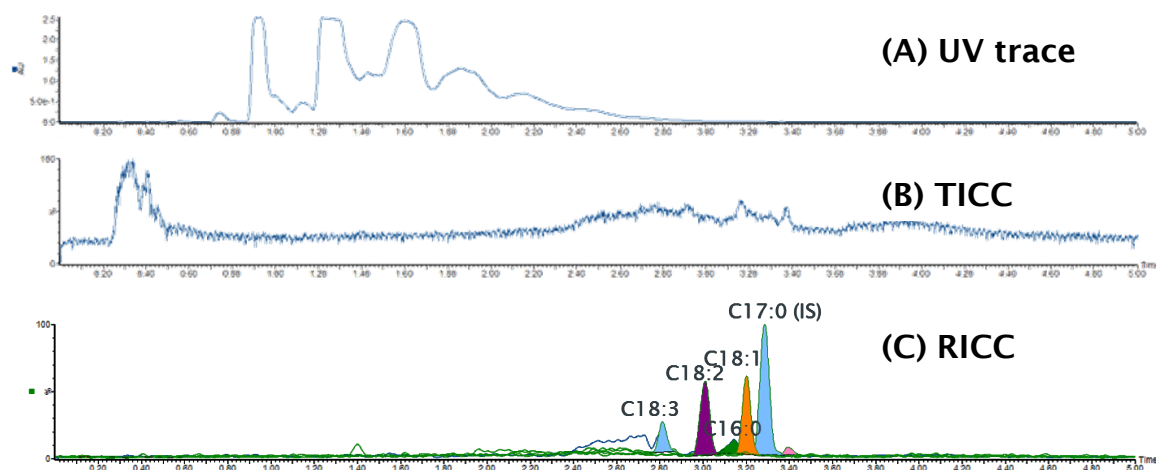
Figure 5-24   Comparison of (A) UV trace, (B) TICC, and (C) RICCs *m/z* 74 and 87 of 5 mg/kg of RME in AF-1 analysed using UHPLC-MS. *m/z* 271 [C16:0 + H]⁺, *m/z* 299 [C18:0 + H]⁺, *m/z* 319 [C18:0 + Na]⁺ and *m/z* 317 [C18:1 + Na]⁺.

5.3.1   Force electrospray ionisation

Generally, a protonated molecule in positive ionisation or deprotonated molecule in negative ionisation is observed in electrospray ionisation. However, several types of adduct ions may be formed depending on the compound, solvent and ESI parameters. The most common adduct ions, sodium and ammonium, are also formed in positive electrospray ionisation. Compounds that have carboxyl, carbonyl, ether or esters functional groups are believed to be responsible for bonding with alkali metal ions. Where adduct ion formation is uncontrolled it is difficult to get a quantitative measurement and so several approaches have been investigated. The first approach is to measure only the adduct ion with the highest response and disregard the other adduct ion forms, but a relative standard deviation (RSD) is unacceptable. This indicates that adduct formation provide the large variation and unreliable results when the

process is uncontrolled. Also the summation complicates experiments. The second approach is to exclude sodium from the ionisation process by adding alkali metal complexation products, such as crown ethers. This is difficult due to the abundant presence of sodium, often originating from the glassware, or as an impurity in chemicals and solvents.

The aim of this study was to use the sodium adduct for quantitative analysis by adding sodium formate solution to the eluent for replacing all adducts by one single desired adduct. The addition of sodium formate is crucial because this forces one ionisation event, *i.e.,* produces only the sodiated molecules. Without the addition of the sodium ions, then an uncontrolled mixture of protonated molecules, ammoniated molecules, sodiated molecules, and potassiated molecules can be produced.[185] A comparison of uncontrolled and forced ESI of C18:3 is shown in Figure 5-25.
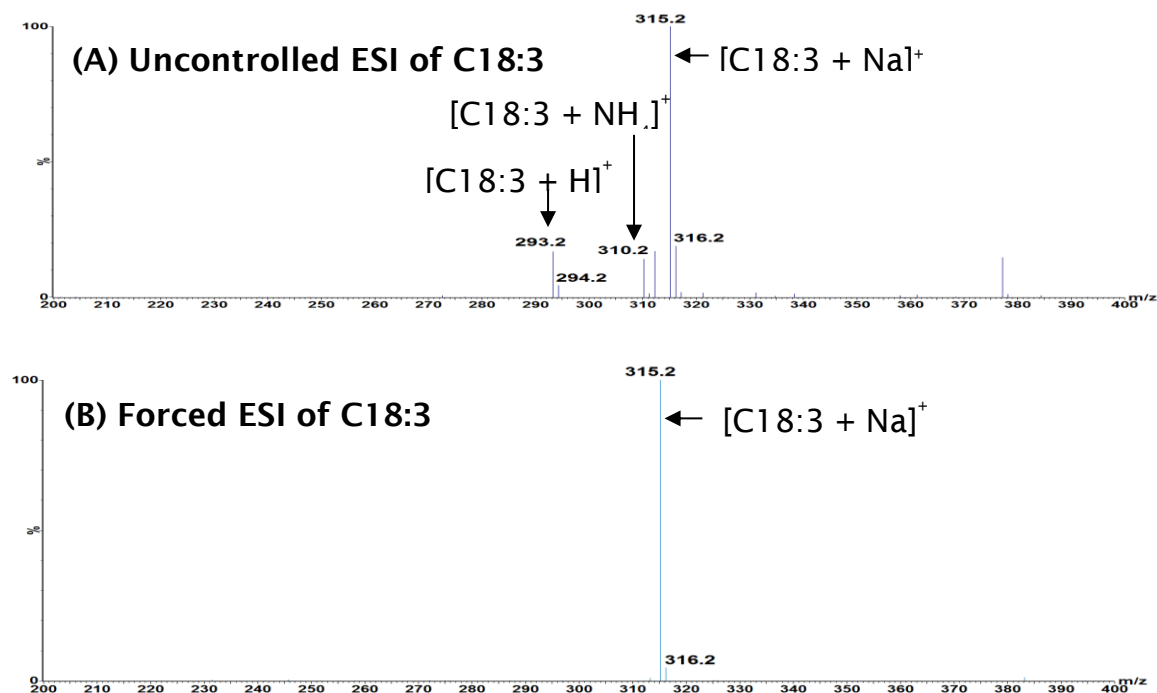
Figure 5-25   Positive ESI mass spectra of uncontrolled and forced ESI of C18:3.

5.4   Analysis of FAMEs in AVTUR using UHPSFC-MS

5.4.1   UHPSFC column screening

The UHPSFC-MS method was developed based on the state-of-art instrumentation (UPC^2-MS) and column technologies (sub 2 μm particles), with the aim to detect and quantify of low-carbon-number fatty acid methyl esters (FAMEs), *e.g.* C8–C14 from coconut oil, and to obtain high throughput analysis. Identical eluent and co-solvent (methanol) composition and gradient were used to ensure that any differences observed in retention behaviour could be directly related to the stationary phase. Figure 5-26 and Figure 5-27 show the elution of FAME species on the four selected stationary phases. The HSS-cyano stationary phase did

not separate the C18:1, C18:2 and C18:3, as shown in Figure 5-26 (A). The

resolution (R_s) of all peaks is zero. The elution of the FAMEs on the BEH

and BEH-amide columns was improved peak resolution, the R_s for the

C18:1 and C18:2 (2.82) and C18:2 and C18:3 (3.53) obtained from the

BEH-amide column whilst the unsaturated FAMEs showed peak tailing, with

unacceptable peak asymmetry factors (As) for C18:1 (2.67), C18:2 (3.67)

and C18:3 (3.25), see Figure 5-26 (C). While the best peak symmetry with

A_s values of 1.0-1.33 acceptable for all FAME species using the BEH

column, see Figure 5-26 (D). The BEH column baseline separated a range

of methyl esters of saturated FAMEs and the unsaturated C18 species,

(C8:0-C18:3, covering the combined CME and RME composition), see

Figure 5-27. The FAMEs eluted according to increasing carbon number,

similarly the unsaturated FAMEs, within the same carbon number, eluted

according to increasing number of double bonds, see Figure 5-27 (D). The

BEH column was subsequently used to investigate the influence of other

parameters.

(A) RME on HSS cyano column

(B) RME on HSS C18 SB column

(C) RME on BEH-amide column
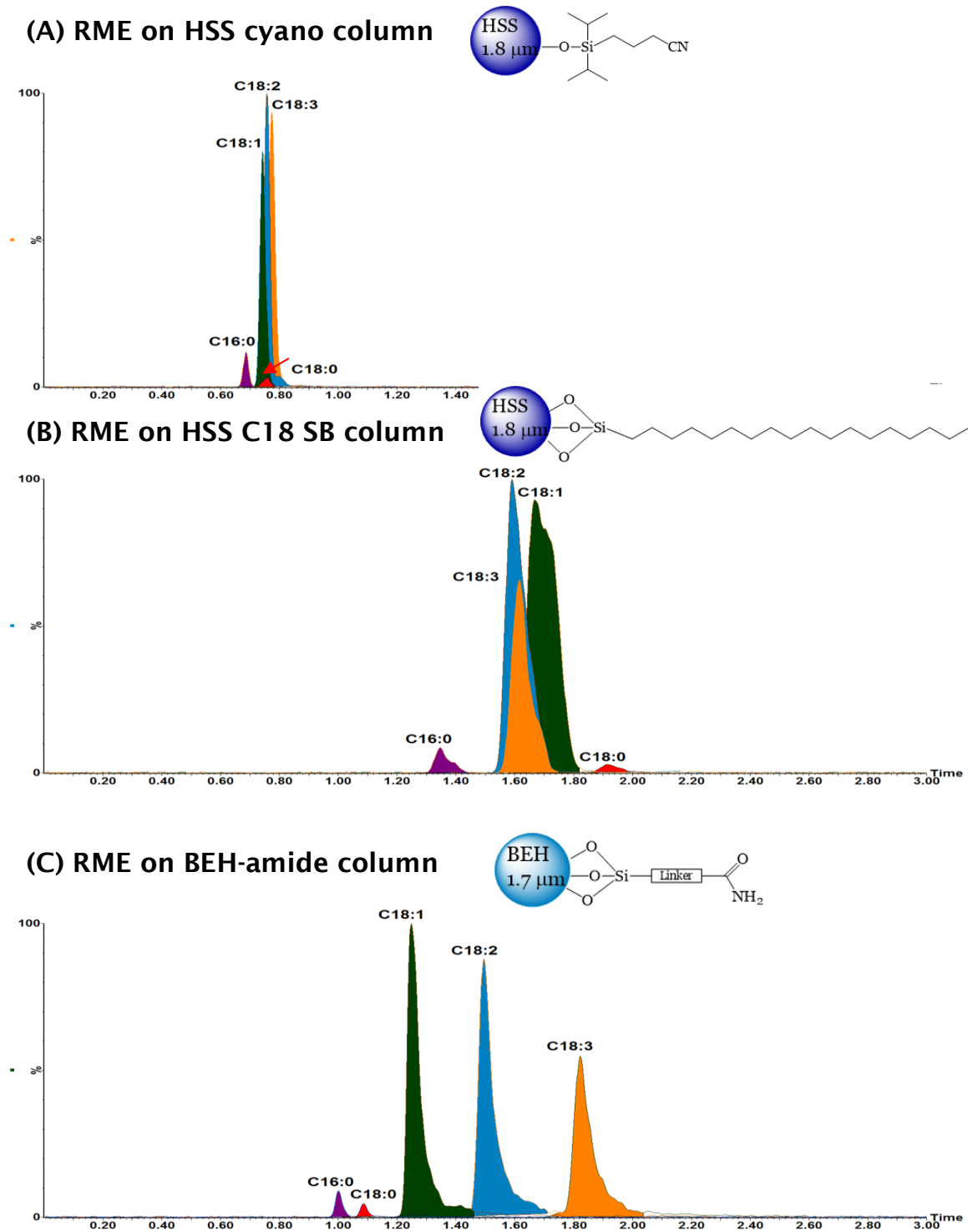
Figure 5-26   Continued overleaf

(D) RME on Ethylene bridged hybrid (BEH)
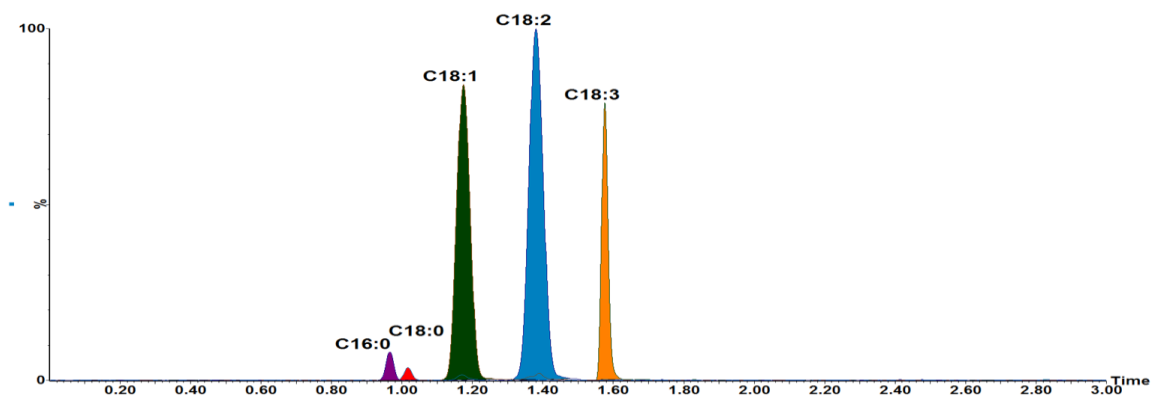
Figure 5-26   Comparison of RICCs for RME separation using different stationary phases. (A) HSS cyano; (B) HSS C18 SB; (C) BEH-amide; and (D) BEH. Chromatographic conditions: CO_2 pressure 105 bar; gradient 0-1% MeOH in CO_2 at 1.5 mL/min in 5 min.

(A) CME on HSS cyano column

(B) CME on HSS C18 SB column
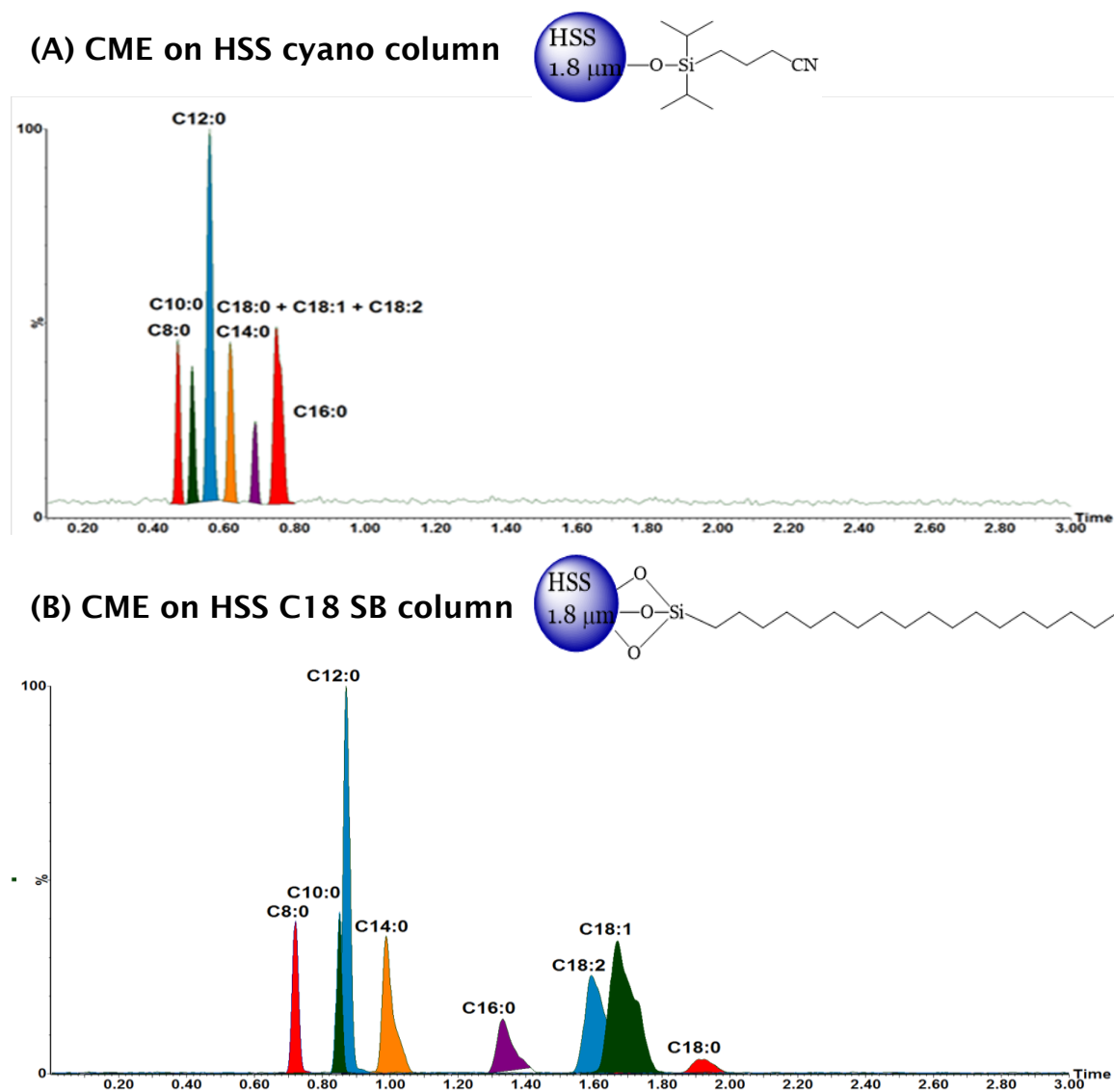
Figure 5-27   Comparison of RICCs for CME separation using different stationary phases. (A) HSS cyano, (B) HSS C18 SB, (C) BEH-amide, and (D) BEH. Chromatographic conditions: CO_2 pressure 105 bar; gradient 0-1% MeOH in CO_2 at 1.5 mL/min in 5 min. (continued overleaf)
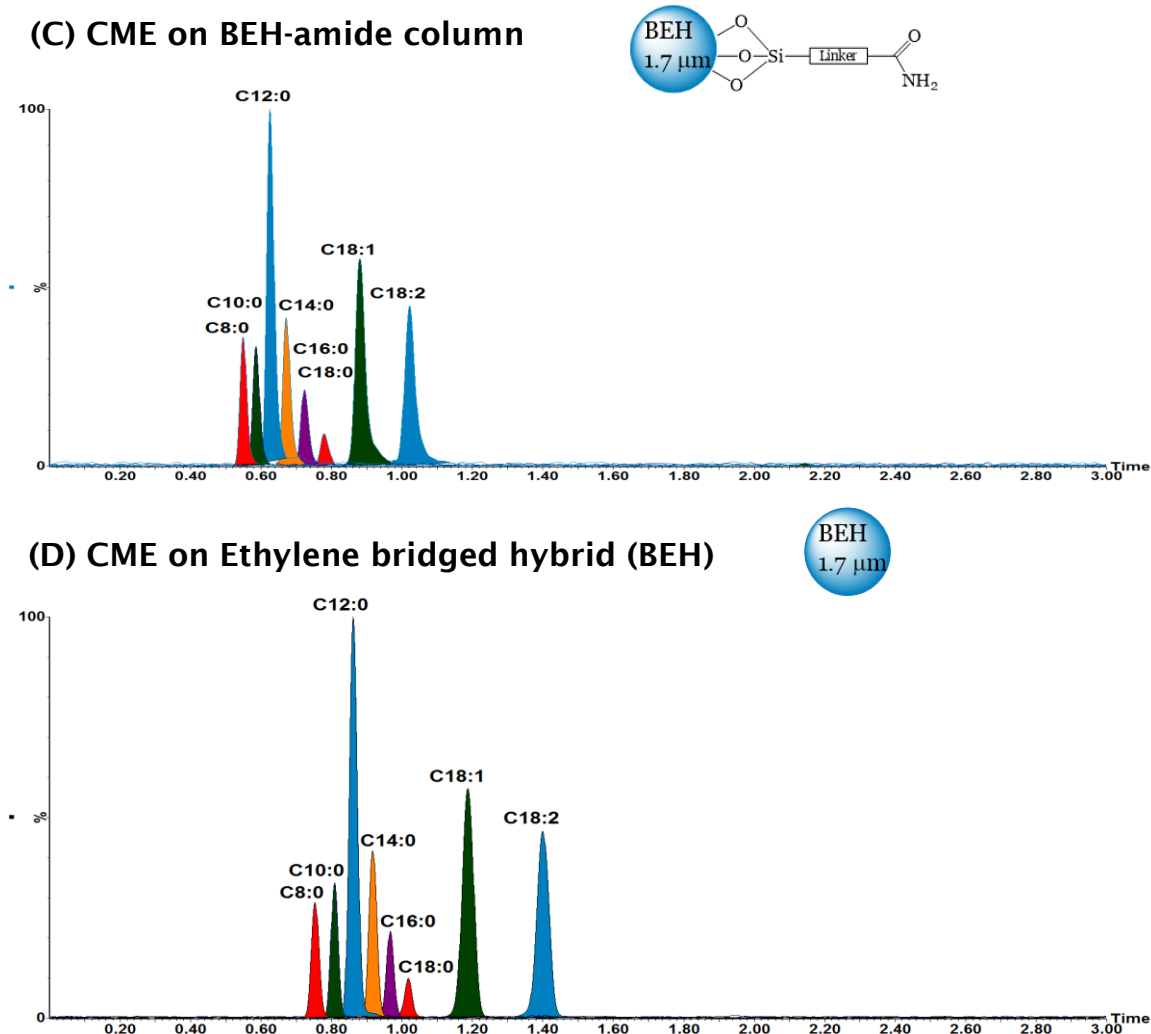
(C) CME on BEH-amide column

(D) CME on Ethylene bridged hybrid (BEH)

Figure 5-27 **Comparison of RICCs for CME separation using different stationary phases. (A) HSS cyano; (B) HSS C18 SB; (C) BEH-amide; (D) BEH. Chromatographic conditions: CO_2 pressure 105 bar; gradient 0-1% MeOH in CO_2 at 1.5 mL/min in 5 min.**

5.4.2   Effect of sample solvents on FAME separation

HPLC protocols recommend a sample should be prepared and diluted in the mobile phase composition used at the start of the analysis, or prepared in a weaker elution strength solvent which is miscible with the mobile phase in order to minimise band spreading.[186][187] A sample

solvent effect was noted when the standard FAME solutions were prepared in different solvents. When methanol was used, poorer peak resolution (R_s = zero) was observed for the FAME when compared to FAME in AVTUR, and subsequently FAME in hexane, giving the R_s for the C18:1 and C18:2 (4.03) and C18:2 and C18:3 (3.53). This loss of chromatographic resolution is thought to be due to residual trace levels of the polar sample solvent from the injection. This issue is only observed when analysis requires very low percentage or no polar co-solvent. Hexane with no H-bond donor capability[188] provided acceptable peak resolution of unsaturated FAME, is a surrogate for AVTUR and was subsequently used for the preparation of all standard solutions, see above. Figure 5-28 and Figure 29 show the BPICC of RME and CME prepared in methanol and hexane analysed using the BEH column. The effect of the presence of trace levels of methanol can be seen in (A) where the C18:1, C18:2 and C18:3 co-elute.
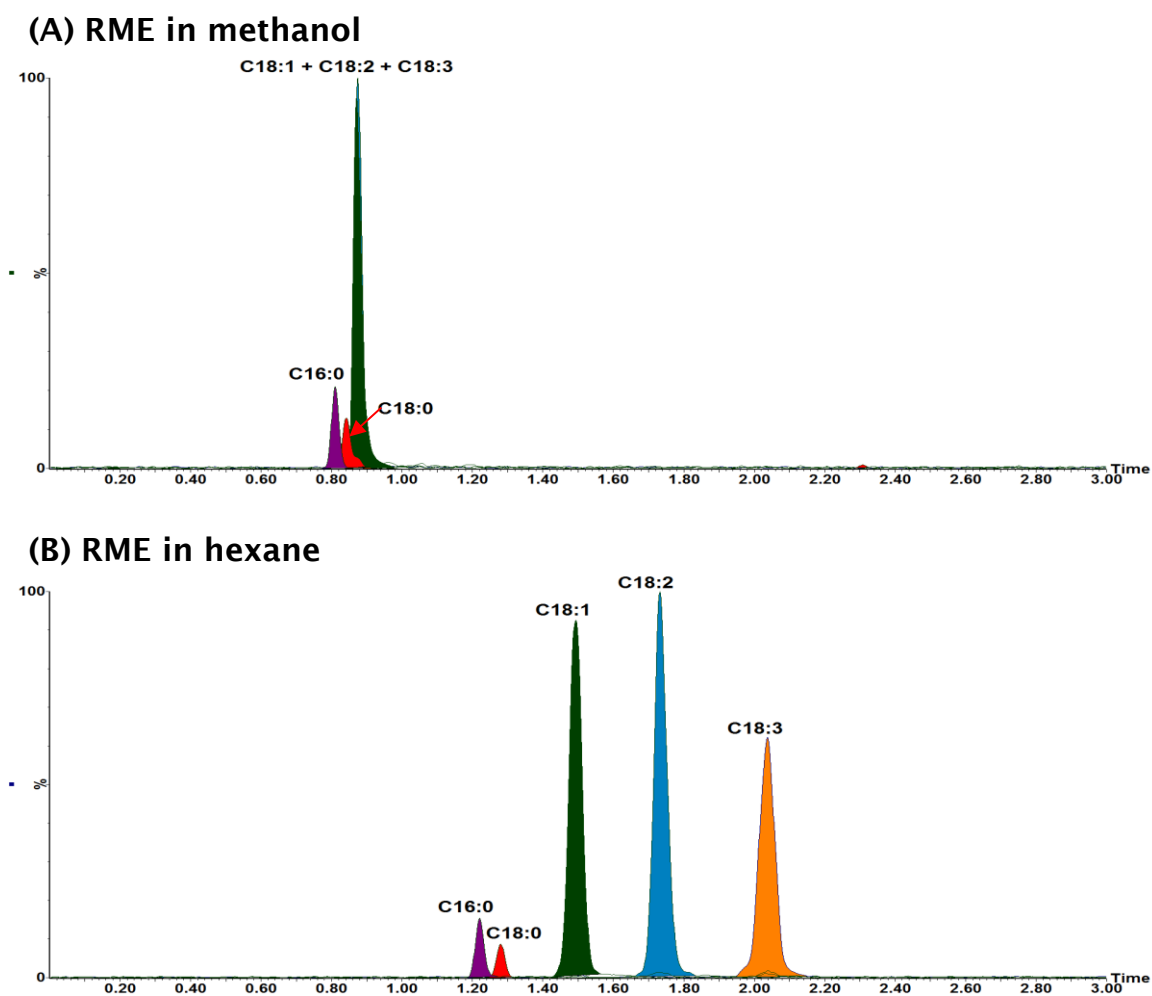
Figure 5-28 **RICCs of RME prepared in methanol (A) and hexane (B) analysed using the BEH column 1.7 μm 3 mm × 100 mm. Conditions: CO_2 pressure 105 bar; gradient 0-1% MeOH in CO_2 at 1.5 mL/min in 5 min.**

(A) CME in methanol

(B) CME in hexane
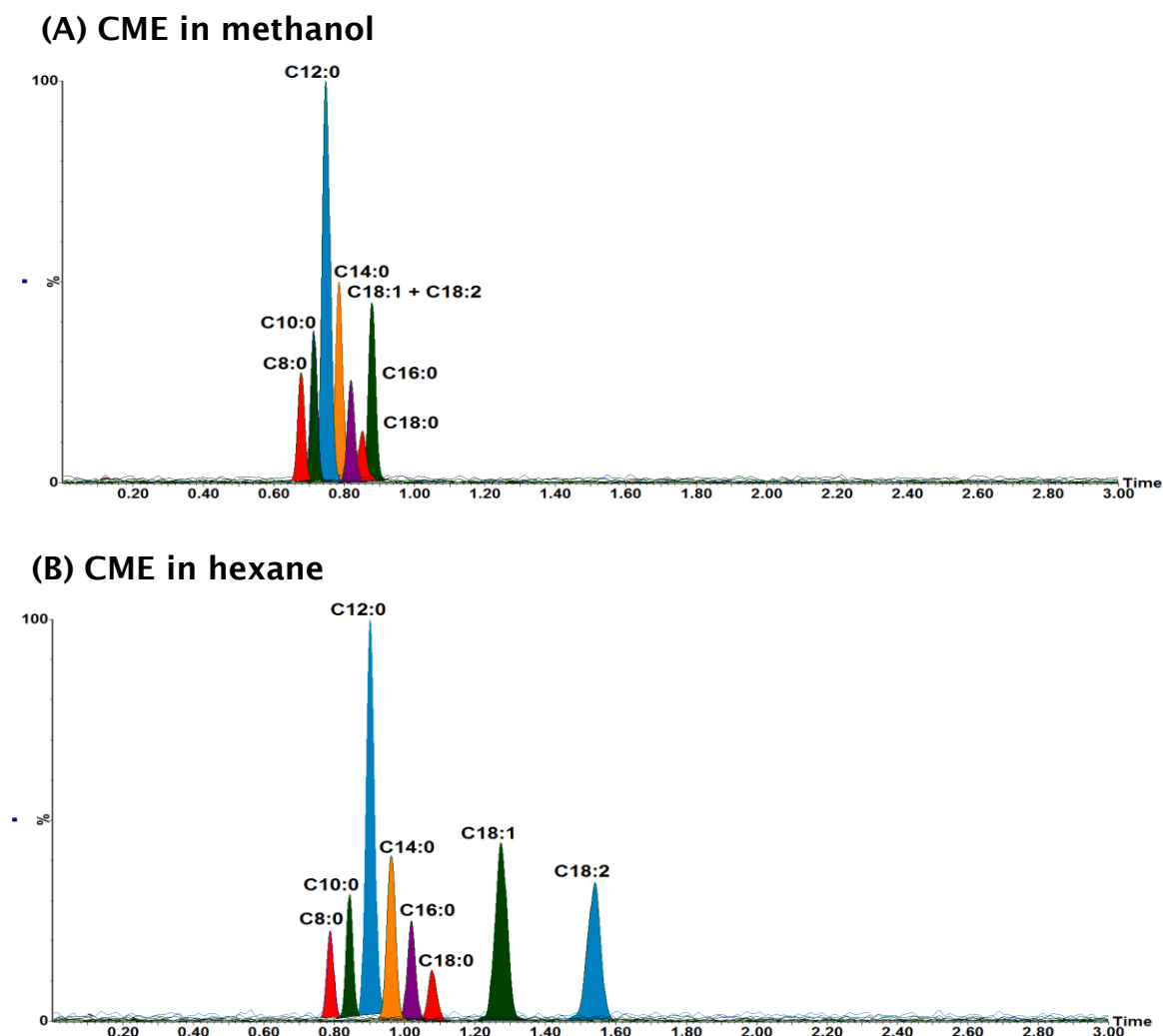
Figure 5-29   RICCs of CME prepared in methanol (A) and hexane
                (B) analysed using the BEH column 1.7 μm 3 mm × 100 mm.
                Chromatographic conditions: CO_2 pressure 105 bar; gradient
                0-1% MeOH in CO_2 at 1.5 mL/min in 5 min.

5.4.3   Effect of modifier on FAME separation

The addition of a polar organic modifier to supercritical fluid CO_2 with the aim to change the mobile phase polarity and enhance the solubility of polar solutes in the mobile phase.[189] The effects of modifiers are; (i) covering the active sites of the stationary phase (silanol group)[190], (ii) swelling or modifying the stationary phase[187], (iii) increased mobile phase density[191], and (iv) increased solvent strength of mobile phase.[189][190]

Four organic modifiers were evaluated in this study (methanol, acetonitrile, isopropanol, methanol 25 mM ammonium acetate) together with no modifier (100% CO_2) the RICCs for RME (see, Figure 5-30) and CME (see, Figure 5-31). The saturated and unsaturated FAMEs were eluted from the BEH column with acceptable peak symmetry (A_s of 0.94-1.51 for unsaturated FAMEs, 0.94-1.51 for saturated FAMEs) and baseline separation using 100% CO_2 as the mobile phase. All subsequent analyses were undertaken using the latter conditions.

(A) RME, MeOH as modifier
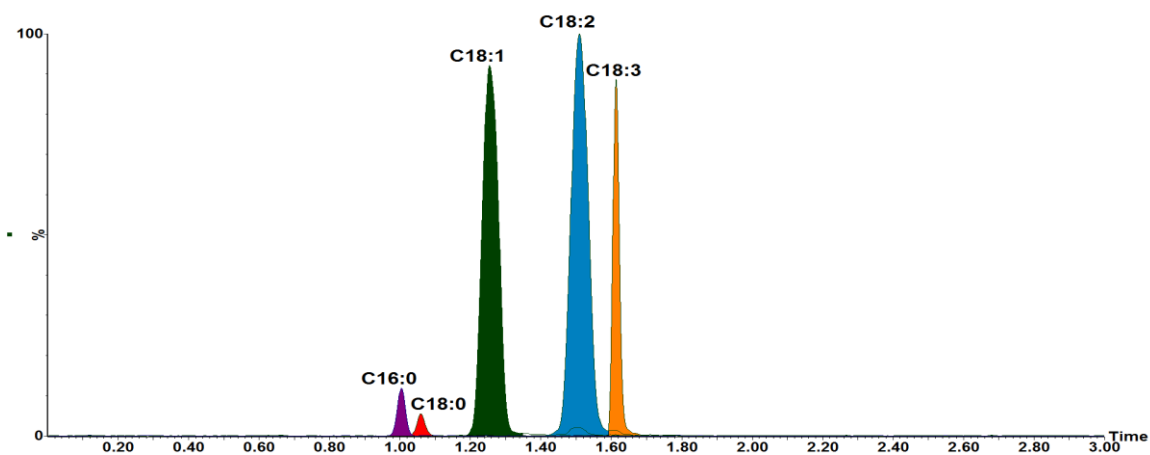
(B) RME, ACN as modifier
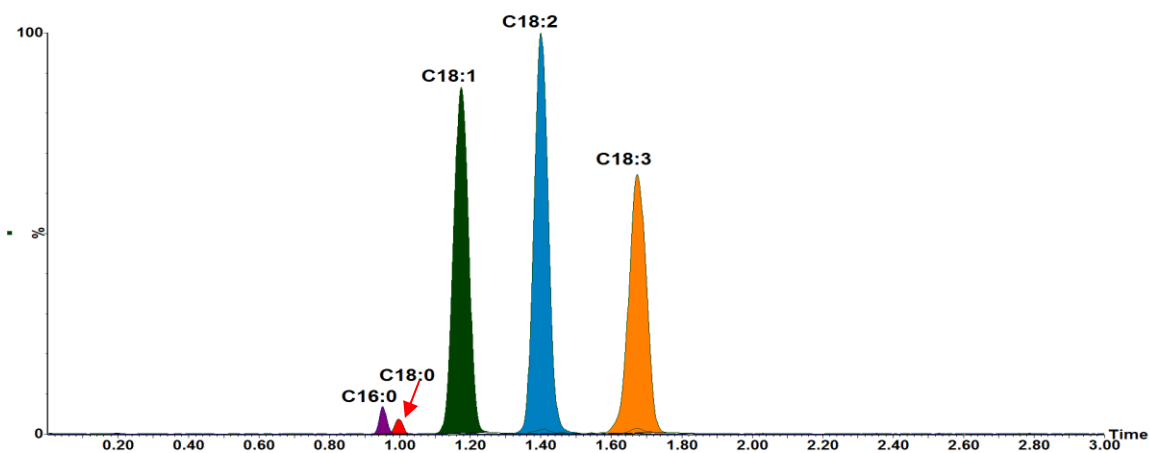
(C) RME, IPA as modifier
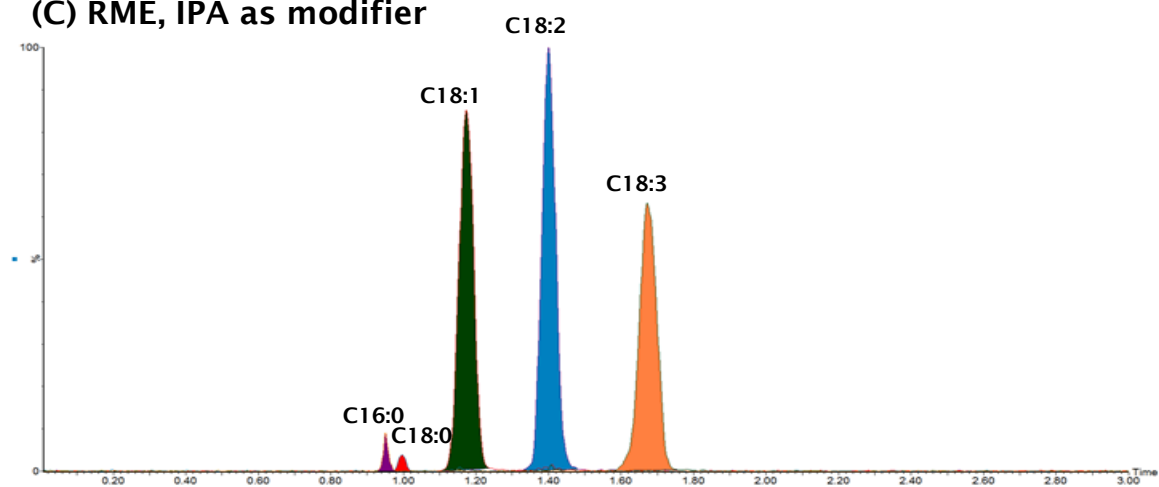
Figure 5-30   Continued overleaf

(D) RME, MeOH 25 mM ammonium acetate

(E) RME, 100% scCO$_2$ as modifier
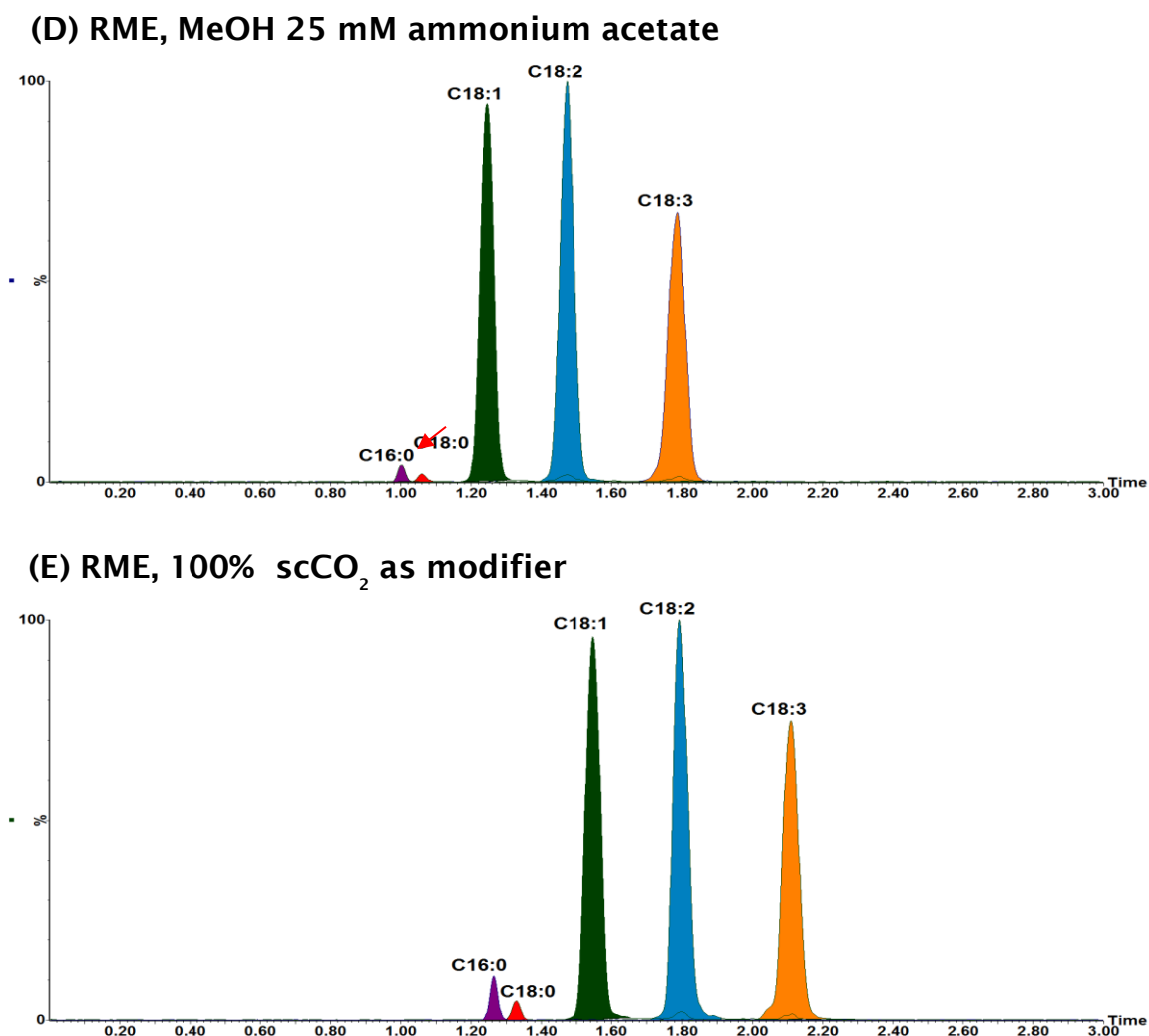
Figure 5-30 **RICCs of RME at *m/z* 271 [C16:0 + H]⁺, 299 [C18:0 + H]⁺, 319 [C18:1 + Na]⁺, 317 [C18:2 + Na]⁺ and 315 [C18:3 + Na]⁺ separation using different organic modifiers. (A) methanol; (B) acetonitrile; (C) isopropanol; (D) methanol 25mM ammonium acetate and; (E) 100% scCO2. Conditions: scCO$_2$ pressure 105 bar; gradient 0-1% modifier in scCO2 at 1.5 mL/min in 5 min.**

(A) CME, MeOH as modifier
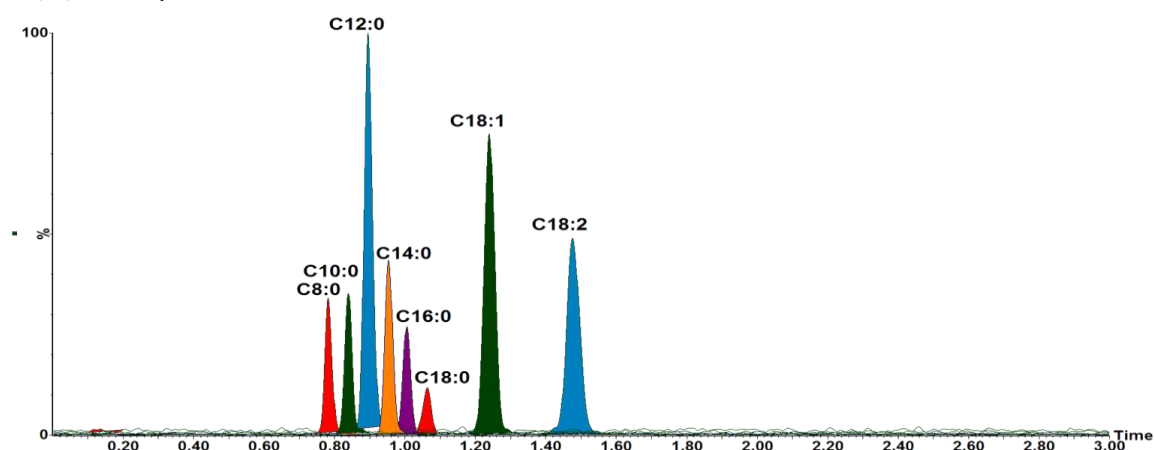
(B) CME, ACN as modifier
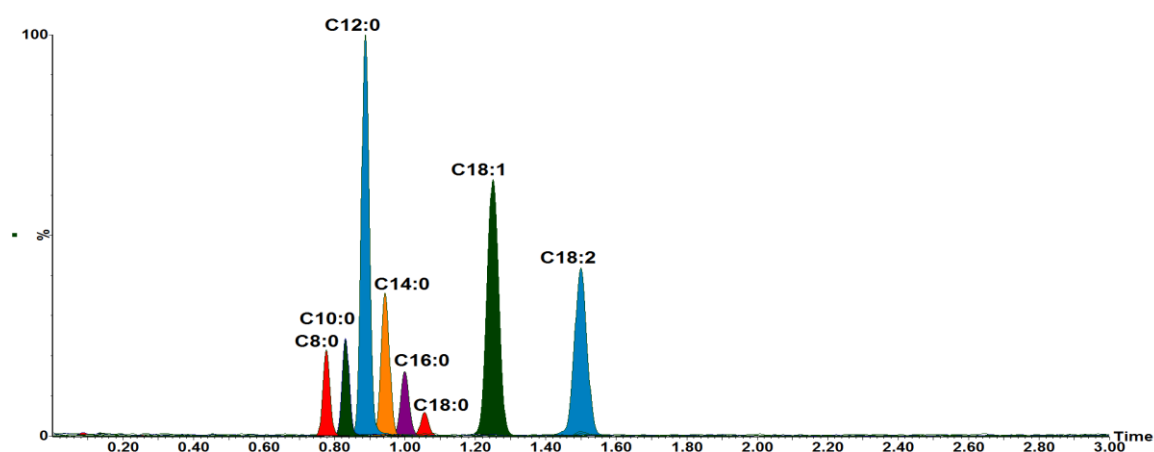
(C) CME, IPA as modifier
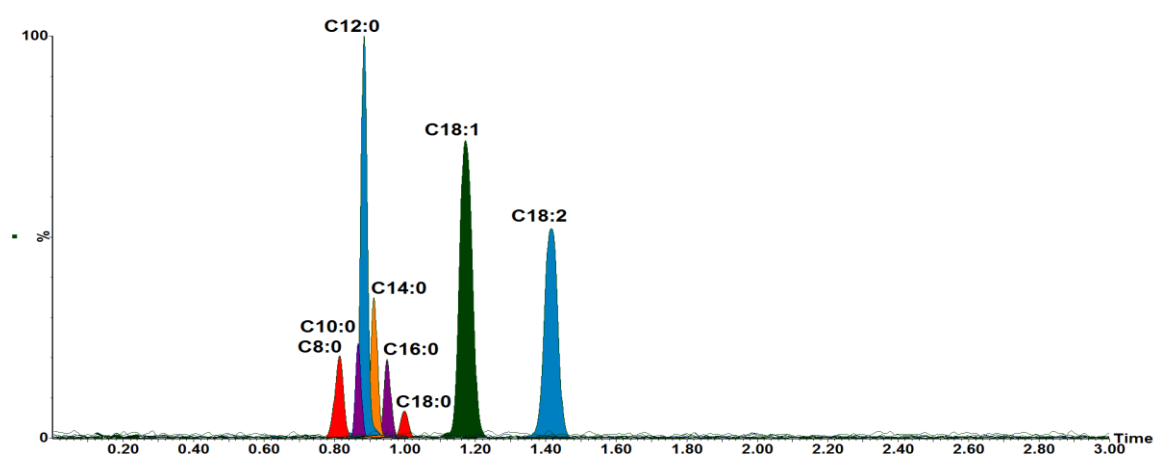
Figure 5-31   Continued overleaf

(D) CME, MeOH 25 mM ammonium acetate as modifier
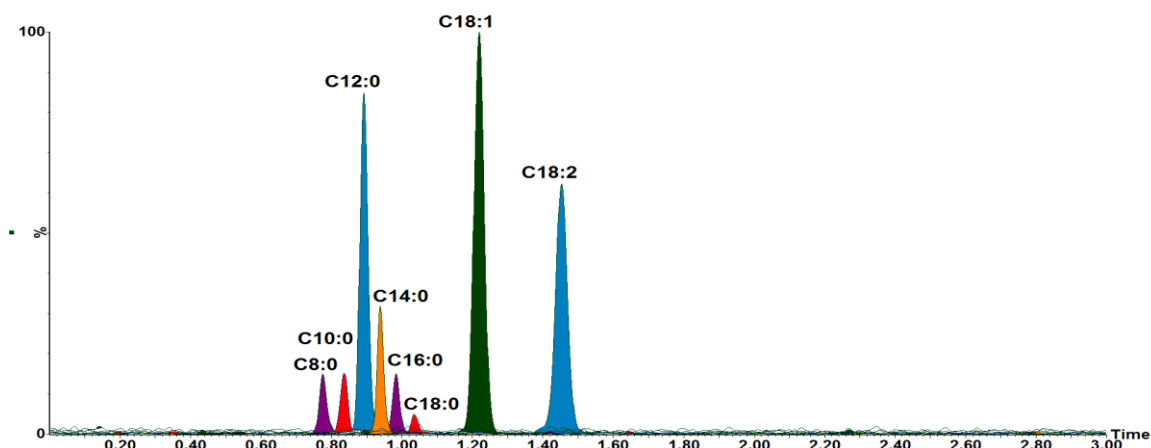
(E) CME, 100% scCO$_2$ as modifier
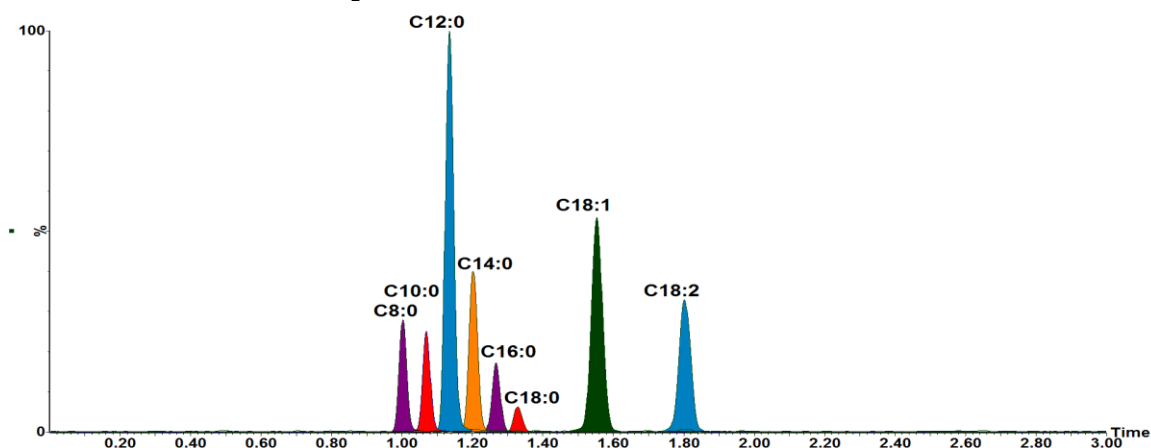
Figure 5-31 RICCs of CME at RICCs of *m/z* 159 [C8:0 + H]⁺, *m/z* 187 [C10:0 + H]⁺, *m/z* 215 [C12:0 + H]⁺, *m/z* 243 [C14:0 + H]⁺, *m/z* 271 [C16:0 + H]⁺, *m/z* 299 [C18:0 + H]⁺, *m/z* 319 [C18:0 + Na]⁺ and *m/z* 317 [C18:1 + Na]⁺. Separation using different organic modifiers. (A) methanol (MeOH); (B) acetonitrile (ACN); (C) isopropanol (IPA); (D) methanol 25 mM ammonium acetate and; (E) 100% scCO$_2$. Conditions: scCO$_2$ pressure 105 bar; gradient 0-1% modifier in scCO$_2$ at 1.5 mL/min in 5 min.

5.4.4   Effect of column temperature FAME separation

This was optimised over the range of 35-50 °C. When using HPLC, an increase in column temperature will cause a decrease in retention factor (k), but this is not straightforward in SFC, here the retention factor of the FAMEs increases with increased column temperature. The density of supercritical fluid decreases as column temperature increases, hence the diffusion rates increase leading to a decrease in fluid elution strength. Therefore, elevated column temperatures increase the retention factor (k) in SFC.[192][193]

The effect of column temperature on FAME separation is presented in Figure 5-32 and Figure 5-33 showing an improvement of the separation when using the BEH column whilst increasing the column temperature from 35 °C to 50 °C. At a column temperature of 50 °C, C16:0 and C18:0 are better resolved whilst the resolution of C18:2 and C18:3 is degraded, *e.g.*, a broader peak profile for the C18:3 FAME was observed, see Figure 5-32 (D) and Table 5-6 to Table 5-8.

(A) RME, column temp. 35 °C

(B) RME, column temp. 40 °C

(C) RME, column temp. 45 °C
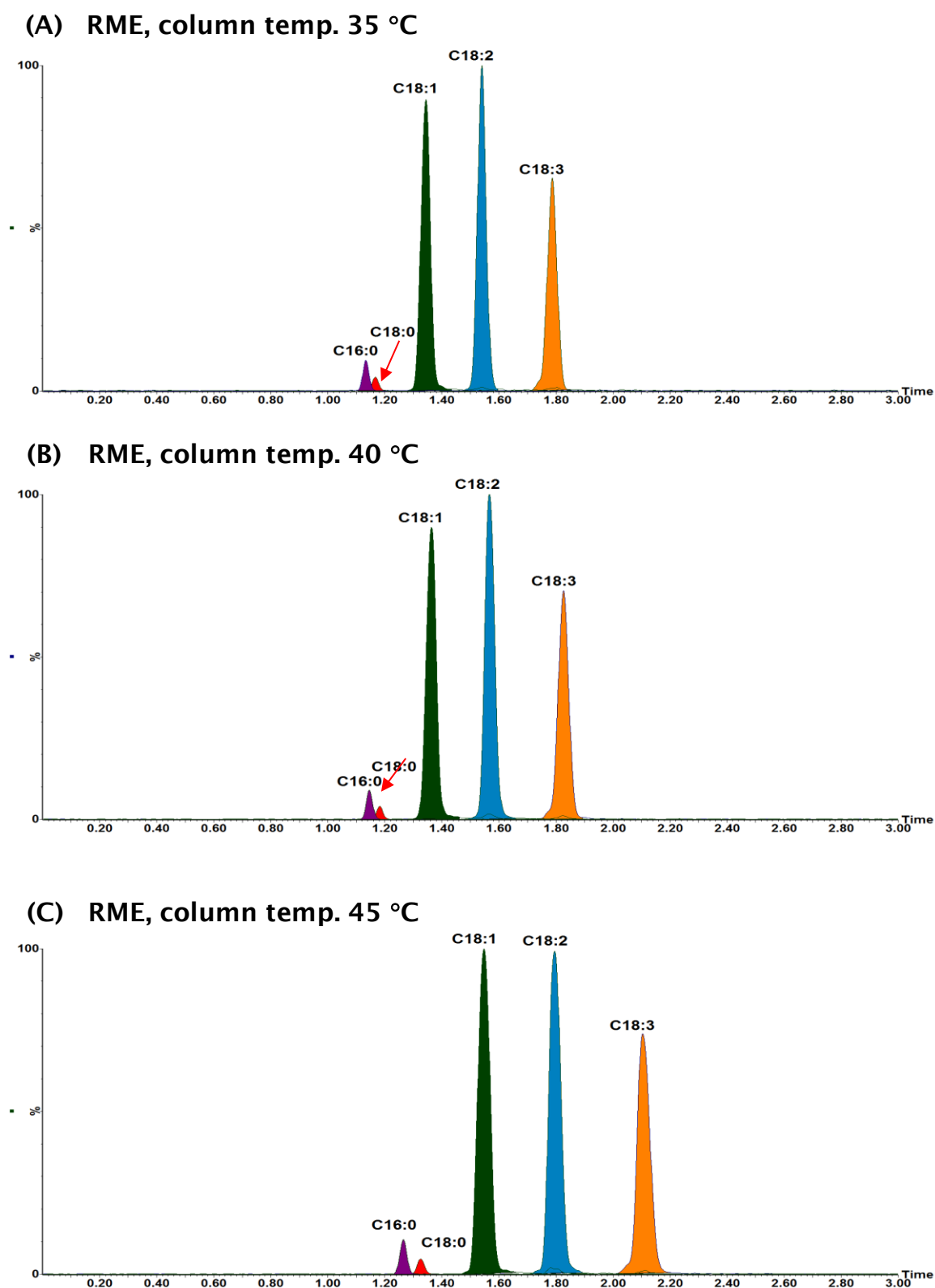
Figure 5-32   Continued overleaf

(D) RME, column temp. 50 °C
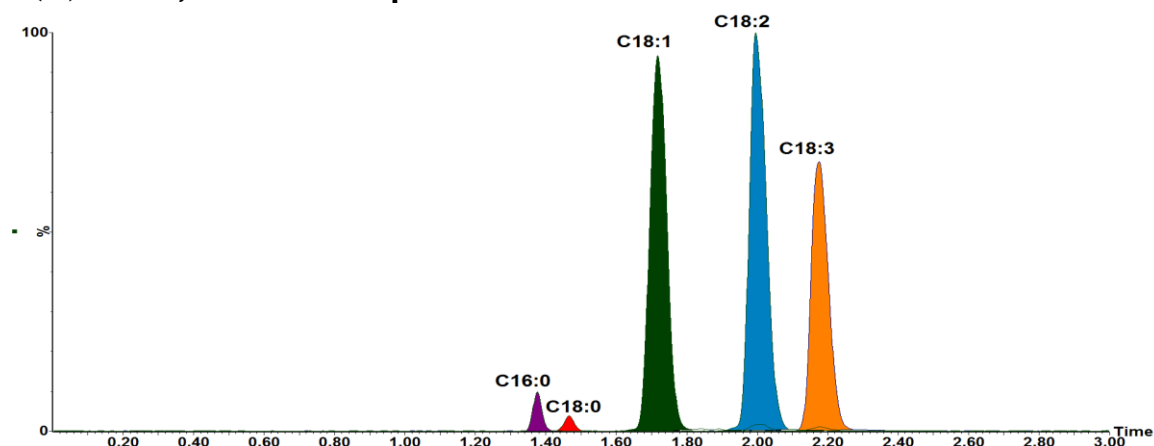
Figure 5-32 RICCs of ions at m/z 271 [C16:0 + H]$^+$, 299 [C18:0 + H]$^+$, 319 [C18:1 + Na]$^+$, 317 [C18:2 + Na]$^+$ and 315 [C18:3 + Na]$^+$ showing RME separation at different column temperatures (A) 35 °C; (B) 40 °C; (C) 45 °C and (D) 50 °C. Chromatographic conditions: scCO$_2$ back pressure of 105 bar using 100% scCO$_2$ as the mobile phase at a flow rate of 1.5 mL/min.

(A) CME, column temp. 35 °C

Figure 5-33 **Continued overleaf**

(B) CME, column temp. 40 °C

(C) CME, column temp. 45 °C

Figure 5-33   Continued overleaf

(D) CME, column temp. 50°C
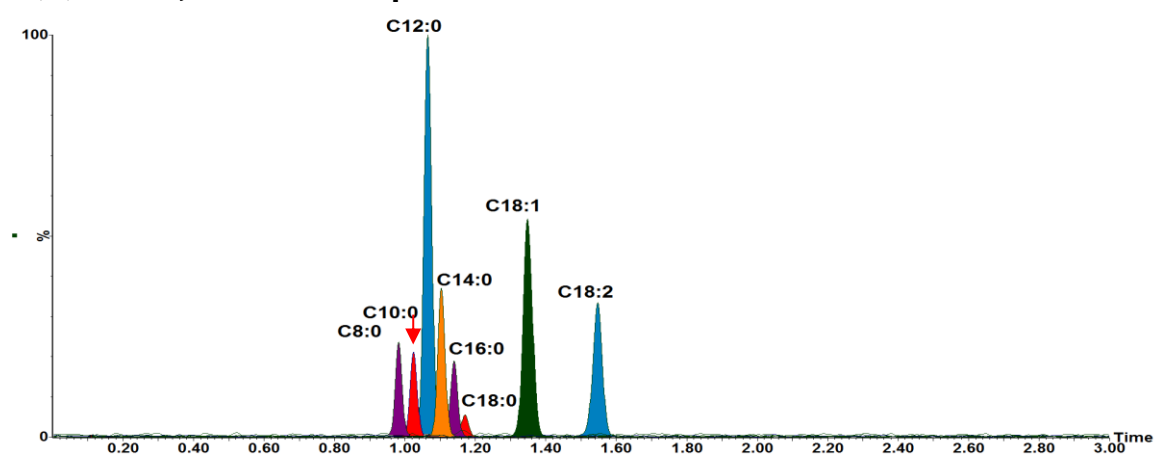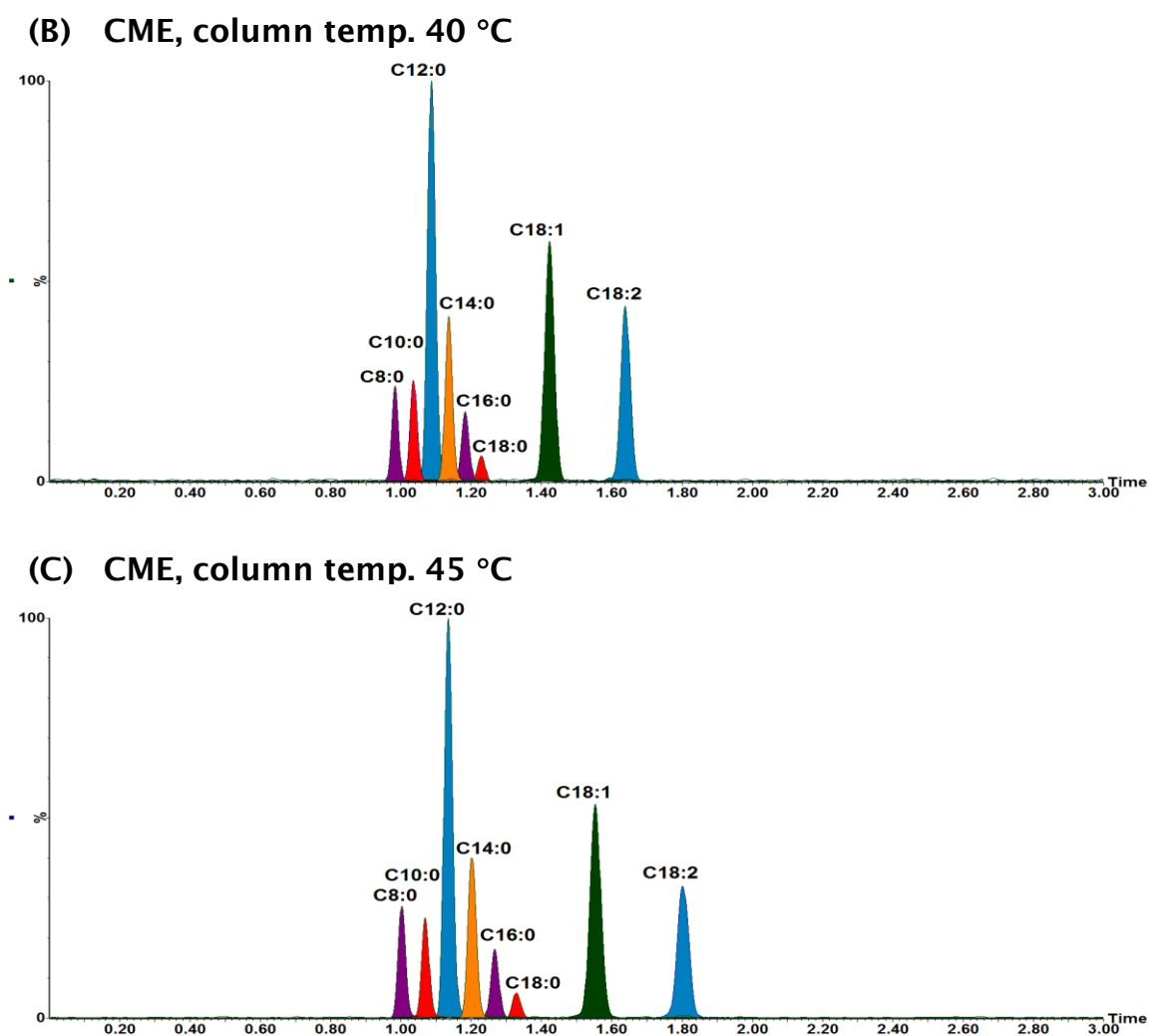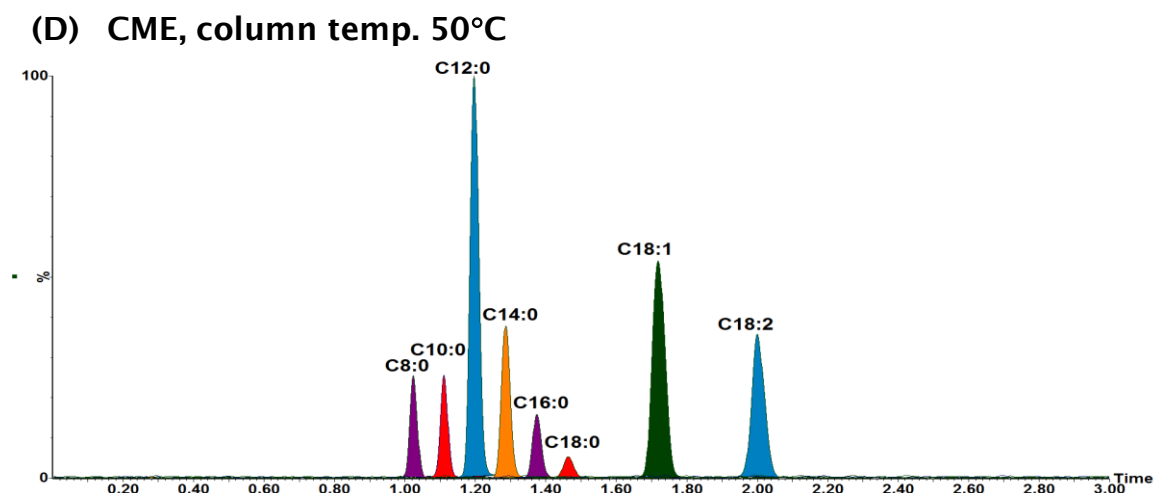
Figure 5-33   RICCs of ions at *m/z* 159 [C8 + H]⁺, 187 [C10 + H]⁺, 215 [C12:0 + H]⁺, 243 [C14:0 + H]⁺, 271 [C16:0 + H]⁺, 299 [C18:0 + H]⁺, 319 [C18:1 + Na]⁺ and 317 [C18:2 + Na]⁺ showing CME separation at different column temperature. (A) 35 °C; (B) 40 °C; (C) 45 °C and (D) 50 °C. Conditions: scCO$_2$ back pressure of 105 bar using 100% scCO$_2$ as the mobile phase at a flow rate of 1.5 mL/min.

Table 5-6 **The results of resolution (R_s) obtained at different Acquity BEH column temperatures**

FAMEs	Column temperature			
	35 °C	40 °C	45 °C	50 °C
	R_s	R_s	R_s	R_s
C16:0	0.81[a]	1.01[a]	1.31[a]	1.69[a]
	(0.14)	(0.15)	(0.14)	(0.17)
C18:0	3.31[b]	3.43[b]	3.26[b]	3.46[b]
	(0.12)	(0.24)	(0.17)	(0.12)
C18:1	3.23[c]	3.10[c]	3.09[c]	3.07[c]
	(0.04)	(0.08)	(0.18)	(0.07)
C18:2	3.93[d]	3.75[d]	3.84[d]	1.98[d]
	(0.10)	(0.13)	(0.14)	(0.00)
C18:3				

Note: The values of resolution (R_s) were calculated from two peaks of interest. [a] is the first pair of peaks, C16:0 & C18:0, [b] is the second pair of peaks C18:0 & C18:1, [b] is the third pair of peak C18:1 & C18:2 and [d] is the fourth pair of peakC18:2 & C18:3. The resolution was calculated using the half-height method. [115][116][194] The values in a bracket () are standard deviation (SD) from number of replicate measurements = 3.

Table 5-7   The results of peak asymmetry (As) obtained at different Acquity BEH column temperatures

FAMEs component	Column temperature			
	35 °C	40 °C	45 °C	50 °C
	A_c	A_c	A_c	A_c
C16:0	1.11	1.26	0.97	0.89
	(0.52)	(0.53)	(0.37)	(0.03)
C18:0	0.98	1.12	0.95	1.30
	(0.24)	(0.45)	(0.04)	(0.47)
C18:1	1.13	1.22	1.07	1.02
	(0.21)	(0.53)	(0.29)	(0.08)
C18:2	1.12	1.15	1.34	1.26
	(0.07)	(0.17)	(0.45)	(0.17)
C18:3	0.96	0.96	1.45	1.28
	(0.14)	(0.22)	(0.35)	(0.17)

Note: The values in a bracket () are standard deviation (SD) from number of replicate measurements = 3.

Table 5-8 **The results of peak width at half height ($w_{0.5}$) obtained at different Acquity BEH column temperatures**

FAMEs component	Column temperature			
	35 °C	40 °C	45 °C	50 °C
	$w_{0.5}$	$w_{0.5}$	$w_{0.5}$	$w_{0.5}$
C16:0	0.02	0.03	0.03	0.89
	(0.00)	(0.00)	(0.00)	(0.03)
C18:0	0.02	0.03	0.03	1.30
	(0.00)	(0.00)	(0.00)	(0.47)
C18:1	0.04	0.04	0.04	1.02
	(0.00)	(0.00)	(0.00)	0.08)
C18:2	0.04	0.04	0.04	1.26
	(0.00)	(0.00)	(0.00)	(0.17)
C18:3	0.04	0.04	0.04	1.28
	(0.00)	(0.00)	(0.00)	(0.17)

Note: The values in a bracket () are standard deviation (SD) from number of replicate measurements = 3.

5.4.5 Effect of scCO$_2$ back pressure on FAMEs separation

The influence of scCO$_2$ back pressure (105-200 bar) on the isocratic elution method (100% scCO$_2$) was investigated (see Figure 5-34). As the pressure of the scCO$_2$ was increased the peaks of C16:0 and C18:0 partially co-eluted and at 200 bar totally co-eluted. At the scCO$_2$ back pressure of 105 bar was selected as the optimum scCO$_2$ pressure, giving the best baseline separation of all species, and, subsequently, was shown to allow retention of the FAMEs away from the fuel matrix.

(A) RME, scCO$_2$ pressure 105 bar
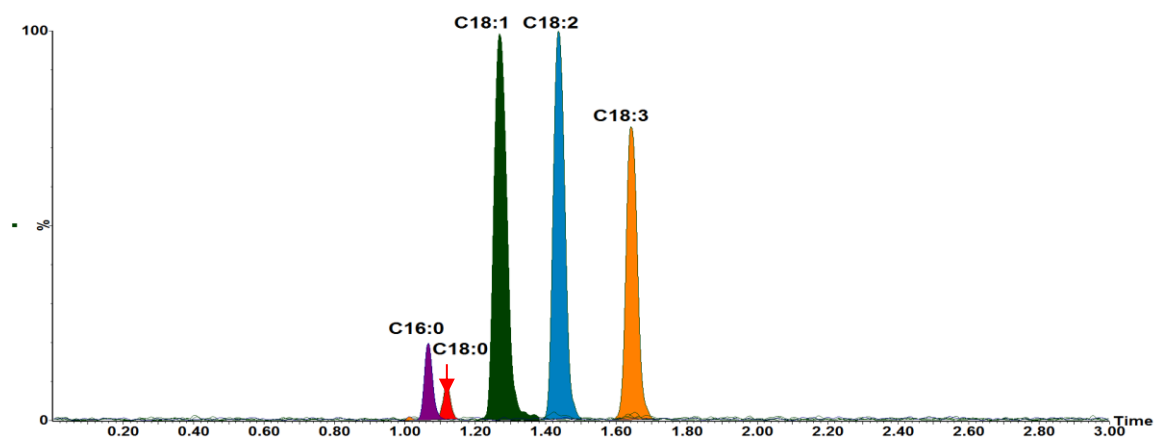
(B) RME, scCO$_2$ pressure 120 bar
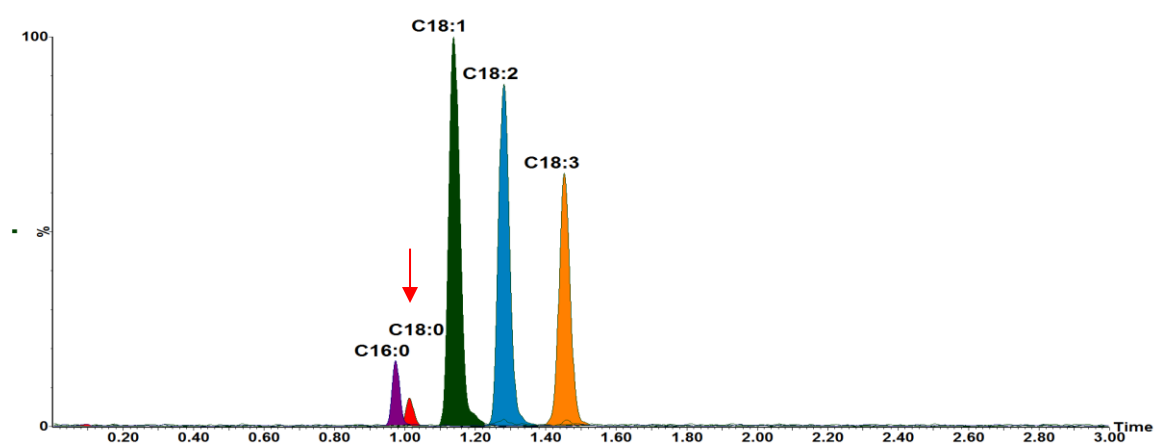
(C) RME, scCO$_2$ pressure 150 bar
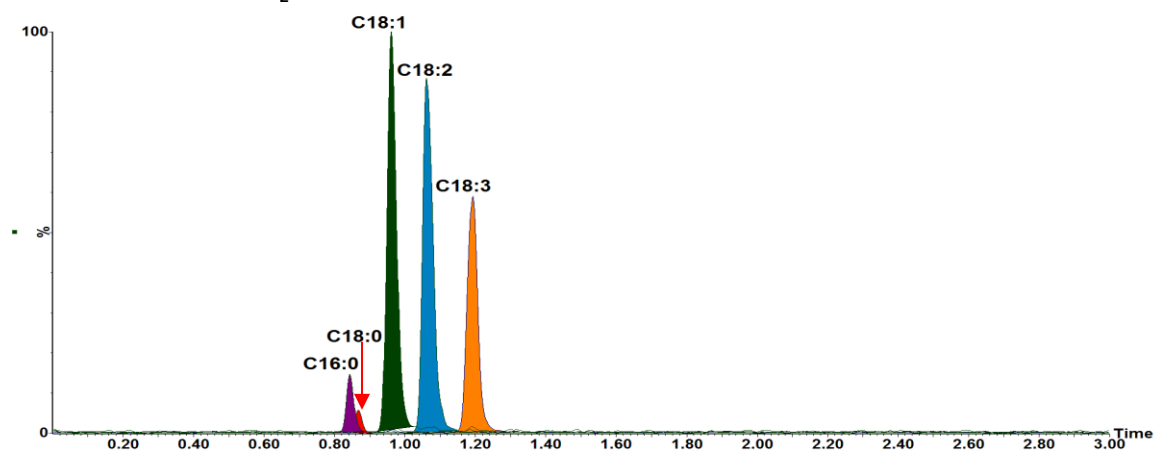
Figure 5-34   Continued overleaf

(D)   RME, scCO$_2$ pressure 180 bar

(E)   RME, scCO$_2$ pressure 200 bar
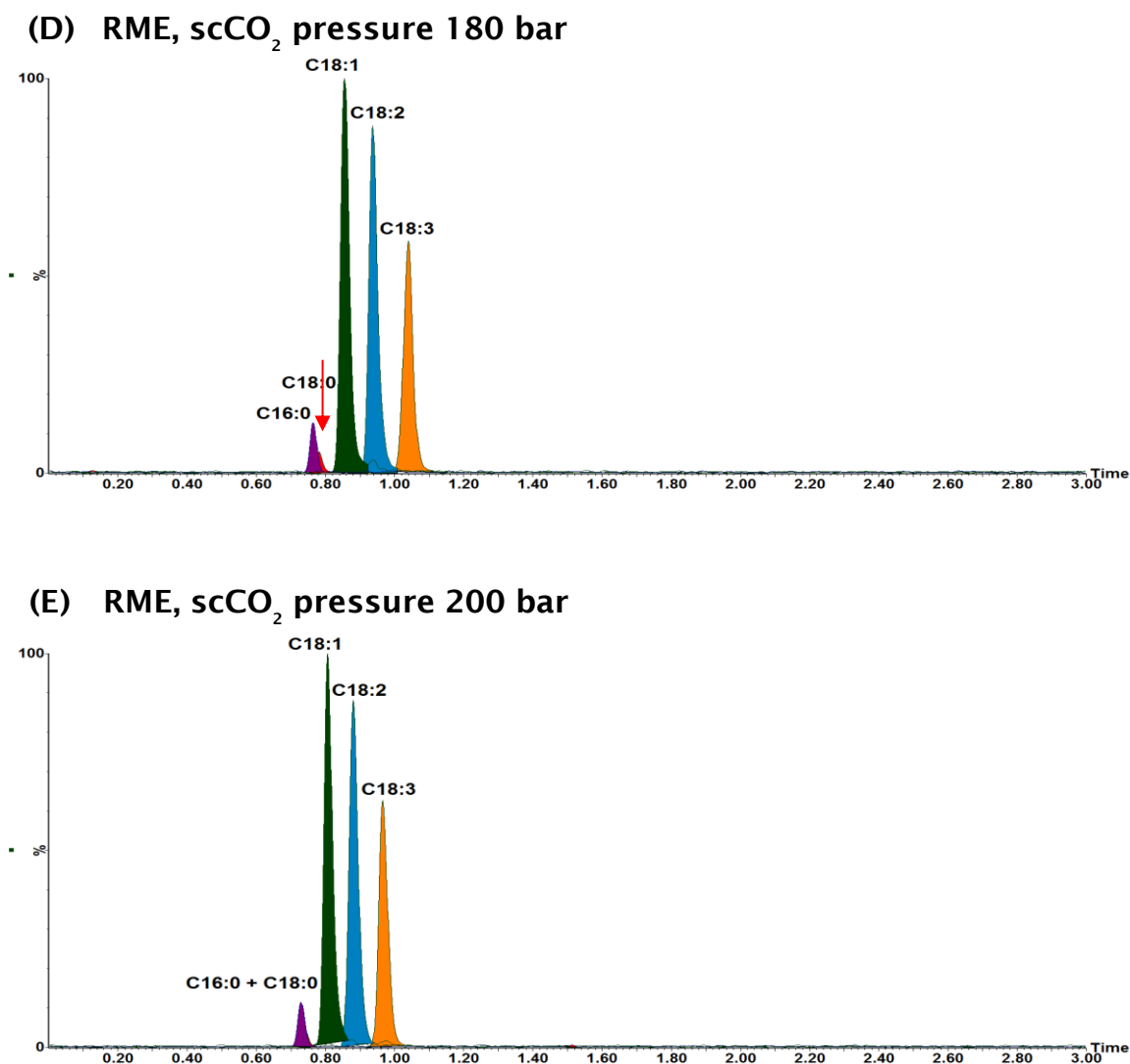
Figure 5-34   RICCs of ions at *m/z* 271 [C16:0 + H]$^+$, 299 [C18:0 + H]$^+$, 319 [C18:1 + Na]$^+$, 317 [C18:2 + Na]$^+$ and 315 [C18:3 + Na]$^+$ showing RME separation at different scCO$_2$ back pressures. (A) 105 bar; (B) 120 bar; (C) 150 bar; (D) 180 bar; (E) 200 bar. Chromatographic condition: scCO$_2$ back pressure of 105 bar using 100% scCO$_2$ as the mobile phase at a flow rate of 1.5 mL/min, at column temperature of 45 °C.

5.4.6   Effect of cone voltage on ESI-MS

'In-source'collisional-induced dissociation (CID) is a feature of atmospheric pressure ionisation techniques where ions are fragmented within the source of the mass spectrometer by applying of a voltage between the 'nozzle' and the 'skimmer', *e.g.* a cone voltage. A change in the cone voltage is made to influence the extent of fragmentation and the relative intensities of the fragment ions. Ion fragmentation can be produced by increasing the cone voltage in the electrospray interface region, where the desolvated ions are transferred into the mass analyser. The potential different between the sample cone and the extraction cone is used to control the internal energy of the ions. Hence, a cone voltage or fragmentor voltage is an important tuning parameter.

To study the effect of cone voltage on ESI-MS, the cone voltage values were adjusted in the range 20–50 V by step of 5 V. Figure 5-35 shows the intensities of ions of FAMEs as a function of cone voltages. Several major ions were observed for FAME, *i.e.*, $[M + H]^+$, $[M + NH_4]^+$ and $[M + Na]^+$. As the cone voltage was increased from 20 V to 30 V the intensity of $[M + Na]^+$ increased and then decreased at the cone voltage 35-50 V, with the highest signal intensity at the cone voltage 30 V for all FAME components. In case of $[M + NH_4]^+$ the maximum response was observed at the cone voltage 20 V, when the cone voltage was increased to 50 V no response was observed for $[M + NH_4]^+$.
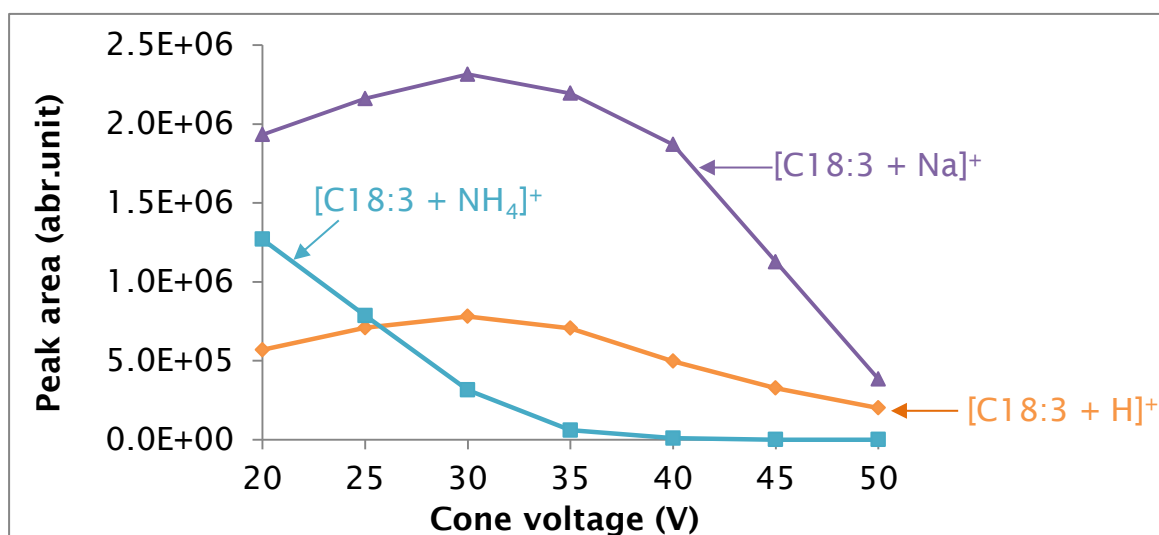
Figure 5-35 **Effect of cone voltages on the ESI signal intensities of [C18:3 + H]+, [C18:3 + NH4]+ and [C18:3 + Na]+ ions.**

Representative of positive ESI mass spectra of methyl linolenate (C18:3) are shown in Figure 5-36. The relative intensity of the ion at *m/z* 310 [C18:3 + NH$_4$]+ obtained at cone voltage of 20 V was higher than the relative intensity of the ion at *m/z* 293 [M + H]+. When the cone voltage was increased, the relative intensity of the ion at *m/z* 310 [M + NH$_4$]+ showed a decreased response. No response for [M + NH$_4$]+ was observed at cone voltage of 50 V.

This indicated that the ammonium adduct ion, [M + NH$_4$]+ is not stable at high cone voltage. The ion [M + NH$_4$]+ can be fragmented to [M + H]+ + NH$_3$.[195] This reaction occurs if M is less basic than ammonia. Then, the relative intensity of the ion at *m/z* 293 [M + H]+ increased up to 30% when cone voltage was increased from 30 V to 50 V. When several adduct ions are formed for a molecule (M), the relative intensities of a particular adduct ion of M depends on is the stability of this adduct ion relative to other

competing adduct ions. The order of stability of the adduct ion of FAMEs is

[M + Na]$^+$ > [M + H]$^+$ > [M + NH$_4$]$^+$.

(A) Cone voltage 20 V
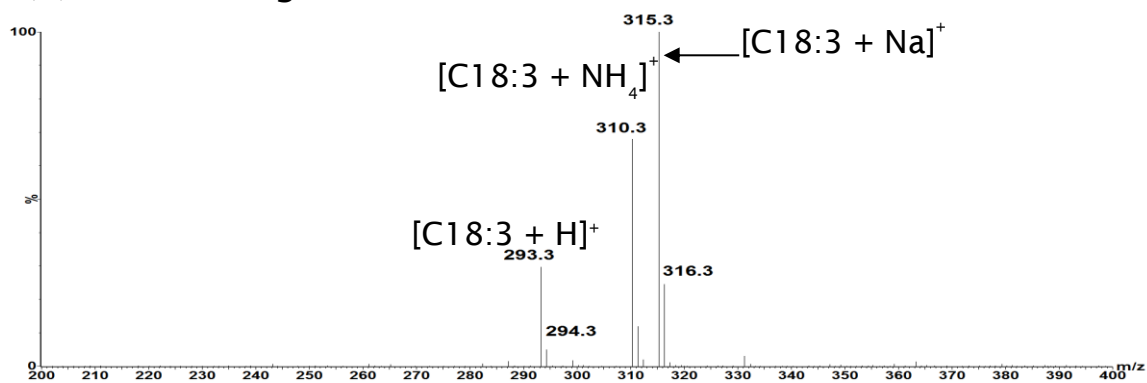
(B) Cone voltage 30 V
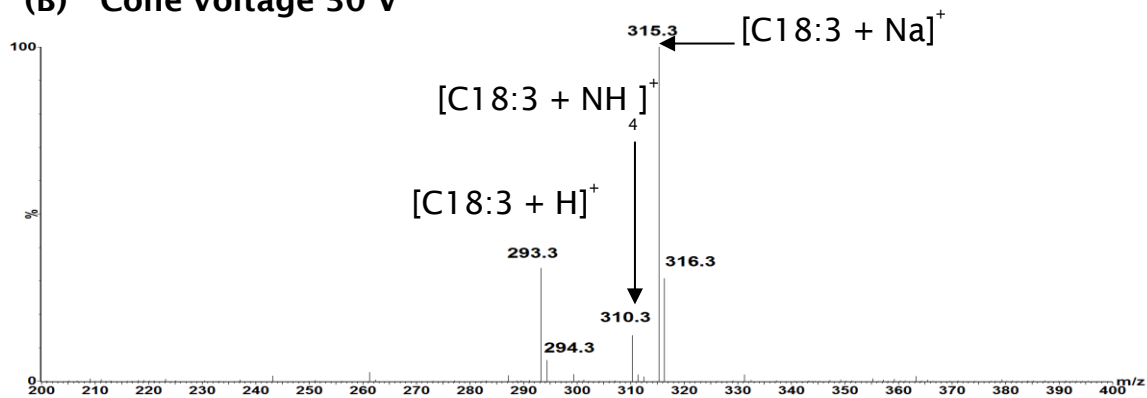
(C) Cone voltage 40 V
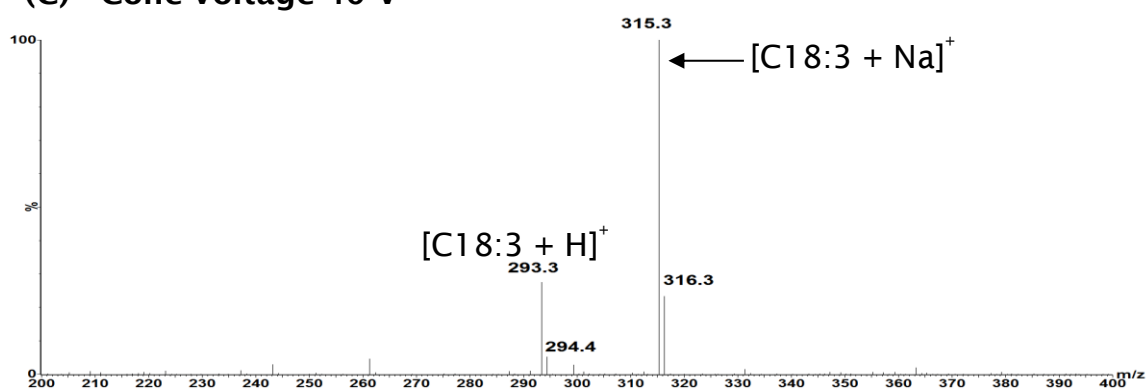
Figure 5-36   Continued overleaf
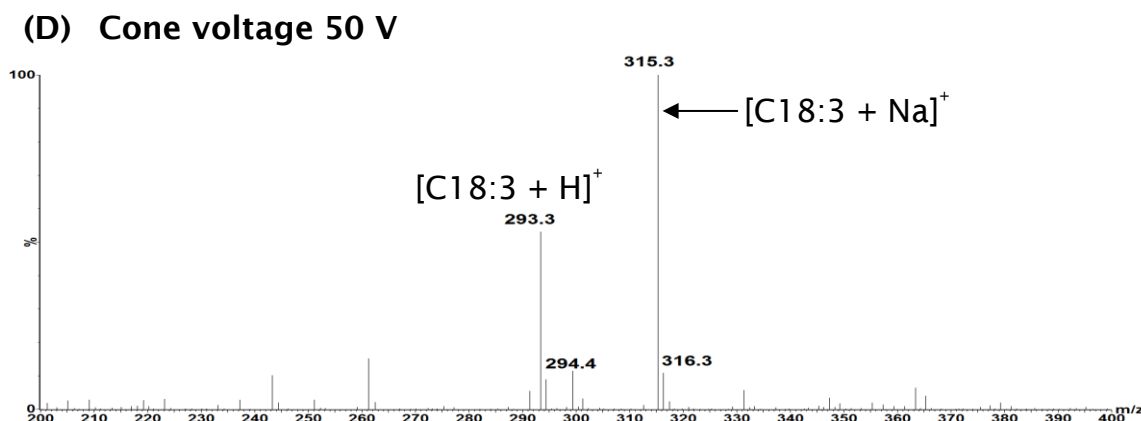
(D) Cone voltage 50 V

Figure 5-36   **Representative of positive ESI mass spectra of C18:3 with different cone voltages (A) 20 V; (B) 30 V; (C) 40 V and (D) 50 V.**

5.5   Limit of detection

Limit of detection (LOD) is a key factor for performance characteristics in method validation. The LOD is the lowest concentration of an analyte in a sample that can be detected, but not necessarily quantified, under the operation conditions. Several methods for the estimation of the LOD are: calculation from the signal-to-noise ratio (S/N), calculation from the standard deviation of the blank and the calibration line at low concentrations.

In this work, the estimation of LOD was calculated by using the signal-to-noise method and performed to display peak-to-peak, see Figure 5-37. This method only can be applied in analytical systems that present noise for the baseline. Calculation of signal to noise can be achieved to display peak-to-peak, or the root mean square value (RMS). Peak-to-Peak is the maximum height of the signal range above the mean noise value divided

by the variance. RMS is the maximum height of the signal above the mean noise divided by the root mean square deviation from the mean of the noise. Generally, a signal-to-noise ratio of 3:1.
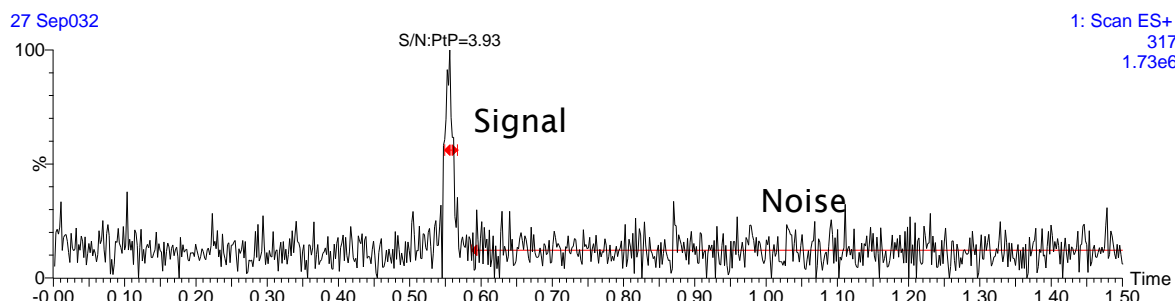
Figure 5-37   **Signal-to-noise ratio calculated.**

5.6   Linearity

It is expected that the response of the instrument is linearly related to the standard concentration for a limited range of concentration. To study linear dynamic range in the UHPLC-ESI-MS and UHPSFC-MS the standard solutions of FAME were prepared in the range 0.5-150 mg/kg. The peak area obtained from reconstructed ion current chromatograms (RICC) of the sodiated ion $[M + Na]^+$ of each FAME component were plotted *versus* FAME concentration, see Figure 5-38.
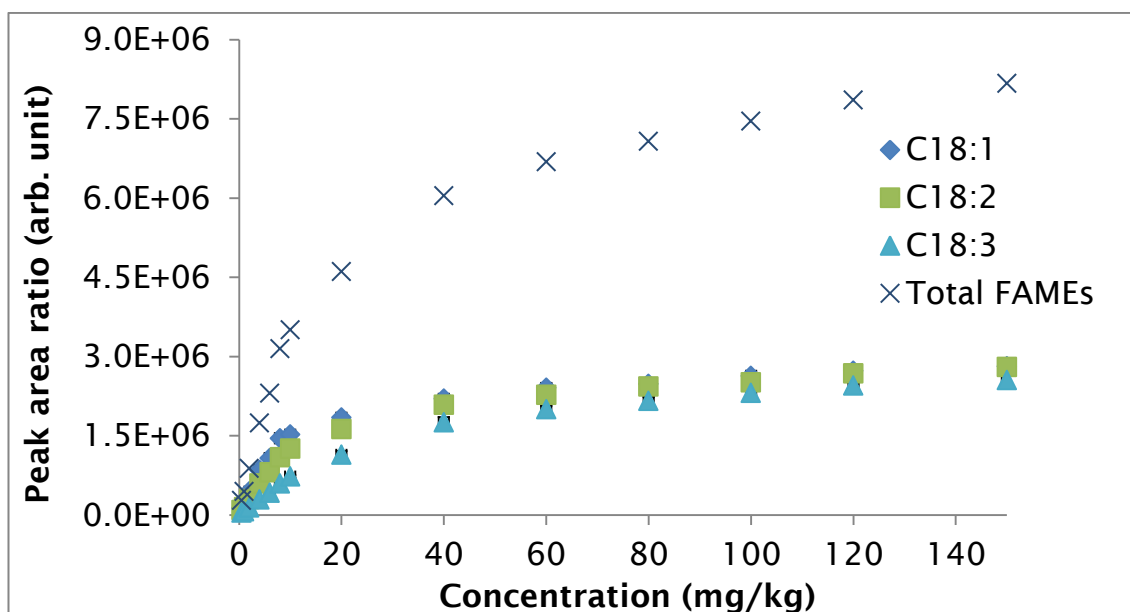
Figure 5-38   Linear plot of measured ESI response (peak area) *versus*
FAME concentration.

The linearity of the UHPSFC-MS was lost at FAME concentration of 20-150 mg/kg. Several reasons have been proposed for why ESI response is limited at upper concentrations. Kebarle and Tang proposed a limitation of linearity in ESI at high concentrations to be a result of an upper limit in the amount of an analyte that can be charged in the ESI process.[196][197] This might be due to a limited amount of excess charge available on ESI droplets or to saturation of the ESI droplets with analytes at their surface at upper concentrations, therefore, obstructing ejection of ions trapped inside the droplets.[198]

As described in the Experimental detail (Chapter 3), following the protocol defined by the international reference method IP585/10. The calibration curves of UHPLC-ESI-MS and UHPSFC-ESI-MS methods was determined by analysis of methanol solutions (UHPLC-ESI-MS) and hexane

solutions (UHPSFC-ESI-MS) of standard FAME species. A total of 10 ppm of

methyl heptadecanoate (C17:0) was used as the internal standard. Peak

areas, relative to the internal standard, of the RICCs of the sodiated

molecules $[M + Na]^+$ of each FAME species were plotted versus the FAME

concentration. Figure 5-39 presents the calibration curves of total FAMEs

for 2-10 mg/kg (R^2 = 0.9958) obtained from the UHPLC-ESI-MS method.
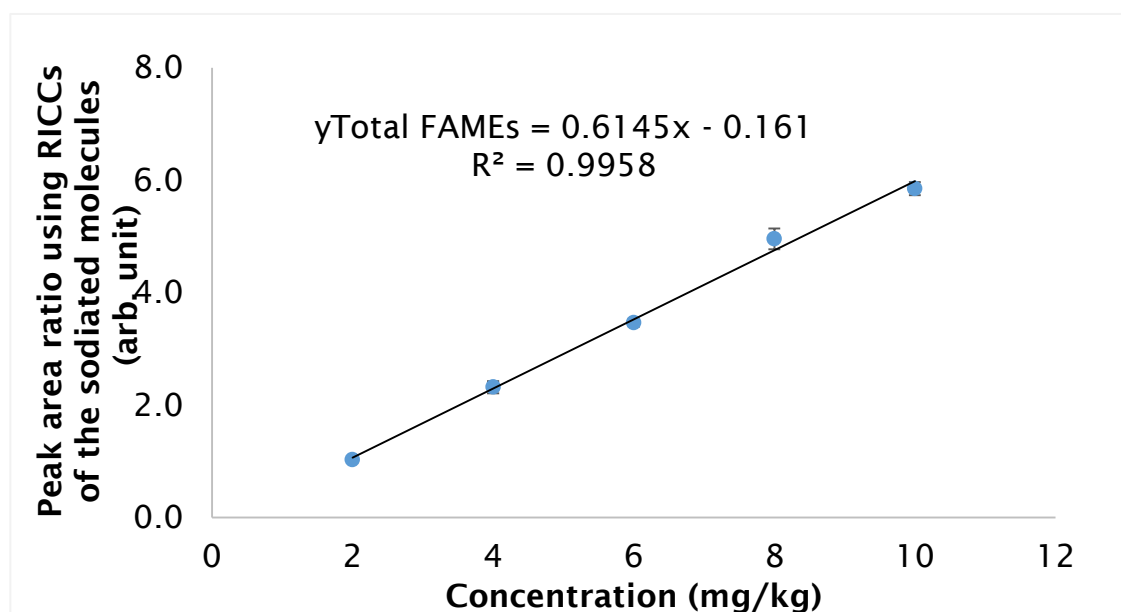
Figure 5-39   Calibration curves of total FAMEs for standard FAMEs (C18:1, C18:2 and C18:3) from the summed RICCs of the sodiated molecules. Number of replicate measurements = 3.

Figure 5-40 presents calibration curves of total FAMEs for 2-10 mg/kg

(R^2 = 0.9983) and 10-100 mg/kg (R^2 = 0.9909). Excellent linearity was

achieved in all cases with a linear correlation (R^2) greater than the required

value for FAMEs in AVTUR, IP585/10 method (R^2 = 0.9850).[98]

(A) RME concentration 2-10 mg/kg
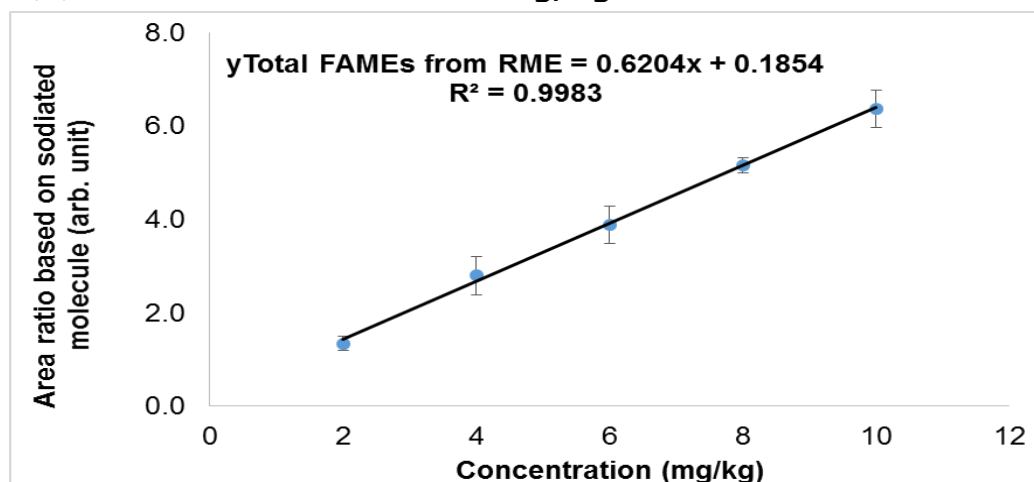
(B) RME concentration 10-100 mg/kg
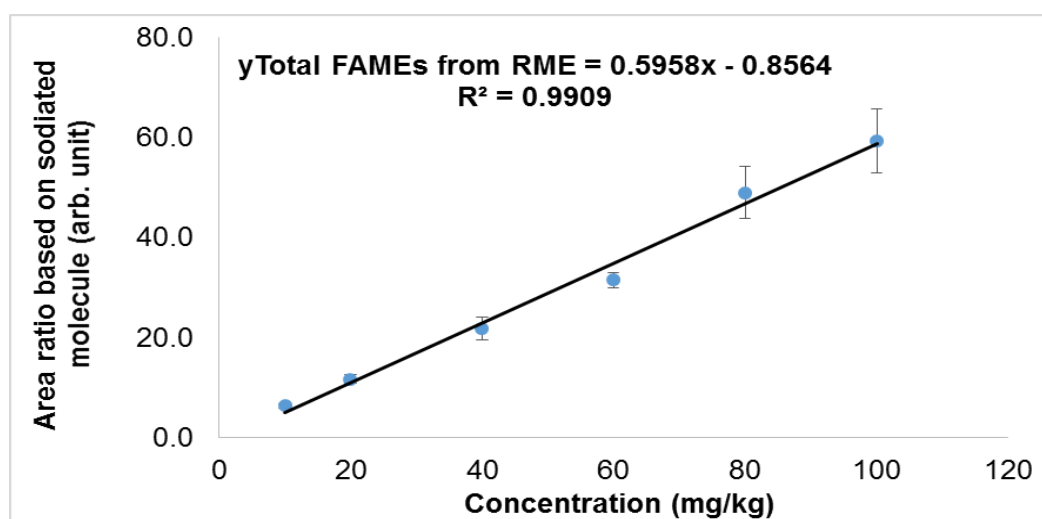
Figure 5-40 **Calibration curves of total FAMEs for RME from the summed RICCs of the sodiated molecules. Number of replicate mea- surements = 3.**

These calibration curves were then applied to determine the levels of FAME in spiked AVTUR samples compared to the expected values for FAME-spiked AVTUR samples.

5.7 Comparison of the GC-EI-MS, UHPLC-ESI-MS, and UHPSFC-ESI-MS methods for the analysis of FAMEs in AVTUR

Comparison of the three different methods shows that UHPSFC-MS is most suitable for analysing a wide range of analytes, and could serve as an alternative or complementary method for UHPLC. Comparison of this new method with the revised GC-MS reference method for FAME in AVTUR shows not only improvement in run time but is also more amenable to the analysis of lower chain length methyl esters, *e.g.*, CME. (see, Figure 5-41).
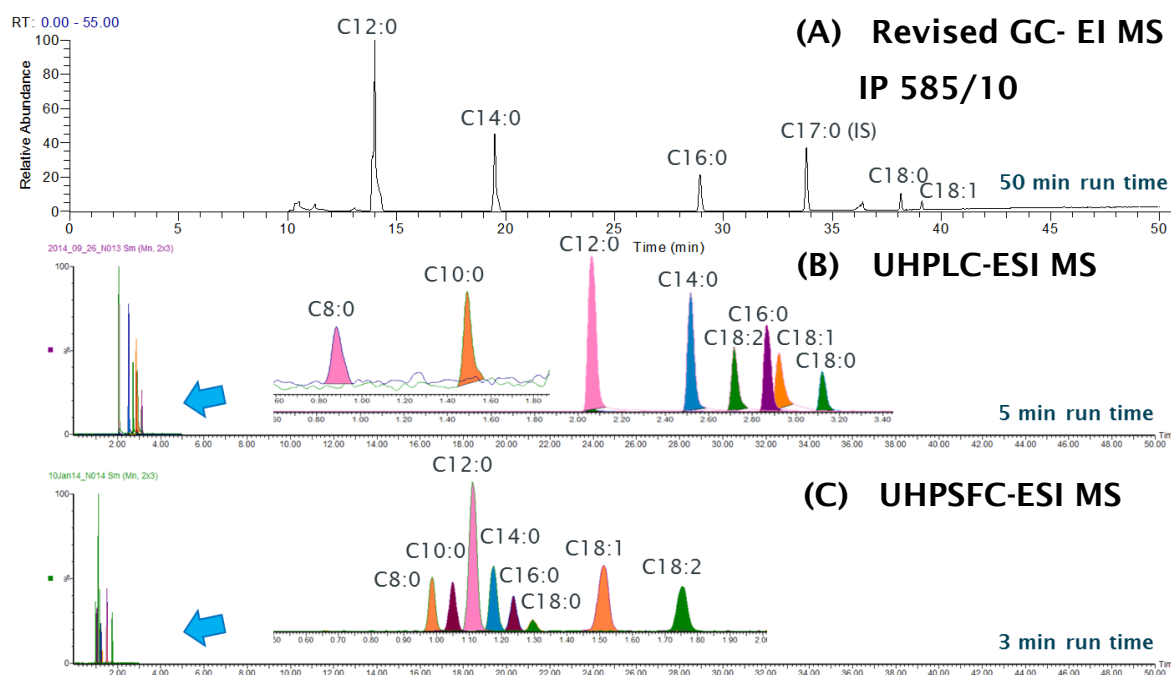
Figure 5-41 **Comparison of biodiesel FAME retention times (RICCs) for (A) the revised GC-EIMS, IP 585/10 method, (B) UHPLC-ESI MS, and (D) UHPSFC−ESI-MS. Reproduced by permission of American Chemistry Society.[185]**

232

Figure 5-42 shows the comparison of the revised GC-MS, UHPLC-MS, and UHPSFC-MS for C12:0 as a surrogate for 100 mg/kg of CME in aviation fuel A-2. UHPLC-MS and UHPSFC-MS also show an ultraviolet (UV) photodiode array (PDA) trace (210-400 nm).
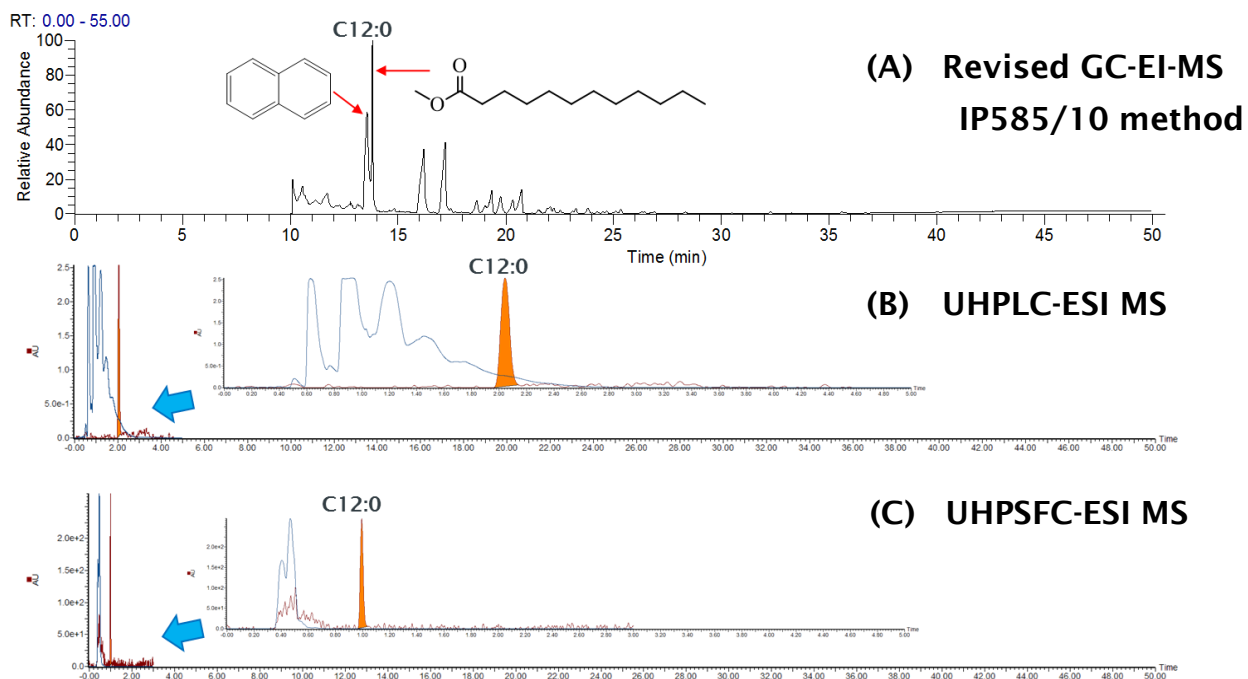
Figure 5-42 **Comparison of C12:0 surrogate CME 100 mg/kg in A-2. (A) the revised GC-EI MS, IP 585/10 method; (B) UHPLC-ESI MS; (D) UHPSFC-ESI-MS. Reproduced by permission of American Chemistry Society.[185]**

Chapter 5: Analysis of FAMEs in AVTUR

A comparison of each method for analysis of FAMEs in AVTUR is shown in Table 5-9.

Table 5-9   Comparison GC-EI/MS, UHPLC-ESI/MS, and UHPSFC-ESI/MS

Method	Analysis time (min)	LOD of total FAMEs (mg/kg)	Linear correlation (R^2)	Duty cycle (min)
GC-EI/MS (full scan)	50	0.10	> 0.99	95
UHPLC-ESI/MS (full scan)	5	0.10	> 0.99	6
UHPSFC-ESI/MS (full scan)	3	0.50	> 0.99	5.30

The developed UHPSFC-ESI-MS method allows sub 5 ppm detection of total FAMEs in hexane and also in AVTUR. It provides a linear dynamic range for the detection of total FAME content, 2-10 and 10-100 ppm, with good linear correlations ($R^2 > 0.99$). This method is approximately twenty times quicker than the existing GC-MS reference method and a revised GC-MS method that attempts to quantify the short chain methyl esters

UHPSFC-MS delivers a method that is free from the FAMEs/fuel matrix co-elution problems inherent with GC-MS and UHPLC-MS methods. Further $scCO_2$ is readily compatible with direct injection of jet fuel into the chromatographic eluent to deliver an effective method for separation and detection of low level FAMEs (sub 5 ppm) in AVTUR. Analysis of short chain FAMEs (C8-C14) with GC-MS is difficult due to them co-eluting with hydrocarbons in AVTUR.

5.8 Analysis of FAMEs in AVTUR using a miniature mass spectrometer (Microsaic system 4000 MiD)

Presently significant development has been on going in the area of miniaturisation of mass spectrometers in order to make transportable mass spectrometers. The Microsaic System was developed and commercialised at the Optical and Semiconductor Devices Group at Imperial College London since 2001.[199] The 4000 MiD is a design that brings together mass spectrometry and silicon micro-electrochemical systems (MEMS) engineering to transform chemical detection. The Microsaic 4000 MiD is a small in size detector system that uses micro-engineering and micro-electrospray ionisation. The 4000 MiD chip-based mass spectrometer was launched by Microsaic System at Pittcon 2013 in Philadelphia, PA, USA.[200]

The spraychip is a microspray device compared to traditional electrospray ion sources. Micro-electrospray ion sources increase ionisation efficiency because it uses lower flow rates, and lower voltages (0.7 and 1.5 kV)[201] are required to provide efficient electrospray. The vac-chip interface is used for transportation of ions from the micro-electrospray ion source into the vacuum system of the 4000 MiD. At the back of the vac-chip, there is a tube lens, an exit lens, an ion guide and an inter-quadrupole lens. Ions produced from the spraychip enter the vac-chip and are focused into the ionchip by using the ion optics. The ionchip is a micro-engineered quadrupole mass analyser based on Microsaic systems

plc patent technology. The functions of the ionchip is similar a conventional quadrupole mass analyser, acting as mass filter, separating ions according to mass-to-charge (*m/z*) ratios.

The vacuum system of miniaturised mass spectrometer consists of a vacuum chamber coupled to turbo molecular pumps, which are backed by small diagram pump. All vacuum pumps are combined within the 4000 MiD, there are no external pumps making it different from conventional mass spectrometers. The vacuum system includes of three main parts; the vac-chip interface, the ion guide chamber and the analytical chamber. The pressure in the chambers are monitored by using pirani gauges which also act as high-voltage interlocks. The system was controlled by Masscape software and all experiment runs using this built-in computer. MiDas™ is designed to connect the 4000 MiD® with a range of high concentration and high flow rate applications. MiDas™ incorporates a make-up pump which dispenses from an external reservoir which is filled with ESI compatible solvent. Here, methanol 0.1% formic acid was used as make-up solvent. MiDas™ automates sampling *via* the run sequence table. In this section, loop method has been produced. The composition of a fixed volume of solution injected into MiDas™ by using syringe port. The sample solution is driven into MiDas™ (Figure 5-43 (A)) by an external pump, where it is diluted and analysed automatically. Figure 5-43 (B) shows a schematic of direct sampling. MiDas™ has an integrated two position six port valves intended for direct injection of sample solution. When triggered the following sequence is initiated. The make-up, attenuator and acquisition are started automatically.

(A)   MiDas interface

(B)   A schematic of MiDas interface
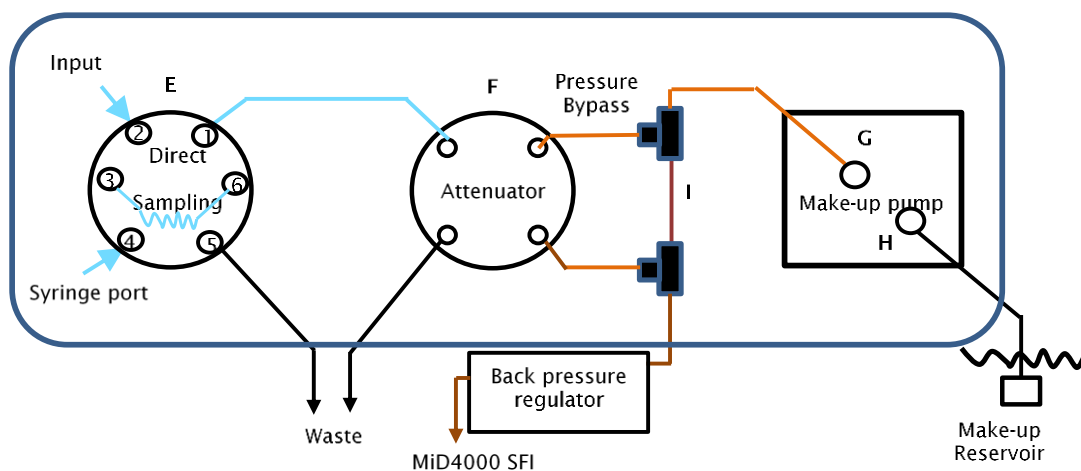
Figure 5-43   (A) MiDas interface module; (B) A schematic of MiDas interface.

A commercially doped sample of AVTUR, AF1 containing 150 mg/kg of FAME was directly injected to MiDas™ by setting desired attenuation to obtained final concentration of 4.5 and 6.0 mg/kg of FAMEs. Figure 5-44 shows the positive ion ESI mass spectra of 5 mg/kg FAMEs in methanol, 4.5 mg/kg and 6.0 mg/kg FAMEs in AVTUR.

(A)   5 mg/kg FAMEs in methanol
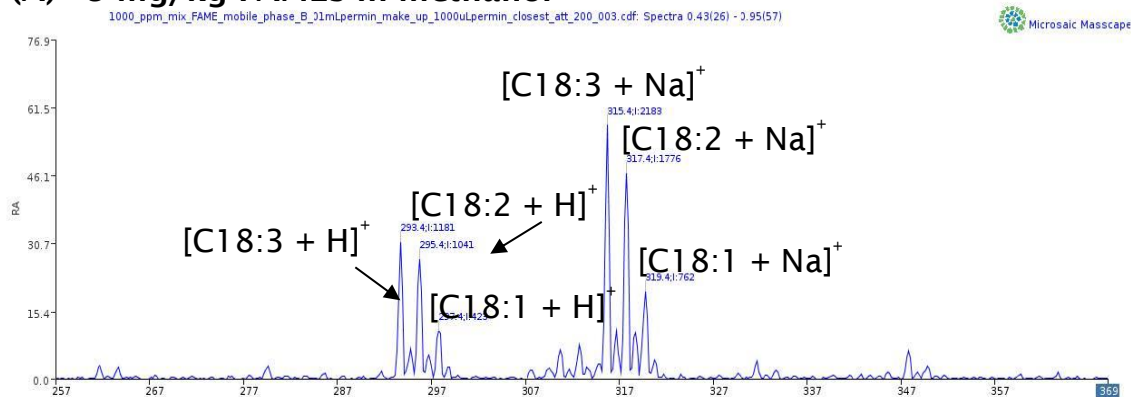
(B)   4.5 mg/kg FAMEs in AF1
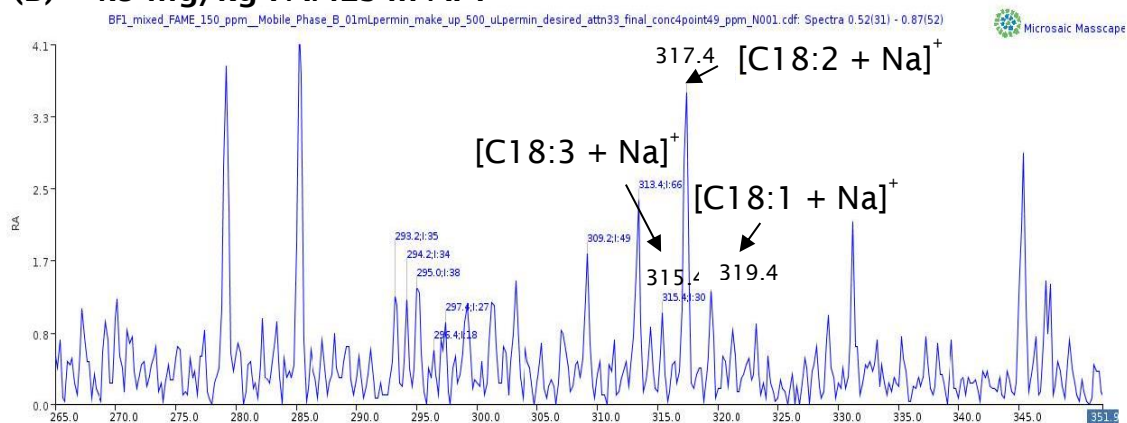
(C) 6 mg/kg FAMEs in AF1
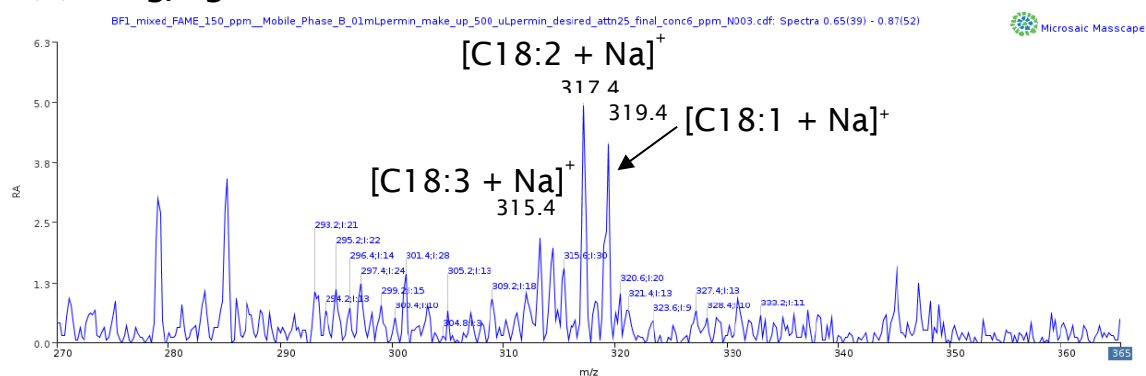
Figure 5-44   ESI mass spectra of (A) 5 mg/kg FAMEs in methanol; (B) 4.5 mg/kg FAMEs in AF1; (C) 6 mg/kg of FAMEs in AF1 analysed using direct from Microsaic 4000 MiD.

Direct dilution of the sample solution to 4000 MiD can qualitatively

detect FAMEs in AVTUR at 5 mg/kg. The method can be used as screening

test but it is not a suitable for a quantitative analysis because the S/N ratio

is below the limit of quantitative (LOQ). Due to natural background of high

end naphtha components present in a sample, the spraychip and vac-chip

parts are easy blocked. Then, a clean-up sample steps is required to

remove interference in the fuel matrix before injecting a sample into a

miniature mass spectrometer.

Hence, a chromatographic methods is required to separate FAMEs

from a complex mixture of hydrocarbons in AVTUR involves a complex

sample preparation procedure, such as to eliminate the interference of

some AVTUR components. This was achieved using a HPLC (Agilent 1100

series) coupled to the Microsaic 4000 MiD® (Figure 5-45) using a split flow

interface (SFI) with a 1:1000 split ratio.
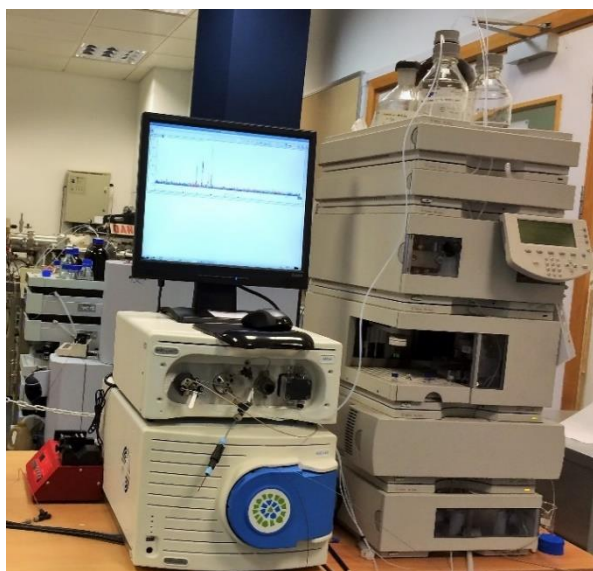
**Figure 5-45   HPLC-miniature mass spectrometer (Microsaic System
        4000 MiD).**

Chapter 5: Analysis of FAMEs in AVTUR

The developed HPLC conditions afforded detection of FAME in methanol at the 5 mg/kg level, (see Figure 5-46).
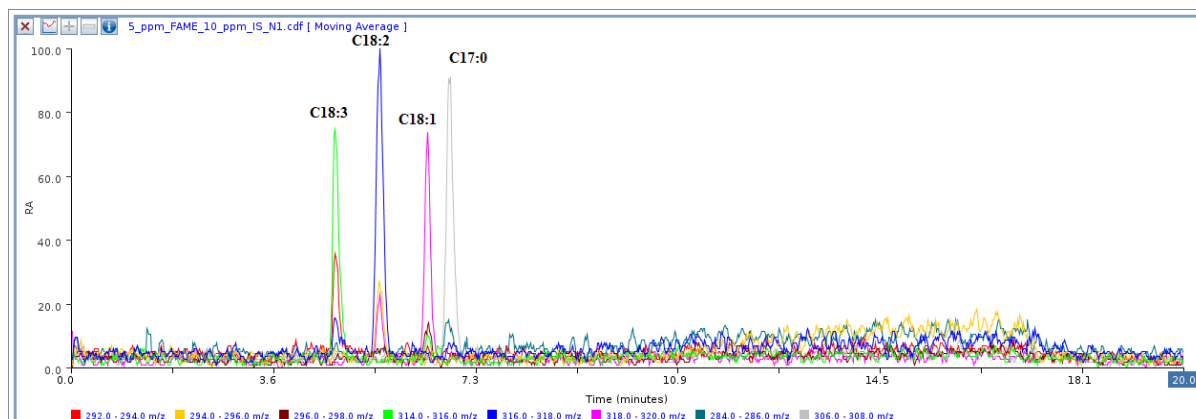
Figure 5-46   **RICCs *m/z* 319, 317, 315 of 5 mg/kg of standard FAMEs (C18:1, C18:2, and C18:3) in methanol analysed using HPLC-Microsaic 4000 MiD.**

5.9   Summary

The objective of this project is to quantify all of the RME (C16:0-C18:3) and the short-chain chain FAMEs (C8-C14), *e.g.* from coconut oil FAMEs in AVTUR at the 5 mg/kg (5 ppm, w/w) level. The aim was to develop methods including GC-MS, HPLC-MS, UHPLC-MS and UHPSFC-MS methods and to compare them to the existing reference GC-MS method for the determination of low-carbon-number FAMEs.

The summary of this chapter were the following as:

- Revision of IP/585 showed partial success and an improvement in qualitative detection and a positive move towards the quantitation of the short chain FAMEs in AVTUR.

- HPLC and UHPLC coupled to MS offer alternative orthogonal approaches for this analysis.

- The selective ionisation afforded by ESI affords ready detection of the FAMEs though the reversed-phase chromatography does not fully separate the FAME from the AVTUR, this would lead to matrix effect and ion suppression issue which would compromise any quantitative assay.

- UHPSFC-MS provides a solution where the FAMEs (CME and RME) are completely separated from the AVTUR whilst still delivering the benefits of the selective ionisation provided by the electrospray interface.

- Further $scCO_2$ is readily compatible with direct injection of the AVTUR with the analytical benefits of supercritical fluid chromatography delivering base-line resolved peaks for all the FAMEs of interest in 3 min.

- Direct dilution of the commercially doped sample of AVTUR to (Microsaic system 4000 MiD) can qualitatively detect FAMEs in AVTUR at 5 mg/kg. The method can be used as screening test but it is not a suitable for a quantitative analysis because the S/N ratio is below the limit of quantitative (LOQ).

- A miniature mass spectrometer coupled to HPLC afforded detection of FAME in methanol at the 5 mg/kg level but further work for the quantitative analysis of FAME in AVTUR will be required. This could not be undertake due to limited the available of Microsaic system 4000 MiD).

Chapter 6:   Conclusions and Future work

6.1   Conclusions

Biodiesel has been used as alternative energy because of the shortage of petroleum fuel resources. Biodiesel is a mixture of fatty acid methyl esters (FAMEs) having different molecular structures with varying chain lengths, and levels of unsaturation. It is generally recognised that the following chemical aspects can have an impact on the oxidation stability of biodiesel. The oxidation stability of biodiesel is lower than fossil fuel and is a significant problem for the use of biodiesel. The oxidation process changes the physical chemistry properties of the fuel, and also forms undesirable compounds. Oxidation products can be formed such as hydroperoxides are the primary products in auto-oxidation of unsaturated fatty acids. They can undergo further oxidation into a variety of volatile and non-volatile secondary products. The introduction of biodiesel into the fuel infrastructure has also given rise to unforeseen problems where these materials can cross-contaminate other fuel types. In the case of aviation turbine fuel (AVTUR) this is a significant issue since the international jet fuel specifications (DEF STAN 91-91) limit FAME content to less than 5 mg/kg (5 ppm w/w). The polar nature of the FAMEs means that they tend to adsorb onto the metal surfaces of pipelines or containers and these materials can then be released by the AVTUR from these shared common pipelines.

Chapter 6: Conclusions and Future work

Following of review literature, the issue of oxidation stability of biodiesel that is the one of the major issues for the use of biodiesel as an alternate fuel to petrodiesel and cross-contamination of biodiesel to AVTUR. Two main objectives of this project were researched.

The first objective was the investigation of the oxidation products of FAME occurring in the on-line EC-ESI MS and autoxidation conditions, and the use of GC–MS, HPLC–MS, UHPLC–MS, UHPSFC–MS, accurate mass measurement, FT-ICR MS to analyse and identify the oxidation product of FAMEs. (see, Chapter 4). The conclusions of this project were the following as:

- Electrochemical (EC) oxidation has been applied as a surrogate system for monitoring FAME oxidation. The oxidation species of oxidised RME and oxidised SME samples with *m/z* 377/379, *m/z* 391/393/395, *m/z* 407/409, *m/z* 423/425/427, *m/z* 437/439/441etc were observed in the EC cell.

- EC-MS been applied for screening method for the analysis of the antioxidant in gasoline samples. EC-MS has proved to be an excellent technique for monitoring of oxidation of FAME and antioxidant oxidation within 10 min.

- Hyphenation of chromatography and MS has also applied to the analysis auto-oxidised of rapeseed methyl ester (RME) and soybean methyl ester (SME). Gas chromatography-mass spectrometry (GC-MS) has provided information of volatile compounds such as 2,4-decadienal and methyl 9-oxo-nonanoate were observed in auto-oxidation of RME and SME samples.

- UHPSFC-MS, HPLC-MS, UHPLC-MS and UHPSFC-MS methods with the preferential ionisation property of positive-ion electrospray ionisation (ESI) has used for the presence of highly oxygenated oxidation products observed in RME and SME.

- UHPSFC-MS method developed can clearly separate oxidation products of FAMEs from parent molecules compared to HPLC-MS and UHPLC-MS.

- Accurate mass measurement using QTOF-MS and FT-ICR MS was a powerful tool for the determination of elemental formula of oxidation products in auto-oxidised FAMEs.

- The elemental formula for these auto-oxidised FAMEs were determined by UHPLC-Q-TOF MS and infusion FT-ICR MS. The presence of oxygenated species up to O (6 oxygen atoms) for the ion at m/z 411.1999 $[C_{19}H_{32}O_8 + Na]^+$ with a 2.6 ppm error was observed. It expected as the hydroperoxy bis-cyclic peroxides from auto-oxidised methyl linolenate. The structures shown (see, section 4.7) for the ion measured are postulated from literatures.

- On-line EC-ESI MS data show similarity with auto-oxidation, however, EC cell produced higher quantities of oxidation species than auto-oxidation. This method shows a great promise for accelerated oxidation studies but further work structural identify of these species will be required.

Chapter 6: Conclusions and Future work

The second objective was the development and optimisation of GC–MS, HPLC–MS, UHPLC–MS, UHPSFC–MS and a miniature MS couple to HPLPC as alternative approaches for analysis of FAMEs contamination in AVTUR (see, Chapter 5). The conclusions of this objective were the following as:

- Revision of IP/585 showed partial success and an improvement in qualitative detection and a positive move towards the quantitation of the short chain FAMEs (*e.g.* C8-C14) in AVTUR.

- The adaption of the new developed GC-MS method improved for the FAME separation. The fuel matrix also limits the application of this approach in relation to the detection and quantification of low-carbon-number fatty acid methyl esters (FAMEs), *e.g.* C8-C14 from coconut oil, a feedstock for FAME production in the Pacific Rim region.

- HPLC and UHPLC coupled to MS offer alternative orthogonal approaches for this analysis.

- A 3 min UHPSFC-MS method has been developed for the analysis of RME and CME. This is compared to the existing reference method and an adapted form of the 60 min reference GC-MS method for the detection of low-carbon-number FAMEs.

- UHPSFC-MS provides a solution where the FAMEs (CME and RME) are completely separated from the AVTUR whilst still delivering the benefits of the selective ionisation provided by the electrospray interface.

- Further scCO$_2$ is readily compatible with direct injection of the AVTUR with the analytical benefits of supercritical fluid chromatography delivering base-line resolved peaks for all the FAMEs of interest in 3 min.

- The selective ionisation afforded by ESI affords ready detection of the FAMEs though the reversed-phase chromatography does not fully separate the FAME from the AVTUR, this would lead to matrix effect and ion suppression issue which would compromise any quantitative assay.

- UHPSFC-MS method is approximately 20 times faster than the ASTM reference method, affords a comparable linear dynamic range for the detection of total FAME content up to 100 ppm with a linear correlation (R^2 > 0.99 for RME), and is more suitable for the detection and quantification of lower chain length methyl esters.

- Direct dilution of the commercially doped sample of AVTUR to (Microsaic system 4000 MiD) can qualitatively detect FAMEs in AVTUR at 5 mg/kg. The method can be used as screening test but it is not a suitable for a quantitative analysis because the S/N ratio is below the limit of quantitative (LOQ).

- A miniature MS coupled to HPLC afforded detection of FAME in methanol at the 5 mg/kg level but further work for the quantitative analysis of FAME in AVTUR will be required. This could not be undertake due to limited the available of Microsaic system 4000 MiD.

6.2   Future work

- Oxidation of fatty acid methyl ester (FAME) in the electrochemical cell in preparative mode and subsequent analysis of the products by HPLC-MS, UHPSFC-MS. Accurate mass measurement and MS/MS will be used for identification and elucidation of chemical structures of FAME oxidation products.

- The developed HPLC coupled with a miniature MS (Microsaic System 4000 MiD) method afforded detection of FAMEs in methanol at the 5 mg/kg level. Future work will apply this method to the analysis of commercially doped samples of aviation turbine fuel (AVTUR) with FAME.

Appendices

Appendix A: Flow diagram of EC-MS method for analysis of FAME oxidation used in Chapter 4

Oxidised FAMEs (RME and SME samples) in EC cell

EC cell
- Glassy carbon working electrode (0-2.5 V)
- Magic diamond working electrode (0-3.0 V)
- HyREF palladium-hydrogen (Pd/H_2) reference
- Titanium as an auxiliary electrode
- Flow rate of 10 µL/min

ESI-QTOF MS
- Positive ion
- Analysis time 10 min

The ions were observed
- *m/z* 331, 333 and 335 correspond to [FAME + (O) + Na]$^+$, estimated as epoxide-FAME or hydroxyl-FAME or keto-FAME
- *m/z* 347, 349, 351 correspond to [FAME + 2(O) + Na]$^+$, expected as hydroperoxides of FAMEs
- *m/z* 379 may correspond to bis-hydroperoxides

Appendix B: Flow diagram of UHPSFC-MS method for analysis of FAME oxidation used in Chapter 4

Autoxidised FAMEs (RME and SME samples)

Samples dissolved in methanol

UHPSFC - MS method

- BEH column (2.1 mm × 100 mm, 1.7 μm)

- Mobile phase A: $scCO_2$

- Mobile phase B: MeOH

- Gradient elution, see Table 3-3

- Column temp.: 45 °C

- $scCO_2$ pressure: 105 bar

- Positive ion ESI

Results

- The elution order:

  Non-oxidised FAMEs (C18:1, C18:2, C18:3), oxidised FAMEs

- m/z 335 [FAME + 1(O) + Na]$^+$, m/z 349 [FAME + 2(O) + Na]$^+$

- m/z 363 [FAME + 3(O) + Na]$^+$, m/z 379 [FAME + 4(O) + Na]$^+$

- More details see section 4.2
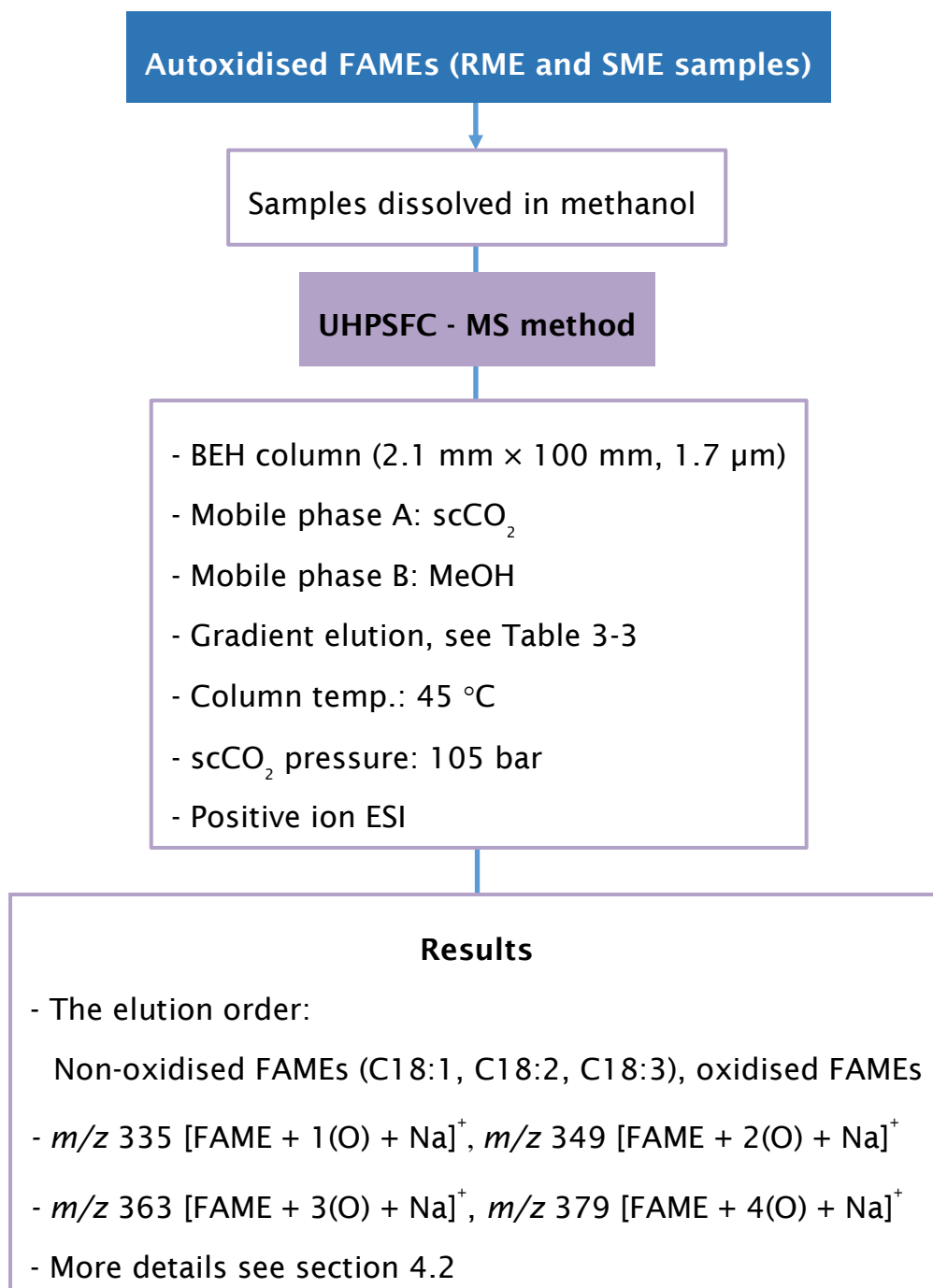
Appendix C: Flow diagram of HPLC–MS and UHPLC-MS methods for analysis of FAME oxidation used in Chapter 4

Autoxidised FAMEs (RME and SME samples)

Samples dissolved in methanol

HPLC-MS method

UHPLC-MS method

- Mobile phase A: water 0.1% formic acid (v/v)

- Mobile phase B: MeOH 0.1% formic acid (v/v)

- Column temp. 40 °C

- Positive ion ESI

- XBridge C18 column

  (2.1mm × 50 mm, 5 µm)

- Gradient elution, see Table 3-1

- Flow rate 0.5 mL/min

- BEH C18 column

  (2.1mm × 100 mm, 1.7 µm)

- Gradient elution, see Table 3-2

- Flow rate 0.6 mL/min

Results

- The elution order:

  Oxidised-FAMEs, non-oxidised FAMEs (C18:3, C18:2, C18:1)

- m/z 335 [FAME + 1(O) + Na]$^+$, m/z 349 [FAME + 2(O) + Na]$^+$

- m/z 365 [FAME + 3(O) + Na]$^+$, m/z 379 [FAME + 4(O) + Na]$^+$

UHPLC-HR MS

Formula of oxidation products from autoxidised FAMEs identified using UHPLC-HR MS, see Table 4-3

Appendix D: Flow diagram of FT-ICR MS method for analysis of FAME oxidation used in Chapter 4

Autoxidised FAMEs (RME and SME samples)

↓

Samples dissolved in methanol

↓

Infusion FT-ICR MS method

↓

- Positive ion ESI

↓

Results

- Formula of oxidation products from autoxidised FAMEs identified using FT-ICR MS,

  e.g. m/z 411.1999 $[C_{19}H_{32}O_8 + Na]^+$

- More details see section 4.5
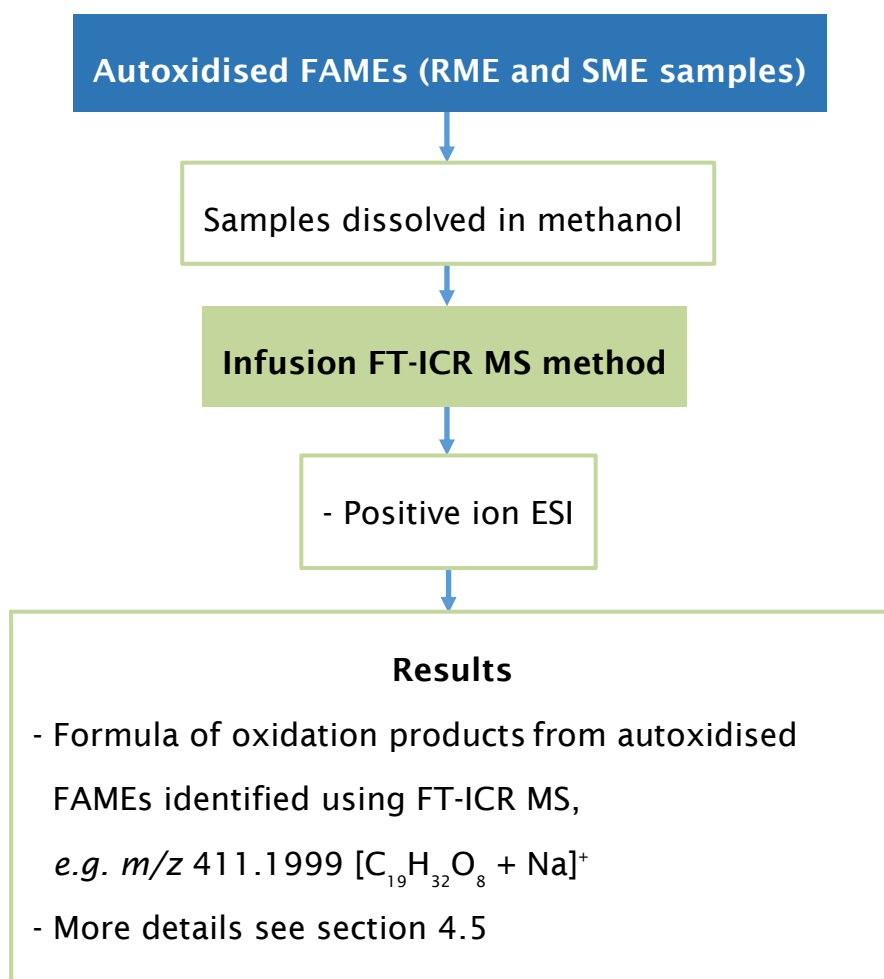
Appendix E: Flow diagram of GC-MS method for analysis of FAME oxidation used in Chapter 4

Autoxidised FAMEs (RME and SME samples)

↓

Samples dissolved in methanol

↓

GC - MS method

↓

- Innowax capillary column

  60 m × 0.25 mm i.d., 0.50 µm film thickness

- Ionisation: 70 eV EI

↓

Results

- Volatile oxidation products:

  2,4-decadienal and methyl 9-oxononanoate

- More details see section 4.7

Appendix F: Flow diagram of GC-MS method for analysis of FAME in AVTUR used in Chapter 5

Analysis of FAMEs (RME and CME samples) in AVTUR

Samples dissolved in n-dodecane

Revised IP585/10 GC - MS method

New GC – MS method

- Innowax capillary column

  60 m × 0.25 mm i.d., 0.50 µm film thickness

- Internal standard: Methyl heptadecanoate (C17:0)

  or methyl heptadecanoate (d_{33})

- Ionisation: 70 eV EI

- Oven temp.: 150 °C (5 min)

12 °C/ min to 200 °C (17 min)

3 °C/min to 252 °C (6.5 min)

- Flow rate 1.0 mL/min

- Analysis time 50 min

- Oven temp.: 130 °C (5 min)

2 °C/ min to 240 °C (5 min)

- Flow rate 1.0 mL/min

- Analysis time 65 min

Results

- Linearity 0 - 150 mg/kg, R^2 > 0.99

- More details see section 5.1.1 and 5.1.2

Appendix G: Flow diagram of HPLC-MS and UHPLC–MS methods for analysis of FAME in AVTUR used in Chapter 5
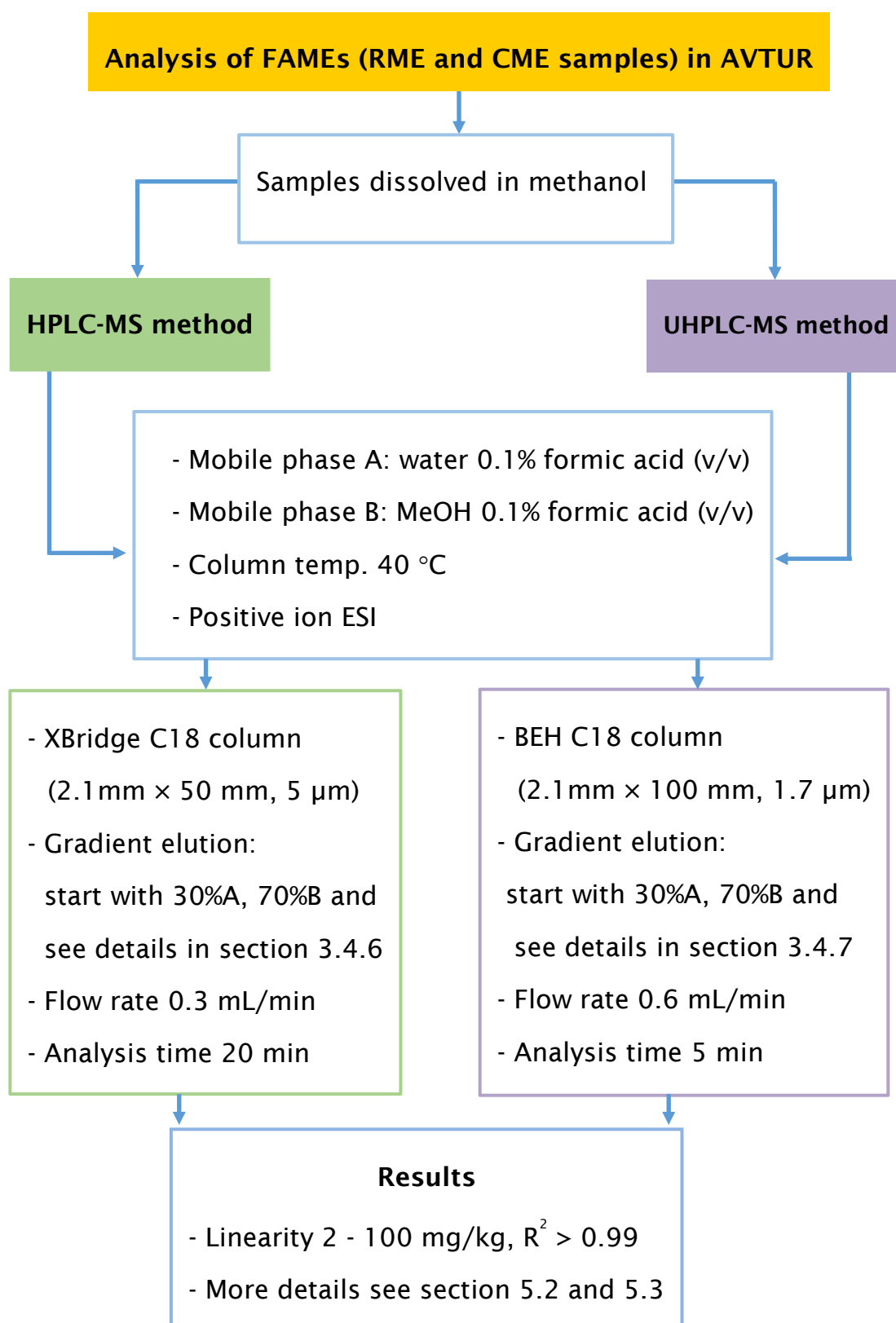
Appendix H: Flow diagram of UHPSFC-MS method for analysis of FAME in AVTUR used in Chapter 5
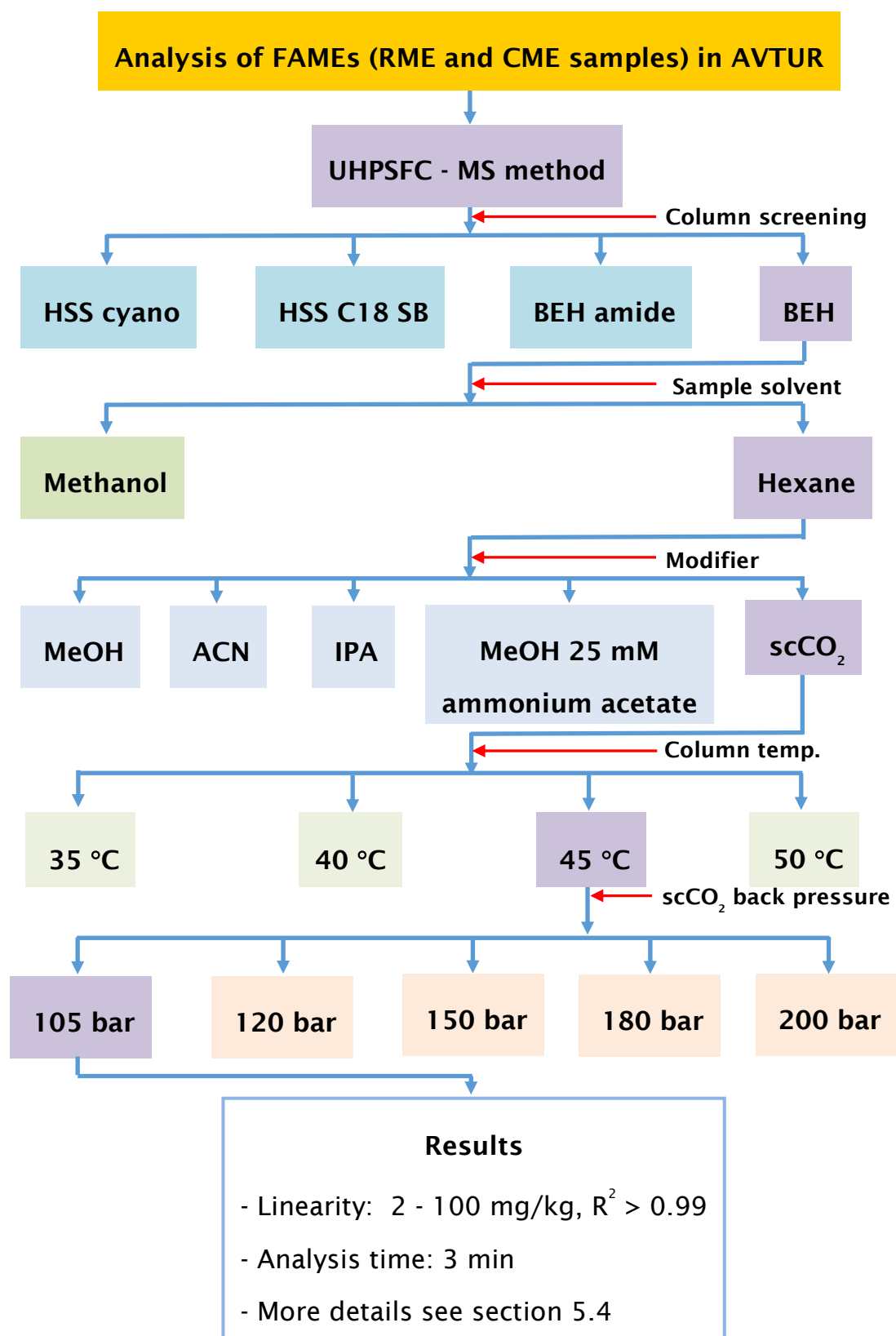
Appendix I: Flow diagram of a miniature mass spectrometer (Microsaic system 4000 MiD) for analysis of FAME in AVTUR used in Chapter 5
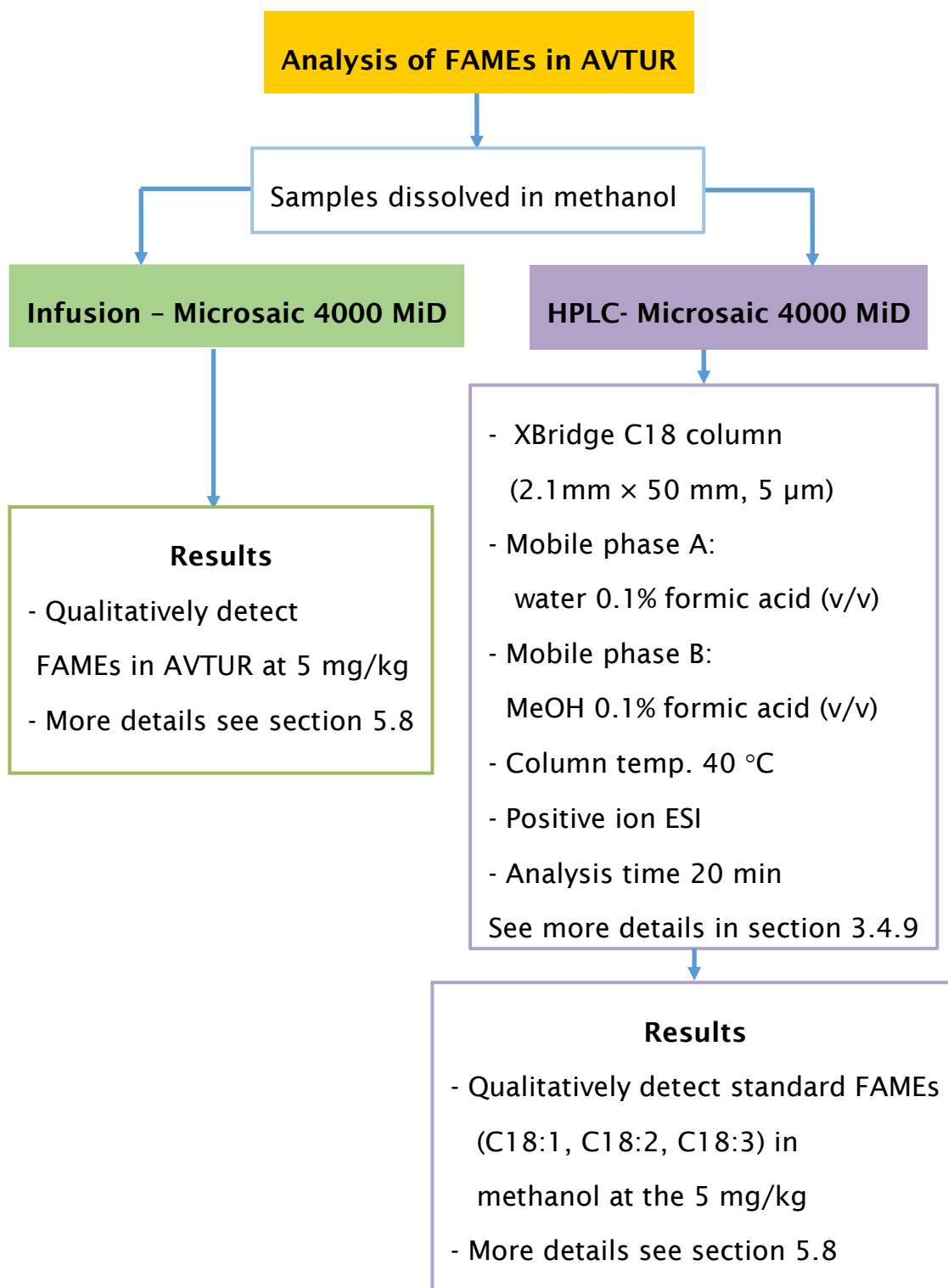
Appendix J: The work has been published

Evaluation of Ultrahigh Performance Supercritical Fluid Chromatography – Mass Spectrometry as an Alternative Approach for the Analysis of Fatty Acid Methyl Esters in Aviation Turbine Fuel. *Energy & Fuels* 2015, 29, 2485–2492, http://dx.doi.org/10.1021/acs.energyfuels.5b00103

Reproduced by permission of American Chemistry Society

Evaluation of Ultrahigh-Performance Supercritical Fluid Chromatography–Mass Spectrometry as an Alternative Approach for the Analysis of Fatty Acid Methyl Esters in Aviation Turbine Fuel

Waraporn Ratsameepakai,[†] Julie M. Herniman,[†] Tim J. Jenkins,[‡] and G. John Langley*,[†]

[†]Chemistry, Faculty of Natural and Environmental Sciences, University of Southampton, Highfield, Southampton SO17 1BJ, United Kingdom

[‡]Waters Corporation, Stamford Avenue, Wilmslow SK9 4AX, United Kingdom

ABSTRACT: The current international reference method (IP585/10) for the determination of rapeseed methyl ester (RME) in jet fuel [aviation turbine fuel (AVTUR), current specifications U.S. ASTM 1655 and DEF STAN 91-91] uses gas chromatography–mass spectrometry (GC–MS). The fuel matrix requirements demand that a slow temperature gradient method (50 min) must be used. The fuel matrix also limits the application of this approach in relation to the detection and quantification of low-carbon-number fatty acid methyl esters (FAMEs), e.g., coconut methyl ester (CME), C8–C14 from coconut oil, a feedstock for FAME production in the Pacific Rim region. A 3 min ultrahigh-performance supercritical fluid chromatography–mass spectrometry (UHPSFC–MS) method has been developed for the analysis of RME and CME. This is compared to the existing reference method and an adapted form of the reference GC–MS method for the detection of low-carbon-number FAMEs. The UHPSFC–MS method is approximately 20 times faster than the ASTM reference method, affords a comparable linear dynamic range for the detection of total FAME content up to 100 ppm with a linear correlation ($R^2 > 0.99$ for RME), and is more suitable for the detection and quantification of lower chain length methyl esters.

■ INTRODUCTION

Limitations of fossil fuel resources combined with environmental concerns have led to increased interest in sustainable or renewable energy resources, e.g., solar, wind, geothermal, and biofuels.[1] Biodiesel (fatty acid esters) has a similar chemical structure and energy content to petrodiesel in terms of the fuel quality.[2] First-generation biodiesel, e.g., fatty acid methyl esters (FAMEs), is produced by base-catalyzed transesterification of vegetable oils or animal fats with methanol. The feedstocks available for producing biodiesel are highly dependent upon the region, climate, soil condition, and geography. Rapeseed is the dominant feedstock for biodiesel production in Europe; soy is the dominant feedstock for biodiesel production in the United States of America; and palm oil is the dominant feedstock for biodiesel production in tropical countries, such as Malaysia and the Philippines.[1,3] Coconut is another feedstock used for biodiesel production in the Pacific Rim region.[4,5] The advantages of biodiesel compared to petrodiesel are renewability, higher cetane number, and higher combustion efficiency, and it is considered to be environmentally friendly.[6] Biodiesel is usually commercially blended with petrodiesel, e.g., EN590 in the U.K., where petrodiesel incorporates 5% biodiesel. However, a major problem related to the use of biodiesel is its inherent instability to oxidation.[7] Biodiesel degradation can change the fuel properties, such as formation of gum, acids, insolubles, and other oxidation products.

The introduction of biodiesel into the fuel infrastructure has also given rise to unforeseen problems, where these materials can cross contaminate other fuel types. In the case of aviation turbine fuel (AVTUR), this is a significant issue because the international jet fuel specifications (U.S. ASTM 1655 and DEF STAN 91-91) limit FAME content to less than 5 mg/kg (5 ppm, w/w).[8]

The polar nature of the FAMEs means that they tend to adsorb onto the metal surfaces of pipelines or containers, and these materials can then be released by the AVTUR from shared pipelines. The presence of FAME at high concentration in AVTUR or jet fuel can significantly impact the thermal stability of the fuel, resulting in coking, and can affect the freezing point of jet fuel, leading to gelling. To avoid such issues, the AVTUR must be B0, i.e., no biodiesel content, which is defined as less than 5 mg/kg (5 ppm).

IP585/10 is the current ASTM reference method for the determination of rapeseed methyl ester (RME) in jet fuel.[9] This gas chromatography–mass spectrometry (GC–MS) method stipulates the use of a 60 m Innowax GC capillary column and slow gradient to ensure separation of the FAME species (C16:0–C18:3) from the nonpolar hydrocarbon matrix of the jet fuel. The GC–MS analysis time is 50 min. However, this method cannot detect and quantify all of the short-chain FAMEs (C8–C14), e.g., from coconut oil (from FAME production in the Pacific Rim region), because of co-elution of these species with the fuel matrix. Comprehensive two-dimensional gas chromatography (GC × GC) has recently been developed for analysis of trace levels of FAME in petroleum-based fuel.[10] This method can be used for the identification and determination of the individual FAME components and total FAME content. Normal-phase high-performance liquid chromatography (NHPLC) has also been used for the determination of FAME in diesel.[11] However, while all of the FAME species eluted as a single peak in the chromatogram, this method can still

Appendix J
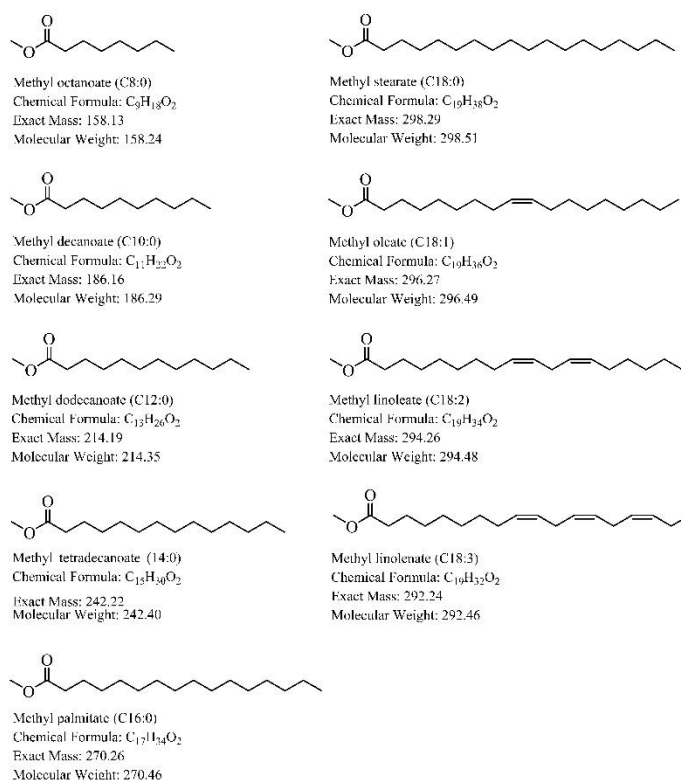
Figure 1. Structures, formulas, and relative molecular masses of selected FAMEs.

Methyl octanoate (C8:0)
Chemical Formula: $C_9H_{18}O_2$
Exact Mass: 158.13
Molecular Weight: 158.24

Methyl decanoate (C10:0)
Chemical Formula: $C_{11}H_{22}O_2$
Exact Mass: 186.16
Molecular Weight: 186.29

Methyl dodecanoate (C12:0)
Chemical Formula: $C_{13}H_{26}O_2$
Exact Mass: 214.19
Molecular Weight: 214.35

Methyl tetradecanoate (14:0)
Chemical Formula: $C_{15}H_{30}O_2$
Exact Mass: 242.22
Molecular Weight: 242.40

Methyl palmitate (C16:0)
Chemical Formula: $C_{17}H_{34}O_2$
Exact Mass: 270.26
Molecular Weight: 270.46

Methyl stearate (C18:0)
Chemical Formula: $C_{19}H_{38}O_2$
Exact Mass: 298.29
Molecular Weight: 298.51

Methyl oleate (C18:1)
Chemical Formula: $C_{19}H_{36}O_2$
Exact Mass: 296.27
Molecular Weight: 296.49

Methyl linoleate (C18:2)
Chemical Formula: $C_{19}H_{34}O_2$
Exact Mass: 294.26
Molecular Weight: 294.48

Methyl linolenate (C18:3)
Chemical Formula: $C_{19}H_{32}O_2$
Exact Mass: 292.24
Molecular Weight: 292.46

determine the total FAME content in diesel fuel faster than the GC–MS method.

Supercritical fluid chromatography (SFC) is a technique that can be considered as an intermediate between gas- and liquid-phase chromatography. At the region above the critical temperature and pressure, a substance cannot be classified as either a gas or a liquid because it has properties of both; therefore, it is termed a supercritical fluid.[12] It has a greater diffusion coefficient and lower viscosity and surface tension than a liquid solvent, which leads to a more favorable mass transfer. Supercritical fluid CO_2 (scCO$_2$) is the most widely used primary mobile phase in SFC because CO_2 has a low critical pressure (P_c of 73.8 bar) and critical temperature (T_c of 31.1 °C)[13–15] and is nontoxic, nonflammable, easy to handle, chemically inert, and inexpensive.[13,14] The hexane-like solvent properties of scCO$_2$ make this an ideal chromatography solvent choice for the direct injection of AVTUR compared to injecting the hydrocarbon fuel matrix directly into an aqueous/organic reversed-phase high-performance liquid chromatography (RP-HPLC) eluent. Ashraf-Khorassani et al. have recently discussed the application of ultrahigh-performance supercritical fluid chromatography–mass spectrometry (UHPSFC–MS) to be a superior analytical tool for both separation and detection of mono-, di-, and triacylglycerols as well as free glycerol itself in biodiesel.[16] Coupling the SFC to a mass spectrometer via an atmospheric pressure ionization source affords a highly sensitive and selective detector that is effective for compound identification and quantification. In the work presented here, the preferential ionization property of positive-ion electrospray ionization (ESI) was used. Here, the FAMEs preferentially ionize compared to the fuel matrix; the hydrocarbons are not ionized by this method because of the lack of suitable chemical functionality for ionization. The UHPSFC–ESI–MS method used here affords the sensitivity, the limit of detection (LOD), and limit of quantification (LOQ) required for RME and is comparable to that delivered by the international reference GC–MS method. Further, this capability is extended to coconut methyl ester (CME).

■ EXPERIMENTAL SECTION

Chemicals. Methanol, acetonitrile, isopropanol, and water [liquid chromatography–mass spectrometry (LC–MS) grade] and hexane (HPLC grade) were purchased from ThermoFisher Scientific (Loughborough, U.K.). Food-grade carbon dioxide was purchased from BOC Special Gases (Manchester, U.K.). Formic acid was purchased from Riedel-de Haën (Seelze, Germany). An internal
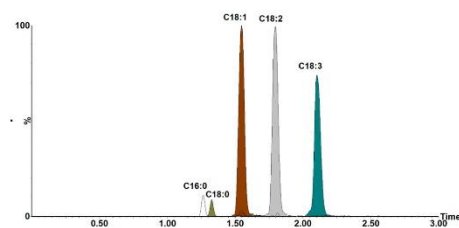
Figure 2. RICCs of FAME separation using 100% $scCO_2$ as the mobile phase.

standard, methyl heptadecanoate (C17:0), was purchased from Sigma—Aldrich (Gillingham, U.K.). RME and CME were supplied by BP (Pangbourne, U.K.). Aviation fuel was obtained from Air BP UK, Ltd. and the Energy Institute. The structures and respective relative molecular weights of the selected FAMEs are shown in Figure 1.

CME and RME Stock Solution Preparation. Preparation of the stock solutions followed the defined protocol of IP585/10.[9] Coconut and rapeseed FAME were used (covering a range of C8:0—C18:3). A total of 0.0100 ± 0.0001 g of CME and RME each was dissolved in hexane to give a total mass of 10 ± 0.05 g, i.e., standard solutions of 1000 mg/kg. These solutions were then diluted by a factor of 2 to give the nominal working solutions (500 mg/kg).

Calibration Solution Preparation. Calibration standards were prepared containing nominally 2, 4, 6, 8, 10, 20, 40, 60, 80, and 100 mg/kg of each FAME using volumetric dilution of the working solution (500 mg/kg) in hexane and included a 10 μL aliquot of an internal standard solution (1000 mg/L).

Internal Standard Solution Preparation. Methyl heptadecanoate, C17:0 (0.0100 ± 0.0001 g), was dissolved in hexane (10 mL) to give a 1000 mg/L solution.

Sample Preparation. AF-1 is a kerosene-grade aviation fuel, and this was used as a surrogate matrix for the standard solutions. A nominal 1000 mg/kg stock solution of CME and RME each was prepared by mixing each FAME (0.0100 ± 0.0005 g) with AF-1 to give a total mass of 10 ± 0.05 g. The samples were further diluted with AF-1 to give final solutions of 5 mg/kg of CME or RME. Commercially doped samples of AVTUR with FAME were supplied by the Energy Institute, and these samples were used neat and analyzed by UHPSFC—MS and GC—MS, respectively.

UHPSFC—MS. The chromatography was performed using an Acquity ultraperformance convergence chromatograph (UPC^2, Waters, Wilmslow, U.K.) with CO_2 as the supercritical fluid. Different sub-2 μm particle size, 3 × 100 mm packed columns (including BEH, HSS C18 SB, BEH-amide, and HSS cyano) were investigated with a variety of organic co-solvents (including methanol, acetonitrile, isopropanol, and methanol 25 mM ammonium acetate). The injection volume was 2 μL, and samples were eluted at a flow rate of 1.5 mL/min. The column temperature was optimized in the range of 35—50 °C. The $scCO_2$ back pressure of the system was optimized and set to 105 bar. Sodium formate (10 mM in methanol) was used as makeup flow (0.45 mL/min).

ESI—MS. Positive-ion ESI mass spectra were recorded using a single quadrupole mass spectrometer (SQD2, Waters, Wilmslow, U.K.) with the following conditions: capillary voltage, 3.6 kV; cone voltage, 30 V; extractor, 3.0 V; source temperature, 150 °C; desolvation temperature, 600 °C; desolvation gas flow, 1000 L/h; and acquisition and data processing achieved using MassLynx, version 4.1. Mass spectra were acquired between m/z 110 and 600 at a scan rate of 10 scans/s.

GC—MS. Electron ionization mass spectra (70 eV) were recorded using a TRACE GC—MS (Thermo Finnigan, Manchester, U.K.) equipped with an Innowax capillary column (J&W Scientific, Berkshire, U.K.), 60 m × 0.25 mm inner diameter, 0.50 μm film thickness, as demanded by IP585/10, the international reference method. Samples
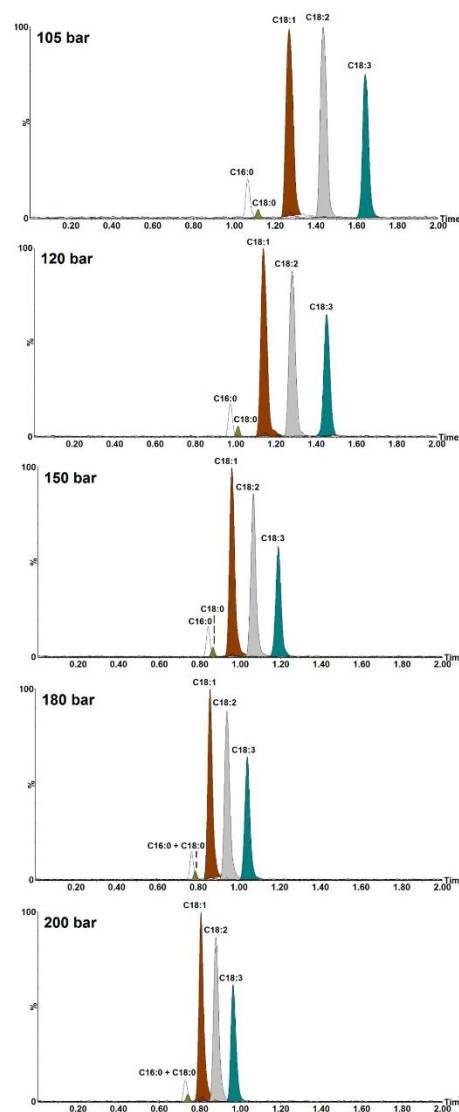
Figure 3. RICCs of FAME separation at different $scCO_2$ back pressures using 100% $scCO_2$ as the mobile phase at a flow rate of 1.5 mL/min.

(1 μL) were introduced via a splitless injector at a temperature of 260 °C. The oven temperature program used was 150 °C for 5 min, ramped at a rate of 12 °C/min to 200 °C for 17 min, then ramped at a rate of 3 °C/min to 252 °C, and held at the final temperature for 6.5 min. Helium was used as the carrier gas at a constant flow rate of 1 mL/min. Mass spectra were acquired between m/z 20 and 510 at a scan rate of 2 scans/s. Each FAME component was identified by comparison of the
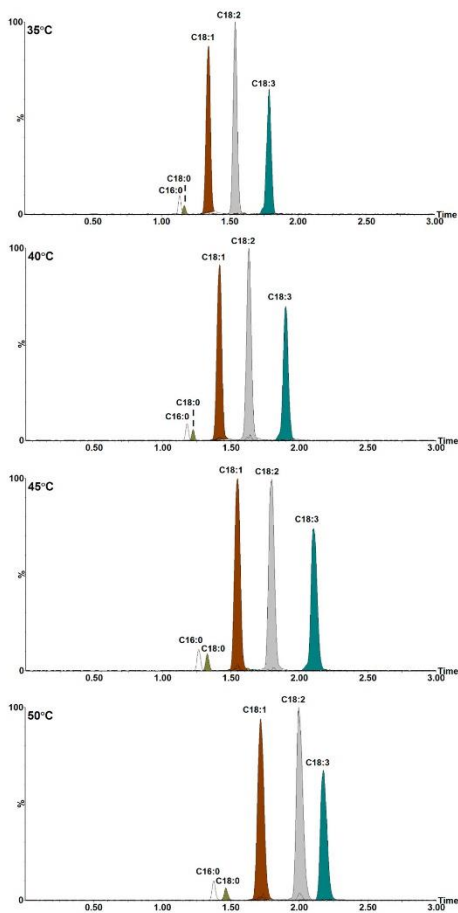
Figure 4. RICCs of FAMEs at different UHPSFC column temperatures at scCO$_2$ back pressure of 105 bar using 100% CO$_2$ as the mobile phase at a flow rate of 1.5 mL/min.

EI mass spectrum with a National Institute of Standards and Technology (NIST) Mass Spectral Library. Xcalibur, version 1.1, was used for control of the GC−MS and data acquisition.

■ RESULTS AND DISCUSSION

UHPSFC Optimization. Initial analyses, following a typical column and modifier screening protocol (5−40% modifier, 5 min), showed elution of the unresolved FAME mixture within 20 s. Iterations of lower percentage modifier gradient experiments initially identified the Acquity UPC² BEH, 3 × 100 mm, 1.7 μm particle size column (Waters, Wilmslow, U.K.) to be the column of choice with a 3 min method and 0−1% methanol modifier gradient. Further optimization of the method afforded an isocratic method without the need of the polar modifier, i.e.,

Table 1. Results of Resolution (R_s),[a] Peak Asymmetry (A_s), and Peak Width at Half Height ($w_{0.5}$) Obtained at Different Column Temperatures

	column temperature											
	35 °C			40 °C			45 °C			50 °C		
FAME component	R_s	A_s	$w_{0.5}$	R_s	A_s	$w_{0.5}$	R_s	A_s	$w_{0.5}$	R_s	A_s	$w_{0.5}$
C16:0	0.81[b] (0.14)	1.11 (0.52)	0.02 (0.00)	1.01[b] (0.15)	1.26 (0.53)	0.03 (0.00)	1.31[b] (0.14)	0.97 (0.37)	0.03 (0.00)	1.69[b] (0.17)	0.89 (0.03)	0.03 (0.00)
C18:0	3.31[c] (0.12)	0.98 (0.24)	0.02 (0.00)	3.43[c] (0.24)	1.12 (0.45)	0.03 (0.00)	3.26[c] (0.17)	0.95 (0.04)	0.03 (0.00)	3.46[c] (0.12)	1.30 (0.47)	0.03 (0.00)
C18:1	3.23[d] (0.04)	1.13 (0.21)	0.04 (0.00)	3.10[d] (0.08)	1.22 (0.53)	0.04 (0.00)	3.09[d] (0.18)	1.07 (0.29)	0.04 (0.00)	3.07[d] (0.07)	1.02 (0.08)	0.04 (0.00)
C18:2	3.93[e] (0.10)	1.12 (0.07)	0.04 (0.00)	3.75[e] (0.13)	1.15 (0.17)	0.04 (0.00)	3.84[e] (0.14)	1.34 (0.45)	0.04 (0.00)	1.98[e] (0.00)	1.26 (0.17)	0.05 (0.00)
C18:3		0.96 (0.14)	0.04 (0.00)		0.96 (0.22)	0.04 (0.01)		1.45 (0.35)	0.04 (0.01)		1.28 (0.17)	0.05 (0.00)

[a]The values of resolution (R_s) were calculated from two peaks of interest. The resolution was calculated using the half-height method.[19−21] [b]First pair of peaks, C16:0 and C18:0. [c]Second pair of peaks, C18:0 and C18:1. [d]Third pair of peaks, C18:1 and C18:2. [e]Fourth pair of peaks, C18:2 and C18:3.
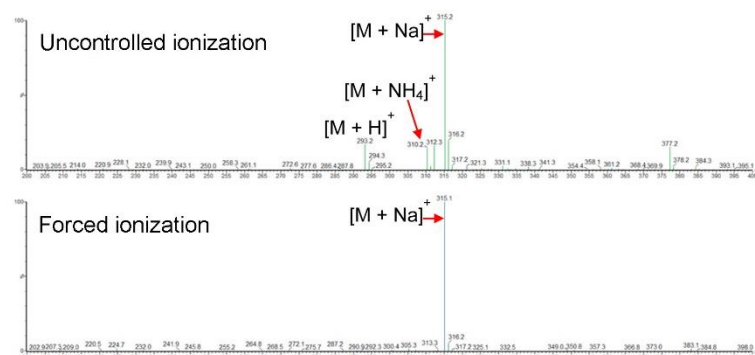
Figure 5. Comparison of uncontrolled and forced ESI of C18:3.

100% scCO$_2$, and all subsequent analyses were undertaken using these conditions (see Figure 2).

The influence of CO$_2$ back pressure (105–200 bar) on the isocratic elution method (100% CO$_2$) was investigated (see Figure 3).

From these experiments, 105 bar was selected as the optimum scCO$_2$ pressure, affording the best baseline separation of all species, and, subsequently, was shown to give retention of the FAMEs away from the fuel matrix.

The UHPSFC column temperature was then optimized over the range of 35–50 °C. The effect of the column temperature on FAME separation is presented in Figure 4, showing an increase in retention with increasing the column temperature (35–50 °C).

For SFC, retention times increase with higher column temperatures because the density of supercritical fluid decreases as the column temperature increases; hence, the diffusion rates increase.[17,18] This is in contrast to HPLC, where an increase in the column temperature will cause a decrease in the retention time. An UHPSFC column temperature of 45 °C was selected and used for all subsequent FAME separations. At a column temperature of 50 °C, C16:0 and C18:0 are better resolved, while the resolution of C18:2 and C18:3 is degraded; e.g., a broader peak profile for the C18:3 FAME was observed (see Table 1).

LOD. The LOD can be calculated using several analytical methods, such as the signal-to-noise ratio (S/N), the standard deviation of the blank, and the calibration plot at low concentrations.[22,23] Here, the LOD was calculated using the S/N method (S/N ≥ 3:1). Detection limits of the reconstructed ion current chromatograms (RICCs) for the sodiated molecules [M + Na]$^+$ were calculated, e.g., C18:1 (0.25 mg/kg), C18:2 (0.50 mg/kg), and C18:3 (0.10 mg/kg).

The addition of sodium formate is crucial because this forces one ionization event, i.e., produces only the sodiated molecule. Without the addition of the sodium ions, then an uncontrolled mixture of protonated molecules, ammoniated molecules, sodiated molecules, and potassiated molecules can be produced (see Figure 5). Sensitivity, repeatability, and quantitation are improved through the production of one ionized species. Thus, enabling this UHPSFC–ESI–MS method to deliver LODs sufficient to detect trace FAMEs in standard solutions (hexane).

Linear Dynamic Range. The linear dynamic range of this UHPSFC–ESI–MS method was determined by analysis of hexane solutions of standard FAME species (0.0–100 mg/kg), as
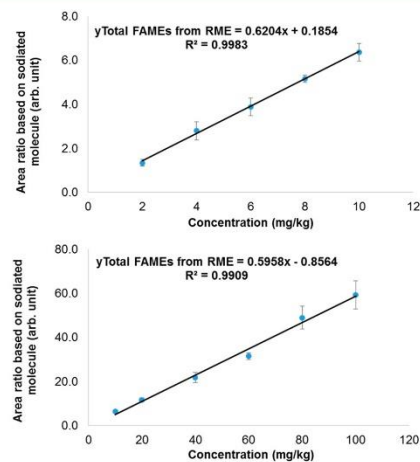
Figure 6. Calibration curves of total FAMEs for RME from the summed RICCs of the sodiated molecules. Number of replicate measurements = 3.

described in the Experimental Section, following the protocol defined by the international reference method IP585/10. A total of 10 ppm of methyl heptadecanoate (C17:0) was used as the internal standard. Peak areas, relative to the internal standard, of the RICCs of the sodiated molecules [M + Na]$^-$ of each FAME species C18:1 (m/z 319), C18:2 (m/z 317), and C18:3 (m/z 315) were plotted versus the FAME concentration. Figure 6 presents calibration curves of total FAMEs for 2–10 mg/kg (R^2 = 0.9983) and 10–100 mg/kg (R^2 = 0.9909). The linear regressions compare favorably to the stipulated value for FAME in AVTUR, IP585/10 (R^2 = 0.9850).[9]

These calibration curves were then used to calculate the levels of FAME in spiked AVTUR samples compared to the expected values for FAME-spiked AVTUR samples.

IP585/10 was originally designed to detect and quantify RME in AVTUR at the 5 ppm level. Figure 7 shows the elution and retention of RME and CME using this method. The introduction
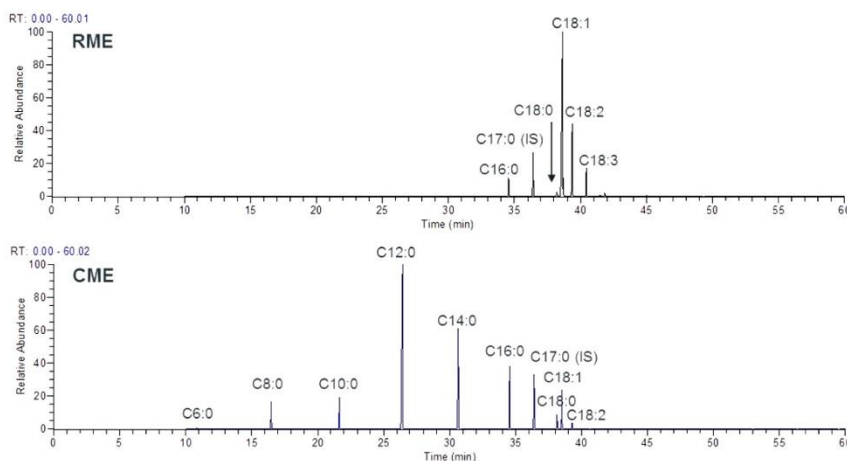
Figure 7. GC−MS of RME and CME. Column: HP Innowax capillary column, 30 m × 0.25 mm inner diameter, 0.25 μm film thickness. Oven temperature: initial temperature of 40 °C, hold for 4 min, ramp at 5 °C/min until 240 °C, and hold for 16 min.

of CME into the fuel chain requires a review of IP585/10 because the shorter chain methyl esters elute in the same chromatographic space as the fuel matrix, before a retention time of 20 min (see Figure 8). Adaptation of this GC−MS method allows for
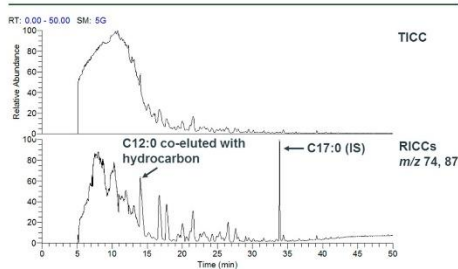
Figure 8. Comparison of (A) total ion current chromatogram (TICC) and (B) RICC m/z 74 and 87 of 5 mg/kg of CME in AF-1 analyzed using GC−MS.

certain CME species (C12:0 and C14:0) to be qualitatively identified, although the quantitation at a low level is still compromised by the co-elution with the hydrocarbon species (fuel matrix). Further, the lighter FAME components (e.g., C8:0 and C10:0) are indistinguishable from the fuel matrix background. While not ideal, this adapted GC−MS method does allow for quantitation of the larger coconut FAMEs (C12:0 and C14:0) at higher levels, from which the total FAME content can then be estimated.

While certain CME species (C12:0 and C14:0) can be qualitatively identified, the quantitation is compromised at low levels by the co-elution with the hydrocarbon species. Further, the lighter FAME (e.g., C8:0 and C10:0) components are indistinguishable from the matrix background (see Figure 8).

Figure 9 compares the GC−MS and UHPSFC−MS chromatograms and also includes UHPLC−MS for the standard FAME mixtures. While UHPLC−MS can be used for the analysis of these species, the fuel samples are less compatible to the reversed-phase solvents and the fuel matrix co-elutes with some of the FAMEs (data not shown).

This UHPSFC−MS method for detection of FAME in AVTUR is more amenable to the analysis of lower chain length methyl esters when compared to an adapted GC−MS method for the inclusion of CME in AVTUR. The adapted GC−MS method has a total duty cycle time (including pre-run, equilibrium, analysis, and cooling time) of 95 min, whereas the UHPSFC−MS method has the equivalent duty cycle of 5.30 min, with both methods giving good correlation for a 5 ppm spiked AVTUR sample of 5.2 and 5.8 ppm, respectively.

Figure 10 shows that co-elution of the CME species with AVTUR is not an issue when using the positive-ion ESI UHPSFC−MS method because the hydrocarbon species are not ionized. In contrast, the C12:0 FAME can be readily identified and quantified.

■ **CONCLUSION**

UHPSFC−MS delivers a robust and quantitative assay for the detection of FAME, affording a linear dynamic range comparable to that of the international GC−MS reference method (IP585/10) for total FAME content in AVTUR, with an excellent linear correlation (R^2 > 0.99 for RME). Further, the UHPSFC−MS method is readily compatible with injection of neat AVTUR, is 17 times faster than the GC−MS method (duty cycle), and is fully compatible with the analysis of short-chain FAMEs, e.g., CME, where these species do not co-elute with the aviation fuel matrix, as seen with IP585/10, the revised version, and UHPLC−MS. Further, quantitative analysis can be achieved at the required 5 ppm level from selected-ion recording (SIR) and scan data (RICCs), with the caveat of the scan data being recorded with sufficient data points (e.g., >15) across the chromatographic peak. The advantage of the use of scan data is

2490

Article
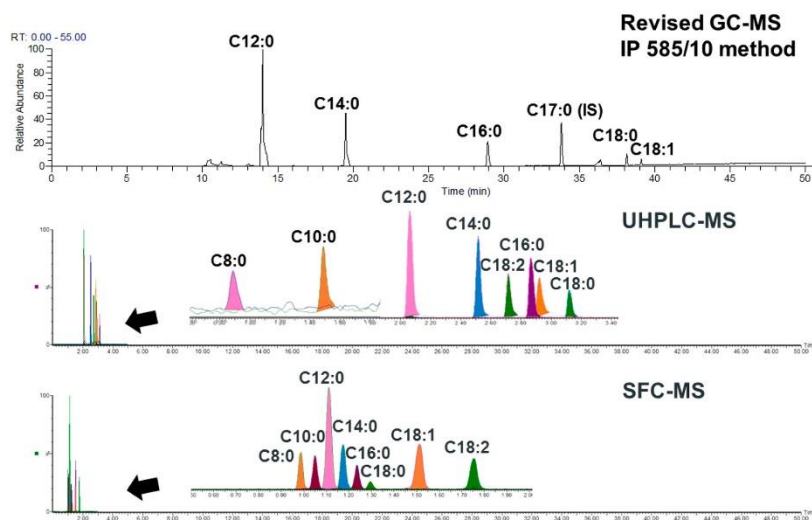
Figure 9. Comparison of biodiesel FAME retention times (RICCs) for GC−MS, UHPLC−MS, and UHPSFC−MS.
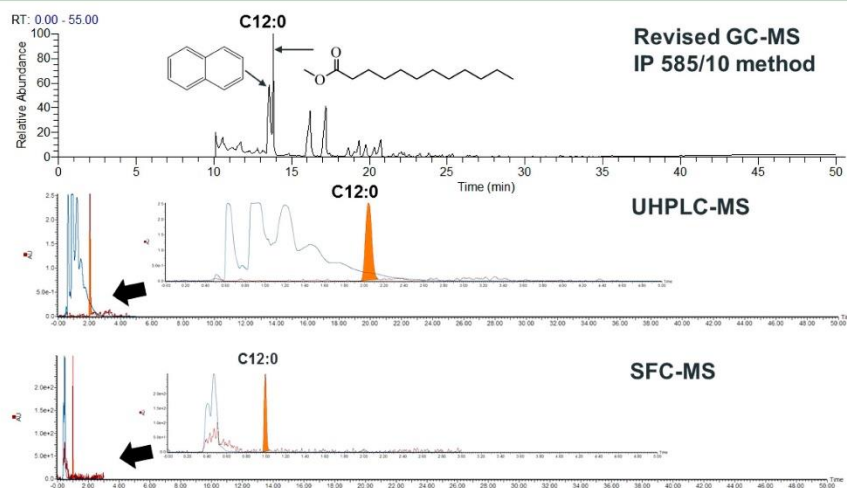
Figure 10. Comparison of revised GC−MS, UHPLC−MS, and UHPSFC−MS for C12:0 as a surrogate for 100 mg/kg of CME in aviation fuel A-2. UHPLC−MS and UHPSFC−MS also show an ultraviolet (UV) photodiode array (PDA) trace (210−400 nm).

that this allows for the observation of new FAME species to be probed through re-interrogation of the scan data and use of appropriate RICCs.

■ **AUTHOR INFORMATION**

Corresponding Author
*Telephone: +44-0-2380-592182. E-mail: g.j.langley@southampton.ac.uk.

Notes
The authors declare no competing financial interest.

■ REFERENCES

(1) Atabani, A. E.; Silitonga, A. S.; Badruddin, I. A.; Mahlia, T. M. I.; Masjuki, H. H.; Mekhilef, S. A comprehensive review on biodiesel as an alternative energy resource and its characteristics. *Renewable Sustainable Energy Rev.* **2012**, *16*, 2070−2093.

(2) Dwivedi, G.; Jain, S.; Sharma, M. P. Impact analysis of biodiesel on engine performance—A review. *Renewable Sustainable Energy Rev.* **2011**, *15*, 4633−4641.

(3) Issariyakul, T.; Dalai, A. K. Biodiesel from vegetable oils. *Renewable Sustainable Energy Rev.* **2014**, *31*, 446−471.

(4) Nakpong, P.; Wootthikanokkhan, S. High free fatty acid coconut oil as a potential feedstock for biodiesel production in Thailand. *Renewable Energy* **2010**, *35* (8), 1682−1687.

(5) Cloin, J. *Liquid Biofuels in Pacific Island Countries*; Pacific Islands Applied Geoscience Commission (SOPAC): Suva, Fiji, 2007; SOPAC Miscellaneous Report 628.

(6) Balat, M. Potential alternatives to edible oils for biodiesel production—A review of current work. *Energy Convers. Manage.* **2011**, *52*, 1479−1492.

(7) Pullen, J.; Saeed, K. An overview of biodiesel oxidation stability. *Renewable Sustainable Energy Rev.* **2012**, *16*, 5924−5950.

(8) Joint Inspection Group (JIG). *Aviation Fuel Quality Requirements for Jointly Operated Systems (AFQRJOS)*; JIG: London, U.K., Feb 2013, Bulletin 60.

(9) Institute of Petroleum (IP). *IP585/10, Determination of Fatty Acid Methyl Esters (FAME), Derived from Biodiesel Fuel, in Aviation Turbine Fuel GC−MS with Selective Ion Monitoring/Scan Detection Method*; IP: London, U.K., 2010; pp 585.1−585.10.

(10) Seeley, J. V.; Bates, C. T.; McCurry, J. D.; Seeley, S. K. Stationary phase selection and comprehensive two-dimensional gas chromatographic analysis of trace biodiesel in petroleum-based fuel. *J. Chromatogr. A* **2012**, *1226*, 103−109.

(11) Kamiński, M.; Gilgenast, E.; Przyjazny, A.; Romanik, G. Procedure for and results of simultaneous determination of aromatic hydrocarbons and fatty acid methyl esters in diesel fuels by high performance liquid chromatography. *J. Chromatogr. A* **2006**, *1122*, 153−160.

(12) Smith, R. M. Supercritical fluids in separation science—The dreams, the reality and the future. *J. Chromatogr. A* **1999**, *856*, 83−115.

(13) Ibañez, E.; Señoráns, F. J. Tuning of mobile and stationary phase polarity for the separation of polar compounds by SFC. *J. Biochem. Biophys. Methods* **2000**, *43*, 25−43.

(14) Saito, M. History of supercritical fluid chromatography: Instrumental development. *J. Biosci. Bioeng.* **2013**, *115*, 590−599.

(15) Li, F.; Hsieh, Y. Supercritical fluid chromatography−mass spectrometry for chemical analysis. *J. Sep. Sci.* **2008**, *31*, 1231−1237.

(16) Ashraf-Khorassani, M.; Yang, J.; Rainville, P.; Jones, M. D.; Fountain, K. J.; Isaac, G.; Taylor, L. T. Ultrahigh performance supercritical fluid chromatography of lipophilic compounds with application to synthetic and commercial biodiesel. *J. Chromatogr. B: Anal. Technol. Biomed. Life Sci.* **2015**, *983−984*, 94−100.

(17) West, C.; Bouet, A.; Routier, S.; Lesellier, E. Effects of mobile phase composition and temperature on the supercritical fluid chromatography enantioseparation of chiral fluoro-oxoindole-type compounds with chlorinated polysaccharide stationary phases. *J. Chromatogr. A* **2012**, *1269*, 325−335.

(18) Nováková, L.; Chocholouš, P.; Solich, P. Ultra-fast separation of estrogen steroids using subcritical fluid chromatography on sub-2-micron particles. *Talanta* **2014**, *121*, 178−186.

(19) Biba, M.; Regalado, E. L.; Wu, N.; Welch, C. J. Effect of particle size on the speed and resolution of chiral separations using supercritical fluid chromatography. *J. Chromatogr. A* **2014**, *1363*, 250−256.

(20) Dolan, J. W. Peak tailing and resolution. *LC·GC Eur.* **2002**, *15*, 334−337.

(21) Kawabe, T.; Tomitsuka, T.; Kajiro, T.; Kishi, N.; Toyo'oka, T. Ternary isocratic mobile phase optimization utilizing resolution Design Space based on retention time and peak width modeling. *J. Chromatogr. A* **2013**, *1273*, 95−104.

(22) Shrivastava, A.; Gupta, V. Methods for the determination of limit of detection and limit of quantitation of the analytical methods. *Chron. Young Sci.* **2011**, *2*, 21.

(23) Ribani, M.; Collins, C. H.; Bottoli, C. B. G. Validation of chromatographic methods: Evaluation of detection and quantification limits in the determination of impurities in omeprazole. *J. Chromatogr. A* **2007**, *115*, 201−205.

Appendix K: Conferences and seminar attended

1. Warwick Mass Spectrometry 80/60 Conference, Warwick, UK. 10th -
    11th December 2012. Poster presentation: "Hyphenation of On-line EC-
    ESI-TOF-MS".

2. The 34th British Mass Spectrometry Society (BMSS) Annual Meeting,
    Eastbourne, UK. 9th - 11th September 2013. Poster presentation:
    "Hyphenation of on-line EC/ESI-Q-TOF/MS for the Generation and
    Identification of FAME Oxidation Products".

3. 13th International Symposium on Hyphenated Techniques in
    Chromatography and Separation Technology (HTC-13), Bruges,
    Belgium. 29th-3st January 2014. Poster presentation: "Ultra Performance
    Convergence Chromatography-Electrospray Ionisation/Mass
    Spectrometry (UPC2-ESI/MS) for Analysis of Trace Fatty Acid Methyl
    Esters (FAMEs) in Aviation Fuels".

4. Meeting the Petrochemical Challenge with Separation Science and
    Mass Spectrometry, Burlington House, London, UK. 14th November
    2014. Oral presentation: "Fatty Acid Methyl Esters (FAMEs) Issues and
    Hyphenated Mass Spectrometry Solutions".

5. 63rd American Society for Mass Spectrometry (ASMS) Conference on
    Mass Spectrometry and Allied Topics. America's Centre, St. Louis,
    Missouri, USA. 31st May - 4th June 2015. Poster presentation: "Analysis
    of biodiesel contamination in jet fuel using supercritical fluid
    chromatography-electrospray ionisation mass spectrometry (SFC-ESI-
    MS)".

Appendix L: Certification
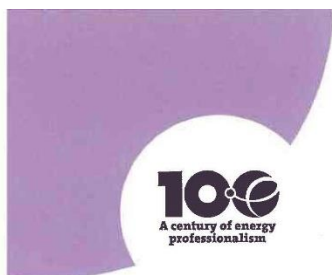
Certificate of Appreciation

awarded to

Waraporn Ratsameepakai

in recognition of her significant contribution to EI technical activities on test method development.

Waraporn has produced an updated version of the IP585/10 GC-MS FAME in Jet Fuel reference test method to address the introduction of short chain methyl esters into the fuel supply chain. She has also developed SFC – MS and UHPLC – MS methods for analysis of FAME in Jet Fuel (Energy & Fuels, submitted Jan 2013). In all cases the Energy Institute has been mentioned in the publications, and the recognition of her contribution will enhance the Energy Institute's profile in Thailand on her return.

Chairman of the Scientific and Technical Advisory Committee

Chief Executive Energy Institute

Issued by:
Energy Institute, 61 New Cavendish Street London W1G 7AR, UK.
Incorporated by Royal Charter 2003.
Registered Charity Number 1097899.
Licensed by the Engineering Council to register engineers and technicians.
Licensed by the Science Council to register chartered scientists.
Licensed by the Society for the Environment to register chartered environmentalists.

www.energyinst.org

References

[1]   N. N. A. N. Yusuf, S. K. Kamarudin, Z. Yaakub. Overview on the current trends in biodiesel production. *Energy Convers. Manag.* **2011**, *52*, 2741.

[2]   G. Knothe. Biodiesel and renewable diesel: A comparison. *Prog. Energy Combust. Sci.* **2010**, *36*, 364.

[3]   S. S. Sidibé, J. Blin, G. Vaitilingom, Y. Azoumah. Use of crude filtered vegetable oil as a fuel in diesel engines state of the art: Literature review. *Renew. Sustain. Energy Rev.* **2010**, *14*, 2748.

[4]   L. Lin, Z. Cunshan, S. Vittayapadung, S. Xiangqian, D. Mingdong. Opportunities and challenges for biodiesel fuel. *Appl. Energy* **2011**, *88*, 1020.

[5]   M. Kumar, M. P. Sharma. Assessment of potential of oils for biodiesel production. *Renew. Sustain. Energy Rev*. **2015**, *44*, 814.

[6]   N. Rashid, M. S. U. Rehman, M. Sadiq, T. Mahmood, J. I. Han. Current status, issues and developments in microalgae derived biodiesel production. *Renew. Sustain. Energy Rev.* **2014**, *40*, 760.

[7]   I. B. Banković-Ilić, O. S. Stamenković, V. B. Veljković. Biodiesel production from non-edible plant oils. *Renew. Sustain. Energy Rev.* **2012**, *16*, 3621.

[8]   A. Demirbas. Potential Resources of Non-edible Oils for Biodiesel. *Energy Sources, Part B Econ. Planning, Policy*. **2009**, *4*, 310.

[9]   A. B. Chhetri, M. S. Tango, S. M. Budge, K. C. Watts, M. R. Islam. Non-edible plant oils as new sources for biodiesel production. *Int. J. Mol. Sci.* **2008**, *9*, 169.

References

[10]   T. M. Y. Khan, A. E. Atabani, I. A. Badruddin, A. Badarudin, M. S. Khayoon, S. Triwahyono. Recent scenario and technologies to utilize non-edible oils for biodiesel production. *Renew. Sustain. Energy Rev.* **2014**, *37*, 840.

[11]   A. S. Ramadhas, S. Jayaraj, C. Muraleedharan. Biodiesel production from high FFA rubber seed oil. *Fuel* **2005**, *84*, 335.

[12]   C. Öner, Ş. Altun. Biodiesel production from inedible animal tallow and an experimental investigation of its use as alternative fuel in a direct injection diesel engine. *Appl. Energy.* **2009**, *86*, 2114.

[13]   A. N. Phan, T. M. Phan. Biodiesel production from waste cooking oils. *Fuel* **2008**, *87*, 3490.

[14]   Z. Yaakob, M. Mohammad, M. Alherbawi, Z. Alam, K. Sopian. Overview of the production of biodiesel from Waste cooking oil. *Renew. Sustain. Energy Rev.* **2013**, *18*, 184.

[15]   P. Nautiyal, K. A. Subramanian, M. G. Dastidar. Production and characterization of biodiesel from algae. *Fuel Process. Technol.* **2014**, *120*, 79.

[16]   J. Huang, J. Xia, W. Jiang, Y. Li, J. Li. Biodiesel production from microalgae oil catalyzed by a recombinant lipase. *Bioresour. Technol.* **2014**, *180*, 47.

[17]   A. L. Ahmad, N. M. Yasin, C. J. C. Derek, J. K. Lim. Microalgae as a sustainable energy source for biodiesel production: A review. *Renew. Sustain. Energy Rev.* **2011**, *15*, 584.

[18]   A. E. Atabani, A. S. Silitonga, I. A. Badruddin, T. M. I. Mahlia, H. H. Masjuki, S. Mekhilef. A comprehensive review on biodiesel as an alternative energy resource and its characteristics. *Renew. Sustain. Energy Rev.* **2012**, *16*, 2070.

[19]   M. H. M. Ashnani, A. Johari, H. Hashim, E. Hasani. A source of renewable energy in Malaysia, why biodiesel? *Renew. Sustain. Energy Rev.* **2014**, *35*, 244.

[20]   A. Demirbas. Importance of biodiesel as transportation fuel. *Energy Policy* **2007**, *35*, 4661.

[21]   Y. C. Sharma, B. Singh. Development of biodiesel: Current scenario. *Renew. Sustain. Energy Rev.* **2009**, *13*, 1646.

[22]   J. Cloin, A. Woodruff, D. Fürstenwerth. Liquid biofuels in Pacific island countries. Community lifelines programme energy section, Pacific Islands applied geoscience commission. **2007**. pp 1-68.

[23]   T. Issariyakul, A. K. Dalai. Biodiesel from vegetable oils. *Renew. Sustain. Energy Rev.* **2014**, *31*, 446.

[24]   A. Karmakar, S. Karmakar, S. Mukherjee. Properties of various plants and animals feedstocks for biodiesel production. *Bioresour. Technol.* **2010**, *101*, 7201.

[25]   G. Knothe, Fuel Properties, in *The Biodiesel Handbook*, (Ed: J.K. Gerhard KnotheJ, Jon Van Gerpen). AOCS Press, Champaign, Illinois, **2005**, pp. 137–247.

[26]   S. T. Keera, S. M. El Sabagh, A. R. Taman. Transesterification of vegetable oil to biodiesel fuel using alkaline catalyst. *Fuel* **2011**, *90*, 42.

[27]   A. Demirbas. Progress and recent trends in biodiesel fuels. *Energy Convers. Manag.* **2009**, *50*, 14.

[28]   A. Abollé, L. Kouakou, H. Planche. The viscosity of diesel oil and mixtures with straight vegetable oils: Palm, cabbage palm, cotton, groundnut, copra and sunflower. *Biomass and Bioenergy* **2009**, *33*, 1116.

References

[29]   K. D. Maher, D. C. Bressler. Pyrolysis of triglyceride materials for the production of renewable fuels and chemicals. *Bioresour. Technol.* **2007**, *98*, 2351.

[30]   T. N. de Castro Dantas, A. C. Da Silva, A. A. D. Neto. New microemulsion systems using diesel and vegetable oils. *Fuel* **2001**, *80*, 75.

[31]   A. Demirbas. Comparison of transesterification methods for production of biodiesel from vegetable oils and fats. *Energy Convers. Manag.* **2008**, *49*, 125.

[32]   R. Kumar, P. Tiwari, S. Garg. Alkali transesterification of linseed oil for biodiesel production. *Fuel* **2013**, *104*, 553.

[33]   A. Abbaszaadeh, B. Ghobadian, M. R. Omidkhah, G. Najafi. Current biodiesel production technologies: A comparative review. *Energy Convers. Manag.* **2012**, *63*, 138.

[34]   A. Demirbas. Comparison of transesterification methods for production of biodiesel from vegetable oils and fats. *Energy Convers. Manag.* **2008**, *49*, 125.

[35]   H. D. Hanh, N. T. Dong, K. Okitsu, R. Nishimura, Y. Maeda. Biodiesel production through transesterification of triolein with various alcohols in an ultrasonic field. *Renew. Energy* **2009**, *34*, 766.

[36]   A. Demirbas. Biodiesel production from vegetable oils via catalytic and non-catalytic supercritical methanol transesterification methods. Prog. *Energy Combust. Sci.* **2005**, *31*, 466.

[37]   E. M. Shahid, Y. Jamal. Production of biodiesel: A technical review. *Renew. Sustain. Energy Rev.* **2011**, *15*, 4732.

[38]   J. C. Bergmann, D. D. Tupinambá, O. Y. A. Costa, J. R. M. Almeida, C. C. Barreto, B. F. Quirino. Biodiesel production in Brazil and alternative biomass feedstocks. *Renew. Sustain. Energy Rev.* **2013**, *21*, 411.

[39]   J. M. Encinar, J. F. González, A. Rodríguez-Reinares. Ethanolysis of used frying oil. Biodiesel preparation and characterization. *Fuel Process. Technol.* **2007**, *88*, 513.

[40]   Q. Li, J. Xu, W. Du, Y. Li, D. Liu. Ethanol as the acyl acceptor for biodiesel production. *Renew. Sustain. Energy Rev*. **2013**, *25*, 742.

[41]   O. S. Stamenković, A. V. Veličković, V. B. Veljković. The production of biodiesel from vegetable oils by ethanolysis: Current state and perspectives. *Fuel* **2011**, *90*, 3141.

[42]   Z. Yaakob, B. N. Narayanan, S. Padikkaparambil. A review on the oxidation stability of biodiesel. *Renew. Sustain. Energy Rev.* **2014**, *35*, 136.

[43]   G. Knothe. Dependence of biodiesel fuel properties on the structure of fatty acid alkyl esters. *Fuel Process. Technol.* **2005**, *86*, 1059.

[44]   D. Berthiaume, A. Tremblay. Study of the Rancimat test method in measuring the oxidation stability of biodiesel ester and blends. *Oleotek Inc. Report, NRCan Project No. CO414 CETC-327.* **2006**

[45]   H. L. Fang, R. L. McCormick. Spectroscopic Study of Biodiesel Degradation Pathways (No. 2006-01-3300). *SAE Tech. Pap.* **2006**, 16.

[46]   R. W. Bruce. Theory and practice of lubrication and tribology in *Handbook of Lubrication and Tribology, Volume II: Theory and Design (Vol. 2).* CRC Press Tarloy & Francis group, Boca Raton, **2012**, p 21-4.

References

[47]   E. C. Zuleta, L. Baena, L. A. Rios, J. A. Calderón. The oxidative stability of biodiesel and its impact on the deterioration of metallic and polymeric materials: A review. *J. Braz. Chem. Soc.* **2012**, *23*, 2159.

[48]   W. E Neff, E. N Frankel, K. Fujimoto. Autoxidative dimerization of methyl linolenate and its monohydroperoxides, hydroperoxy epidioxides and dihydroperoxides. *J. the American Oil Chemists' Society* **1988**, *65*, 616.

[49]   E. N. Frankel, Hydroperoxide decomposition, in *Lipid Oxidation*, (Ed: E.N. Frankel), 2nd edition. Woodhead Publishing Limited, Cambridge, **2012**. pp. 67-96.

[50]   J. A. Waynick. Characterization of biodiesel oxidation and oxidation products (CRC project No. AVFL-2b Task 1 results Technical literature review SwRI® Project No. 08-10721. Texas, **2005**. pp.1-51.

[51]   A. S. Silitonga, H. H. Masjuki, T. M. I. Mahlia, H. C. Ong, W. T. Chong, M. H. Boosroh. Overview properties of biodiesel diesel blends from edible and non-edible feedstock. *Renew. Sustain. Energy Rev.* **2013**, *22*, 346.

[52]   G. Knothe, The history of vegetable oil-based diesel fuels, in *The Biodiesel Handbook*, (Eds: G. Knothe, J. Van Gerpen, J. Krahl). **2005**. pp. 5-19.

[53]   G. Dwivedi, S. Jain, M. P. Sharma. Impact analysis of biodiesel on engine performance—A review. *Renew. Sustain. Energy Rev.* **2011**, *15*, 4633.

[54]   A. M. Ashraful, H. H. Masjuki, M. A. Kalam, I. R. Fattah, S. Imtenan, S. A. Shahir, H. M. Mobarak. Production and comparison of fuel properties, engine performance, and emission characteristics of biodiesel from various non-edible vegetable oils: A review. *Energy Convers. Manag.* **2014**, *80*, 202.

[55] S. K. Hoekman, A. Broch, C. Robbins, E. Ceniceros, M. Natarajan. Review of biodiesel composition, properties, and specifications. *Renew. Sustain. Energy Rev.* **2012**, *16*, 143.

[56] H. K. Ng, S. Gan, J. H. Ng, K. M. Pang. Simulation of biodiesel combustion in a light-duty diesel engine using integrated compact biodiesel-diesel reaction mechanism. *Appl. Energy* **2013**, *102*, 1275.

[57] N. De Lima Da Silva, C. B. Batistella, R. M. Filho, M. R. W. Maciel. Investigation of biofuels properties. *Chem. Eng. Trans.* **2011**, *25*, 851.

[58] M. Johansson, J. Yang, R. Ochoterena, S. Gjirja, I. Denbratt. NOx and soot emissions trends for RME, SME and PME fuels using engine and spray experiments in combination with simulations. *Fuel* **2013**, *106*, 293.

[59] M. Chinnamma, S. Bhasker, H. Madhav, R. M. Devasia, A. Shashidharan, B. C. Pillai, P. Thevannoor. Production of coconut methyl ester (CME) and glycerol from coconut (Cocos nucifera) oil and the functional feasibility of CME as biofuel in diesel engine. *Fuel* **2015**, *140*, 4.

[60] A. Broatch, B. Tormos, P. Olmeda, R. Novella. Impact of biodiesel fuel on cold starting of automotive direct injection diesel engines Economic Commission for Europe. *Energy* **2014**, *73*, 653.

[61] A. E. Atabani, M. Mofijur, H. H. Masjuki, I. A. Badruddin, M. A. Kalam, W. T. Chong. Effect of Croton megalocarpus, Calophyllum inophyllum, Moringa oleifera, palm and coconut biodiesel-diesel blending on their physico-chemical properties. *Ind. Crops Prod.* **2014**, *60*, 130.

[62] C. Guido, C. Beatrice, P. Napolitano. Application of bioethanol/RME/diesel blend in a Euro5 automotive diesel engine: Potentiality of closed loop combustion control technology. *Appl. Energy* **2013**, *102*, 13.

References

[63]   B. R. Moser. Fuel property enhancement of biodiesel fuels from common and alternative feedstocks via complementary blending. *Renew. Energy* **2016**, *85*, 819.

[64]   A. Demirbas. Potential resources of non-edible oils for biodiesel. *Energy Sources, Part B Econ.* **2009**, *4*, 310.

[65]   M. M. K. Bhuiya, M. G. Rasul, M. M. K. Khan, N. Ashwath, A. K. Azad, M. A. Hazrat. Second Generation Biodiesel: Potential Alternative to-edible Oil-derived Biodiesel. *Energy Procedia* **2014**, *61*, 1969.

[66]   R. M. Joshi, M. J. Pegg. Flow properties of biodiesel fuel blends at low temperatures. *Fuel* **2007**, *86*, 143.

[67]   F. D Gunstone, J. L. Harwood, A. J. Dijkstra. Occurrence and characterisation of oils and fats, in *The Lipid Handbook with CD-ROM*. CRC Press., Boca Raton, **2007**. p 70.

[68]   A. C. Hansen, B. B. He, N. J. Engeseth. Food versus fuel characteristics of vegetable oils and animal fats. *Trans. ASABE* **2011**, *54*, 1407.

[69]   N. Strömberg, A. Saramat, H. Eriksson. Biodiesel degradation rate after refueling. *Fuel* **2013**, *105*, 301.

[70]   J. Pullen, K. Saeed. An overview of biodiesel oxidation stability. *Renew. Sustain. Energy Rev.* **2012**, *16*, 5924.

[71]   R. Garcés Mancheño, E. Martínez-Force, J. J. Salas. Vegetable oil basestocks for lubricants. *grasas y aceites* **2011**, *62*, 21.

[72]   G. Yildiz, R. L. Wehling, S. L. Cuppett. Comparison of four analytical methods for the determination of peroxide value in oxidized soybean oils. *J. Am. Oil Chem. Soc.* **2003**, *80*, 103.

[73]   A. Morales, S. Marmesat, M. C. Dobarganes, G. Márquez-Ruiz, J. Velasco. Evaporative light scattering detector in normal-phase high-performance liquid chromatography determination of FAME oxidation products. *J. Chromatogr. A* **2012**, *1254*, 62.

[74]   A. Morales, S. Marmesat, M. V. Ruiz-Méndez, G. Márquez-Ruiz, J. Velasco. Formation of oxidation products in edible vegetable oils analyzed as FAME derivatives by HPLC-UV-ELSD. *Food Res. Int.* **2014**, *62*, 1080.

[75]   N. Gladovič, L. Zupančič-Kralj, J. Plavec. Determination of primary oxidation products of linoleic acid and triacylglycerols. *J. Chromatogr. A* **1997**, *767*, 63.

[76]   R. F. Garwood, B. P. Khambay, B. C. Weedon, E.N. Frankel. Allylic hydroperoxides from the autoxidation of methyl oleate. *J.C.S. Chem.Comm.,* **1977**, *178*, 364.

[77]   E. N. Frankel, W. E. Neff, W. K. Rohwedder, B. P. S. Khambay, R. F. Garwood, B. C. L. Weedon. Analysis of autoxidized fats by gas chromatography-mass spectrometry: I. Methyl oleate. *Lipids* **1977**, *12*, 901.

[78]   E. N. Frankel, W. E. Neff, E. Selke. Analysis of autoxidized fats by gas chromatography-mass spectrometry: VII. Volatile thermal decomposition products of pure hydroperoxides from autoxidized and photosensitized oxidized methyl oleate, linoleate and linolenate. *Lipids* **1981**, *16*, 279.

[79]   I. Ontañon, J. Sanz, a Escudero, S. de Marcos, V. Ferreira, J. Galbán. A modified commercial gas chromatograph for the continuous monitoring of the thermal degradation of sunflower oil and off-line solid phase extraction gas-chromatography-mass spectrometry characterization of released volatiles. *J. Chromatogr. A* **2015**, *1388*, 52.

[80]   S. Jain, M. P. Sharma. Thermal stability of biodiesel and its blends: A review. *Renew. Sustain. Energy Rev.* **2011**, *15*, 438.

References

[81]   G. Fontaras, G. Karavalakis, M. Kousoulidou, L. Ntziachristos, E. Bakeas, S. Stournas, Z. Samaras. Effects of low concentration biodiesel blends application on modern passenger cars. Part 2: Impact on carbonyl compound emissions. *Environ. Pollut.* **2010**, *158*, 2496.

[82]   W. E. Neff, E. N. Frankel, C. R. Scholfield, D. Weisleder. High-pressure liquid chromatography of autoxidized lipids: I . methyl oleate and linoleate. *Lipids* **1978**, *13*, 415.

[83]   W. E. Neff, E. N. Frankel, D. Weisleder. High pressure liquid chromatography of autoxidized lipids: II. Hydroperoxy-cyclic peroxides and other secondary products from methyl linolenate. *Lipids* **1981**, *16*, 439.

[84]   G. G. Pereira, R. M. Alberici, G. D. Fernandes, I. B. S. Cunha, M. N. Eberlin, M. C. Dobarganes, R. J. Daroda, D. Barrera-Arellano. Ambient sonic-spray ionization mass spectrometry for rapid monitoring of secondary oxidation products in biodiesel. *Eur. J. Lipid Sci. Technol.* **2014**, *116*, 952.

[85]   G. Lercker, M. T. Rodriguez-Estrada, M. Bonoli, Analysis of the oxidation products of cis- and trans-octadecenoate methyl esters by capillary gas chromatography-ion-trap mass spectrometry: I. Epoxide and dimeric compounds, in *Journal of Chromatography A.* **2003**, pp. 333–342.

[86]   M. M. Rashed, M. A. Kalam, H. H. Masjuki, H. K. Rashedul, A. M. Ashraful, I. Shancita, A. M. Ruhul. Stability of biodiesel, its improvement and the effect of antioxidant treated blends on engine performance and emission. *RSC Adv.* **2015**, *5*, 36240.

[87]   S. Korcek, M. D. Johnson, R. K. Jensen, M. Zlnbo. Determination of the high-temperature antioxidant capability of lubricants and lubricant components. *Ind. Eng. Chem. Prod. Res. Dev.* **1986**, *25*, 621.

[88]   M. A. Huang, L. M. Turner. Analysis of phenolic antioxidants in JP-5 aviation fuels. In abstract of papers of the Anerican chemical society (Vol. 200, pp. 92-FUEL). 1155 16Th St, NW, Washigton, DC 20036, **1990**. 1255.

[89]   M. del Nogal Sánchez, P. Glanzer, J. L. Pérez Pavón, C. García Pinto, B. Moreno Cordero. Determination of antioxidants in new and used lubricant oils by headspace-programmed temperature vaporization-gas chromatography-mass spectrometry. *Anal. Bioanal. Chem.* **2010**, *398*, 3215.

[90]   E. S. Almeida, F. M. Portela, R. M. Sousa, D. Daniel, M. G. Terrones, E. M. Richter, R. A. Muñoz. Behaviour of the antioxidant tert-butylhydroquinone on the storage stability and corrosive character of biodiesel. *Fuel* **2011**, *90*, 3480.

[91]   X. Lin, Y. Ni, S. Kokot. Glassy carbon electrodes modified with gold nanoparticles for the simultaneous determination of three food antioxidants. *Anal. Chim. Acta* **2013**, *765*, 54.

[92]   Z. Zhou, F. Bing, W. Tao, X. Song. Alternative method for the determination of the antioxidant content in transformer oil by electrochemical techniques. *IEEE Trans. Dielectr. Electr. Insul.* **2012**, *19*, 1498.

[93]   T. F. Tormin, R. R. Cunha, E. M. Richter, R. A. Munoz. Fast simultaneous determination of BHA and TBHQ antioxidants in biodiesel by batch injection analysis using pulsed-amperometric detection. *Talanta* **2012**, *99*, 527.

[94]   L. A. Goulart, A. R. L. Teixeira, D. A. Ramalho, A. J. Terezo, M. Castilho. Development of an analytical method for the determination of tert-butylhydroquinone in soybean biodiesel. *Fuel* **2014**, *115*, 126.

[95]   P. I. Ortiz. Determination of *tert*-butylhydroxytoluene by flow injection analysis at polymer modified glassy carbon electrodes. **1998**, *10*, 832.

References

[96]   B. R. Moser. Impact of fatty ester composition on low temperature properties of biodiesel-petroleum diesel blends. *Fuel* **2014**, *115*, 500.

[97]   Joint Inspection Group (JIG). Aviation fuel quality requirements for jointly operated systems (AFQRJOS). **2013**, *60*, 1.

[98]   Institute of Petroleum (IP). IP585/10, Determination of Fatty Acid Methyl Esters (FAME), Derived from Biodiesel Fuel, in Aviation Turbine Fuel GC-MS with Selective Ion Monitoring/Scan Detection Method. **2010**, 585.1–585.10.

[99]   J. V Seeley, C. T. Bates, J. D. McCurry, S. K. Seeley. Stationary phase selection and comprehensive two-dimensional gas chromatographic analysis of trace biodiesel in petroleum-based fuel. *J. Chromatogr. A* **2012**, *1226*, 103.

[100]   M. Kamiński, E. Gilgenast, A. Przyjazny, G. Romanik. Procedure for and results of simultaneous determination of aromatic hydrocarbons and fatty acid methyl esters in diesel fuels by high performance liquid chromatography. *J. Chromatogr. A* **2006**, *1122*, 153.

[101]   L. S. Ettre. MS Tswett and the Invention of Chromatography. *LC GC North Am.* **2003**, *21*, 458.

[102]   K. S. Cleaves, M. S. Lesney. Capitalizing on Chromatography: LC and GC have been key to the central science. *Enterp. Chem. Sci.* **2009**. 75.

[103]   K. D. Bartle, P. Myers. History of gas chromatography. *TrAC Trends Anal. Chem.* **2002**, *21*, 547.

[104]   L. R. Snyder. Peer reviewed: HPLC: Past and Present. *Analytical chemistry*. **2000**, *72*, 412-A.

[105]   The Theory of HPLC Introduction. [Online] Available from: http://www.chromacademy.com/hplc-training.html. [Accessed 26th October 2014].

[106]   Waters Corporation. Title Beginners Guide to UPLC, [Online] Available from: http://www.waters.com/waters/en_GB/Beginners-Guide-to-UPLC/nav.htm?cid=134803622&locale=en_GB. [Accessed 30th July 2014].

[107]   L. T. Taylor. Supercritical fluid chromatography for the 21st century. *J. Supercrit. Fluids* **2009**, *47*, 566.

[108]   R. M. Smith. Supercritical fluids in separation science-the dreams, the reality and the future. *J. Chromatogr A,* **1999,** *856,* 83.

[109]   H. J. Hübschmann. Basics, in *Handbook of GC/MS: Fundamentals and Applications.*, John Wiley & Sons, the Federal Republic of Germany, **2008**. p 36.

[110]   E. Ibañez, F. J. Señoráns. Tuning of mobile and stationary phase polarity for the separation of polar compounds by SFC. *J. Biochem. Biophys. Methods* **2000**, *43*, 25.

[111]   T. Bamba, J. W. Lee, A. Matsubara, E. Fukusaki. Metabolic profiling of lipids by supercritical fluid chromatography/mass spectrometry. *J. Chromatogr. A.* **2012**, *1250*, 212.

[112]   G. Guiochon, A. Tarafder. Fundamental challenges and opportunities for preparative supercritical fluid chromatography. *J. Chromatogr. A* **2011**, *1218*, 1037.

[113]   F. Li, Y. Hsieh. Supercritical fluid chromatography-mass spectrometry for chemical analysis. *J. Sep. Sci.* **2008**, *31*, 1231.

[114]   X. Gong, N. Qi, X. Wang, J. Li, L. Lin. A new method for determination of α-tocopherol in tropical fruits by ultra performance convergence chromatography with diode array detector. *Food Anal. Methods* **2014**, *7*, 1572.

[115]   J. W. Dolan. Peak tailing and resolution. *LC GC Nort America*, **2002**, *20 (5),* 430-437.

References

[116]   M. Biba, E. L. Regalado, N. Wu, C. J. Welch. Effect of particle size on the speed and resolution of chiral separations using supercritical fluid chromatography. *J. Chromatogr. A* **2014**, *1363*, 250.

[117]   S. Jahn, U. Karst. Electrochemistry coupled to (liquid chromatography/) mass spectrometry-current state and future perspectives. *J. Chromatogr. A* **2012**, *1259*, 16.

[118]   Antec. Introduction, in *µ-PrepCell TM User Manual*. 204.0010, 5th Edition, Zoeterwoude, The Netherlands, **2013**. p 9.

[119]   R. M. Smith. Instrumentation in *Understanding Mass Spectra: A Basic Approach*. John Wiley & Sons, Inc., New Jersey, **2004**. p 4.

[120]   J. H. Gross. *Mass Spectrometry: A Textbook*. Springer, **2011**.

[121]   Electron Ionization for GC-MS-Tutorial. [Online] Available from: http://www.chromacademy.com/Electron Ionization for GC-MS-Tutorial. [Accessed 29th June 2015].

[122]   E. D. Hoffmann, V Stroobant. Mass analyser. *In Mass Spectrometry: principles and applications*. 3rd Edition, John Wiley and Sons, Chichester. **2007,** pp. 85-173.

[123]   LCGC Editors. Introduction to Electron Impact Ionization for GC–MS. *LCGC North America, 2012,* 30. [Online] Available from: http://www.chromatographyonline.com/introduction-electron-impact-ionization-gc-ms. [Accessed 29th June 2015].

[124]   J. T. Watson, O. D. Sparkman. The mass spectrometer, in *Introduction to Mass Spectrometry Instrumentation, Applications and Strategies for Data Interpretation*. John Wiley & Sons Ltd, Chichester, West Sussex, England, **2007,** p 65.

[125]   L. Hejazi, D. Ebrahimi, D. B. Hibbert, M. Guilhaus. Compatibility of electron ionization and soft ionization methods in gas chromatography/orthogonal time-of-flight mass spectrometry. *Rapid Commun. Mass Spectrom*. **2009**, *23*, 2181.

[126]   E. D. Hoffmann, V Stroobant. Ion Source in *Mass Spectrometry: principles and applications*. John Wiley and Sons, Chichester **2007,** pp.15-83.

[127]   T. Portolés, E. Pitarch, F. J. López, F. Hernández, W. M. A. Niessen, Use of soft and hard ionization techniques for elucidation of unknown compounds by gas chromatography/time-of-flight mass spectrometry, in *Rapid Communications in Mass Spectrometry*. **2011**, pp. 1589–1599.

[128]   S. J. Gaskell. Special feature: Electrospray : principles and practice. *J. mass Spectrom.* **1997**, *32*, 677.

[129]   P. Kebarle, U. H. Verkerk. Electrospray: from ions in solution to ions in the gas phase, What we know now. *Mass Spectrom. Rev.* **2009**, *28*, 898.

[130]   P. Kebarle. Special feature: A brief overview of the present status of the mechanisms involved in electrospray mass spectrometry. *J. Mass Spectrom.* **2000**, *35*, 804.

[131]   S. Crotti, R. Seraglia, P. Traldi. Some thoughts on electrospray ionization mechanisms. *Eur. J. Mass Spectrom. (Chichester, Eng).* **2011**, *17*, 85.

[132]   P. Kebarle, L. Tang. From ions in solution to ions in the gas phase-the mechanism of electrospray mass spectrometry. *Anal. Chem.* **1993**, *65*, 972A.

[133]   P. Kebarle, M. Peschke. On the mechanisms by which the charged droplets produced by electrospray lead to gas phase ions. *Anal. Chim. Acta* **2000**, *406*, 11.

[134]   T. C. Rohner, N. Lion, H. H. Girault. Electrochemical and theoretical aspects of electrospray ionisation. *Phys. Chem. Chem. Phys.* **2004**, *6*, 3056.

References

[135]   K. K. Murray, R. K. Boyd, M. N. Eberlin, G. J. Langley, L. Li, Y. Naito. Definitions of terms relating to mass spectrometry (IUPAC Recommendations 2013). *Pure and Applied Chemistry*, **2013**, *85*, 1515-1609.

[136]   J. H. Batey. The physics and technology of quadrupole mass spectrometers. *Vacuum* **2014**, *101*, 410.

[137]   P. E. Miller, M. B. Denton. The quadrupole mass filter: Basic operating concepts. *J. Chem. Educ.* **1986**, *63*, 617.

[138]   D. J. Douglas. Linear quadrupooles in mass spectrometry. **2009**, *28*, 937.

[139]   S. Mikhail, A. Maria. Perturbation theory for ion motion in quadrupole radio frequency field. *Int. J. Mass Spectrom.* **2012**, *325-327*, 58.

[140]   Z. Du, D. J. Douglas, N. Konenkov, C. Vt. Elemental analysis with quadrupole mass filters operated in higher stability regions Potential and fields. *J. Anal. At. Spectrom.,* **1999**, *14*, 1111.

[141]   G. Bracco. Comparison of quadrupole mass filters with hyperbolic and cylindrical rods working in the third stability zone. *Int. J. Mass Spectrom.* **2011**, *303*, 212.

[142]   M. S. Lesney. Spectacular Spectrometry:The corporate-led evolution of MS produced an irreplaceable tool. *Enterp. Chem. Sci.* **2001**, 93.

[143]   A. W. T. Bristow. Accurate mass measurement for the determination of elemental formula-a tutorial. *Mass Spectrom. Rev.* **2006**, *25*, 99.

[144]   B. Mamyrin, V. Karataev, D. Shmikk, V. Zagulin. The mass-reflectron, a new nonmagnetic time-of-flight mass spectrometer with high resolution. *Sov Phys JETP* **1973**, *37*, 45.

[145]   I. J. Amster. Fourier Transform Mass Spectrometry. *J. mass Spectrom.* **1996**, *31*, 1325.

[146]   D. G. Schmid, P. Grosche, H. Bandel. FTICR-Mass Spectrometry for High-Resolution Analysis in Combinatorial Chemistry. **2001**. *71*, 149.

[147]   C. L. Hendrickson, J. P. Quinn, N. K. Kaiser, D. F. Smith, G. T. Blakney, T. Chen, A. G. Marshall, C. R. Weisbrod, S. C. Beu. 21 Tesla Fourier Transform Ion Cyclotron Resonance Mass Spectrometer: A National Resource for Ultrahigh Resolution Mass Analysis. *J. Am. Soc. Mass Spectrom.* **2015**, *26*, 1626.

[148]   E. N. Nikolaev, Y. I. Kostyukevich, G. N. Vladimirov. Fourier transform ion cyclotron resonance (FT ICR) mass spectrometry: Theory and simulations. *Mass Spectrom. Rev.* **2014**, 1-40.

[149]   D. G. Schmid, P. Grosche, H. Bandel, G. Jung. FTICR-mass spectrometry for high-resolution analysis in combinatorial chemistry. *Biotechnol. Bioeng.* **2001**, *71*, 149.

[150]   A G. Marshall, C. L. Hendrickson, G. S. Jackson. Fourier transform ion cyclotron resonance mass spectrometry: a primer. *Mass Spectrom. Rev.* **1998**, *17*, 1.

[151]   A. G. Marshall, P. B. Grosshans. Fourier transform ion cyclotron resonance mass spectrometry: the teenage years. *Anal. Chem.* **1991**, *63*, 215A.

[152]   S. Forcisi, F. Moritz, B. Kanawati, D. Tziotis, R. Lehmann, P. Schmitt-Kopplin. Liquid chromatography-mass spectrometry in metabolomics research: Mass analyzers in ultra high pressure liquid chromatography coupling. *J. Chromatogr. A* **2013**, *1292*, 51.

[153]   J. V. Johnson, R. A Yost, P. E. Kelley, D. C. Bradford. Tandem-in-space and tandem-in-time mass spectrometry: triple quadrupoles and quadrupole ion traps. *Anal.Chem.* **1990**, *62*, 2162.

References

[154]   E. de Hoffmann. Tandem mass spectrometry: a primer. *J. Mass Spectrom.* **1996**, *31*, 129.

[155]   E. N. Frankel. Lipid oxidation: Mechanisms, products and biological significance. *J. Am. Oil Chem. Soc.* **1984**, *61*, 1908.

[156]   F. D. Gunstone. Reaction of oxygen and unsaturated fatty acids. *J. Am. Oil Chem. Soc.* **1984**, *61*, 441.

[157]   K. Miyashita, N. Hara, K. Fujimoto, T. Kaneda. Decomposition products of dimers arising from secondary oxidation of methyl linoleate hydroperoxides. *Agric. Biol. Chem.* **1985**, *49*, 2633.

[158]   E. Choe, D. B. Min. Comprehensive Reviews in Food Science and Food Safety Mechanisms and Factors for Edible Oil Oxidation. *Compr. Rev. Food Sci. Food Saf.* **2006**, *5*, 169.

[159]   S. Jain, M. P. Sharma. Review of different test methods for the evaluation of stability of biodiesel. *Renew. Sustain. Energy Rev.* **2010**, *14*, 1937.

[160]   J. R. Pedersen, Å. Ingemarsson, J. O. Olsson, Oxidation of rapeseed oil, rapeseed methyl ester (RME) and diesel fuel studied with GC/MS.*Chemosphere*, **1999**, *38*, 2467.

[161]   L. D. N. Batista, V. F. Da Silva, É. C. Pissurno, T. da Conceição Soares, M. R. de Jesus, C. N. Kunigami, M. G. Brasil, M. G. da Fonseca. Formation of toxic hexanal, 2-heptenal and 2,4-decadienal during biodiesel storage and oxidation. *Environ. Chem. Lett.* **2015**, *13*, 353.

[162]   C. J. Chuck, C. D. Bannister, R. W. Jenkins, J. P. Lowe, M. G. Davidson. A comparison of analytical techniques and the products formed during the decomposition of biodiesel under accelerated conditions. *Fuel* **2012**, *96*, 426.

[163]   P. C. Smith, Y. Ngothai, Q. D. Nguyen, B. K. O'Neill. Alkoxylation of biodiesel and its impact on low-temperature properties. *Fuel* **2009**, *88*, 605.

[164]   A. Morales, S. Marmesat, M. C. Dobarganes, G. Márquez-Ruiz, J. Velasco. Quantitative analysis of hydroperoxy-, keto- and hydroxy-dienes in refined vegetable oils. *J. Chromatogr. A* **2012**, *1229*, 190.

[165]   L. Steenhorst-Slikkerveer, A. Louter, H. G. Janssen, C. Bauer-Plank. Analysis of nonvolatile lipid oxidation products in vegetable oils by normal-phase high-performance liquid chromatography with mass spectrometric detection. *J. Am. Oil Chem. Soc.* **2000**, *77*, 837.

[166]   M. Yamane. High-performance liquid chromatography-thermospray ionization-mass spectrometry of the oxidation products of polyunsaturated-fatty acids. *Anal. Chim. Acta* **2002**, *465*, 227.

[167]   B. S. Levison, R. Zhang, Z. Wang, X. Fu, J. A DiDonato, S. L. Hazen. Quantification of fatty acid oxidation products using online high-performance liquid chromatography tandem mass spectrometry. *Free Radic. Biol. Med.* **2013**, *59*, 2.

[168]   G. G. Pereira, R. M. Alberici, L. L. Ferreira, J. M. Santos, H. L. Nascimento, M. N. Eberlin, D. Barrera-Arellano. A screening method to evaluate soybean oil-based biodiesel oxidative quality during its shelf life. *J. the American Oil Chemists' Society.* **2015**, *92*, 967.

[169]   A. T. Godoy, G. G. Pereira, L. L. Ferreira, I. B. S. Cunha, D. Barrera-Arellano, R. J. Daroda, M. N. Eberlin, R. M. Alberici. Biodiesel Oxidation Monitored by Ambient Desorption/Ionization Mass Spectrometry. *Energy & Fuels* **2013**, *27*, 7455.

[170]   E. N. Frankel. Lipid oxidation. *Prog. Lipid Res.* **1980**, *19*, 1.

[171]   A. K. Endalew, Y. Kiros. Catalytic autoxidation of fatty acid methyl esters from jatropha oil. **2014**, *2014*. 1.

References

[172]   P. Bondioli, A. Gasparoli, L. Della Bella, S. Tagliabue, G. Toso. Biodiesel stability under commercial storage conditions over one year. *Eur. J. Lipid Sci. Technol.* **2003**, *105*, 735.

[173]   R. M. Smith, S. Cocks. Separation of saturated and unsaturated fatty acid methyl esters by supercritical fluid chromatography on a silica column. *Analyst* **1994**, *119*, 921.

[174]   E. N. Frankel, W. E. Neff, R. D. Plattner. Chemical ionization-mass spectrometry of secondary oxidation products from methyl linoleate and linolenate. *Lipids* **1986**, *21*, 333.

[175]   C. Pera, V. Knop. Methodology to define gasoline surrogates dedicated to auto-ignition in engines. *Fuel* **2012**, *96*, 59.

[176]   European Committee for Standardization. Automotive Fuels-Diesel Requirements and Test Methods, En 590. **2003**, 1-11.

[177]   Ministry of Defence Defence Standard 91-91. Turbine fuel, aviation kerosine type, Jet A-1 NATO Code: F-35, Joint service designation: AVTUR. **2011**, *7*, pp.1-38.

[178]   M. Froment. Jet fuel contaminayion with FAME-World jet fuel supply. *Fast* 46, 8.

[179]   M. Kamiński, E. Gilgenast, A. Przyjazny, G. Romanik. Procedure for and results of simultaneous determination of aromatic hydrocarbons and fatty acid methyl esters in diesel fuels by high performance liquid chromatography. *J. Chromatogr. A* **2006**, *1122*, 153.

[180]   J. V. Seeley, S. K. Seeley, E. K. Libby, J. D. Mccurry. Analysis of Biodiesel/Petroleum Diesel blends with comprehensive two-dimensional gas chromatography. *J. chromatographic science.* **2007**, *45*, 650.

[181]   F. Adam, F. Bertoncini, V. Coupard, N. Charon, D. Thiébaut, D. Espinat, M. C. Hennion. Using comprehensive two-dimensional gas chromatography for the analysis of oxygenates in middle distillates. I. Determination of the nature of biodiesels blend in diesel fuel. *J. Chromatogr. A* **2008**, *1186*, 236.

[182]   H. Budzikiewicz, C. Djerassi, D. H. Williams. Esters and lactones, in *Mass Spectrometry of Organic Compounds*. Holden-Day, Inc., San Francisco, **1967**, p. 176.

[183]   Chem. agilent. Setting up a SIM acquisition method MS chemStation. can be found under http://www.chem.agilent.com/Library/Support/Documents/a050 42.pdf., [Accessed 8th March 2015].

[184]   R. Raina, P. Hall. Comparison of gas chromatography-mass spectrometry and gas chromatography-tandem mass spectrometry with electron ionization and negative-ion chemical ionization for analyses of pesticides at trace levels in atmospheric samples. *Anal. Chem. Insights* **2008**, *2008*, 111.

[185]   W. Ratsameepakai, J. M. Herniman, T. J. Jenkins, G. J. Langley. Evaluation of ultrahigh performance supercritical fluid chromatography – mass spectrometry as an alternative approach for the analysis of fatty acid methyl esters in aviation turbine fuel. *Energy & Fuels* **2015**, *29*, 2485.

[186]   J. N. Fairchild, J. F. Hill. P. C. Iraneta. Influence of sample solvent composition for SFC separations. *LCGC North Am.* **2013,** *31*, 326.

[187]   L. Nováková, A. Grand-Guillaume Perrenoud, I. Francois, C. West, E. Lesellier, D. Guillarme. Modern analytical supercritical fluid chromatography using columns packed with sub-2μm particles: A tutorial. *Anal. Chim. Acta* **2014**, *824*, 18.

[188]   M. S. Victor Abrahamsson. Impact of injection solvents on supercritical fluid chromatography. *J. Chromatogr. A.* **2013**, 1306, 80.

References

[189]   W. Zou, J. Dorsey, T. Chester. Modifier effects on column efficiency in packed-column supercritical fluid chromatography. *Anal. Chem.* **2000**, *72*, 3620.

[190]   L. T. Taylor. Trends in Supercritical Fluid Chromatography: 1997. *J. chromatographic science*, **1997**, *35*, 374.

[191]   M. T. Combs, M. Ashraf-Khorassani, L. T. Taylor. Packed column supercritical fluid chromatography-mass spectroscopy: A review. *J. Chromatogr. A* **1997**, *785*, 85.

[192]   C. West, A. Bouet, S. Routier, E. Lesellier. Effects of mobile phase composition and temperature on the supercritical fluid chromatography enantioseparation of chiral fluoro-oxoindole-type compounds with chlorinated polysaccharide stationary phases. *J. Chromatogr. A* **2012**, *1269*, 325.

[193]   L. Nováková, P. Chocholouš, P. Solich. Ultra-fast separation of estrogen steroids using subcritical fluid chromatography on sub-2-micron particles. *Talanta* **2014**, *121*, 178.

[194]   T. Kawabe, T. Tomitsuka, T. Kajiro, N. Kishi, T. Toyo'oka. Ternary isocratic mobile phase optimization utilizing resolution Design Space based on retention time and peak width modeling. *J. Chromatogr. A* **2013**, *1273*, 95.

[195]   X. J. Yang, Y. Qu, Q. Yuan, P. Wan, Z. Du, D. Chen, C. Wong. Effect of ammonium on liquid- and gas-phase protonation and deprotonation in electrospray ionization mass spectrometry. *Analyst* **2013**, *138*, 659.

[196]   L. Tang, P. Kebarle. Dependence of ion intensity in electrospray mass spectrometry on the concentration of the analytes in the electrosprayed solution. *Anal.Chem.* **1993**, *65*, 3654.

[197]   L. Tang, P. Kebarle. Effect of the conductivity of the electrosprayed solution on the electrospray current. Factors determining analyte sensitivity in electrospray mass spectrometry. *Anal. Chem.* **1991**, *63*, 2709.

[198]   K. Tang, J. S. Page, R. D. Smith. Charge competition and the linear dynamic range of detection in electrospray ionization mass spectrometry. *J. Am. Soc. Mass Spectrom.* **2004**, *15*, 1416.

[199]   O. D. Sparkman. Mass spectrometry PittCon® 2006. *J. Am. Soc. Mass Spectrom.* **2006**, *17*, 873.

[200]   A. Clayton, H. Peinado. In the news. *TrAC Trends Anal. Chem.* **2013**, *46*, v.

[201]   Microsaic system plc 4000 MiD® User Guide Version 5 (2nd Edition). pp. 1-99.